# PROCEEDINGS OF THE 12TH WORKING MEETING ON EUROPEAN VLBI FOR GEODESY AND ASTROMETRY

Edited by Bjørn R. Pettersen

STATENS KARTVERK
GEODESIDIVISJONEN

# PROCEEDINGS OF THE 12TH WORKING MEETING ON EUROPEAN VLBI FOR GEODESY AND ASTROMETRY

Hønefoss, Norway,
September 12 and 13, 1997

Edited by Bjørn R. Pettersen

ISBN 82-90408-41-2

# PREFACE

The 12th Working Meeting on European VLBI for Geodesy and Astrometry was held at the Norwegian Mapping Authority in Hønefoss, Norway on September 12 and 13, 1997. Technical observatory reports and scientific analyses and results pertaining to space geodesy, geodynamics and astrometry were presented. These *Proceedings* collect the written versions as submitted in camera ready format by each author(-group).

Members of the Geodetic Institute of the Norwegian Mapping Authority and its Space Geodetic Observatory at Ny-Ålesund, Svalbard participated in the planning, preparations and practical implementations necessary to run the meeting. The efforts of secretary Lilliann Lorentzen are very much appreciated. The unforgettable slide show of the majestic nature of Svalbard and the video presentation of the Space Geodetic Observatory by Gunn Marit Hernes and Leif Morten Tangen was a well appreciated appetizer between a full day of lectures and the conference evening meal. VLBI happens at fascinating places and brings together friendly and enjoyable people.

Hønefoss, November 22, 1997.

Bjørn Ragnvald Pettersen

# TABLE OF CONTENTS

# "MEASUREMENT OF VERTICAL CRUSTAL MOTION IN EUROPE BY VLBI" - Status of the EU-TMR Network

*James Campbell, Geodetic Institute, Bonn University, Germany*

## 1. Introduction

The first operational phase of the European Geodetic VLBI Network has been supported by the EU under the title "European VLBI for Crustal Dynamics" (Period 1993-1996). In this first phase the work has been concentrated on the determination of horizontal crustal motions, which presently are showing up clearly in the data analyses.

The proposal for a continuation and expansion of the project has been accepted by the European Commission under the "Training and Mobility of Researchers (TMR)"-programme thus enabling the second phase to start with new funding in October 1996. This second phase stresses the determination of vertical motions, which are, due to the adverse effects of systematic errors, much more difficult to detect than horizontal motions.

The present TMR-contract includes 5 positions of visiting researchers assigned to 4 different countries: Italy (2), Spain (1), Germany (1), Sweden (1), where they will take responsabilities as full staff members and will be involved in the ongoing research work. Up to now, three of these positions have been filled and candidates for the remaining two are in the process of negociation.

The main concern of the scientific work in the second phase is the treatment of tropospheric refraction causing elevation dependent excess path delays in the observations. The effects are very much the same for VLBI and GPS observations, although different strategies may have to be applied due to the difference in observing modes. At present, several studies are underway to assess the benefits of existing and develop new ways to solve these problems.

The immediate goal is to produce refined results for the height components of the sites in the network using both VLBI and GPS data for comparison and reliability studies. The expected achievement of the project will consist of the first reliable estimates of changes in the vertical position of the stations in the European VLBI-network. The results derived from the campaigns will constitute the much needed basis for the geophysical interpretation of crustal uplift and subsidence as well as sea level changes and other vertical motion applications.

## 2. Project status

At the last Meeting of the European Geodetic VLBI Group a detailed overview of the project has been presented (Campbell 1996). The main activities have been concentrated on the persuit of the regular EUROPE VLBI campaigns which are being organised at Bonn in coordination with the global geodetic VLBI programmes (Tab. 1). On the technical side the new station of Yebes (Instituto Geografico Nacional) is being included in the campaigns and assistance is given in determining the initial problems in the data acquisition process (see Lopez-Fernandez in this Volume).

| | | |
|---|---|---|
| 90JAN26X | EUROPE-1/90 | WET-ONS-MED-MAD-NOT |
| 90SEP05AN | EUROPE-2/90 | WET-ONS-MED-MAD-NOT-MAT |
| 90DEC20XE | EUROPE-3/90 | WET-ONS-MED-MAD-NOT-MAT |
| 91JAN06X | EUROPE-1/91 | WET-ONS- MAD- MAT |
| 91SEP08X | EUROPE-2/91 | WET-ONS-MED-MAD-NOT-MAT |
| 91DEC01X | EUROPE-3/91 | WET- MED-MAD- MAT-EFL |
| 92JAN14X | EUROPE-1/92 | WET-ONS-MED-MAD-NOT-MAT |
| 92APR08XE | EUROPE-3/92 | ONS-MED-MAD-NOT-MAT |
| 92MAY12XA | EUROPE-4/92 | MED-MAD- MAT- MV2 |
| 92JUL07X | EUROPE-5/92 | ONS-MED-MAD- MAT- MV2 |
| 92NOV03XA | EUROPE-7/92 | WET-ONS-MED-MAD- MAT |
| 92DEC01XA | EUROPE-8/92 | WET-ONS-MED-MAD- MAT-EFL |
| 93FEB16XA | EUROPE-1/93 | WET-ONS-MED-MAD-NOT-MAT |
| 93APR27XA | EUROPE-2/93 | WET- MED-MAD-NOT-MAT |
| 93AUG18XA | EUROPE-3/93 | WET-ONS-MED-MAD- MAT |
| 93DEC11XE | EUROPE-4/93 | WET-ONS-MED-MAD- MAT-EFL |
| 94FEB09XN | EUROPE-1/94 | WET- MED- not-MAT |
| 94APR27XE | EUROPE-2/94 | WET-ONS-MED-MAD-not-MAT-EFL |
| 94JUN29XE | EUROPE-3/94 | WET-ONS-MED-MAD-not-MAT |
| 94AUG31XE | EUROPE-4/94 | WET-ONS-MED-MAD-not-MAT- CRI |
| 94OCT26XE | EUROPE-5/94 | WET-ONS-MED- not-MAT-EFL-CRI-NYA |
| 94DEC28XA | EUROPE-6/94 | WET-ONS-MED-MAD-not-MAT- NYA |
| 95FEB01XE | EUROPE-1/95 | WET-ONS-MED-MAD-not-MAT- CRI-NYA |
| 95APR12XA | EUROPE-2/95 | WET-ONS-MED-MAD-not-MAT-EFL-CRI-NYA |
| 95JUN08XA | EUROPE-3/95 | WET-ONS-MED-MAD-not-MAT- CRI-NYA-YEB |
| 95AUG31XA | EUROPE-4/95 | WET-ONS- MAD- NYA |
| 95NOV09XA | EUROPE-5/95 | WET-ONS-MED-MAD-NOT-MAT- |
| 95DEC06XA | EUROPE-6/95 | WET-ONS-MED-MAD-NOT-MAT-EFL- NYA |
| 96FEB07XM | EUROPE-1/96 | WET-ONS-MED-MAD-NOT-MAT |
| 96APR25XA | EUROPE-2/96 | WET-ONS- MAD- CRI-NYA |
| 96JUN12XA | EUROPE-3/96 | WET-ONS- MAD-NOT-MAT |
| 96SEP09XA | EUROPE-4/96 | WET-ONS- MAD-NOT-MAT |
| 96NOV03XA | EUROPE-5/96 | WET-ONS-MED-MAD-NOT-MAT- NYA-YEB |
| 96DEC05XA | EUROPE-6/96 | WET-ONS-MED-MAD-NOT-MAT-EFL- NYA-YEB |
| 97JAN29XA | EUROPE-1/97 | WET-ONS-MED- MAT |
| 97MAR17XA | EUROPE-2/97 | WET-ONS-MED- MAT- YEB |

Tab. 1: Geodetic European VLBI sessions carried out in the period Jan. 1990 - March 1997. WET = Wettzell/Germany, ONS = Onsala/Sweden, MED = Medicina/Italy, MAD = Madrid/Spain, NOT = Noto/Italy (not = obs. with frequency subset), MAT = Matera/Italy, EFL = Effelsberg/Germany, MV2 = Mobile VLBI Unit, CRI = CRIMEA/Ukraine, NYA = Ny Alesund/Norway, YEB = Yebes/Spain

Of great concern are the TV interference problems that beset the stations in Italy, especially in Matera and Noto. New frequency sequences have to be worked out for the S-band at regular intervals because of the new TV links appearing at varying directions and frequencies. Up to now an exclusion zone could not be realized due to insufficient political pressure.

Another concern is the transition to the next generation VLBI system MkIV, which entails a number of technical changes, from new thin tapes to wider banwidth and new formatters. These changes will cause technical problems and may push up the failure rate again. Therefore increased attention will be required for the observing crews at the telescopes as well as at the correlator.

At the telescope sites the local surveys and the monitoring of the motion of the baseline reference points are underway. At the stations of Wettzell and Onsala the temperature effects on the height and the tilt of the telescope mounts are being observed with specially designed techniques (see e.g. Johansson et al. 1996).

## 3. Problems in relative height determination

Because the main thrust of the project is now being concentrated on the determination of vertical motions, all aspects of this task should be discussed from the onset with the necessary rigour. In this paragraph the basis for the critical evaluation of our results will be outlined, relying mostly on the relevant literature on this subject.

### *3.1 Formal errors from the adjustment*

Generally, the relative height determination is achieved by performing a least squares solution of an observing session which contains the observations of two or more stations for any given period of time. The solved quantities include relative station coordinates, tropospheric zenith path delays and many other parameters. The so-called formal errors are obtained by propagating the observational errors through the least squares estimator. A detailed discussion of the behaviour of the height component in the least squares solutions of VLBI observations has been given e.g. by Herring (1986). His conclusions remain valid, although his study is limited to some degree by concentrating on the special case of only one tropospheric parameter estimated per station and per session.

The formal errors of the adjustment are derived from the covariance matrix using the variance calculated from the post fit residuals:

$$\sigma_h = \sigma_0 \cdot \sqrt{q_{hh}} \qquad (1)$$

$$\sigma_0 = \sqrt{\Sigma p_i v_i^2 / n_f} \qquad (2)$$

where $p_i$ are the weights of the individual observations, $v_i$ the corresponding residuals and $n_f$ is the number of degrees of freedom of the solution. The vertical error $\sigma_h$ represents the actual error estimate from the observational sample. By means of the covariance term $q_{hh}$ the effects of the geometric model, the parametrisation and the number of observations as well as their individual weights contribute their share to the resulting error $\sigma_h$.

For the correct interpretation of the results of the least squares solutions two cases are of interest:

a) If we use the standard error as computed from eqn. (1) and (2), $\sigma_h$ will contain the observational noise as well as part of the mismodelling effects (e.g. variations of the zenith delay during the session and shortcomings of the mapping function).

b) If we use a constant a-priori observational error $\sigma_0$ in (1), we obtain a measure of the geometrical strength of the solution. With $\sigma_0 = 1$ this quantity may also be called relative HDOP (in allusion to the DOP-numbers used in GPS navigation solutions):

$$\sigma_{hdop} = 1 \cdot \sqrt{q_{hh}} \qquad (3)$$

So, as output from the least sqares solution we have two indicators on the quality of our results, one a pure geometrical indicator of the stability of the solution and the other a combined measure of stability *and* observational and model fitting errors.

These indicators are, however, not sufficient to estimate the 'true' error of our results. In order to achieve this, we have to look at the *repeatability* of the results between different sessions conducted under different conditions, in order to sample the variability of the unmodeled components in the observational process. But before we consider a series of different sessions we should exploit the possibilities of studying the behaviour of individual sessions more closely.

Due to the elevation dependence of most errors in VLBI- (and GPS-) observations, it has become

common practice to perform so-called cut-off tests, i.e. to compare solutions made at different elevation cut-offs. A typical example of such tests is reproduced here (Fig. 1 in Herring 1986) to explain some specific points.

The two dash-dotted curves marked I and II refer to $\sigma_h$ of case a) and contain both the effects of the geometry *and* the observational errors. Curve I is of prime importance, because it shows the behaviour of the error of the estimated height component (of station 2 of a baseline) if the tropospheric zenith delay is also estimated (which is the standard procedure in most cases). From this curve we can deduce that the optimum result for the height component is achieved if we use an elevation cut-off of about 8°. The steep rise of both curves at the very low elevations is due to the predominance of mismodeling effects, which are getting out of hands near the horizon.

Curve II represents the height error obtained without estimating the tropospheric zenith delay, a situation which cannot be achieved until a reliable method is found to determine the zenith delay independently (e.g. from meteorological data and WVR).

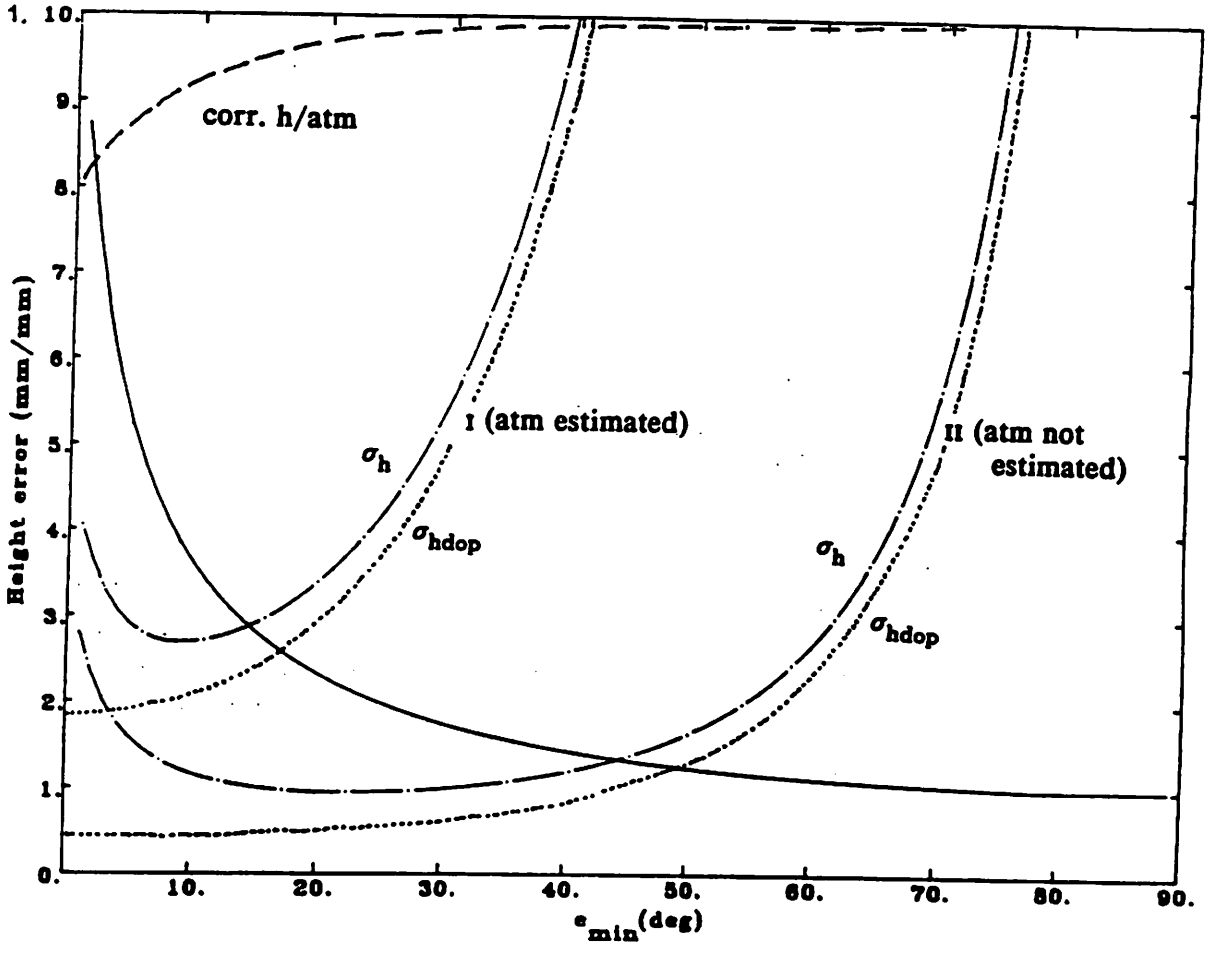


Fig. 1: Accuracy of the height component as a function of the elevation cut-off angle (adapted from Herring 1986)

The fact that curve I is much less favourable with respect to an accurate height determination than curve II is due to the correlation between the vertical component and the zenith delay parameters. This correlation tends to be very high and decreases only slightly with lower elevation cutoff (see dashed curve in fig.1). The correlation inflates the HDOP-values, but more seriously, it allows the effects of mismodeling to contaminate the vertical adjustment results.

We added the dotted curves in order to show the pure geometric effect (HDOP), which continues to improve (albeit more slowly) right down to zero elevation.

The solid curve is a different matter: it shows what happens when the constant zenith delay is not estimated *and* is in error by a fixed amount. But this curve is similar in nature to the curve of $\sigma_0$ from eqn. (2) and shows how the effect of the unmodeled errors increases with decreasing elevation. Thus the behaviour of the value of $\sigma_0$ as a function of elevation (or any other parameter) is a good indicator for studying the presence of unmodeled errors.

### *3.2 Repeatability*

In addition to the HDOP and the formal errors from the adjustment we can also include the repeatability in our error investigation, if we have a series of observing sessions spread over a period of time. Here we have to distinguish beween short term repeatability (e.g. from a number of adjacent sessions) and long term repeatability (from sessions spread over a longer period of time). The corresponding error can be calculated from the weighted mean or from a straight line fit through the results at N epochs. Usually the wrms (weighted rms) is given as

$$\sigma_{wrms} = \sqrt{\Sigma p_i v_i^2 / \Sigma p_i} \qquad (4)$$

which represents the scatter of a fictitious observation with average weight. The individual weights are usually calculated by $p_i = 1/\sigma_i^2$ , where the $\sigma_i$ are the (formal) errors of the individual session results.

An example for the baseline *length* repeatability as a function of the cut-off angle is reproduced from MacMillan and Ray (1991) in fig. 2. However, here we have to pay attention because the term 'formal error' is used for case b), i.e. the pure geometric effect, which 'arises from the propagation of (a priori) measurement noise and the atmospheric and clock model process noise though covariances with the geodetic parameters' (p. 429 of MacMillan and Ray 1991). Therefore the behaviour of $\sigma_{wrms}$ has to be described by adding a so-called unmodeled error to the 'formal error'.

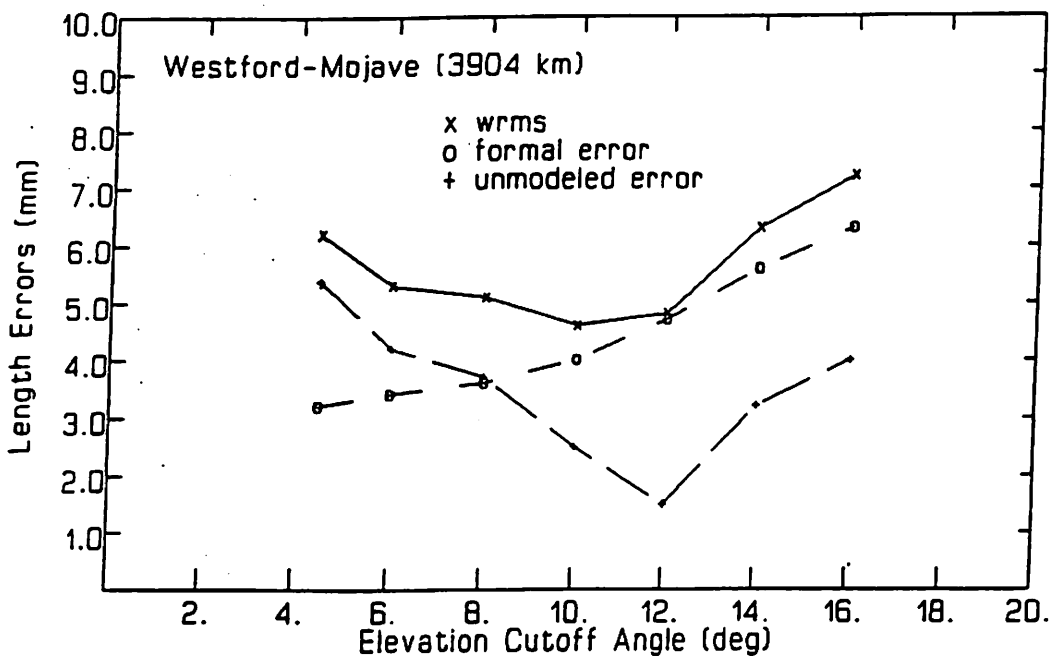


Fig. 2: Baseline length repeatability on a 4000km baseline (MacMillan and Ray 1991)

If calculated and interpreted correctly, this wrms scatter (i.e. the repeatability) is a good indicator of the 'true' accuracy of the results (as stated also by MacMillan and Ray 1991). If the repeatability improves, there is a good chance that the modeling refinements have been successful.

*3.3 Strategies*

In view of our goal to obtain accurate estimates of the height component from the VLBI (and GPS) data and with the above definitions in mind, we may summarise what should be done to cope with the atmospheric path delays:

a) Zenith delays

"Hydrostatic" delay: proportional to total surface pressure.
This part of the delay can be computed using the met data of the station (or we may ignore these and use a seasonal model adapted to certain climatic areas or use data from the world weather centers)

Wet delay: too difficult to model from surface measurements.
Alternatives: wet delays derived from WVR (Dodson et al. 1996) and from GPS. Developments are in progress: see e.g. Carlsson et al. 1996 and Niell et al. 1996.
Routinely the corrections to the wet zenith delay are estimated for each station at certain intervals in time (piecewise linear functions, Kalman filter, etc.)

b) Mapping function (elevation dependence)

Separation in "dry" and "wet" mapping funtions. The zenith delay estimation uses the wet mapping function. Alternatives: Global mapping fuctions dependent on time of year and station location (Niell 1996)

c) Estimation of atmospheric gradients ("tilted atmosphere")

- observed azimuthal asymmetry
- analysis shows improved repeatability of baseline results (MacMillan 1996)
- drawback: still more parameters included in the solutions

## 4. Validation strategies

In order to create a sound basis for improving the accuracy of the height component more cut-off tests have to be carried out on different baselines in the European VLBI network. At the same time studies of the GPS-data taken at the permanent stations should be included in the investigation. In the evaluation of the behaviour of the results at different elevation cut-offs the statistical indicators as defined by equations (1) to (3) should be used (and clearly stated). The principal test indicator will be the vertical repeatability of the individual sessions in a longer time series. Additionally, the repeatability should also be looked at in absolute terms: this means that the actual change in the vertical component at different cut-off angles should be displayed (Görres 1996) and correlated with possible external influences. In this way we should also be able to validate the use of atmospheric gradients.

## 5. Repeatability of the vertical component from VLBI and GPS observing sessions

In their paper on the current precision of VLBI Vertical determinations, MacMillan and Ray (1991) decided to use the baseline length repeatability in order to infer the vertical accuracy achieved in the VLBI data sets they analysed. The main reason for this resided in the fact that they used the data of a large network containing baselines of 1000 to 5000km baselines, which are affected (in the components) by rotational errors of the entire network. The European network contains much shorter baselines (down to a few hundred kms) and is therefore much less affected by these errors. Thus it will be justified to try to estimate the error behaviour directly from the results obtained for the vertical component.

From their analysis of the series of specially designed R&D experiments (research and development) conducted under the CDP in 1987 and 1988 MacMillan and Ray (1991) obtain a vertical (inferred) precision of 11mm compared to 2.3mm in the horizontal and 3.5mm in lenght (for the 1000km baselines). So the ratio between vertical and horizontal (or length) in these 'best' VLBI experiments is between 4:1 and 3:1. For these experiments the cut-off tests showed the elevation limits of 10° and 12° to be the optimum in terms of repeatability. In a later study Gipson & MacMillan (1995) find the optimum rather more close to 8°, i.e. the same as Herring (1986).

Examples of the repeatability of the baseline length as well as the components in the European VLBI network are given by Nothnagel (1996). These results show a length (and horizontal) repeatability of ±2.7 - ±4.9 mm and a vertical repeatability of ±11.7 - ±18.6 mm, which is a ratio of 3 - 4. The elevation limits used in the analysis have been set initially at 5° (but with a great deal of editing out of low elevation observations) and from June this year onwards at 8°. Extensive cut-off tests are planned for the near future.

The GPS horizontal and vertical repeatability can be readily seen from the plots of daily solutions for the permanent GPS stations (fig. 3). The results shown here are being produced on a routine basis by the Bundesamt für Kartographie und Geodäsie (BKG, formerly IfAG) in Frankfurt (Seeger et al. 1997) and give a clear indication that the repeatability between sessions with a time lag of ≥1 month is quite similar to the results from VLBI, i.e. about ±5 mm in the horizontal and ±20 mm in the vertical component.

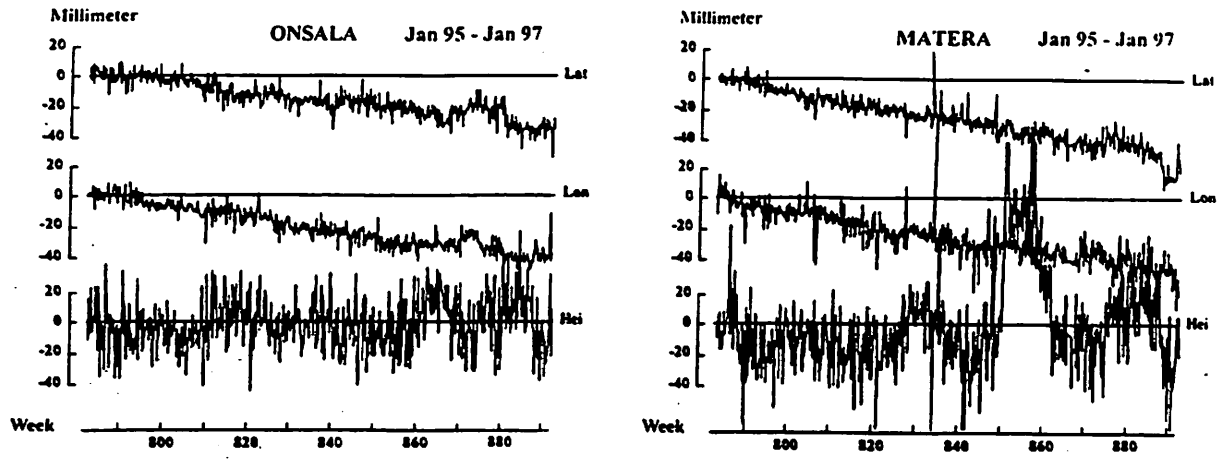


Fig. 3: Daily repeatability of coordinate determinations of the European Permanent GPS Stations (Examples from the IfAG-analysis (Seeger et al. 1997)) in a North America fixed frame (positive lat., long. axes point downwards).

By the fact that daily GPS solutions are now routinely becoming available from many computing centers it will be much easier to detect and study anomalous behaviour in the results, such as can be seen in the evolution of the heigt component in Matera, where changes had been made at the antenna support during 1996. Annual fluctuations which are most probably associated with atmospheric changes are visible in the height variations at most stations. The experience gained from the investigation of the GPS data will certainly be of great value also for the improvement of the VLBI results.

## 6. References

Campbell J.: Measurement of vertical crustal motion in Europe by VLBI - Further Support of the European Geodetic VLBI Network by the European Union. Proc. 11th Working Meeting on European VLBI for Geodesy and Astrometry. Research Report No 177, Onsala Space Observatory, p. 227-231, 1996

Carlsson T.R., G. Elgered, J.M. Johansson: A Quality Assessment of the Wet Path Delay Estimated from GPS Data. Proc. 11th Working Meeting on European VLBI for Geodesy and Astrometry. Research Report No 177, Onsala Space Observatory, p. 89-95, 1996

Dodson A.H., Shardlow P.J., Hubbard L.C.M., Elgered G., Jarlemark P.O.J.: Wet tropospheric effects on precise relative GPS height determination. Journal of Geodesy, Vol.70, p. 188-202, 1996

Gipson, J.M., D.S. MacMillan: How low should you go? Optimizing elevation limits in VLBI. Abstract GA51 G-14 in IUGG XXI General Assembly, Boulder, Colorado, July 2-14, 1995, p. A56-A57, 1995

Görres, B.: Determination of Height Changes in Regional GPS Networks. Proc. 11th Working Meeting on European VLBI for Geodesy and Astrometry. Research Report No 177, Onsala Space Observatory, p. 143-152, 1996

Herring T.A.: Precision of Vertical Position Estimates From Very Long Baseline Interferometry. JGR, Vol. 91, p. 9177-9182, 1986

Johansson L.Å., F. Stodne, S. Wolf: The PISA Project. Variations in the height of the foundation of the 20 meter radio telescope. Research Report No 178, Onsala Space Observatory, Göteborg 1996

MacMillan D.S., J.R. Ray: Current Precision of VLBI Vertical Determinations. In: Proceedings of the AGU Chapman Conference on Geodetic VLBI: Monitoring Global Change. NOAA Technical Report NOS 137 NGS 49, 1991

MacMillan D.S.: Atmospheric Delay Gradients in Geodetic Analysis. Abstract GA32 A-3, AGU Spring Meeting 20-25 May 1996 Supplement to EOS Transactions of the AGU, Vol 77, 1996

Niell A.E.: Global mapping functions for the atmosphere delay at radio wavelengths. Journ. Geophys. Res. Vol. 101, p. 3227-3246, 1996

Niell A.E.: A.J. Coster, F.S. Solheim, V.B. Mendes, P.C. Toor, R.B. Langley, C.A. Ruggles: Measurement of Water Vapor by GPS, WVR, and Radiosonde. Proc. 11th Working Meeting on European VLBI for Geodesy and Astrometry. Research Report No 177, Onsala Space Observatory, p. 96-101, 1996

Nothnagel A.: Update on European Geodetic VLBI Analyses at the Geodetic Institute of the University of Bonn. Proc. 11th Working Meeting on European VLBI for Geodesy and Astrometry. Research Report No 177, Onsala Space Observatory, p. 110-120, 1996

Seeger H., G. Weber, W. Schlüter, B. Richter: Status of IfAG GPS Permanent Network Analysis. Presented at the 8th General Assembly of the WEGENER Project, Maratea, Italy, 9 - 11 June 1997 *(Proceedings to be published)*

# Radioastronomy at the NASA Madrid Deep Space Communications Complex

Status Report, September 1997

*A. Rius*[1,2], *A. Alberdi*[1,3], *C. García-Miró*[1], *J.A. Perea*[4]
([1]LAEFF, INTA, Spain , [2]IEEC/CSIC, Barcelona, Spain, [3]IAA/CSIC, Granada, Spain , [4]MDSCC, Madrid, Spain,)
e-mail: alberdi@laeff.esa.es, rius@laeff.esa.es, cgm@laeff.esa.es, japerea@oort.mdscc.nasa.gov

## Introduction

The purpose of this report is to summarize the radioastronomical activities which have been performed during the year 1996 and the first half of 1997, using the facilities provided by the **NASA Madrid Deep Space Communications Complex (MDSCC)**. The projects performed at the MDSCC required the unique resources available at the DSN: **large antennas, precise and accurate clocks, low noise receivers and high sensitivity ...** and its geographical location (in the case of interferometry observations).

We note that the reported activities have been performed in a specific environment: **a NASA spacecraft tracking station.** The positive action of many individuals at JPL and at the MDSCC/INTA have been necessary for the successful accomplishment of this work. We hope that our activities have also contributed to improve the primary activities of the DSN: **tracking spacecrafts.**

More details on the radioastronomical activities can be obtained from the different authors, and in the Technical Reports included in the Web-pages of the DSN-radiobservatory and of the MDSCC URL Addresses:
http://dsnra.jpl.nasa.gov and http://www.laeff.esa.es/~alberdi/mdscc.html.

## The radio astronomy program in the DSN

It is composed of the following segments:

- **Applied Radio Astronomy** in direct support of the DSN.

- **Support of the NASA** Office of Space Sciences and Applications (OSSA).

- **Host Country Observations: they include both interferometric and spectroscopic observations.**

- **Radio Astronomical Observations which require the unique capabilities of the DSN.** An agreement has been signed with the EVN (European VLBI

Network) permitting the participation of the NASA dishes in a few projects, requiring very high sensitivity, in each EVN observing session. The proposals must be submitted to the Program Committees of the VLBA (Very Long Baseline Array) and of the EVN (European VLBI Network). Moreover, DSS63 will co-observe with VSOP at 18cm and eventually at 1.3cm.

## News about the MDSCC

• Madrid MkIII system was sent in February 1997 to JPL for its upgrade to MKIV. **This upgrade has been completed.** MKIV is back installed in Madrid. The MKIV terminal of the MDSCC uses **only thin tapes.**

We are in the process of integration of the MkIV terminal in the station network via **new interface systems** (the RAC -Radio Astronomy Controller- and EAC -Equipment Activity Controller-) with other peripherals (e.g. antennae, front ends, Phase-Cal systems, communications, etc.).

The first tests of the whole equipment will be performed in September 15; hopefully, Madrid will come back in operation at the end of September. A detailed report will be sent to all the users when the integration tests are completed.

• The DSS65 antenna has been down all the month of May 1997 for Azimuth bearing repair (this action was strongly required to correct its pointing accuracy and its stability). Several campaigns ,before and after this repair, have been performed in order to provide data to study variations in the reference point. These data is being studied.

## Instrumentation

(See the 'Radio Astronomy and the Deep Space Network' reports generated yearly by the JPL Telecommunications and Data Acquisition Science Office, M/S 303-401, Pasadena, California 91109, for details on the available instrumentation).

**a) VLBI Antennas:**

The antennas considered for VLBI work are:

- DSS63 (70m)
- DSS65 (34m)
- DSS54 (34m) (This antenna will be operational in October-November 1997)

**b) Info about DSS63 (70m):**

| BAND | L | S | X | K |
|---|---|---|---|---|
| Freq. Range (GHz) | 1.60-1.70 | 2.2-2.3 | 8.4-8.5 | 18-26 |
| Antenna Beamwidth (arcmin) | 10.8 | 6.5 | 1.8 | 0.75 |
| Apert. Efficiency(%) | 60 | 72 | 65 | 50 |
| Sensitivity (K/Jy) | 0.84 | 1.0 | 0.9 | 0.7 |
| Feed Polarization | LCP | RCP-LCP | RCP-LCP | LCP |
| Low noise Amplifier | FET | Maser | Maser | HEMT |
| Tsys (K) | 35 | 16 | 21 | 70 |

**c) Info about DSS65 (34m):**

| BAND | S | X | X |
|---|---|---|---|
| Freq. Range (GHz) | 2.2-2.3 | 8.4-8.5 | 8.2-8.6 |
| Antenna Beamwidth (arcmin) | 16.2 | 4.2 | 4.2 |
| Apert. Efficiency(%) | 57 | 72 | 72 |
| Sensitivity (K/Jy) | 0.19 | 0.24 | 0.24 |
| Feed Polarization | RCP-LCP | RCP-LCP | RCP-LCP |
| Low noise Amplifier | FET | Maser | HEMT |
| Tsys (K) | 40 | 21 | 38 |

**d) Info about DSS54 (34m) :**

Antenna has to become operational in November 1997. To start it will have only S and X band, but future expansions are contemplated (like K-Band , which is already planned ). Technical characteristics will be available after the performance tests which are performed during August/September/October 1997.

**e) Recording Terminals**

1 Mark IV A DAT (with two recorders)
It is controlled through the Linux-based Field System FS9 (GSFC), version FS9.3.14

The Video Converters will have 2, 4, 8 and 16 Mhz filters, with the capability to use them in the USB or LSB or both at the same time. Some of the Video Converters might have some other narrower filters.

**f) The Local Oscillators:**

- X Band: 8100 MHz
- S Band: 2000 MHz
- K Band: Tunable ( from 18 to 26.5 GHz )
- L Band: 1380 MHz

**g) Time and Frequency**

2 Redundant Hydrogen MASERS.

**h) Other equipment**

- SNR-8 ROGUE GPS Receiver.
- Pressure, humidity and temperature sensors integrated in the system.
- Water Vapour Radiometre: Method to estimate the wet delay.

## Experiments performed at the MDSCC during 1996 and the first half of 1997

**Year 1996:**

**Geodesy Experiments:**

- **Europe 1/96** - DOY 38-39 - DSS65 - S/X Band
- **RDSATL** - DOY 71-72 - DSS65 - S/X Band
- **Europe 2/96** - DOY 116-117 - DSS65 - S/X Band
- **Europe 3/96** - DOY 164-165 - DSS65 - S/X Band
- **RDMSA1** - DOY 241-242 - DSS65 - S/X Band
- **Europe 4/96** - DOY 253-254 - DSS65 - S/X Band
- **Europe 5/96** - DOY 308-309 - DSS65 - S/X Band
- **RDMSA2** - DOY 330-331 - DSS65 - S/X Band
- **Europe 6/96** - DOY 341 - DSS65 - S/X Band

**Astronomy Experiments:**

- **JPL_ST2** - DOY 6-7 - DSS63 - S Band
- **MAH18** - DOY 23 - DSS63 - K Band
- **MT044** - DOY 44 - DSS63 - L Band
- **JPL_ST3** - DOY 48-49 - DSS63 - S Band
- **BW24** - DOY 49-50 - DSS63 - K Band
- **MAH19** - DOY 91-92 - DSS63 - K Band
- **GR12T** - DOY 98-99 - DSS63 - X Band
- **MAH21** - DOY 139 - DSS63 - L Band
- **BR40** - DOY 146 - DSS63 - X Band
- **GM28** - DOY 155 - DSS63 - S Band

- **JPL_ST4** - DOY 167 - DSS63 - S Band
- **VT003** - DOY 168 - DSS63 - K Band
- **JPL_ST5** - DOY 195 - DSS63 - S Band
- **BR40C** - DOY 257 - DSS63 - X Band
- **JPL_ST6** - DOY 280 - DSS63 - S Band
- **EG14** - DOY 302 - DSS65 - X Band
- **EA10A** - DOY 303 - DSS65 - X Band
- **EA12A** - DOY 303-304 - DSS65 - X Band
- **EA12B** - DOY 304-305 - DSS65 - X Band
- **EA10B** - DOY 305-306 - DSS65 - X Band
- **ET03A** - DOY 306 - DSS65 - S/X Band
- **EP019** - DOY 306-307 - DSS65 - S/X Band
- **GM28B** - DOY 343-344 - DSS63 - S Band

Year 1997:

- **JPL_ST7** - DOY 6 - DSS63 - S Band
- **BR47A** - DOY 16 - DSS63 - X Band
- **BR47B** - DOY 18 - DSS63 - X Band
- **JPL_ST8** - DOY 25 - DSS63 - S Band
- **GM28C** - DOY 33 - DSS63 - S Band

- **Multiple non-VLBI radioastronomical observing sessions.**

## Scientific objectives and results

The scientific objectives included:

- **Study of the angular expansion of SN1993J.** A sequence of images from VLBI (DSS63 and DSS14 were essential part of the array due to their very high sensitivity) shows that the young radio supernova SN1993J is expanding with circular symmetry. A scenario in which freely expanding supernova ejecta shock mostly isotropic circumstellar material is strongly favoured. With VLBI observations at 3.6 and 6cm in the period 6 to 42 months after explosion, we have discovered that the expansion has begun to slowdown. The precise determination of the deceleration allows to parametrize the density profiles of the supernova ejecta and circumstellar medium (CSM) in standard supernova explosion models.

- **Study of the parsec-scale relativistic jets** associated with quasars and Active Galactic nuclei. DSS63 has taken part in dual polarization VLBI experiments at X-band.

- **VLBI differential astrometry.** High precision VLBI differential astrometry observations have permitted to i) study the stability of the cores of the

compact radio sources and ii) determine absolute motions of the VLBI components with precisions better than a tenth of a milliarcsecond.

- **Single-dish monitoring** of variable radiostars and galactic plane variable radio sources. The 70 meter antenna (DSS63) has been used to monitor the flux density of variable radiostars (as X-ray binaries, flare stars). Several campaigns were performed coordinated with X-ray, millimetre and sub-millimetre observations at other observatories.

- **VLBI Observations of radio stars.** The flare stars with strongest radio emission (a few tenths of milliJanskies, e.g. Algol) and some nearby radio stars (e.g. LAMAND, UVCETI_B, HR_581) were observed with VLBI with the participation of DSS63 (essential due to sensitivity reasons).

- **VLBI astrometry**, using the phase-referencing technique, provides sub-milliarcsecond-precision positions **of weakly-emitting radio stars.** ¿From a combination between multi-epoch VLBI astrometric observations and Hipparcos satellite data a low-mass companion has been detected orbiting the radio star AB Doradus, a member of the Pleiades Moving Cluster. The dynamical mass of the newly-discovered companion (0.08 – 0.11 $M_\odot$) inferred from the observed reflex motion of AB Doradus, places this object on the boundary between a brown dwarf and a very low-mass star. This result is the first detection of a low mass stellar companion using the VLBI technique, a technique which will become an important tool in future searches for planets and brown dwarfs orbiting other stars.

- **VSOP Pre-launch survey.** 6 experiments have been performed in order to determine which $H_2O$ masers (at 22 GHz) and which $OH$ masers (at 1.6 GHz) could be detected with VSOP.

- **Applications of VLBI to Geodynamics.** The antenna DSS65 have participated in the VLBI Geodesy campaigns, in particular in the *Europe* and in the *GTRF -Global Terrestrial Reference Frame-* experiments. The DSS65 antenna has been surveyed during this period to establish possible displacements of the VLBI reference point. The results of the different campaigns are under comparison and analysis.

- **Applications of GPS ("Global Positioning System")** observations to the study of the ionosphere and its effects on the proper calibration of the radioastronomical observations. During the period 22nd to 26th April 1996, a local network of seven GPS receivers was implemented around the complex with the purpose of gathering data to compare estimates of the water vapor content obtained with VLBI, GPS and WVR.

# Publications in refereed journals in 1996-1997 containing data from DSS63-DSS65


1. Alberdi, A., Krichbaum, T.P., Marcaide, J.M., Witzel, A., Zensus, J.A., Graham, D.A., Standke, K., Greve, A., Grewing, M., Schalinski, C.J., Booth, R.S., Baath, L.B., Colomer, F., Rogers, A.E.E., Doeleman, S. 1997, "The high frequency compact radio structure of the peculiar quasar 4C 39.25", Astronomy & Astrophysics, in press

2. Elósegui, P., Rius, A., Davis, J.L., Ruffini, G., Kehim, S., Burki, B. 1997, "An experiment for estimation of the spatial and temporal variations of water vapor using GPS and WVR data", Physics and Chemistry of the Earth, submitted

3. Guirado, J.C., Reynolds, J.E. et al. 1997, "Astrometric Detection of a very low mass companion orbiting a late-type radio star", Astrophysical Hournal, in press

4. Juan, M., Rius, A., Hernández-Pajares, M. 1997, "A two-layer model of the ionosphere using GPS data", Geophysical Research Letters, 24, 393

5. Kniffen, D.A., ..., Paredes, J.M., et al. 1997, "EGRET observations of the gamma-ray source 2CG 135+01", Astrophysical Journal, 486, 126

6. Lara, L., Marcaide, J.M., Alberdi, A., Guirado, J.C. 1996, "VLBI differential astrometry at large angular separation: 3C 395 - 3C 382", Astronomy & Astrophysics, 314, 672-678

7. Lara, L., Muxlow, T.W.B., Alberdi, A., Marcaide, J.M., Junor, W., Saikia, D. 1997, "Radio Observations of the Quasar 3C 395 from parsec to kiloparsec scales", Astronomy & Astrophysics, 319, 405

8. Marcaide, J.M., Alberdi, A., Ros, E., Diamond, P., Shapiro, I.I., Guirado, J.C., Jones, D.L., Mantovani, F., Pérez-Torres, M.A., Preston, R.A., Schilizzi, R.T., Sramek, R.A., Trigilio, C., Van Dyk, S.D., Weiler, K.W., Whitney, A.R. 1997, "Deceleration in the expansion of SN 1993J", Astrophysical Journal, 486, L1

9. Paredes, J.M., Marti, J., Peracaula, M., Ribó, M. 1997, "Evidence of X-ray periodicity in LSI+61°303", Astronomy and Astrophysics, 320, L25

10. Peracaula, M. 1997, "The radio emitting X-ray binary systems LSI+61°303and Cygnus X-3", PhD Thesis, Universitat de Barcelona

11. Rius, A., Ruffini, G., Romeo, A. 1997, "Analysis of Ionospheric Electron Content density distribution from GPS/MET occultations", IEEE Transactions on Geoscience and Remote Science, in press

12. Rius, A., Ruffini, G., Cucurull, L. 1997, "Improving the vertical resolution of Ionospheric tomography", Geophysical Research Letters, in press

13. Ruffini, G., Flores, A., Rius, A. 1997, "GPS tomography of the Ionospheric Electron Content with a correlation functional", IEEE Transactions on Geoscience and Remote Science, in press

### Conference Proceedings

14. Alberdi, A., Lara, L., Marcaide, J.M., Leppanen, K., Patnaik, A., Porcas, R. 1997, "Dual high frequency polarization images of the quasar 3C395", in "Blazars, Black Holes and Jets", ed. M. Kidger and J.A. de Diego, Kluwer Academic Publishers (Dordrecht, The Netherlands), in press

15. Alberdi, A., Lara, L., Gómez, J.L., Marcaide, J.M., Pérez-Torres, M.A., Kemball, A., Leppänen, K., Marscher, A.P., Patnaik, A., Porcas, R. 1997, "Magnetic Field Configuration in 4C39.25", in "Radio Emission from Galactic and Extragalactic Compact Sources", ed. G. Taylor, J. Wrobel and J.A. Zensus, Cambridge University Press, 1997, in press

16. Lara, L., Alberdi, A. 1996, "Velocity and Orientation of Accelerating Components in Relativistic Jets", in "Extragalactic Radio Sources", ed. R. Fanti and C. Fanti, Kluwer Academic Publishers (Dordrecht, The Netherlands), 447-448

17. Marcaide, J.M., Alberdi, A., Ros, E., Diamond, P., Shapiro, I.I., Guirado, J.C., Jones, D.L., Krichbaum, T., Mantovani, F., Preston, R.A., Rius, A., Schilizzi, R.T., Trigilio, C., Whitney, A.R., Witzel, A. 1996, "Spectral-Index Map and Rate of Expansion of SN 1993J", in "Radio Emission from the Stars and the Sun", ed. A.R. Taylor & J.M. Paredes, Astronomical Society of the Pacific Conference Series, 156-158

18. Marcaide, J.M., Alberdi, A., Ros, E., Diamond, P., Shapiro, I.I., Guirado, J.C., Jones, D.L., Mantovani, F., Pérez-Torres, M., Preston, R.A., Schilizzi, R.T., Trigilio, C., Whitney, A.R. 1997, "Expansion of SN1993J: new 6 and 13cm images", in "Vistas in Astronomy", ed. F. Colomer and M. Garrett, Elsevier Science, in press

19. Marcaide, J.M., Alberdi, A., Ros, E., Diamond, P., Shapiro, I.I., Guirado, J.C., Jones, D.L., Mantovani, F., Pérez-Torres, M.A., Preston, R., Schilizzi, R.T., Sramek, R.A., Trigilio, C., Van Dyk, S.D., Weiler, K.W., Whitney. A.R. 1997, "Deceleration in the Expansion of SN 1993J", in "Radio Emission from Galactic and Extragalactic Compact Sources", ed. G. Taylor, J. Wrobel and J.A. Zensus, Cambridge University Press, 1997, in press

## Future plans and hopes

- **K-band HEMT Receiver**: 18-26.5 GHz Modules.
  + a second down-converter chain in the MMS:

2 polsns or 2 spectral lines simultaneously!

- **22 GHz Tunable Maser**: End 1997

- **Digital Espectrometre**:

1024 channels correlator, with a bandwidth ~10 MHz.

1.6 GHz Receiver: $OH$ Masers; 22 GHz: $H_2O$ Masers

It is already in the process of characterization of the instrument.

| | | **1612** | **MHz** | **22** | **GHz** |
|---|---|---|---|---|---|
| Bandwidth (MHz) | Channel Spacing (Hz) | Velocity Range (Km/sec) | Velocity Resolution Km/sec | Velocity Range Km/sec | Velocity Resolution Km/sec |
| 16 | 15.625 | 2978 | 5.82 | 218 | 0.426 |
| 8 | 7.813 | 1489 | 2.91 | 109 | 0.213 |
| 4 | 3.906 | 744 | 1.45 | 54.5 | 0.107 |
| 2 | 1.953 | 372 | 0.73 | 27.3 | 0.053 |
| 1 | 0.976 | 186 | 0.36 | 13.6 | 0.027 |
| 0.5 | 0.488 | 93 | 0.18 | 6.82 | 0.013 |
| 0.25 | 0.244 | 47 | 0.09 | 3.41 | 0.007 |

# Status Report at OAN - Yebes VLBI Station

OAN-Yebes VLBI group[1] (presented by I. López-Fernández)

*Centro Astronómico de Yebes, Observatorio Astronómico Nacional, Guadalajara, Spain*

**Abstract**

We briefly present the current status of Yebes station concerning Geodetic VLBI, reporting recent technical upgrades and future trends and overviewing its results during the observations carried out last year.

## 1 VLBI Operational activities 1996-97

Since November 1996 [1], Yebes Observatory (Observatorio Astronómico Nacional – OAN) has participated in the geodetic experiments of the EUROPE and CORE (B3 subnet) campaigns, making a total of 9 experiments (we could not take part in CB303 due to a computer hardware breakdown). We also have participated in another 6 astronomical VLBI experiments during the EVN session X.

Details about the results of the observations can be found in the correlator report. Table 1 presents short remarks about some problems found during the experiments. Most of them have a common origin: intermitent errors originated in the VLBA formatter, not always reported by the *field system*[2]. The information we get from the correlator is that there sometimes are channels either lost, with low amplitude or offset a number of sampling intervals. This usually affects only even or odd tracks.

It could be inferred from this symptoms that the problem is very similar (if not the same) to the one repaired by Interferometrics last year. There may be sampling ticks missing, probably in some FIFO buffers which make the corresponding channels be ahead or behind the others. This will produce low or undetectable fringe amplitude when correlated with the nominal offset.

The fault is very difficult to detect, due to its erratic nature. It also depends highly on external conditions (for instance, using a VME extender to measure the board could make the formatter stop failing). We have already ordered some chip replacements, but our small technical group could not dedicate all its efforts to this problem. Sending the formatter to Interferometrics would imply a long period without observing, and the promised Mark IV upgrade for VLBA terminals could be ready soon.

---

[1] Presently formed by (in alphabetical order): J. Alcolea, A. Barcia, F. Colomer (coordinator), P. de Vicente, J. D. Gallego, J. Gómez-González (director), I. López-Fernández.

[2] When the formatter is failing, the *field system* sometimes, after a period of time, reports FIFO or sample clock dropout errors

| CAMPAIGN | EXPERIMENT | DATE | COMMENTS |
|---|---|---|---|
| EUROPE | EUROP5 96 | 11/03/96 | Rx warm due to faulty amplifier. |
| | EUROP6 96 | 12/05/96 | Form. jump of 6 sec.; data lost from this point. |
| | EUROP1 97 | 01/29/97 | Form. hw error 9000. Corr. reports no data in fw passes nor in odd channels of even passes. |
| | EUROP2 97 | 03/17/97 | Corr. reports spread phase in X band. |
| | EUROP3 97 | 06/16/97 | Form. hw error a000. Corr. reports low amplitude and spread phase in odd channels of X band. It is possible to refringe odd channels obtaining the same deterioration in even channels. |
| | EUROP4 97 | 08/28/97 | No correlation yet. |
| CORE | CB301 | 01/08/97 | Corr. reports godd data, but 3 scans with even/odd/all channels affected by 1 sampling interval offset. |
| | CB302 | 03/24/97 | |
| | CB303 | | No participation due to HP1000 breakdown. |
| | CB304 | 05/01/97 | Form. hw error 9000. Corr reports good even channels with -0.5 us offsets or good odd scans with +0.5 us offsets. |

**Table 1:** *Geodetic VLBI experiments since september 1996*

## 2 Technical upgrades

We briefly describe here only the technical developments in our station related to VLBI observing.

- **Receivers**
  - This year the Q band receiver has been upgraded, exchanging the IF amplifiers by a HEMT amplifier designed and built in our station, which has improved 20 K the receiver noise temperature.
  - The vacuum leaks in the S/X cryostat have been fixed in our labs. They were responsable of observing with the receiver uncooled in EUROP5 96.
- **Computers and software**
  - The *field system* has been continuously upgraded with the latest versions available. It is currently installed vs 9.3.16.

    Some commands particular to our station have been revised or programmed for the first time following the field system managers recommendations [3]. This has required in some cases hardware modifications to automatically command and/or collect data from the maser (`gps-fmout`), the weather station (`wx`), the cable calibrator (`cable`), the noise source (`calnoise`) and the phase calibrator (`calphase`).
  - The antenna control computer (HP 1000) and the *field system* PC are finally synchronized and no human intervention is necessary [3]. VLBI observations are fully

automatic; this greatly reduces the security time needed between scans. Software tools have been developed to generate HP 1000 *obs* command files from the *snap* files.

- **VLBA terminal and Recorder**
  - The whole DAR underwent a complete revision after we received the suposedly repaired formatter from interferometrics. As a result of this, some BBCs with locking problems at certain frequencies or which did not synchronize with the 1 pps were repaired (we found bad contacts in some chips and critical feed voltage in the lower BBCs).
  - The recorder has been succesfully upgraded for thin tape operation by L. Parry. Accordingly, the vacuum motor and vacuum pressure switch have been adjusted for mixed thick and thin tape operation.

A new air conditioning system was installed in the control room (this decision was partly taken in order to preserve our "delicate" formatter from any environmental changes).

| | | *S BAND* | *X BAND* | *Q BAND* |
|---|---|---|---|---|
| **Structure** | Type | Cassegrain, radome enclosed | | |
| | Slew rate (°/sg) | < 1 (azimut and elevation) | | |
| | Pointing (″) | 10 | | |
| **Main ref.** | Diameter (m) | 13.7 | | |
| | rms ($\mu$m) | 313 | | 228 [1] |
| | $\eta_s$ (%) | 65 | | 80 [1] |
| **Subreflector** | Diameter (cm) | 220 [2] | | 108.6 |
| **Feeder** | Horn type | Coaxial [2] | Conical [2] | Corrugated [3] |
| | Polarization | RCP | RCP | LCP |

[1] after reshaping the secondary from holographic measurements

[2] tilted subreflector (6.29°) and off axis multiangled shaped feeders for S ($\phi$ = 46 cm) & X ($\phi$ = 10 cm) bands

[3] sole horn cooled ($\phi$ = 6.8 cm)

**Table 2:** *Antenna characteristics*

# 3 Present Situation

Tables 2 and 3 summarize the main characteristics of our station [2]. In table 2, the parameters of the 13.7 m antenna an feeders, at X, S and Q bands are given, while table 3 refers to the VLBI receivers features, including the VLBA terminal. All receivers, including HEMT amplifiers were designed and built at Yebes. Note that with our present focalization system we have to change the subreflector when switching from 7 mm to S/X observation modes. The process requires 4 people and takes about 1 hour.

| | | *S BAND* | *X BAND* | *Q BAND* |
|---|---|---|---|---|
| **Front-end** | Type | HEMT - 15 K | HEMT - 15 K | Schottky-20 K |
| | $T_{rec}$ [1] (K) | 12 | 13 | 65 |
| | $T_{sys}$ [1] (K) | 65 | 45 | 100 |
| | Frequency (GHz) | 2.28 | 8.38 | 41 - 49 |
| **Back-end** | BW (MHz) | 140 | 500 | 400 |
| **(VLBI)** | Terminal | VLBA, 14 BBC | | |
| | Recorder | Honeywell, thin tape upgraded | | |

[1] $T_{rec}$ measured at vacuum window and $T_{sys}$ includes waveguides, polarizers and horns

**Table 3:** *Receivers characteristics*

Figure 1 shows the gain curve at 8.4 GHz obtained this year observing *Taurus A* rise up to 70°. It is basically flat, with an efficiency around 0.475. It has to be taken into account that Yebes antenna is enclosed in a radome which degrades the performance of the receiverws at these frequencies.

The VLBA DAR and recorder is commanded by version 9.3.13 of the Field System running on a 486-33 PC under slackware version 1.2.13 of Linux. This PC is not controlling the antenna; an old HP1000 is in charge.

The timing system includes the KVARZ CH1-75 hydrogen active maser [4], a TRIMBLE 5000A GPS (locked to the maser 5 MHz) with a 1 pps comparator, and an OAY-11 (in house) 1 pps synthesizer. A 286 PC records every 15 minutes the output of the pps comparison from the GPS. Another 286 monitors the meteorological data.

The OAY-15 and OAY-16 Ground an Antenna Units of the phase calibration system are complemented by an HP 52131 A counter to measure the cable delay.

The overall performance of our system is summarized in table 4.

| **Sky frequencies** (GHz) | 2.21 - 2.35 | 8.13 - 8.63 | 41 - 49 |
|---|---|---|---|
| $\eta_A$ (%) | 38 | 48 | 34 |
| $T_{sys}$ (K) | 87 | 77 | 250 |
| **SEFD** (Jy) | 3800 [2] | 3300 [2] | 10500 |

[1] $\eta_A$, $T_{sys}$ and SEFD measurements include radome effects (not optimized for S & X bands)

[2] measured using *Tau A* with assumed flux density of 810 Jy (S) and 563 Jy (X)

**Table 4:** *Overall performance*

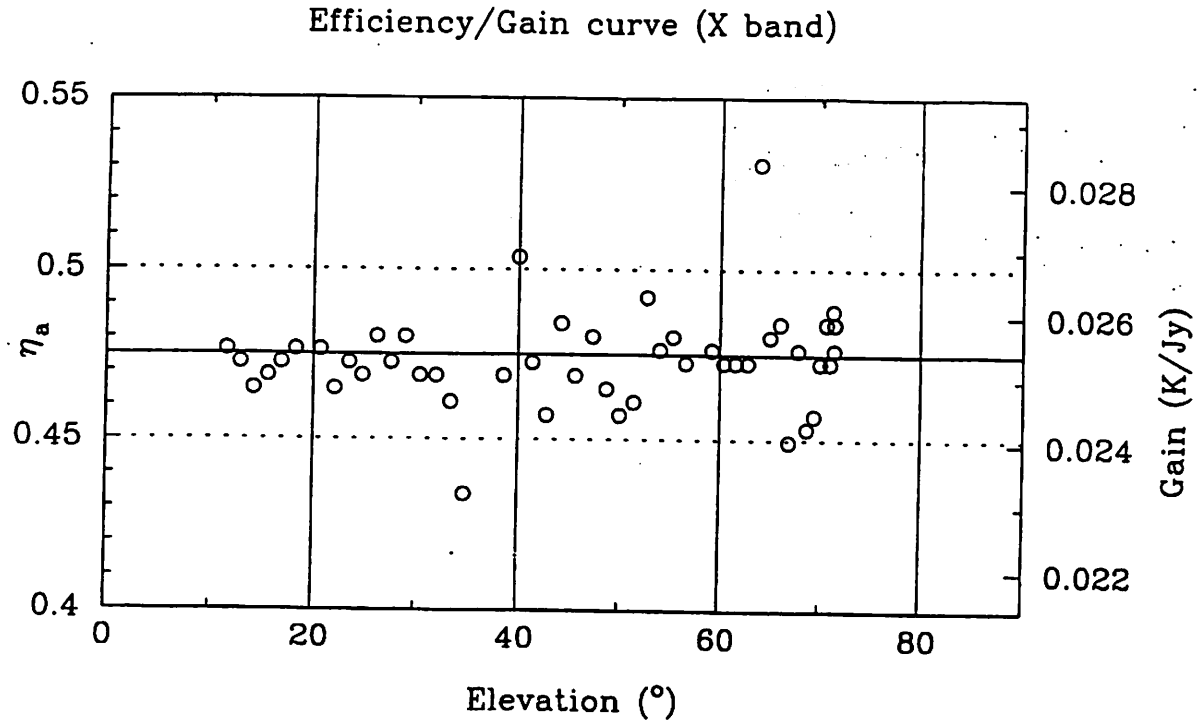


**Figure 1:** *Gain curve at X band. The mean efficiency value is 0.475*

## 4 Future plans

The new 22 GHz dual polarization receiver is already designed and some parts of the IF had been manufactured. A new focal arrangement able to accomodate the four receivers is under study. The HEMT amplifiers are being made at Yebes.

We are expecting the new Mark IV upgrade for the VLBA terminals (the so called VLBA4) which includes a completely new formatter. This would in any case solve our present problems with our VLBA formatter.

We also continue with the developement of a new control system 68040 based for the radiotelescope, whose first version will be ready early next year.

Several steps have been taken towards the possible construction of a new 40 m antenna at Yebes, which would be mainly devoted to VLBI. This year it was contracted an engineering design project, but funding for its building has not been completely assured yet.

On the observational side, we will continue our regular participation in EUROPE experiments. If the results provided by our station continue its degradation due to the formatter, we do not discard the possibility of not taking part in a number of sessions until we completely fix the problem. We are conscious of the efforts of the correlator group to cope with our data.

We also intend to participate in the CORE sessions of 1998.

## References

[1] I. López Fernández, Status report at OAN-Yebes VLBI station, *Proc. of the XI Working meeting on European VLBI for geodesy and astrometry*, Göteborg, 1996.

[2] P. de Vicente, I. López Fernández, J. D. Gallego, Characteristics of the 14 m radiotelescope at S and X bands, *CAY Technical report 1995/13*, Centro Astronómico de Yebes, 1995.

[3] P. de Vicente, J. Alcolea, I. López Fernández, J. D. Gallego, Process automatization for VLBI observations, *CAY Technical report 1996/6*, Centro Astronómico de Yebes, 1996.

[4] N.A. Demidov *et al.*, Investigations of the frequency instability of CH-75 hydrogen masers, *Proc. of the 22nd Anual Precise Time and Time Interval (PTTI) Aplications and Planning Meeting*, 1990.

# *Matera VLBI Station Status Report*

G. Bianco

agenzia spaziale italiana

G.Colucci, D.Del Rosso, L.Garramone

nuova telespazio spa

## INTRODUCTION

This report summarizes the present status (up to August 1997) of the operational activities at the Matera Space Geodesy Centre (CGS).

## THE SYSTEM

The Matera VLBI system is operated, on behalf of Italian Space Agency (**ASI**), by Nuova Telespazio at **Centro di Geodesia Spaziale (CGS)** of Matera.

The CGS came into operation on 1983 in the framework of an agreement with the Basilicata Regional Government and ASI.

A fixed SLR system and a network of permanent GPS receivers (including one at Matera site) are also operated at CGS.

The Matera VLBI system includes

- X/S bands receiver
- 20 meter diameter cassegrain antenna;
- MARK-III D.A.T. and VLBA Recorder;

## OPERATIONS

The following figure shows the summary of the activities performed and planned starting from the beginning of the Matera activities

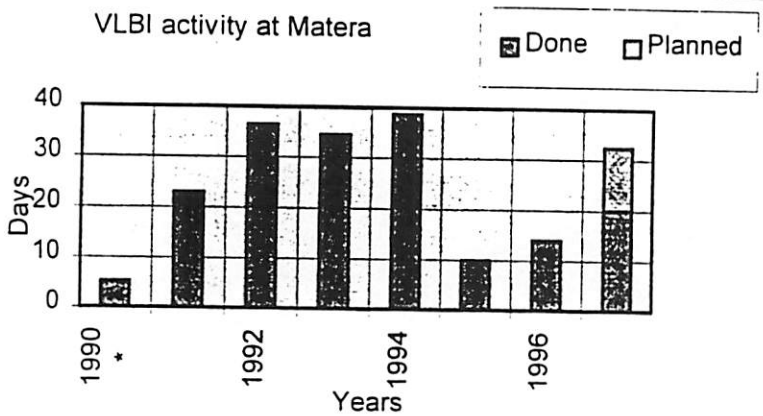


**Summary of the Matera activity**

Particularly, this is the plan for the 1997:

- 25 Core-A experiments;
- 6 Europe experiments;

- 2 EVN (astron.) experiments;
- 2 MARS experiments.

## PERFORMED UPGRADE

In December 1996, in order to upgrade the system to the NASA Wide Band Standard, a new receiver (by ATSC) front end was installed with the following characteristics (input frequencies: S-band 2210 MHz to 2450 MHz, X-band 8180 MHz to 8980 MHz)

An IF3 module (by MIT Haystack Observatory) was also installed in the Mark-III rack.

## PERFORMANCES

In order to evaluate the performances of the new system, an ONOFF session by Field System was started. Measures was performed using IF1 as X-Band device and VC13 ((272.99 MHz)) as S-Band device. Also SEFD measurement was performed obtaining ~900 Jy in X-Band and ~800 Jy in S-Band

The following figures shows the Tsys results.

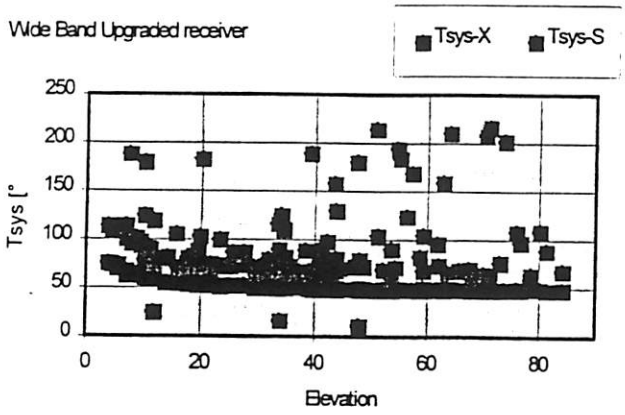


**Tsys measured by ONOFF program**

## PROBLEMS

New L.O. had large position dependent Phase Cal Phase scatter. The old LO (by Selenia) was installed into the new receiver in order to avoid this effect.

To avoid strong RFI at Matera, starting from CA012, the CORE experiments are performed using CDP-WBCA Modified CDP wide-band SX sequence.

Europe experiments performed using EUR-SX sequence.

## PLANNED UPGRADE

A new Linux FS 9.x PC was bought and is at moment at GSFC for system installation and testing; the Antenna Control SW will be ported on the new platform at Matera.

Procurement phase for Mark-IV upgrade (DAT and Recorder) started. It includes Thin Tape upgrade.

## MORE INFO

More detailed information about all the Matera activities are available *on-line*, at this address:

GeoDAF Web Server: `http://geodaf.mt.asi.it`

# The upgrading of the Medicina Station

A. Orfei, G. Maccaferri, M. Morsiani, G. Zacchiroli

*Istituto di Radioastronomia, C.N.R., Bologna, Italy*

## Abstract

Last year two big jobs were completed at the Medicina Station on the VLBI antenna. First, the track and wheels have been replaced and all of the azimuth axis has been realigned. Second, a new subreflector mechanics has been mounted to allow a fast and automatic switching among the receivers.

Both of these tasks were successfully completed and the Station now has a more reliable antenna with the capability of switching among five frequencies (i.e. seven observing configurations) within four minutes maximum. The new subreflector mechanics also allows to perform beam switching ten times faster than by moving the antenna.

## Track and wheels replacement

Since many years the track of the VLBI antenna at the Medicina Station was suffering of progressive wear, showing lateral cracks and rolling of the contact surface with the wheels. These last have also worned out being of the same hardness of the track.

In Summer 1996 the replacement and the realigning of all the azimuth axis, i.e. track, wheels and the central bearing, which was discovered to be tilted outside of the mounting limits, was funded.

All the jobs have been completed successfully. The measurements and the calibrations showed how much the performance of the antenna was improved. In figures 1a and 1b a survey of the track status are plotted, before (1a) and after (1b) the replacement. The measurements were taken by two levelmeters, mounted perpendicular each other. Fig. 1a shows:

- the tilt of the azimuth plane, detected by the sinusoidal trend (recoverable by pointing calibration)
- the superimposed non-smooth behaviour of the antenna with a not easily recoverable pointing error. As a whole the rms is about 9 arcsec, but locally the error is much higher in many azimuth places.

In fig. 1b the same sort of measures, taken after the job, are shown. The scale used is the same in order to show the improvement achived. As it can be seen the plot is very smooth at the level of 2 arcsec and, more important, at any azimuth place.

These results were confirmed by performing pointing calibration observations and accumulating in the long term several gain curves of the antenna. The gain curves repeat quite well even at different frequencies. The residuals of the pointing calibration are of the same order of magnitude at any antenna position with rms values better than any previously achieved.

It is worth to mention that the position of the antenna has changed: the azimuth plane has rotated by 57 arcsecs and the antenna is higher (vertically) of $4.4 \pm 2$ mm (the error is an estimate).

## Frequency agility

In the meantime another big task was performed: the completion of the new mechanics for the primary focus of the antenna. This was the second step of the upgrade of the Medicina dish (Orfei et al. 1993). It consists of a new mechanical structure which allows to move the subreflector aside when the primary focus receiver box has to be used.

In the past, we had to dismount the huge subreflector system using a crane, a lot of manpower and loosing observing time. Moreover, to dismount the subreflector was not a safe operation since a technician had to climb part of the antenna in order to do that. Last but not least, the mounting/dismounting of the subreflector was dependent from the weather condition.

The new system overcomes all the problems above. The system is also under computer control. With a touch of the mouse it is possible to select any of the primary focus receivers or the receiver mounted in the secondary focus. The available observing configurations are:

- 2.3/8.4 GHz receiver, one channel for each band
- 2.3 GHz double channel
- 8.8 GHz double channel
- 1.6 GHz double channel
- 1.4 GHz double channel
- 22 GHz double channel
- 5 GHz double channel

The time needed to switch among these configuration last from a few seconds to four minutes maximum. The needed time depends on which pair of configurations are involved in the operation. Four minutes are nedeed any time the subreflector must be moved either aside or back to the focal axis.

Another important improvement of the new mechanics is that it allows the subreflector to be tilted. It is possible to point a circle in the secondary focus room (vertex room) or to make a beam switching ten times faster than that obtainable by moving the antenna. The beam can be pointed off source in a very short time (about 1 second). Because of that a better recovering of the fluctuations due to the atmosphere, particularly at 22GHz, is possible. Moreover, less time is wasted allowing longer integration time.

## Future plan

As pointed out above, the new mechanics of the subreflector allows us to select a secondary focus receivers mounted off focus in the vertex room. We can now keep the receivers permanently mounted in the secondary focus room switching among them tilting the subreflector. This further step of the upgrading will complete the frequency agility of the antenna.

This task implies the redesign of all the receivers. Our aim is to get a new generation of receivers, with as large bandwidth as possible, good performances and very low crosstalk polarisation, exploiting what the up to date technology allows. We plan to achieve a sort of continuum covering in the microwave range 5–43 GHz. The design of the new receiver system is already started.

## References

A. Orfei, G. Maccaferri, S. Mariotti, M. Morsiani, G. Zacchiroli " The upgrade proposal for the VLBI Medicina antenna" Proceedings on VLBI Technology, Progress and Future Observational Possibilities, Kyoto September 1993 pag. 165 -170

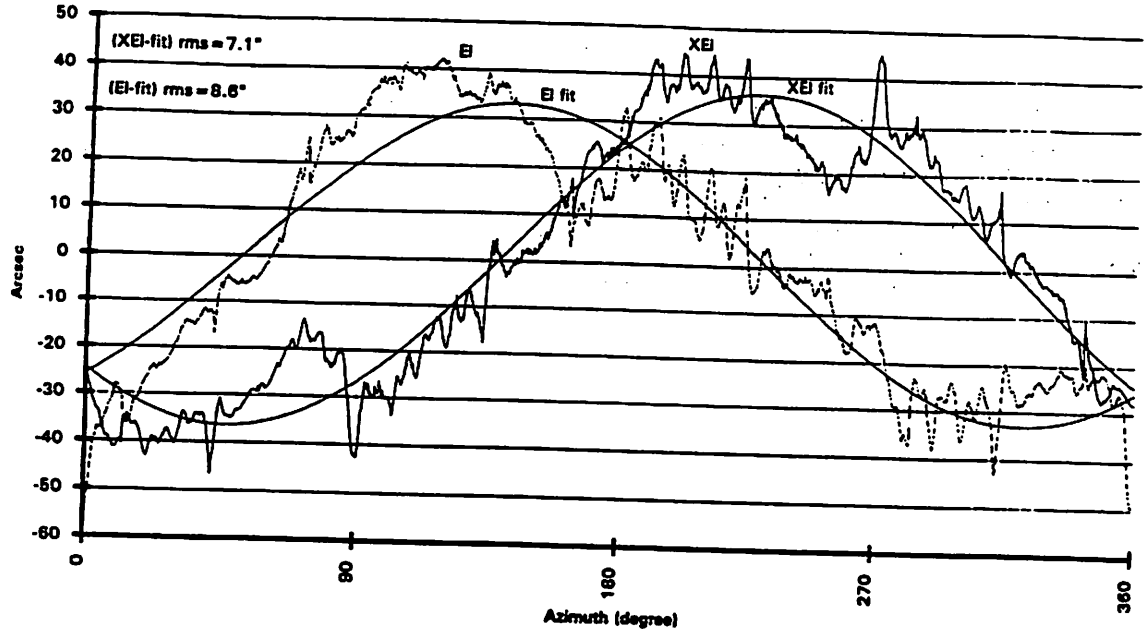
(XEl-fit) rms = 7.1°
(El-fit) rms = 8.6°
El
El fit
XEl
XEl fit
Arcsec
Azimuth (degree)

Fig. 1a

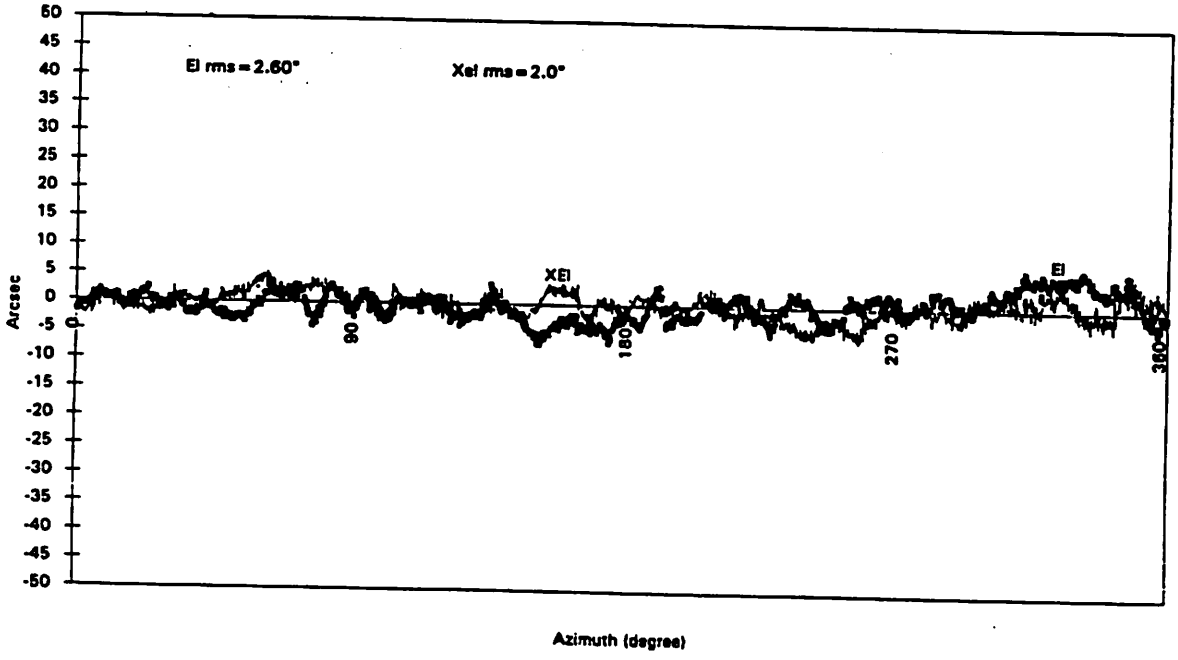
El rms = 2.60°
Xel rms = 2.0°
XEl
El
Arcsec
Azimuth (degree)

Fig. 1b

# NOTO STATION UPGRADE PROGRAM

G. Tuccari

Radioastronomy Institute
National Research Council - Italy

*Abstract*

Noto VLBI station this year started a project in order to get better performances in the existing equipment and to acquire new features. This project involves a deep upgrade program covering the following topics: frequency agility, new receiver bands availability, improving performances in the operating receivers, MKIV terminal conversion, new observation equipment, new station control equipment, new laboratory instrumentation, new calculation center, new power supply security.
The main goal is to obtain a station able to produce optimum quality VLBI observations for astronomy and geodesy, to extend single dish observation possibility, all in fully automatic fashion with minimum human contribution in order to reduce failure percentage. Technical personnel will be principally devoted to the preventive maintenance of the equipment and to the develop the new features. Moreover the new instrumentation in the laboratories is and still will be used for the technological research and development including international collaboration with the VLBI community.
The paper illustrates the program and the scheduled time in the different areas.

## 1. Frequency agility

Possibility to change in few tens of seconds or less observing frequency is one of the main goal for the station. Indeed this feature allows to improve antenna usage, drastically reducing time needed to change receiver in secondary focus (SF) or changing primary focus (PF) allocation with receivers or the secondary mirror. Two actions are necessary: automatic subreflector positioning and continuous working status for more receivers in vertex room. Tab. 1 shows the actions. Medicina group developed a system able to place secondary mirror in PF or in displaced position in order to have a receiver in PF. Such a mechanical implementation translate linearly the mirror and is in use in the Medicina antenna where was successfully tested. Automatic positioning includes X, Y and 3 Z motion axis. A new version will be replicated for the Noto antenna including some modifications become clear when the equipment has been tested.

Table 1

**FREQUENCY AGILITY**

- AUTOMATIC SUBREFLECTOR POSISTIONING
  Fast switching between Primary Focus Receiver System and Secondary Focus Receiver System

  Planned: summer 1998

- PRIMARY FOCUS RECEIVER SYSTEM
  Fast swithing between 3.6/13cm, 18cm, 21cm, 49cm, 92cm

  Planned: summer 1998

- SECONDARY FOCUS RECEIVER SYSTEM
  Fast switching between 0.7cm,1.3cm,2cm,6cm

  Planned: end 1999

The orders for the parts are already started and the construction will be realized in the first part of the 1998. Installation is scheduled for the summer 1998.

During the installation a new secondary mirror will be used to replace the old one damaged for incorrect positioning at ground when PF receivers are used. Indeed deformations up to 2 millimeters in the shape of the surface seriously affected antenna efficiency at the higher frequency used, but no effect has been detected in X band.

A new concept for the receivers is going to be adopted for the station. Functionality will be concentrated and full automatic switching is needed. Lower frequency bands will be implemented in PF, while higher frequency will be covered by receiver in SF. In this area improved performances, double circular polarization, additional observative bands quickly and automatically switched are the main goals.

A multifrequency receiver is under construction for the PF. The project is managed by the Noto technological group in strong collaboration with Medicina receiver group. The feed system, consisting in one S/X feed, one L band and two microstrip antennas is designed and probably is going to be realized by CSELT in Turin, cooling system including dewar and cryogenic section is

designed by Noto group, all the front-end amplifiers, with only exception of the X band ones furnished by NRAO, are developed in Medicina. Tab. 2 summarizes the possible configurations.

TABLE 2

**PRIMARY FOCUS RECEIVER SYSTEM**

4 CHANNELS ARE POSSIBLE:

| 2 CHANNEL CONFIGURATIONS | | 2 CHANNEL CONFIGURATIONS |
|---|---|---|
| | + | |
| 3.6 cm Left and Right Polarizations | | 49 cm Left and Right Polarizations |
| 13 cm Left and Right Polarizations | | 92 cm Left and Right Polarizations |
| 18 cm Left and Right Polarizations | | 49/92 cm Left Polarization |
| 21 cm Left and Right Polarizations | | 49/92 cm Right Polarization |
| 3.6/13 cm Right Polarization | | 3.6/13 cm Left Polarization |

Sky frequency for all the bands of such a receiver are transferred from the PF to the vertex room before any frequency conversion using low attenuation cables (Andrew LDF2-50) long about 30 m. A general IF conversion module is placed in vertex room and as local oscillator a HP synthesizer, able to generate CW signals up to 20 GHz, is used. S/X and L band feed and amplifiers are cooled and a new CTI compressor has been acquired able to maintain three systems cooled at the same time. In Noto this receiver is the first to be cooled in PF and pipelines have to be mounted for such purpose.

Scheduled time for the installation of the multifrequency receiver is the same of the automatic subreflector system, the summer 1998.

Receiver system in the vertex room will be deeply revised in order to get better performances and finally all the receivers in line. A new feed system will be studied by CSELT and in Noto the feeds covering the VLBI bands up to 43 GHz will be installed. As it was already said a unique IF module will be adopted including the SF receivers and two LO synthesizer. IF signal transfer up to the antenna control room, where the acquisition terminal is placed, will be realized using 1 GHz bandwidth optical fibers. The solution is adopted in order to avoid frequency dependent attenuation

due to the coaxial cables. The scheduled time for this second stage in the receivers area will be realized starting in the second part of 1998 and should be completed before the 1999's end. Tab. 3 shows vertex receiver system possible configurations.

TABLE 3

**SECONDARY FOCUS RECEIVER SYSTEM**

2 CHANNELS ARE POSSIBLE:

0.7 cm Left and Right Polarizations
1.3 cm Left and Right Polarizations
2 cm Left and Right Polarizations
6 cm Left and Right Polarizations

## 2. Acquisition related facilities

A complete VLBA terminal is at present available in Noto, including delay cable module. The VLBI terminal allows the MKIIIA and VLBA modes to be recorded. The terminal will be upgraded to MKIV when the formatter will be available. Mixed operation with either thin or tick tapes is now possible and the first EVN session including both support is currently observed.

A Canadian S2 terminal has been installed in the last part of 1996 and it has been successfully used for VSOP observation program with Halca satellite.

A 2048 channels autocorrelator with 160 MHz instantaneous bandwidth is available for single dish spectrometry; the instrument is at present used with the analog part of the VLBA terminal and its own dedicated SSB converters and filter banks are under construction. The instrument should be fully operative for the end of this year.

A digital polarimeter is under development. The system will be used to determine the receivers instrumental polarization and for single dish polarimetry.

The section including the computers used to drive the different part in the station will also improved and deeply modified in order to get automatic setting for antenna driving and instrumentation control. The structure is the following: a user terminal is adopted to access all the equipment. The hardware included in such a computer presents a multiserial interface and a general purpose A/D multichannel board, it can drive GPIB instruments, it can access the spectrometer, the VLBA terminal, the receiver system, the antenna. A second PC is dedicated to the Field System and acts as interface between schedule files, VLBA terminal and antenna. Antenna computer is going to be under WIN95 and will be accessible through network, as the two previous ones, for monitoring. A fourth computer will be dedicated to the subreflector control.

Main goal for this section is to achieve full automatic operations in order to avoid human mistakes and possibility to remotely control all the system. Completion for this upgrade section will follow the hardware implementations.

A new GPS receiver (Track system 9000B) was bought to replace the Totally Accurate Clock; the former will be externally clocked with H-Maser reference for improving stability of the internal clock and the last will be used as secondary for backup purposes. Its installation is scheduled for the last part of this year.

The station to monitor interference is under completion. New attention is now given to the interference contribution for the damage in the data utilization it involves. An antenna was developed for 3-8 GHz and will be installed completing a continuous coverage between decametric up to centimetric bands. Moreover a study was undertaken in order to evaluate a possible system able to decrease interference effects on the VLBI recorded data.

New continuity groups have been acquired and will be installed in the next months. Two independent 15 KVA equipment will be used to cover the gap between the main power supply and the station generators. The two groups will be devoted at different loads: a first priority set including all the equipment needed during observation, and a second priority group including workstation for post processing and laboratories equipment. An automatic selection will be

performed whether a failure occurs to the principal group during observative sessions. Also in this case the main goal is improve reliability for network operations.

### 3. Laboratories

Technical personnel is at present mainly involved in the operation devoted to frequency change and other manual activities. The upgrade program will bring to get an automatic system, that will get better working conditions. As consequence of upgrade technicians could spend most of their time in preventive maintenance and project developments. An adequate laboratories upgrading is then necessary. Three laboratories are defined and will get new instrumentation: an high frequency section involves receivers related techniques (microwave and cooling technology), a digital section devoted to acquisition and correlator techniques, a Time&Frequency section including also IF , low frequency and optical fibers technology.

The first laboratory will acquire instrumentation and will develop methods to operate for noise figure and gain analysis and improvement in the receivers components, to learn know-how in the large vacuum microwave window and vacuum methods. The digital laboratory is already collaborating with the International MKIV Correlator Consortium in the development of some part of the new MKIV correlator and is involved in the digital polarimeter development. T&F laboratory is developing the filter section for the autocorrelator spectrometer in collaboration with Florence Arcetri Observatory group, the IF section for the receiver system and is involved in the interference effects reduction in the VLBI data; moreover this laboratory will develop instrumentation and methods related to optical fibers for use in radioastronomy.

A workshop will be constructed in order to realize in situ the mechanical parts for the receivers and for the vertex room modification.

The main goals for the laboratories is to gain knowledge and instrumentation in order to bring state of art technology to the station.

# Status Report of RT-Wettzell

presented at

12th Working Meeting on European VLBI
for Geodesy and Astrometry

in Hoenefoss, Norway

**Richard Kilger**

This report presents an overview of the activities at the 20m-Radiotelescope in Wettzell since our last meeting in Goeteborg in August 1996. TIGO (Transportable Integrated Geodetic Observatory) with its 6m-offset VLBI-antenna will be described in a separate paper. The first section shows our participation in international VLBI-campaigns, the second deals with our activities in upgrading hard+software.

Since the 20m-Radiotelescope is dedicated to geodesy our main VLBI-activities and VLBI-partners donot change too much over the years and still are:

- NEOS-A, alias IRIS-A, alias POLARIS,
- INTENSIVE or Δ (UT1) measurements,
- IRIS-S,
- EUROPE,

- GSFC [CORE (Continuos Observation of Rotation of the Earth), GLOBAL-TRF/CRF, GOLDEN GLOBAL, XASIA, MARS...]
- USNO [NAVEX, NVSAT],

- MPIfR.

Table 1 gives an overview over the different campaigns over the years.

Special activities since our last meeting were:

- VLBI-observation during and after landing of interplanetary mission "Mars Pathfinder", to improve our knowledge of the planet Mars.

- Time transfer measurements with 34m-antenna in Koganei, Japan, recorded with Sony cassette recorders in K4 technology.

- Special astronomical VLBI-measurements for investigators in the MPIfR.

Wettzell performed following technical upgrades within its VLBI-measuring system:

**regarding software:**

- Field System software has been changed from HP-1000/A400 computer to FS-PC version 9.1.7 in July/Aug 1997. We started with a fairly old PC and intend to implement the latest version of Fs on a new PC.

**regarding hardware:**

- our DAT and tape unit shall be upgraded from Mark-III to -IV; Mr. Wunderlich from MPIfR in Bonn started with a more mechanical part of the thin tape upgrade at the tape unit. The still necessary components, as Formatter, read/write electronics for the tape, filters for VC's etc have been ordered from NASA. We expect to get the hardware in time before the next step of CORE is started.
- we plan to modernize our antenna pointing; in spite of the fact, that it works still reliable we have to replace:
  - antenna pointing computer DEC 11/23; it simply is no longer supported by the manufacturer DIGITAL EQUIPMENT.
  - CAMAC-module; its a parallel interface system between antenna pointing computer and FS-computer and after 14 years of service out of fashion and no longer supported by the manufacturer in the case of technical problems; additionally it caused severe problems, when we tried to move from HP-A400 to FS-PC.
  - Servo Control Unit (SCU) and Analog Control Unit (ACU)
  - Azimuth and Elevation encoder.

Another statement refers to 2 subsystems I mentioned in my talk in Goeteborg already.
One Water Vapor Radiometers (WVR) works permanently at the Fundamentalstation in Wettzell since 1996. Our practical experience at Wettzell with the WVR is, that it needs a lot of maintenance. Obviously the WVR suffers a lot due to our weather conditions (rain, snow and ice). The mechanical portion, as Azimuth- and Elevation drive unit, are too weak to accomodate to additional influences caused by ice, snow and wind. The electronical portion suffer due to the fact, that the housing cannot be tightened against water.

Our system to measure height changes of the reference point of the antenna also made problems, but we have now a set of reliable measurements and hope to integrate a value to the log-file at every scan during a VLBI-measurement indicating the height of the reference point of the antenna. Taking into account the accuracy of VLBI-measurements today and in near future with Mark-IV technology, we have to consider relative height changes of the antennas, during one day and also over the year.

The best way to do this is a measuring system, for instance with a wire made of invar-material; but if there is none available, there is a good chance to do this with reasonable assumptions, we have to do for every antenna individually, taking into account:

- radome : yes/no
- material: steel with thin wall thickness,
  concrete with thicker walls,

For Wettzell I tried to make following assumptions:

- Height of concrete tower : H = 8000 mm;
- Height of steel construction: H = 4000 mm;

Assumtions for air temperatures (normally from LOG):

- Winter day : $t$ = -20 °C; $t$ = -10 °C; $t$ = 0 °C;
- Summer day : $t$ = 17 °C; $t$ = 25 °C; $t$ =33 °C;

Temperature of concrete tower : $t$ = ( $t$ + $t$ )/2;

The temperature of the thick concrete part of the tower is represented by the middle of the outside temperature (from LOG) and an inside temperature $t$ being considered to be constant over the year. This has the consequence (in Wettzell), that the concrete tower shows no daily variations, but only seasonal effects and temperature changes over more than one day.

- $t$ is mean value of $t$ of LOG for that day;
- $t$ is temperature inside of tower ~ 15 °C (experience);

in Winter day: $t$ = (-10 + 15)/2 °C = + 2.5 °C;
in Summer day: $t$ = ( 25 + 15)/2 °C = + 20 °C;

Temperature of steel construction: $t$ = $t$ (from LOG);

Temperature of the thin steel construction equals the ambient temperature. This has the consequence, that the steel construction shows daily **and** seasonal height changes.

This causes following height changes:

- Concrete tower :
  per day : $\Delta H$ = 0 mm;
  Summer/winter : $\Delta H$ = E-05 * 8000mm * 17.5 = 1.4 mm;

- Steel construction:
  per winter day : $\Delta H$ = E-05 * 4000mm * 20 = 0.8 mm;
  per summer day : $\Delta H$ = E-05 * 4000mm * 16 = 0.64mm;
  total variation: $\Delta H$ = E-05 * 4000mm * 53 = 2.12mm;

- Concrete+steel : $\Delta H$ = E-05(8000*17.5+4000*53)= 3.52mm;

- only steel : $\Delta H$ = E-05 *12000mm * 53 = 6.36mm.

# OBSERVATORY REPORT FROM EFFELSBERG

R.W.Porcas (MPIfR, Bonn)

September 1997

1. September 1996 saw the celebration of 25 years of Effelsberg operation !

2. The new azimuth track and elevation encoders have improved the telescope performance. Values for the height increase resulting from the changes are listed below:

| | |
|---|---|
| 12 mm | predicted, and reported at the Onsala meeting |
| 18 mm ± 1 mm | measured at the telescope |
| 29 mm ± 6 mm | deduced by M. Eubanks from geodetic experiment |

3. The outer, wire-mesh panels (80-100m) are being replaced by perforated aluminium panels, to improve gain and reduce ground noise. Work started this summer.

4. The MK3A terminal has now been upgraded to MK4 (November 1996) and is controlled by the FS9 field system. A vacuum switch for switching between thin and thick tape operation will be installed later this year. The VLBA terminal is now used exclusively with thin tape (high density) recording. R. Boesel has been stationed at Effelsberg for maintainance of both the MK4 and VLBA terminals.

5. Frequency agility is now working well between the secondary focus receivers at 13, 6, 3.6, 2, 1.3, and 0.7 cm wavelengths. Efforts are needed to improve the 1.3 and 0.7 cm performance.

6. The new 8.4 GHz receiver is still under construction. No wide-band geodesy system is planned.

7. The increased occurence of VLBI observations outside of EVN "sessions", particularly together with the VLBA, has revealed a need for improved operator training.

# TIGO - Transportable Integrated Geodetic Observatory A Fundamental Station for Geodynamic Research

HAYO HASE, WOLFGANG SCHLÜTER, ARMIN BÖER,
REINER DASSING, PETER SPERBER
Bundesamt für Kartographie und Geodäsie
*former: Institut für Angewandte Geodäsie (IfAG)*
Fundamentalstation Wettzell
D-93444 Kötzting, Germany

RICHARD KILGER
Forschungseinrichtung Satellitengeodäsie (FESG) der Technischen Universität München
Fundamentalstation Wettzell
D-93444 Kötzting, Germany

12th Working Meeting on European VLBI for Geodesy and Astrometry, Hønefoss, September 12-13, 1997

## Introduction

Dynamical processes within the Earth system are causing global changes. They can be investigated from:

- the dynamical behaviour of the Earth motion, e.g. in the variation of the length of day and the polar motion,
- changes of the lithosphere, as tectonic plate motion or earthquakes and vulcanism,
- climate changes and
- changes within the biosphere.

Precise modelling of the dynamic processes regarding the correlation between the geodynamical events has risen to a complex physical theory in post Newton approximations.

For the development of such models a wide spread spectrum of observables has to be collected from a network of stationary and transportable observatories.

## Fundamental Stations for Geodynamical Applications

For geodynamical research a globally distributed network of *Fundamental Stations*, equipped with VLBI-, SLR-, GPS- and other observation techniques, is required in order to obtain precise and reliable results.

The objectives of Fundamental Stations coordinated within a network are to:

- represent the Earth and its motion in space,
- define and realize a terrestrial reference frame,
- maintain the reference frame by observing the Earth rotation parameters and plate motions with respect to an extraterrestrial reference frame represented by quasars.

Various observables have to be provided which are sensitive to the Earth rotation and the variations, to the movements of the lithosphere and to the gravity of the Earth.



## Basic Characteristics of Fundamental Stations

The basic characteristics of Fundamental Stations are:

1. *permanency*, to provide data on a long term basis,
2. *complementary*, to carry out a broad spectrum of supplementary observations,
3. *redundancy*, to employ various, independent techniques for controlling the results.

The instrumentation of a Fundamental Station for geodetic and geodynamical applications should be able to carry out:

- VLBI-observations to quasars,
- laser ranging to artifical satellites (and to the Moon),
- GPS-observations,
- gravity and seismic observations,
- supplementary terrestrial measurements,
- time and frequency measurements.

# Concept of TIGO

The global network consists of *only a few* existing Fundamental Stations, which are globally *insufficient* and *unbalanced* distributed (lack in southern hemisphere) and has to be improved by additional geodetic observatories

The Bundesamt für Kartographie und Geodäsie (former IfAG) is realizing the *Transportable Integrated Geodetic Observatory (TIGO)* based on the principles:

- provision of a broad spread spectrum of observations,
- minimum observation period of 1 year per site,
- preference for sites in the southern hemisphere,
- cooperation based on agreements with host agencies,

- modular design, state-of-the-art,
- high degree in automatisation,
- transportation in 40-feet seacontainers,
- setup time less than 1 week.

Realisation in the period from 1992 to 1998.



# Distribution of ITRF94 Sites (IERS Technical Note 20)

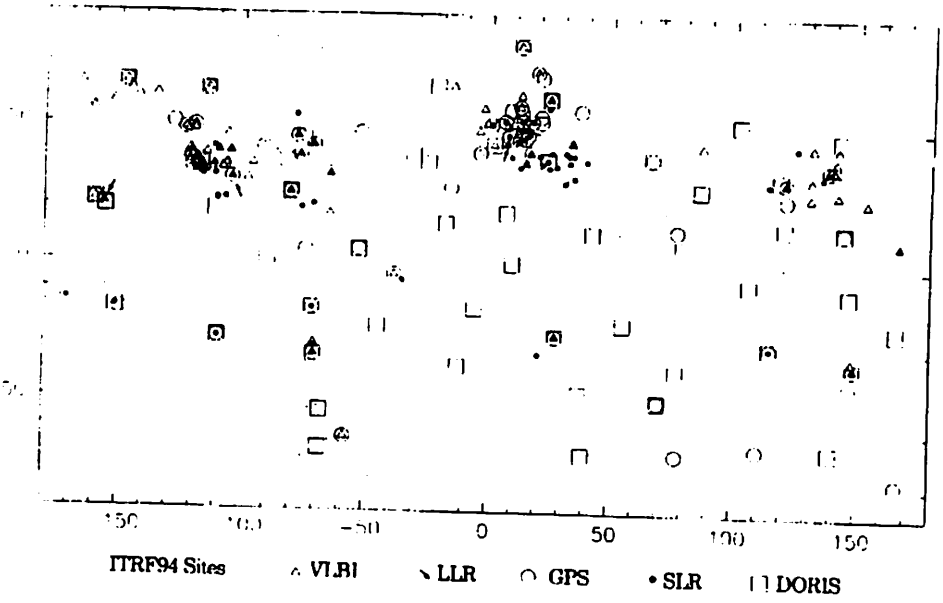

# TIGO: Spectrum of Observations and Equipment

Space techniques:

- VLBI = Very Long Baseline Interferometry,
- SLR = Satellite Laser Ranging,
- GPS = Global Positioning System.

In-situ observations:

- gravity,
- seismic,
- meteorology,
- time and frequency,
- supplementary terrestrial measurements.

Additional devices:

- central control computer,
- WAN/LAN, communication,
- power system (solar, generators).

For transportation and housing:

- 6 standard seacontainers (40 feet),
- platform and monumentation.



# TIGO: VLBI-Module Specifications

- Mk IV data acquisition terminal,
- Mk IV PC field system,
- standard geodetic cryogenic dualband S/X receiver,
- Antenna parameters:

| | |
|---|---|
| diameter, type | 6 m, offset-primary focus |
| f/D | 0.3629 |
| surface accuracy | 0.4 mm |
| azimuth velocity | 6 deg/s |
| elevation velocity | 3 deg/s |

- Receiver parameters:

| Band | Frequencies | Efficiencies | noise temperature |
|---|---|---|---|
| S | 2.216 ... 2.350 GHz | $> 64\%$ | 53 K |
| X | 8.108 ... 9.036 GHz | $> 68\%$ | 50 K |

# TIGO: 6m-Offset-Radiotelescope for VLBI

**Transportation and Various Elevations**

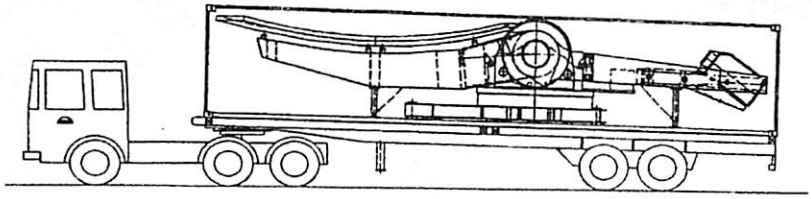

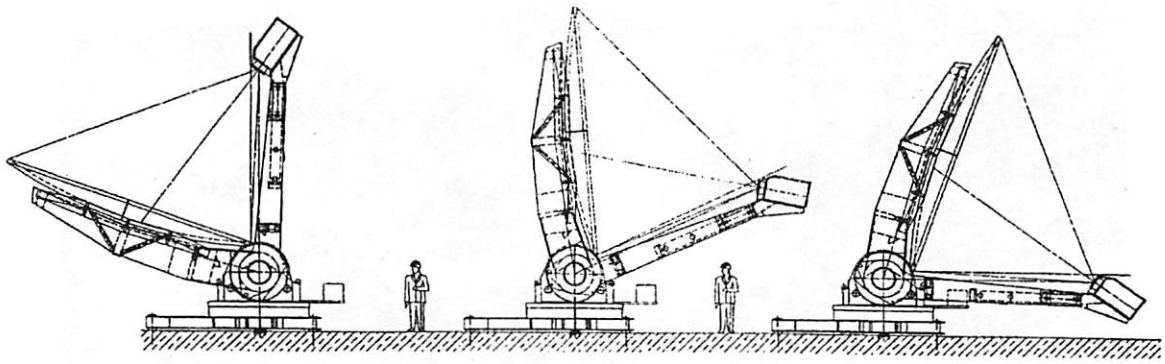



# TIGO: Setup of the Radiotelescope within 2 days

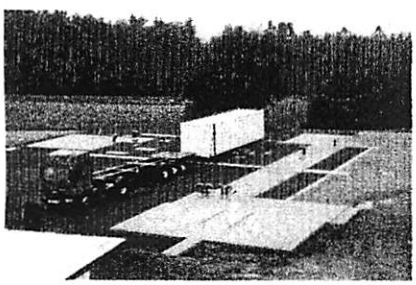

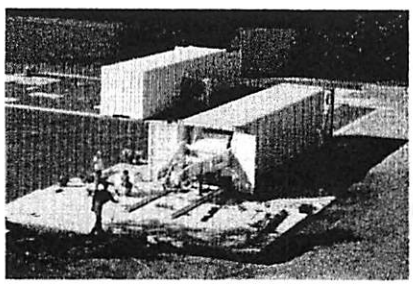

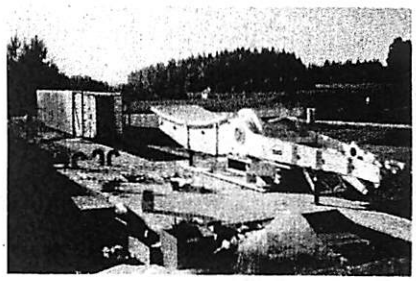

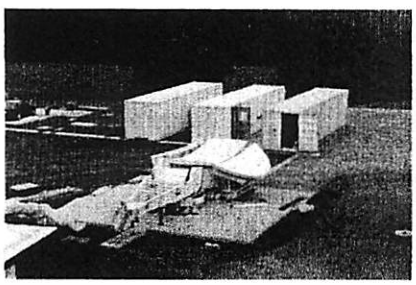

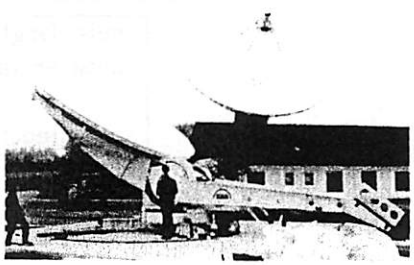

# TIGO: Operational Radiotelescope

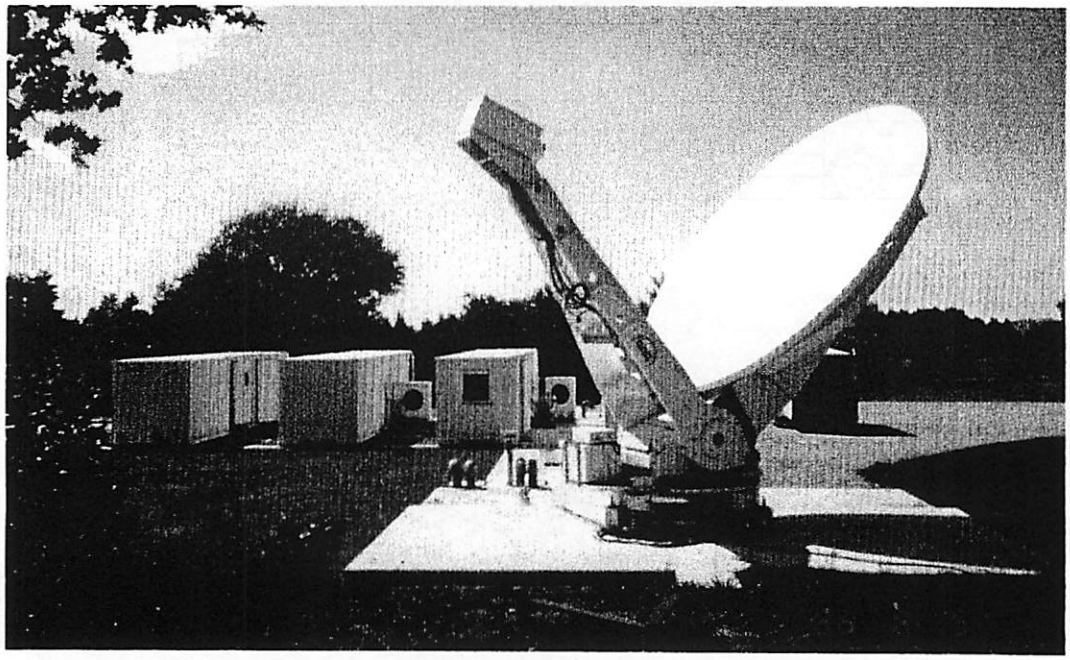



# TIGO: SLR-Module Specifications

- subcentimeter system,
- ranging up to 40.000 km,
- day and night capability,
- two colour system,
- high degree in automatisation,
- 50cm-telescope for transmit and receive,
- high efficiency in transmission,
- precise pointing,
- internal and external calibration,
- Titan Sapphire Laser:

| | |
|---|---|
| pulse length | 50 ps |
| pulse energy | $\leq$ 40 mJ at 424 nm wavelength |
| | $\leq$ 100 mJ at 847 nm wavelength |
| pulse repetition rate | 10 Hz |

- 3 detector ports (SPAD),
- Setup within 2 days.

# TIGO: SLR-Configuration

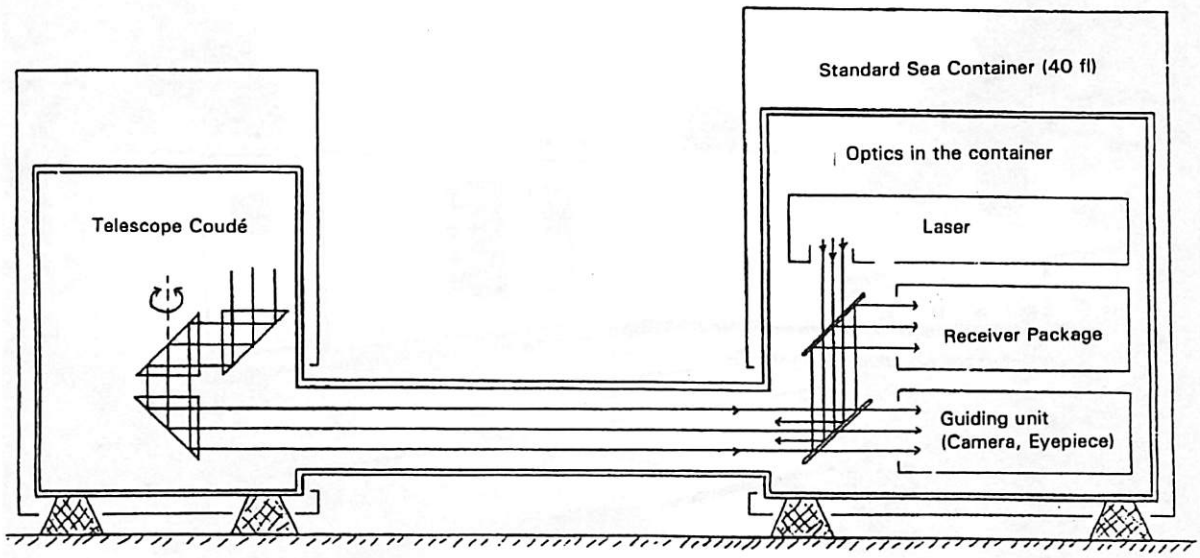




# TIGO: 50cm-Telescope for SLR

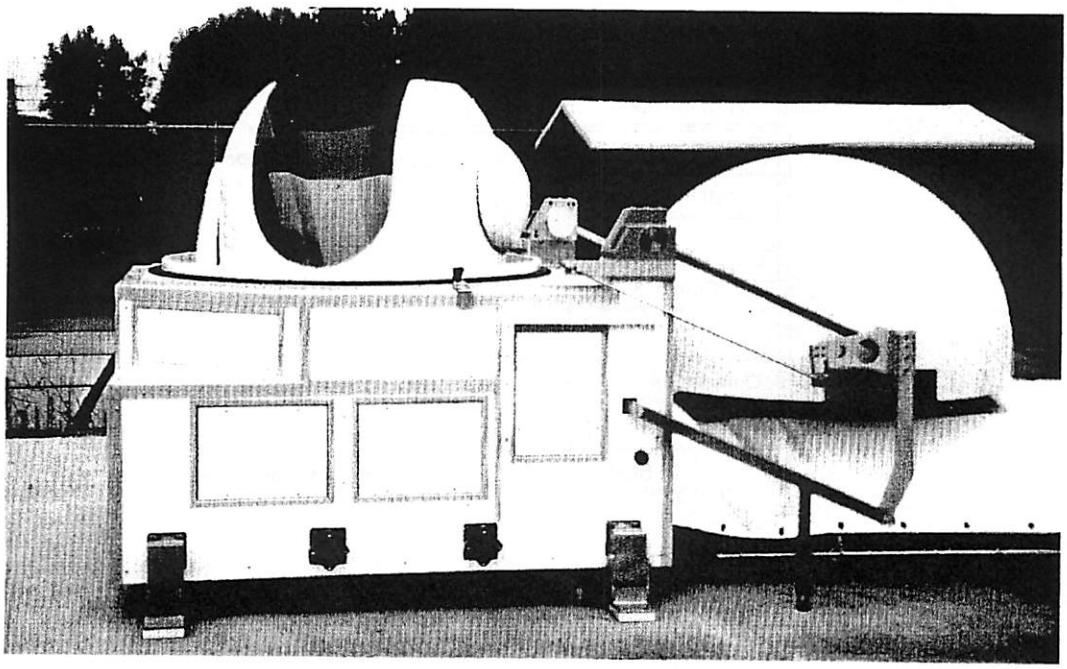

# TIGO: SLR-Module Operational at Platform

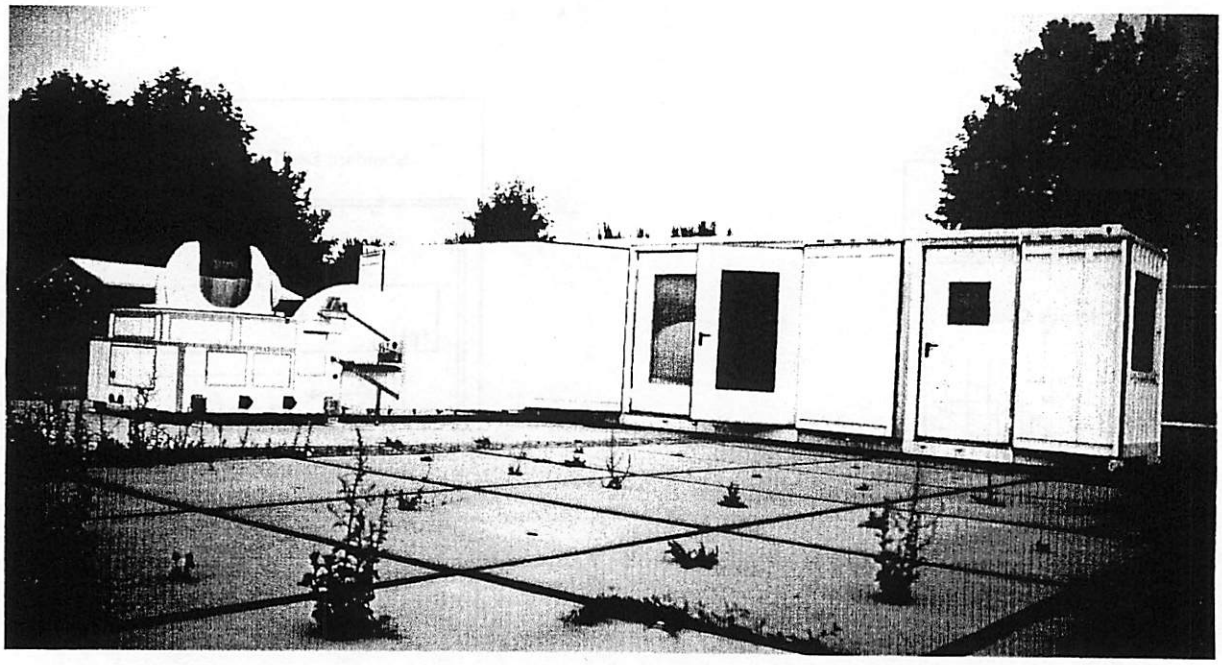



# TIGO: Platform and Monumentation

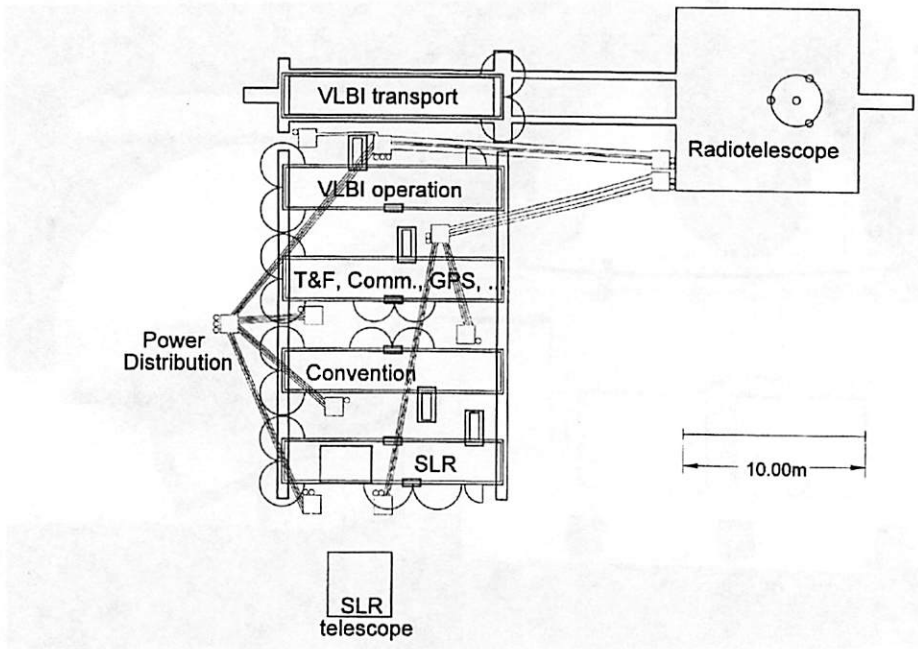

# TIGO: Overview

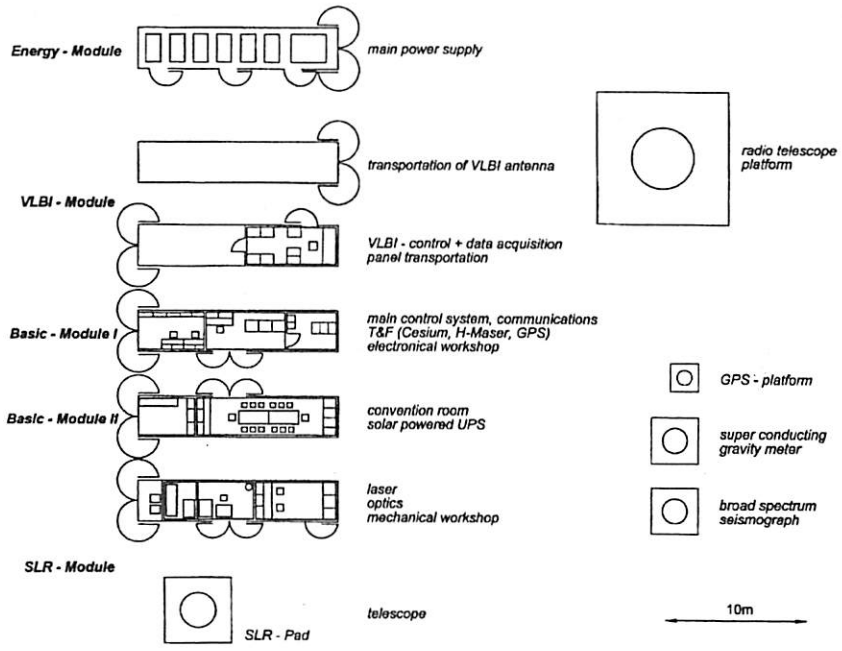




# TIGO at Wettzell during Summer 1997

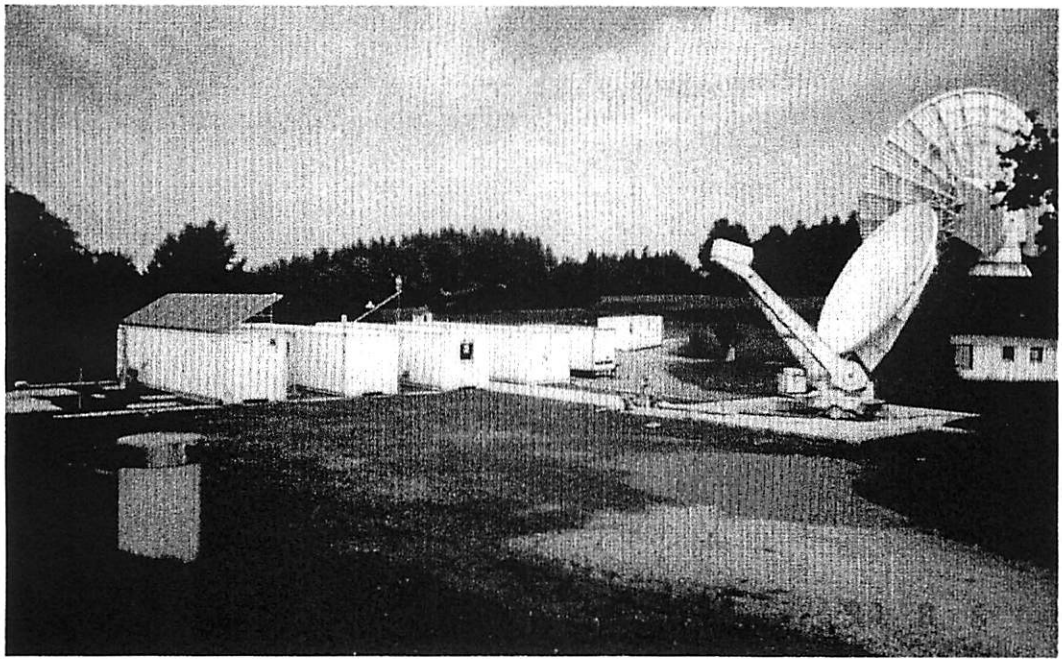

# TIGO: Schedule

| | | |
|---|---|---|
| 1992 | general design and request for offers | VLBI antenna |
| | first contracts | SLR-module |
| | | small size H-Maser |
| 1993 | detailed design | VLBI-module |
| | begin of manufacturing | SLR-module |
| 1994 | offers/contracts | VLBI receiver and Mk IV DAT |
| | | Titan Sapphire Laser |
| | | Containers |
| 1995 | setup the TIGO platform at Wettzell | |
| | delivery of | VLBI antenna |
| | | SLR module |
| | | H-Maser |
| | start of implementation of the systems | |
| 1996 | offers/contracts | GPS, time & frequency systems |
| | | central control computer, WAN, LAN |
| | | gravity meter, seismometer |
| | | energy module (solar, generators) |
| 1997-1998 | final integration and test period at Wettzell | |



# Cooperation with Host Agencies

| | |
|---|---|
| 1997/1998 | international agreements |
| | agreements between Bundesamt für Kartographie und Geodäsie and host agencies |
| 1999 | start of field campaigns |

Objectives:

- Optimal support for ITRF and geodynamic research.

Expected support for TIGO from host agencies:

- protected property to set up the TIGO system,
- facilities to provide power, water, communications,
- construction of the base platform,
- manpower to support the operation.

# Geodetic Very-Long-Baseline Interferometry at the Onsala Space Observatory 1996–1997

Gunnar Elgered and Ruediger Haas

Onsala Space Observatory, Department of Radio and Space Science, Chalmers University of Technology, SE–439 92 Onsala, Sweden

**Abstract.** We summarize the performed and planned geodesy VLBI activities at the Onsala Space Observatory for the period 1996–1997. A total of fourteen experiments were carried out during 1996 and another eighteen experiments are planned for 1997. We discuss the installation of a new hydrogen maser. A new S- and X-band feed for dual polarizations is being developed for the 20 m telescope and we report about the progress of the implementation of this system. A measurement system for monitoring of the height of the concrete foundation of the 20 m telescope has been in operation for one year. This first year of data shows that the foundation was approximately 3 mm higher in the summer compared to the winter. All observed variations larger than 0.1 mm can be explained by a linear model based on the measured variations in the temperature of the concrete.

## 1 VLBI observations

The Onsala 20 m antenna participated in fourteen geodetic VLBI experiments during 1996. Six of these were in the European network; two were Global Terrestrial Reference Frame (GTRF) experiments; and six were a part of the "continuous" session during the autumn of 1996 (CONT–96).

In total eighteen experiments are planned for 1997; six are European; six are in the CORE–B network; and six are together with Medicina and the US Very-Long-Baseline Array (VLBA).

So far (October 1997) these experiments have been carried out according to the plan, but of course some problems have also occurred. For example, there was a jump in the formatter clock in the RDV04 experiment in July 1997; and during the CORE–B105 experiment in August 1997 many scans were lost due to problems with the Field System control of the vacuum motor.

## 2 Installation of a second H-maser

There are now two H-masers operating side-by-side at the observatory. The "old" maser, the Oscilloquartz EFOS–7, has been used since 1987. The more recent maser is the Kvartz CH1–75. It was purchased and delivered in March, 1997. The two masers are shown in Figure 1. The new maser has so far only been used in one VLBI experiment, namely the CORE–B105 on August 20–21, 1997. Diagnostic tests, including an evaluation of the stability, are ongoing.

## 3 The S- and X-band feed

The present S/X-feed system at Onsala consists of separate feed horns for the two frequency bands. A tertiary reflector with a dichroic surface is used for the S-band. The dichroic surface is flat which reduces the efficiency at S-band. It also has some transmission loss at X-band.

The planned new feed system consists of two feed reflectors, used by both the S- and the X-band. The principle of such a feed system is shown in Figure 2; and the main features of the dual-frequency feed horn are shown in Figure 3. The horn has been manufactured and its radiation patterns have been measured. The results of the test measurements are encouraging. The other components of the new system are partly produced and the characteristics will be measured and compared

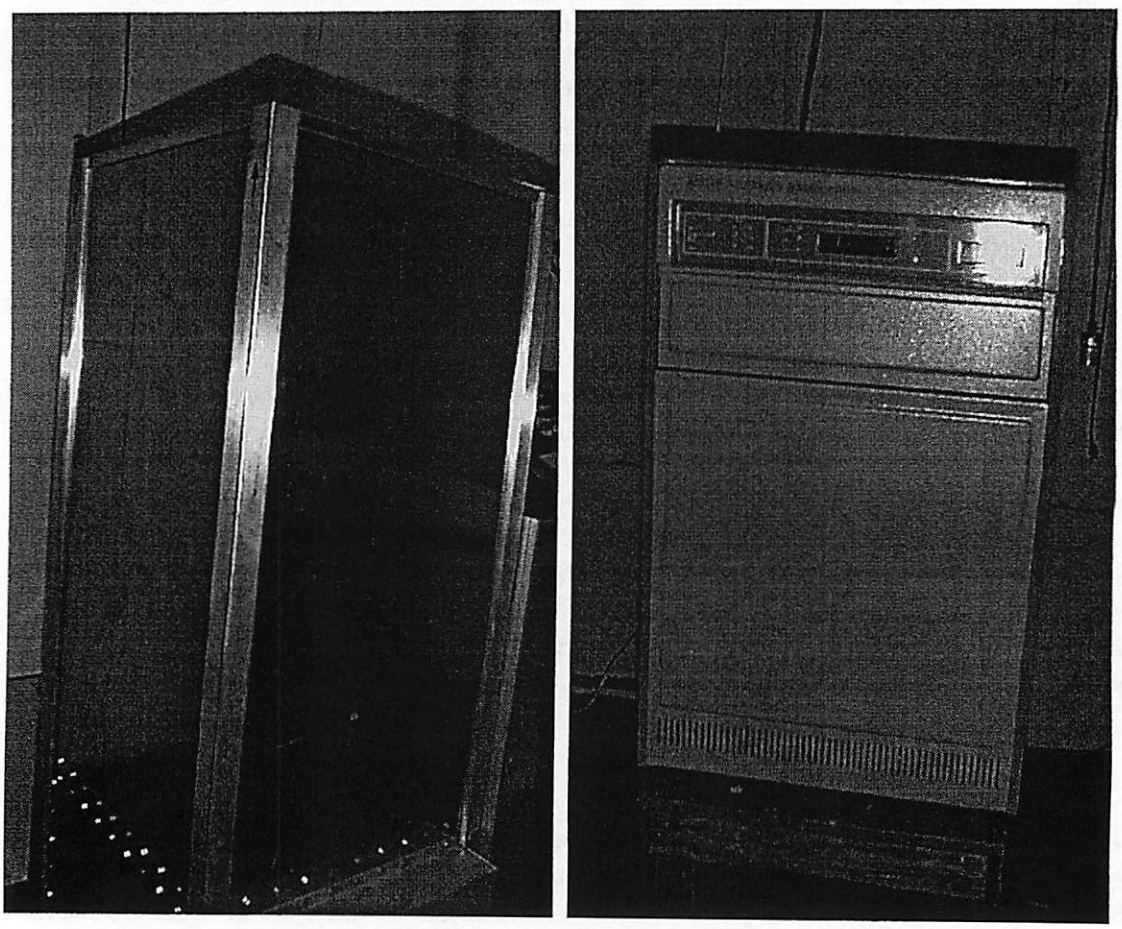

Figure 1: The two masers operating at the Onsala site. To the left the Oscilloquartz maser EFOS–7; and to the right the new Kvartz CH1–75.

to the simulated performance, e.g., the coaxial wave transformer for the S-band, and the two septum polarizers (one for each frequency band). More details of the new feed system can be found in *Elgered et al.* [1997].

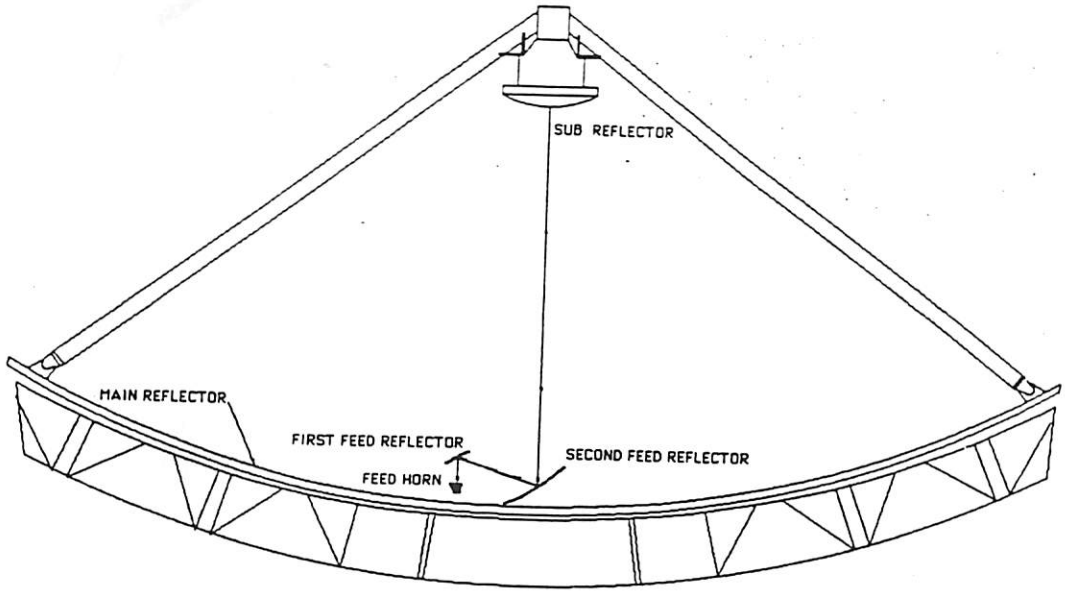


Figure 2: A sketch showing the possible feed arrangement. The two feed reflectors are removable. The mm-wave feed array is located in the antenna cabin below the second feed reflector.

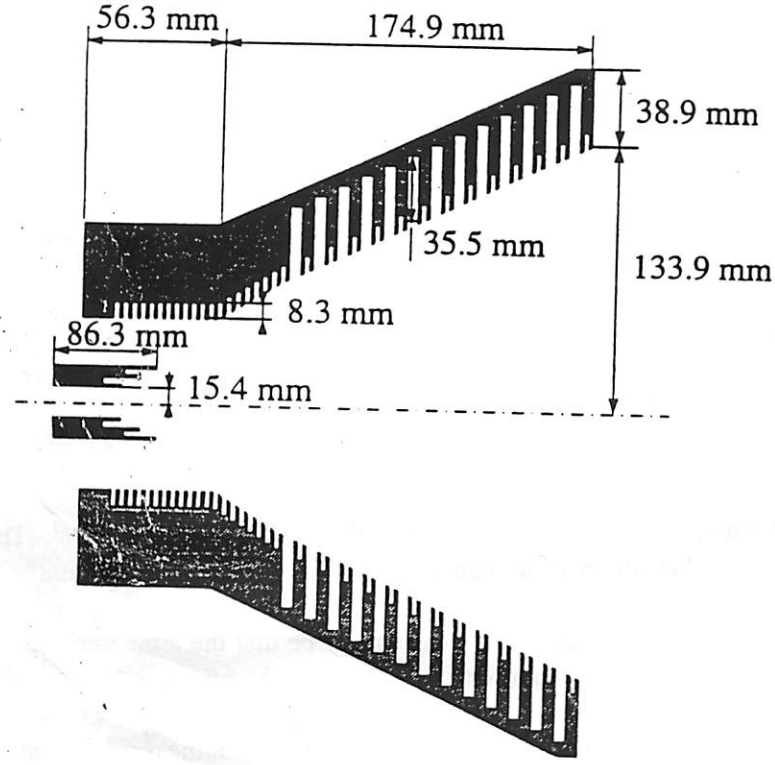


Figure 3: The cross section of the dual-frequency corrugated horn.

# 4 Mark-IV upgrade

The upgrade to the Mark-IV system has been completed. The tape recorder upgrade and the Mark-IV formatter were installed in November–December 1996. Hardware and software, allowing quick switching between thin and thick tape recording, were installed in August 1997. The first experiment using thin tape recording was the RDV05 on September 8, 1997.

The Field System (FS) software was first used with the LINUX operating system in February 1996 (version 9.0.8). Several updates of the FS have been made since then and presently the version 9.3.15 is running at Onsala.

# 5 Measurements of the stability of the antenna tower

A data acquisition system for monitoring of the temperature and the vertical motion of the concrete tower of the 20-m antenna was described at last year's meeting [*Elgered*, 1996].

Figure 4 presents a summary of the data acquired so far, from October 1, 1996 to September 30, 1997. The estimates of the height variations in Figure 4 are corrected for the modelled expansion of the invar rod estimated by measuring the temperature at the mid point and using the theoretical temperature coefficient of invar, $1.5 \cdot 10^{-6}$ (° C)$^{-1}$.

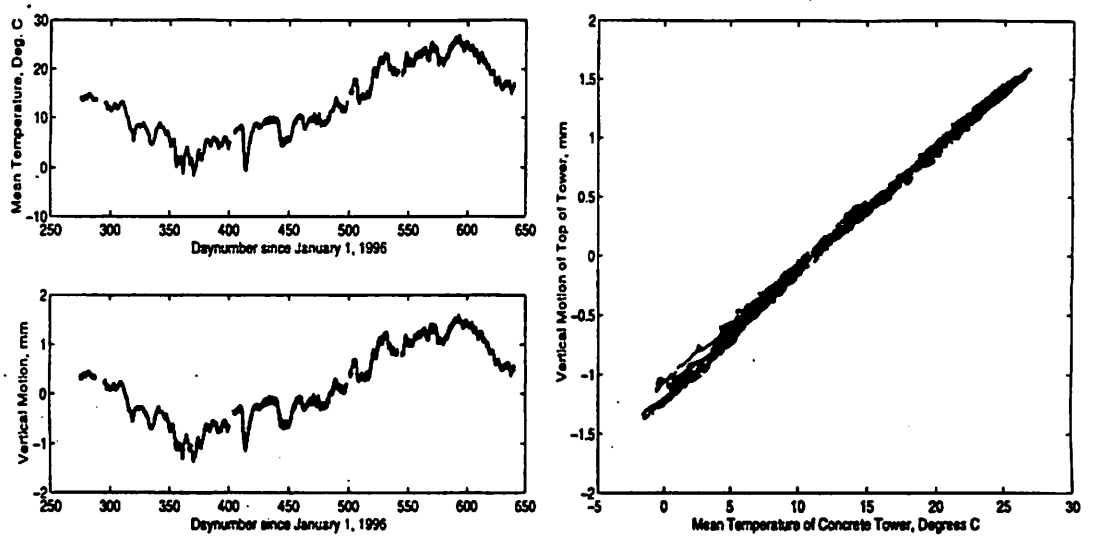


Figure 4: The first year's data from measurements of the temperature and the vertical motion of the concrete tower of the 20 m antenna. The time series to the left show the mean concrete temperature (upper plot to the left) and the vertical motion (lower plot to the left). The strong correlation is obvious from the time series but especially when the motion is plotted versus the observed mean temperature (to the right).

A least squares fit of the data in Figure 4 gives a height change of 0.10 mm(° C)$^{-1}$. This is slightly less than the expected value for an 11 m high concrete tower, which is 0.13 mm(° C)$^{-1}$. This is consistent with the results presented for the initial measurements made during the summer of 1996. A possible explanation for the disagreement can simply be that the temperature sensors are not located correctly in order to yield a representative mean for the effective temperature of the concrete. For example, there are no sensors located close to the ground where the temperature variations may be significantly smaller. It is, however, important to note that the rms residual about the estimated straight line in Figure 4 is only 0.04 mm. This means that the unmodeled variations in the height of the concrete tower can be neglected for a model using the presently available concrete mean temperature.

We see in Figure 4 that the measured yearly variation (peak-to-peak) is approximately 3 mm corresponding to variations in the mean concrete temperature from $-2$ to $+27$ ° C.

## 6 Conclusions and future work

The recent technical improvements, the Mark-IV VLBI system, are now starting to be used and the improved sensitivity lays the ground for more observations per observing session which in turn makes it possible to further investigate systematic errors at the millimeter level. An additional improvement in sensitivity is expected when the new feed system is installed.

## References

Elgered, G., Geodetic very-long-baseline interferometry at the Onsala Space Observatory 1995–1996, *Proc. of the 11th Working Meeting on European VLBI for Geodesy and Astrometry, Research Report 177*, Ed. G. Elgered, Onsala Space Observatory, Chalmers University of Technology, 55–61, 1996.

Elgered, G, P.-S. Kildal, J. Flodin, B. Hansson, L. Pettersson, S. Raffaelli, J.Ó. Rubiños-López, and A. Tengs, A dual frequency feed system for the 20 m radio telescope at the Onsala Space Observatory, *Proc. Antenn–97*, 279–287, (available from: Försvarets Materielverk, SE–115 88 Stockholm), 1997.

# Ny-Ålesund Geodetic Observatory
# Station Report 1996-1997

Gunn Marit Hernes, Svein Rekkedal

Norwegian Mapping Authority
Geodetic Institute
N-3500 Hønefoss
NORWAY

*email: gunnm@gdiv.statkart.no, sveinr@gdiv.statkart.no*

## Abstract

**Since last annual report Ny-Ålesund Geodetic Observatory has continued to participate in international geodetic sessions. In addition the Observatory participated in two astrometry sessions. The MkIV has been completed, thin tape has been ordered via Arthur Niell, Haystack, and a fringe test is scheduled in mid September. The local control network around the VLBI-antenna has been determined with GPS as well as terrestric methods. In addition levelling of the network has been redone. An automated relative gravimeter has been running for a year. A GPS Rogue receiver runs in parallel with a GPS TurboRogue receiver to provide IGS data. The receivers will run in parallel for a year. PRARE has been running since late 1995 and a SAR - reflector was installed late 1996.**

## Ny-Ålesund participation in international geodetic sessions

Since the 11th working meeting in Onsala, Ny-Ålesund has participated in the following geodetic sessions:

### 1996

| | | | | | | |
|---|---|---|---|---|---|---|
| CONT96-GA | CRD96A | 02-SEP | 16:00 | Fb-Kk-G2-Ny-Wz | NASA | HAYS |
| NEOS-A175 | NA175 | 03-SEP | 18:00 | G2-Kk-Wz-Bz-Fb-Ny | USNO | WASH |
| CONT96-GB | CRD96B | 04-SEP | 20:00 | Fb-Kk-G2-Ny-Wz | NASA | HAYS |
| CONT96-GC | CRD96C | 05-SEP | 20:00 | Fb-Kk-G2-Ny-Wz | NASA | HAYS |
| CONT96-GD | CRD96D | 06-SEP | 20:00 | Fb-Kk-G2-Ny-Wz | NASA | HAYS |
| CONT96-GE | CRD96E | 16-SEP | 16:00 | Fb-Kk-G2-Ny-Wz | NASA | HAYS |
| NEOS-A177 | NA177 | 17-SEP | 18:00 | G2-Kk-Wz-Bz-Fb-Ny | USNO | WASH |
| CONT96-GF | CRD96F | 18-SEP | 20:00 | Fb-Kk-G2-Ny-Wz | NASA | HAYS |
| CONT96-GG | CRD96G | 19-SEP | 20:00 | Fb-Kk-G2-Ny-Wz | NASA | WASH |
| CONT96-GH | CRD96H | 20-SEP | 20:00 | Fb-Kk-G2-Ny-Wz | NASA | WASH |
| CONT96-GI | CRD96I | 30-SEP | 16:00 | Fb-Kk-G2-Ny-Wz | NASA | WASH |
| NEOS-A179 | NA179 | 01-OCT | 18:00 | G2-Kk-Wz-Bz-Fb-Ny | USNO | WASH |
| CONT96-GJ | CRD96J | 02-OCT | 20:00 | Fb-Kk-G2-Ny-Wz | NASA | WASH |
| CONT96-GK | CRD96K | 03-OCT | 20:00 | Fb-Kk-G2-Ny-Wz | NASA | WASH |
| CONT96-GL | CRD96L | 04-OCT | 20:00 | Fb-Kk-G2-Ny-Wz | NASA | WASH |
| CONT96-GM | CRD96M | 14-OCT | 16:00 | Fb-Kk-G2-Ny-Wz | NASA | WASH |
| CONT96-GN | CRD96N | 16-OCT | 20:00 | Fb-Kk-G2-Ny-Wz | NASA | WASH |
| CONT96-GO | CRD96O | 17-OCT | 20:00 | Fb-Kk-G2-Ny-Wz | NASA | WASH |
| CONT96-GP | CRD96P | 18-OCT | 20:00 | Fb-Kk-G2-Ny-Wz | NASA | WASH |
| NEOS-A182 | NA182 | 22-OCT | 18:00 | G2-Kk-Wz-Bz-Ag-Ny | USNO | WASH |
| EUROPE-5 | EUROP5 | 03-NOV | 14:10 | Wz-Ma-Os-Nt-Md-Mt-Cr-Ny-Yb | BONN | BONN |
| CONT96-GQ | CRD96Q | 04-NOV | 16:00 | Fb-Kk-G2-Ny-Wz | NASA | WASH |
| CONT96-GR | CRD96R | 06-NOV | 20:00 | Fb-Kk-G2-Ny-Wz | NASA | WASH |
| CONT96-GS | CRD96S | 07-NOV | 20:00 | Fb-Kk-G2-Ny-Wz | NASA | WASH |
| CONT96-GT | CRD96T | 08-NOV | 20:00 | Fb-Kk-G2-Ny-Wz | NASA | WASH |
| CONT96-GU | CRD96U | 11-NOV | 16:00 | Fb-Kk-G2-Ny-Wz | NASA | WASH |
| NEOS-A185 | NA185 | 12-NOV | 18:00 | G2-Kk-Wz-Bz-Fb-Ny | USNO | WASH |
| CONT96-GV | CRD96V | 13-NOV | 20:00 | Fb-Kk-G2-Ny-Wz | NASA | WASH |
| CONT96-GW | CRD96W | 14-NOV | 20:00 | Fb-Kk-G2-Ny-Wz | NASA | WASH |
| CONT96-GX | CRD96X | 15-NOV | 20:00 | Fb-Kk-G2-Ny-Wz | NASA | WASH |
| GOLDEN GLOBAL4 | GGLB04 | 21-NOV | 22:00 | Kk-G2-Ny-Hb-Ta-Sc-Wf-Bz-Wz-Fb | USNO | WASH |
| GLOBAL TRF-13 | RDGT13 | 25-NOV | 16:00 | Mk-Yb-Kp-Nl-Ny-Mt-Nt-Fb-Os-Ks | USNO | WASH |
| NEOS-A187 | NA187 | 26-NOV | 18:00 | G2-Kk-Wz-Bz-Ag-Ny | USNO | WASH |
| GOLDEN GLOBAL5 | GGLB05 | 02-DEC | 16:00 | Kk-G2-Ny-Hb-Ta-Sc-Wf-Bz-Wz-Fb | NASA | WASH |
| GEO-VLBA5 | RDGEO5 | 04-DEC | 20:00 | VLBFb-KK-G2-Os-Ny-Gf | NASA | VLBA |
| EUROPE-6 | EUROP6 | 05-DEC | 22:15 | Wz-Ma-Os-Nt-Md-Mt-Cr-Ny-Ef-Yb | BONN | BONN |
| NEOS-A189 | NA189 | 10-DEC | 18:00 | G2-Kk-Wz-Bz-Fb-Ny | USNO | WASH |
| GOLDEN GLOBAL6 | GGLB06 | 16-DEC | 14:00 | Kk-G2-Ny-Hb-Ta-Sc-Wf-Bz-Wz-Fb | USNO | WASH |

In addition we participated in two astrometry sessions:

| | | |
|---|---|---|
| ET3A | 01-NOV | 08:00 |
| ET3B | 02-NOV | 06:00 |

The FS-computer malfunctioned on several occations in late 1996. It has been replaced by a new computer with Field System built on a linux platform.

A failing power supply produced a noisy phase cal in Golden Global 4.

Another technical problem concerns Tsys-measurements. A burned relay in the monitor computer located in the receiver unit prevented the noise diodes to be turned on and off. Limited time between sessions and severe weather conditions in Ny-Aalesund prevented a fixing of the problem until summer 1997. Procedures were temporarily changed to get pointing results and SEFD-measurements, and the lack of Tsys did not influence the quality of the data produced.

**1997**

| | | | | | | |
|---|---|---|---|---|---|---|
| NEOS-A194 | NA194 | 14-JAN | 18:00 | Gn-Ft-Kk-Ny-Wz | USNO | WASH |
| CORE-B201 | CB201 | 22-JAN | 18:30 | Ft-Gc-Kk-Ka-Mc-Ny | NASA | HAYS |
| NEOS-A196 | NA196 | 28-JAN | 18:00 | Gn-Ft-Kk-Ny-Wz | USNO | WASH |
| CORE-B101 | CB101 | 03-FEB | 16:00 | Ap-Ft-Gc-Ka-On-Ny-Wz | NASA | HAYS |
| NEOS-A198 | NA198 | 11-FEB | 18:00 | Gn-Ft-Kk-Ny-Wz | USNO | WASH |
| NEOS-A200 | NA200 | 25-FEB | 18:00 | Gn-Ft-Kk-Ny-Wz | USNO | WASH |
| CORE-B302 | CB302 | 19-MAR | 18:30 | Gn-Ft-Gc-Kk-Nt-Yb-Ny | NASA | HAYS |
| NEOS-A204 | NA204 | 25-MAR | 18:00 | Gn-Ft-Kk-Ny-Wz | USNO | WASH |
| NEOS-A206 | NA206 | 08-APR | 18:00 | Gn-Ft-Kk-Ny-Wz | USNO | WASH |
| CORE-B102 | CB102 | 16-APR | 18:30 | Ap-Ft-Gc-Ka-On-Ny-Wz | NASA | HAYS |
| NAVEX-S13 | NAXS13 | 21-APR | 12:00 | Gn-Ap-Kk-Gc-On-Mc-Ny | USNO | WASH |
| NEOS-A208 | NA208 | 22-APR | 18:00 | Gn-Ft-Kk-Ny-Wz | USNO | WASH |
| NAVEX-S14 | NAXS14 | 28-APR | 12:00 | Gn-Ap-Kk-Gc-On-Nt-Ny | USNO | WASH |
| NEOS-A210 | NA210 | 06-MAY | 18:00 | Gn-Ft-Kk-Ny-Wz | USNO | WASH |
| CORE-B202 | CB202 | 14-MAY | 18:30 | Ft-Gc-Kk-Ka-Mc-Sm-Ny-45 | NASA | HAYS |
| NEOS-A212 | NA212 | 20-MAY | 18:00 | Gn-Ft-Kk-Ny-Wz | USNO | WASH |
| NEOS-A214 | NA214 | 03-JUN | 18:00 | Gn-Kk-Ny-Wz | USNO | WASH |
| EUROPE-3 | EUROP3 | 16-JUN | 14:00 | Wz-On-Mc-Ma-Yb-Nt-Sm-Ny | BONN | BONN |
| NEOS-A216 | NA216 | 17-JUN | 18:00 | Gn-Kk-Wz-Ny | USNO | WASH |
| NEOS-A218 | NA218 | 01-JUL | 18:00 | Gn-Kk-Ny-Wz-Ap | USNO | WASH |
| CORE-B203 | CB203 | 09-JUL | 18:30 | Gc-Kk-Ka-Mc-Sm-Ny | NASA | WASH |
| NEOS-A220 | NA220 | 15-JUL | 18:00 | Gn-Kk-Ny-Wz-Ap | USNO | WASH |
| NEOS-A222 | NA222 | 29-JUL | 18:00 | Gn-Kk-Ny-Wz-Ap | USNO | WASH |
| NEOS-A224 | NA224 | 12-AUG | 18:00 | Gn-Kk-Ny-Wz-Ap | USNO | WASH |
| CORE-B105 | CB105 | 20-AUG | 18:30 | Ap-Gc-Ka-On-Ny-Ur | NASA | WASH |
| EUROPE-4 | EUROP4 | 25-AUG | 14:00 | Wz-On-Mc-Ma-Yb-Nt-Sm-Ny | BONN | BONN |
| NEOS-A226 | NA226 | 26-AUG | 18:00 | Gn-Ap-Kk-Ny-Wz | USNO | WASH |
| NEOS-A228 | NA228 | 09-SEP | 18:00 | Gn-Ap-Kk-Ny-Wz | USNO | WASH |
| NEOS-A230 | NA230 | 23-SEP | 18:00 | Gn-Ap-Kk-Ny-Wz | USNO | WASH |

Dewer malfunction in the receiver lead to NEOS-A198 and NEOS-A200 beeing run with a warm receiver. Roger Allshouse, AlliedSignal Inc., visited for three weeks during which time the dewer and the noise diode problems were fixed and a general maintanance program was carried out. Late arrival of spare parts during this effort prevented us from participating in NEOS-A202 and EUROP2.

CORE-B104 was lost because of problems encountered with the formatter and the tape station during installation of MkIV read/write electronics.

## MkIV Upgrade

The new formatter from AlliedSignal Inc. was received in February -97. It was installed and tested together with the read/write electronics and though it seems as if the formatter still have some problems the correlator feed back on sessions run as a MkIII station is good.

The read/write electronics was delivered from Metsaehovi in March -96. Parts were mounted and installed by station personnel. The job was completed in July 1997.

A fringe test in MkIV mode was done with Fairbanks and Wettzell mid September. Preliminary report is OK.

The first MkIV mode session, VLBA6, is planned to take place on December 17.

Thin tapes have been ordered and are on the way to Ny-Ålesund. Ny-Ålesund will try to avoid vacuum switching if possible, and will switch to a thin tape only station from NEOS-A242 on December 16.

## The local control network

In Ny-Ålesund we have established eight pillars in the local area around the antenna. All of them are equipped with a central top screw for horizontal reference and an excentric levelling bolt for height reference. The pillars are approximately 1.3 m high to give comfortable workingheight when geodetic instruments are mounted to the pillar.

We have started to enlarge the control network to other geological structures. In the same peninsuela, but approximately 2 km away, we have fixed a control marker in the sesmic station (concrete building blasted into bedrock). Approx. 12 and 15 km. away, at Ny London and Observasjonsholmen the same kind of control markers are fixed directly to solid bedrock. Whereever possible, we try to select the site in such a way that it is possible to determine its position both with terrestric - as well as spacebased techniques (collocation).

The control network around the VLBI-antenna has been determined with GPS as well as terrestric methods this autumn. In addition levelling of the network has been redone.

## Maintenance and building activity

Through the whole summer a company has removed rust, redone welding on the gearboxes and painted the entire antenna white.

In the basement of the control building an electronic- and mechanical lab in addition to a mechanical workshop and a storage room are about to be established.

Two small appartments for station personell are built up close to the Observatory.

## Miscellaneous

IGS (International GPS Service for Geodynamics)
With the changeover to a 12 channel TurboRogue GPS receiver (replacing the old 8 channel Rogue), the new antenna is located in a new steel tower fixed to the solid bedrock, hopefully with less multipath. The two systems will work in paralell for a year to map systematic differences.

PRARE (Navigation system on ERS-2):
PRARE has been operating since late 1995. Due to the weather conditions in Ny-Ålesund we have experienced problems with the equipment. The system was down for several months because of broken coaxial cables.

Earthtide study
An automated relative gravimeter was installed in the University of Bergen seismic station in November 96. The first preliminary analysis is about to be completed.

ERS-2 SAR Interferometry
Together with Norwegian Defence Resarch Establishment, we have installed a SAR reflector near Kullhaugen. The reflector is used to produce reference signal in the SAR images covering Brøggerhalvøya and Oscar II Land. Goals for the study is to detect movement of glaciers and land uplift.

## Staff information

At present three persons work at the Observatory, one Station Manager and two operators. The Station Manager and one of the operators have electronic background, the other operator has mechanical background. In addition, one position in Hønefoss works full time in VLBI technology.

This year we have tried to establish a VLBI-operator group in Hønefoss. In the group there will be four persons and each of them are expected to work 3 months per year in Ny-Ålesund. We hope this will establish a good back-up for the staff in Ny-Ålesund.

# MPIfR BONN CORRELATOR REPORT

R.W. Porcas and W. Alef (MPIfR, Bonn) A. Müskens (University of Bonn)

September 1997

## 1 CORRELATOR HARDWARE

The correlators work reliably, with a low failure rate. Unfortunately, HP hardware support for the old (1982 !) control computer was cancelled from 1997. We are collecting old HP 1000F computers to use for spare parts - any offers ? We await eagerly the replacement MK4 correlator !

## 2 TAPE DRIVE STATUS

Of the 9 Metrum/Honeywell playback drives, 8 have been upgraded with MK4/VLBA style control electronics, and equipped for thick and thin tape playback (both high and low density). The 9th recorder is undergoing the upgrade, which should be completed by the end of 1997. Further upgrading to full MK4 capability must be synchronised with MK4 developments at Haystack Observatory.

In addition, a Penny and Giles playback drive is still operating, and brings to 10 the total number of drives. This helps to make efficient parallel use of the MK3 and MK3a correlators.

## 3 THIN TAPE

The correlation of thin tapes recorded at high density works well. The vacuum is switched between 15″ water (thick tape) and 5″ water (thin tape); this has been automated to avoid head damage being caused by playing thick tape at 5″ water. However, we expect mixed tape operation is likely to decrease the head life (normally ca. 1.5 years). To reduce wear we are atempting to lower the relative humidity at the head. We are experimenting by blowing on dry warm air from behind the drives. We are also testing playback using a new "triple cap" head on one drive.

The EVN and MPIfR purchased a batch of 232 thin tapes in 1996. Regrettably, due to a manufacturing defect, only about 25 % are useable. These have been re-spooled onto glass reels at MPIfR.

## 4 OPERATIONAL ISSUES

MPIfR has appointed a new tape librarian, and is training one new operator. Up to 40 % of correlator time is used by the geodesy community, for correlating EUROPE, IRIS, CORE-OHIG and XASIA observations.

→ Operations would be greatly helped if all geodesy
→ stations used the TRACK program to log tape shipments !

For astronomy experiments, the backlog of uncorrelated projects has now reached ca. 1 year, due to a mixture of over-scheduling and under-correlating. We expect (not for the first time !) that the load will soon be reduced, since much of EVN observing can now be done using VLBA-mode recording, which is correlated at the VLBA correlator in Socorro. This includes observations with the Japanese orbiting telescope, HALCA.

## 5 SOFTWARE DEVELOPMENT

We plan to transfer FRNGE and archiving to a unix machine within the next few months. There are two new AIPS tasks of interest to astronomers. M3TAR is equivalent to task MK3IN, but reads the tar archive from the correlator (instead of the SAVEM archive) to create an AIPS u-v data file. PHREF runs in special versions of AIPS. It allows one to "replace the MK3 correlator model" with the CALC8 model (i.e. residual phases are as if this had been used at correlation). This is important for phase-referenced observations.

# Correlation of the data of the Geodetic VLBI European Network

Mauro SORGENTE
*Geodetic Institute of the University of Bonn (GIUB), Germany*

## Abstract

*Six Geodetic VLBI campaigns with the European network have been conducted and correlated since the August'96. It will be shown the main problems found during the correlation of these campaigns.*
*I will also report some results of a comparison of the expected and observed SNR for each baseline.*

## Introduction

The European Network consists of eight core stations (Wettzell, Onsala, Madrid, Ny Alesund, Noto, Matera, Medicina and Yebes), plus two other stations that occasionally take part in the network (Effelsberg and Crimea).

The problems found during the correlation of the campaigns conducted since August'96 will be here discussed. Then it will be shown the results of a comparison between the expected and the observed SNR for the different baselines. Finally there will be a synthesis of the problems of the stations and at the end some conclusions.

The dates of the campaigns and the stations that took part to it are presented in the table 1.

| Experiment | date | Stations |
|---|---|---|
| Europe-4/96 | 09Sep96 | Wet-Ons-Mad-Not-Mat |
| Europe-5/96 | 03Nov96 | Wet-Ons-Mad-Not-Mat-Efl-Nya-Yeb |
| Europe-6/96 | 05Dec96 | Wet-Ons-Med-Mad-Not-Mat-Efl-Cri-Nya-Yeb |
| Europe-1/97 | 29Jan97 | Wet-Ons-Med-Mat-Yeb |
| Europe-2/97 | 17Mar97 | Wet-Ons-Med-Mat-Yeb |
| Europe-3/97 | 16Jun97 | Wet-Ons-Med-Not-Mat-Cri-Nya-Yeb |

**Table n.1: European campaigns in 96/97**

Since the Europe2-97, the campaigns had as many stations as possible in each session, as it was before the summer 1995.

# Stations' Problems

Crimea : The station should have had to participate to some campaigns since November'96, but due to different problems, it was possible successfully only in the Europe3-97. The main problem was that the fringe phase was scattered even if the SNR level was good.

Madrid : The phase calibration voltage was less than the acceptable threshold in the Europe4-96 for all the scans experiment and for some scans in the Europe5/6-96.

Effelsberg: There was a phase offset of about 100 degree at frequency 2267.99 in the both experiment in which it took part.

Matera : Interferences were found at frequency 2297.99 and frequency 2222.99 during the experiment Europe4-96, Europe2-97 and Europe3-97 in more than 70% of the scans. It was necessary to refringe all data without these two frequencies. This problem occurred also in other experiments in most of the scans at one of these frequencies and sometime at the other frequency.

Some interferences were found also at the frequency 2212.99, but it was quite sporadic so that it was not necessary to refringe the data without this frequency.

Until the Europe2-97 the phase of the phase calibrator was scattered on all the tracks in S and X.

Noto : Problems of phase-offset at freq 8420.99 and 8570.99 in all the experiments in which it took part. It was of about -60 and -130 degrees in the Europe4-96, Europe5-96, Europe6-96 and about 25 and -13 degrees in the Europe3-97. This was easily solved by making manual phase-offset on these frequencies.

In the Europe5-96 and Europe6-96 the data at frequency 2212.99 in all the reverse passes were not reproducible and it was necessary to refringe the data without this frequency. On the contrary in the Europe4/96 this problem occurred only in the last 2 hours and in the Europe3-97 it has affected only 10 scans.

Onsala : High parity errors level was found at frequency 8550.99 in all the experiments of 1996. All data had to be refringe with the increase of the acceptable error level threshold from 0.001 to 0.05. It was decided to use as normal threshold for parity errors the level 0.01 since Europe1-97. This does not degrade the quality of the output.

Yebes : Many problems, some repetitive and some occasional, were found in the experiments in which the station took part. Now I will describe them more detailly.

Europe5-96: The quality of the data was very poor because the receiver was uncooled (system temperature was more than 200K). Many scans were lost because the head positions were not set in the correct way and some tracks were overwritten. This happened more frequently during the recording of reverse passes, but not exclusively.

Many left scans at frequency 2222.99 were not reproduced sufficiently.

Europe6-96: The station reported a clock jump of about 6 sec at the scan 341-0443. The exact offset could not be recovered at the correlator and no fringe were found after this epoch.

Fringe phase residuals of unknown origin were present in 15 scans (QF=5-6-7).

Some scans had very low SNR.

Europe1-97: All the scans in forward passes yielded no fringe, the reason was unknown. Clock informations and data were found on the tape with an autocorrelation test.

No fringes were found at frequencies 8210.99, 8250.99, 8420.99, 8550.99, 2212.99, 2237.99, 2292.99 at all the reverse passes. The station reported that reverse passes were affected by a problem of FIFO 3 in the HC formatter.

All data in this experiment were rejected.

Europe2-97: The fringe amplitude at frequency 2237.99 was only 10% of the average level from scan 077-0024 to scan 077-1104. This problem happened also from scan 076-1450 to scan 076-1540. It may be due to a connection problem. All data were refringed without this frequency.

More than 30 scans had SNR lower than the minimum threshold and in about 10 scans no signal was detected.

Europe3-97: During the whole experiment more than 40 scans had no fringe amplitude at freq. 8210.99, 8250.99, 8420.99 8550.99. All data were refringed without these frequencies. It happened also the freq. 2212.99 2237.99 and 2292.99 but the problem was less serious. The station reported it could have been a problem at the formatter. After a test I discovered that there was a different offset of about 1 usec. between the data registered on the odd tracks and the even tracks. But it was not constant so I could not synchronise the tracks and recover all the data.

## SNR Expected and Observed

Average observed and predicted SNR for each baseline is presented in the table 2. The predicted values were derived from the values of the SEFD in Jansky of the antennas taken from the skedfile and compared with the real values obtained in the correlation.

**Values of SEFD in Jansky of the antennas**

| | |
|---|---|
| CRIMEA | X 3000 S 2000 |
| DSS65 | X 220 S 195 |
| EFFELSBERG | X 40 S 100 |
| MATERA | X 1500 S 850 [X 3000 S 5000 (europ4/5/6-96; europ1-97)] |
| MEDICINA | X 310 S 500 |
| NOTO | X 1000 S 900 [X 1725 S 1100 (europ4/5/6-96; europ1/2-97)] |
| NY ALESUND | X 900 S 1200 [X 1200 S 1200 (europ5-96)] |
| ONSALA | X 2450 S 3200 |
| WETTZELL | X 750 S 1115 |
| YEBES | X 3000 S 5000 |

Here are reported the values obtained for the campaigns Europe6-96 and Europe3-97.

| Baseline | X-Band prediction | SNR results | Obs/Pred% X | Chan X | S-Band prediction | SNR results | Obs/Pred% S | Chan S |
|---|---|---|---|---|---|---|---|---|
| 65-EB | 860 | 566 | 65.8 | 8 | 332 | 177 | 53.3 | 6 |
| 65-MC | 336 | 314 | 93.5 | 8 | 168 | 143 | 85.1 | 6 |
| 65-MA | 125 | 114 | 91.2 | 8 | 55 | 43 | 78.2 | 5 |
| 65-NT | 158 | 184 | 116.5 | 8 | 114 | 125 | 109.7 | 5 |
| 65-NY | 138 | 121 | 87.7 | 8 | 84 | 73 | 86.9 | 6 |
| 65-ON | 87 | 94 | 108.0 | 8 | 50 | 48 | 96.0 | 6 |
| 65-WZ | 197 | 152 | 77.2 | 8 | 100 | 86 | 86.0 | 6 |
| 65-YB | No Data | | | | | | | |
| EB-MC | 718 | 421 | 58.6 | 8 | 217 | 109 | 50.2 | 6 |
| EB-MA | 243 | 129 | 53.1 | 8 | 70 | 34 | 48.6 | 5 |
| EB-NT | 320 | 239 | 74.7 | 8 | 148 | 86 | 58.1 | 5 |
| EB-NY | 351 | 206 | 58.7 | 8 | 120 | 67 | 55.8 | 6 |
| EB-ON | 256 | 174 | 68.0 | 8 | 81 | 49 | 49.4 | 6 |
| EB-WZ | 494 | 294 | 59.5 | 8 | 145 | 98 | 67.6 | 6 |
| EB-YB | 200 | 100 | 50.0 | 8 | 90 | 34 | 37.7 | 6 |
| MC-MA | 99 | 76 | 76.7 | 8 | 36 | 26 | 72.2 | 5 |
| MC-NT | 132 | 137 | 103.8 | 8 | 77 | 76 | 98.7 | 5 |
| MC-NY | 134 | 104 | 77.6 | 8 | 58 | 48 | 82.8 | 6 |
| MC-ON | 91 | 83 | 91.2 | 8 | 38 | 33 | 86.8 | 6 |
| MC-WZ | 190 | 147 | 77.4 | 8 | 72 | 70 | 97.2 | 6 |
| MC-YB | 80 | 59 | 73.8 | 8 | 47 | 28 | 59.6 | 6 |
| MA-NT | 52 | 51 | 98.1 | 8 | 30 | 28 | 93.3 | 4 |
| MA-ON | 40 | 34 | 85.0 | 8 | 16 | 15 | 93.7 | 5 |
| MA-WZ | 67 | 44 | 65.7 | 8 | 24 | 20 | 83.3 | 5 |
| MA-YB | 31 | 19 | 61.3 | 8 | 19 | 11 | 57.9 | 5 |
| NT-NY | 60 | 64 | 106.7 | 8 | 44 | 47 | 106.8 | 5 |
| NT-ON | 46 | 55 | 125.0 | 8 | 31 | 35 | 112.9 | 5 |
| NT-WZ | 87 | 77 | 88.5 | 8 | 51 | 54 | 105.9 | 5 |

*Continuation on the next page ...*

*Continuation ...*

| Baseline | X-Band prediction | SNR results | Obs/Pred% X | Chan X | S-Band prediction | SNR results | Obs/Pred% S | Chan S |
|---|---|---|---|---|---|---|---|---|
| NT-YB | 38 | 31 | 81.6 | 8 | 37 | 24 | 64.9 | 5 |
| NY-ON | 60 | 56 | 93.3 | 8 | 28 | 27 | 96.4 | 6 |
| NY-WZ | 91 | 67 | 73.6 | 8 | 40 | 41 | 102.5 | 6 |
| NY-YB | 42 | 36 | 85.7 | 8 | 28 | 19 | 67.9 | 6 |
| ON-WZ | 65 | 57 | 87.7 | 8 | 27 | 31 | 114.8 | 6 |
| ON-YB | 32 | 28 | 87.5 | 8 | 22 | 14 | 63.6 | 6 |
| WZ-YB | 53 | 31 | 58.5 | 8 | 32 | 21 | 65.6 | 6 |

**Table n.2: Europe6-96**

| Baseline | X-Band prediction | SNR results | Obs/Pred% X | Chan X | S-Band prediction | SNR results | Obs/Pred% S | Chan S |
|---|---|---|---|---|---|---|---|---|
| SM-MA | 43 | 71 | 165.1 | 8 | 44 | 32 | 72.7 | 4 |
| SM-MC | 87 | 114 | 131.0 | 8 | 51 | 58 | 113.7 | 6 |
| SM-NT | 54 | 71 | 131.5 | 8 | 42 | 51 | 121.4 | 6 |
| SM-NY | 47 | 64 | 136.2 | 8 | 32 | 39 | 121.9 | 6 |
| SM-ON | 38 | 53 | 139.5 | 8 | 26 | 30 | 115.4 | 6 |
| SM-WZ | 54 | 75 | 138.9 | 8 | 34 | 46 | 135.3 | 6 |
| SM-YB | 27 | 28 | 103.7 | 4 | 27 | 18 | 66.7 | 6 |
| MA-MC | 117 | 112 | 95.7 | 8 | 75 | 39 | 52.0 | 4 |
| MA-NT | 78 | 72 | 92.3 | 8 | 65 | 37 | 56.9 | 4 |
| MA-NY | 62 | 58 | 93.5 | 8 | 47 | 27 | 57.4 | 4 |
| MA-ON | 47 | 46 | 97.9 | 8 | 33 | 19 | 57.6 | 4 |
| MA-WZ | 81 | 79 | 97.5 | 8 | 52 | 33 | 63.5 | 4 |
| MA-YB | 37 | 29 | 78.4 | 4 | 38 | 11 | 28.9 | 4 |
| MC-NT | 147 | 111 | 75.5 | 8 | 75 | 65 | 86.7 | 6 |
| MC-NY | 120 | 94 | 78.3 | 8 | 54 | 47 | 87.0 | 6 |
| MC-ON | 88 | 70 | 79.5 | 8 | 37 | 32 | 86.5 | 6 |
| MC-WZ | 159 | 131 | 82.4 | 8 | 62 | 63 | 101.2 | 6 |
| MC-YB | 66 | 43 | 65.2 | 4 | 41 | 20 | 48.8 | 6 |
| NT-NY | 74 | 54 | 73.0 | 8 | 45 | 40 | 88.9 | 6 |
| NT-ON | 55 | 42 | 76.4 | 8 | 30 | 27 | 90.0 | 6 |
| NT-WZ | 100 | 76 | 76.0 | 8 | 50 | 52 | 104.0 | 6 |
| NT-YB | 46 | 27 | 58.7 | 4 | 36 | 20 | 55.6 | 6 |
| NY-ON | 56 | 48 | 85.7 | 8 | 26 | 23 | 88.5 | 6 |
| NY-WZ | 84 | 68 | 81.0 | 8 | 38 | 39 | 102.6 | 6 |
| NY-YB | 38 | 26 | 68.4 | 4 | 26 | 15 | 57.7 | 6 |
| ON-WZ | 60 | 50 | 83.3 | 8 | 25 | 27 | 108.0 | 6 |
| ON-YB | 31 | 21 | 67.7 | 4 | 21 | 11 | 52.4 | 6 |
| WZ-YB | 46 | 31 | 67.4 | 4 | 28 | 17 | 60.7 | 6 |

**Table n.3: Europe3-97**

The observed average value of the SNR in the X-Band is generally good for all the stations except Effelsberg. Its observed value is only 60-70% of the expected one. However

it is nevertheless higher than the threshold (22). Sometime the values of the SNR for baselines with Yebes are lower than the average of the other baselines. The baselines with stations DSS65, Simeiz, Onsala and Wettzell have very good average values.

On the contrary the average observed levels in S-Band are in general lower than the predicted one. For the baselines with Matera or Yebes it brings a problem because there are some values lower than the acceptable threshold (15). For this reason there are scans with no signal detectable or even when the signal is detectable the fringe phase is not constant during the time of the scan. This gives results of poor quality. The observed average value for the baselines with Effelsberg in S-Band are only 50-60% of the expected one.

The values of the SEFD for Matera have been changed from the Europe2-97 because they got a new receiver. But it has to be said that the ratio of the observed over the predicted SNR is decreased in the S-Band from the 80% to the 50%, this means that perhaps the new receiver is not working as it was expected.

## Stations' problems Resuming

Crimea : The quality of the data of the Europe3-97 was quite good. The problem found was that some scans with high SNR showed an unstable fringe phase and there was more or less the same behaviour on all the channels. I tried to fringe the data using a constant value for the phase offset during the scan and using a phase offset estimated accumulation period by accumulation period. I found no differences.

Matera : Phase cal phase has a more regular behaviour in the last experiment than in the previous one.

It is still present the problem of the two frequencies in S- Band (2222.99; 2297.99) for which the fringe amplitude is mainly lower than 50% of the average. I noted that in the logfiles of Matera the "tsys2" of Video Converter corresponding to these two frequencies were in overflow in more than the 70% of the scans. With the data of the Europe3-97 I made a test and I tried to see if there was a correspondence between these two facts, but there was no direct correspondence. Then I tried to check if there were special azimuth or elevations where this problem was present or if there was a relation between the azimuth and the time, or between the elevations and the time, but also in these case I did not find any relation.

Yebes : The main problem is that the SNR collected on S-Band is still too low. As result the fringe phase is scattered in the scans that have lower SNR. The SNR collected on X-Band is sometime lower than the other stations even if not lower than the acceptable threshold. It has to be noted that the SEFD values for Yebes in the skedfile are already high (see the previous table).

Another problem founded in some scans was that the channels had different phase offset, but it appeared only in some scans. This could be resolved using the manual phase calibration but this would imply to alter the alignment of the fringe phase of the good scans. At the moment this problem does not appear very often, about 10 scans in each experiment, but however to be taken in consideration.

Effelsberg: The observed SNR is substantially lower than the predicted one on X and S Band and a phase offset at freq. 2267.99 S-Band was found in both the experiments I have correlated since August 1996.

Madrid : Phase cal ampl. sometime is lower than the expected threshold.

Noto : Phase offset found at frequencies 8420.99 and 8570.99 in all the last experiments. This problem was solved easily introducing a manual phase offset for both frequencies.

Medicina : No particular problem.

Ny Alesund: No particular problem.

Onsala : No particular problem.

Wettzell: No particular problem.

## Conclusions

I would like to point out that I also started to analyse the phase cal difference between the reference frequency and the other frequencies. I found generally good results for all the station. The phase calibration diferrences were flat lines that means that the receivers do not show internal problems due the collection of the signal. The only peculiar aspect I found was analysing the Crimea phase calibration difference for the channel 5,7,8, in X Band that showed a diurnal variation.

At the end I would like to say that also if there are still some problems that have to be solved, it is usually possible to correlate about the 99% of the total amount of the scheduled data.

# On the Effects of Missing Tracks

Axel Nothnagel, Geodetic Institute of the University of Bonn, Nussallee 17, D-53115 Bonn

E-mail: nothnagel@uni-bonn.de

## 1 Introduction

In recent VLBI sessions of the Europe series we suffered a considerable loss of data and, even more importantly, a loss of data quality from radio frequency interference (RFI), formatter failures, and data recording deficits. In this paper we try to summarize the basics of bandwidth synthesis with special emphasis on the effects of missing data channels. It should be understood that each channel scheduled to be observed is necessary for achieving the good data quality which we aim at. In this paper frequencies and bandwidths are used according to the current Mark III (narrow band) setup. All explanations apply to the wide band case (720 MHz and 125 MHz) in the same way.

The Signal-to-Noise-Ratio (SNR) of an interferometer, defined as the inverse of the standard deviation of fringe phase in radians, is given by

$$SNR = \eta \sqrt{\frac{A_1 A_2 2BT}{T_{s1} T_{s2}}} \cdot \frac{F}{2k} \tag{1}$$

where k = Boltzmann's Constant, F = correlated flux density of the source in units of watts per steradian of the emitting region per $m^2$ of antenna collecting area per Hertz of observing bandwidth, $T_{si}$ = system temperature at station i, $A_i$ = effective area of antenna i, B = total recorded bandwidth, T = total integration time (2BT is the total number of bits at the Nyquist rate), $\eta$ = loss factor to account for clipping and signal losses (Clark et al., 1985).

The accuracy of a group delay $\sigma_\tau$ determined from a cross-correlated stream of bits representing the coherent signal of a radio source received by two telescopes may be deduced from the SNR as

$$\sigma_\tau = \frac{1}{2\pi \; SNR \; \Delta f_{rms}} \tag{2}$$

with $\Delta f_{rms}$ = root-mean-squared spanned bandwidth or rms frequency deviation about the mean of the observing frequencies.

$$\Delta f_{rms} = \sqrt{\sum_{i=1}^{n} \frac{\omega_i^2}{n} - \left( \sum_{i=1}^{n} \frac{\omega_i}{n} \right)^2} \tag{3}$$

where $\omega_i$ are the individual center frequencies and n is the number of channels. Combining (1) and (2) leads to

$$\sigma_\tau = \frac{2k}{F} \cdot \sqrt{\frac{T_{s1} T_{s2}}{A_1 A_2 2BT}} \cdot \frac{1}{2\pi\eta\Delta f_{rms}} \tag{4}$$

Under the assumption that we cannot increase the effective aperture of the telescopes with economical costs and that the noise of the receivers is at their lower limits we may only use an increased recording bandwidth to improve the accuray of the delay determination.

## 2 The Single-Channel Case

In order to understand the basics of and the necessity for bandwidth synthesis we should first look at the single band delay determination. Consider that we have recorded a single channel of a certain bandwidth B with a rectangular bandpass. After cross-correlating two coherent signals of the same source the cross correlation function would become

$$R_{xy}(\tau) = 2\cos[\theta + \omega^0(\tau) + \pi B\tau]\frac{\sin \pi B\tau}{\pi B\tau} \tag{5}$$

with $\theta$ being the local oscillator phase difference, $\omega^0$ the local oscillator frequency and $\tau$ the group delay (Rogers, 1970).

The envelope function of this cross-correlation function has the form of a so-called sinc-function ((sin x)/x) which would be equivalent to a Fourier transform of the bandpass from the frequency domain into the lag domain. The sinc-function has a delay width of approximately

$$\Delta_\tau = \frac{1}{B} \tag{6}$$

with B being the bandwidth of the bandpass. The delay width is important since it determines, at least in part, the inherent accuracy of the delay determination, i.e the sharper the peak, the more accurate the determination of the location of the maximum on the $\tau$ axis (Fig. 1). From (6) and figure 1 it can easily be deduced that we could improve the delay accuracy just by increasing the bandwidth (e.g. Beyer, 1985). This, however, has its limitations since it requires coherence across the whole band and an enormous, ever increasing, recording capacity.

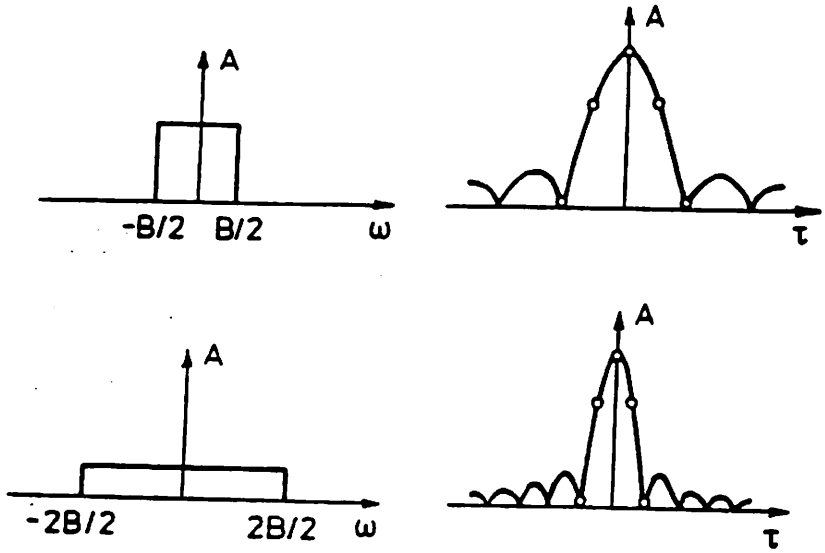


Fig. 1: Fourier transform from frequency domain into lag domain with bandwidth B and 2B (Beyer, 1985)

## 3 Bandwidth Synthesis

In order to improve the delay determination under economic restrictions Rogers (1970) "solved the problem in a rather ingenious way" - as Whitney (1974) wrote - by developing the bandwidth synthesis

method. Similar to antenna aperture synthesis where a number of small telescopes synthesise the aperture of a much larger telescope (e.g. VLA or Westerbork Synthesis Radio Telescope) a wide frequency band is sampled using a number of narrow bands, in the case of Mark III of 2 MHz bandwidth. This is achieved by placing two channels at the extreme frequencies defining the total spanned bandwidth, 360 MHz at X band and 85 MHz at S'band. In addition, a number of intermediate frequency channels are introduced in between according to a certain scheme which is discussed later. Using only these narrow bands the whole bandwidth (between the first and the last frequency) is synthesised and the accuracy of the delay determination is improved.

In order to describe the frequency band - time lag (delay) relationship Rogers (1970) defined a complex delay function for an ideal situation

$$D(\tau) = \int_0^\infty S_{xy}(\omega) e^{-i\omega\tau} e^{-i\omega^0\tau} \frac{d\omega}{2\pi} \tag{7}$$

with $S_{xy}(\omega)$ being the cross-spectral function, $\omega$ the radio frequency and $\omega_0$ the local oscillator frequency. The envelope or magnitude of this function is called the delay resolution function (DRF).

The delay resolution function of any synthesis frequency setup has an envelope which represents the Fourier transformed of the channel bandwidth similar to Fig. 1a with a main peak at 0 delay and first nulls at plus and minus 1/B. In the case of Mark III with 2 MHz channel bandwidths (Fig. 2) the envelope has a base width of about -500 nsec to +500 nsec (from $(2MHz)^{-1}$). Underneath this envelope there are distinguished peaks with sharp edges. The lower dashed line represents the level of the sidelobes if the total bandwidth would be synthesised perfectly.

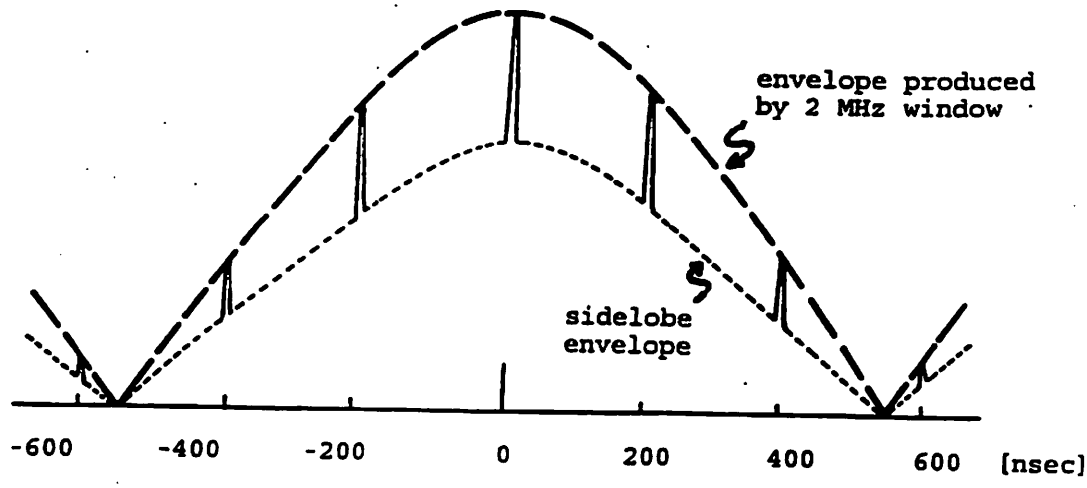


Fig. 2: Semi-complete delay resolution function with envelope of 2 MHz channel bandwidth with main lobe, ambiguous peaks and envelope of sidelobes.

Now, let's turn to the criteria of how and where to place the intermediate channels. If we would use only the two bands at the lower and upper edge of the current Mark III S band bandpass spanning about 85 MHz there would be peaks underneath the envelope every $(85MHz)^{-1}$ or about 12 nsec. This of course would be an ambiguity spacing too narrow to be solved in the analysis. One way to overcome this problem is the introduction of one or more frequency channels in between.

The basis for the selection of the band separations is the fact that the sharp peaks in figure 2 are spaced 1/S where S is the greatest common denominator of all n(n- 1)/2 frequency differences of n frequency bands used to synthesise the total bandwidth (currently 5 MHz at S band and 10 MHz at X band). 1/S is the so-called ambiguity spacing. If, for example, one introduces another band at $\omega_1$ + 5 MHz the smallest common denominator of all frequency differences would be 5 MHz. The resulting ambiguity spacing is then $(5MHz)^{-1}$ or 200 nsec as it is in the current Mark III standard S band setup. However, there is a large number of sidelobes within one ambiguity spacing almost as high as the main peak (Fig. 3).

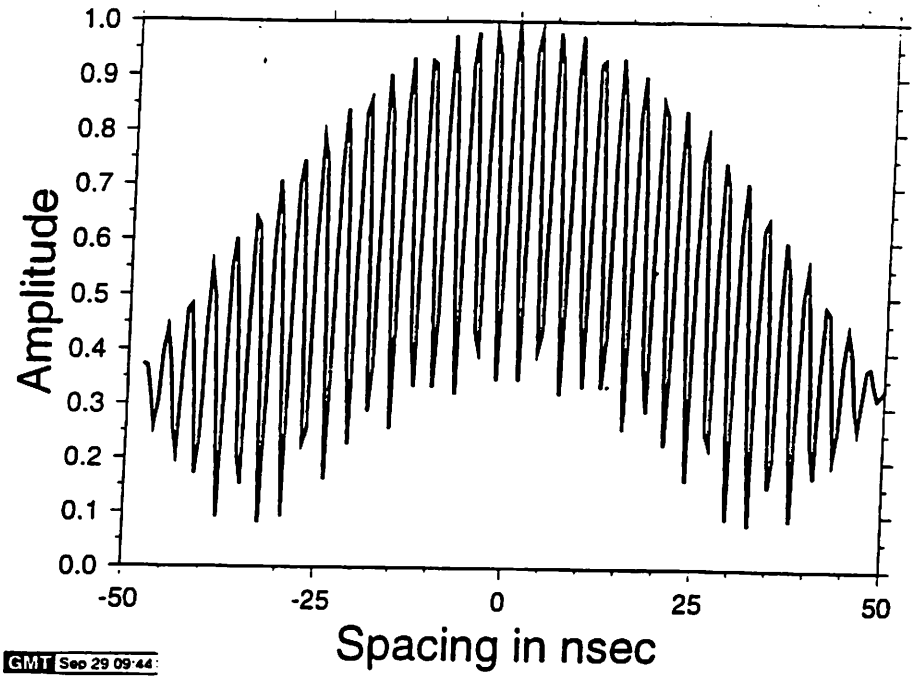


Fig. 3: Central part of the delay resolution function for a 0, 5, 85 MHz frequency setup. N.B.: This is only the portion between -100 and +100 nsec of figure 2.

If we consider that the delay resolution function represents the ideal situation it is quite understandable that the fringe fitting process which uses a "maximum likelyhood method" (Rogers, 1970) may select the wrong peak in the case of bandpass irregularities and/or a high noise level. Therefore, more frequency channels are introduced between the two bandpass edges which serve the purpose of reducing the level of the sidelobes to a level which is uncritical for the fringe fitting process. In addition, more channels increase the signal-to-noise-ratio (SNR) by providing more bits to be correlated and subsequently more reliable cross-correlation coefficients.

The frequency channel separation is selected for an optimal suppression of the sidelobes with an optimal ambiguity spacing. The initial selection of the channel separation was done using an algorithm which is based on the Golomb ruler theory (Taylor and Golomb, 1985). A Golomb ruler describes the separation of elements (e.g. frequency bands or antenna separation in an array) on the basis of non-redundant difference sequences, i.e. integer sequences which have the property that the difference of each pair of integers is distinct from the difference of each other pair (Robertson, 1991). However, in practice technical limitations like harmonic interference and limited bandwidth require a certain compromise. Therefore,

0, 1, 4, 10, 21, 29, 34, 36 times 10 MHz are used to span the 360 MHz bandwidth of Mark III X band observations and 0, 2, 5, 11, 16, 17 times 5 MHz synthesise 85 MHz of S band. The central parts of the resulting delay resolution functions within the limits of plus/minus one and a half ambiguity spacings are shown in figures 4 and 5. It is immediately obvious that with only 6 channels at S band the suppression of the sidelobes is less successful than with 8 channels at X band. In addition, more channels at X band produce a higher SNR according to formula (1).

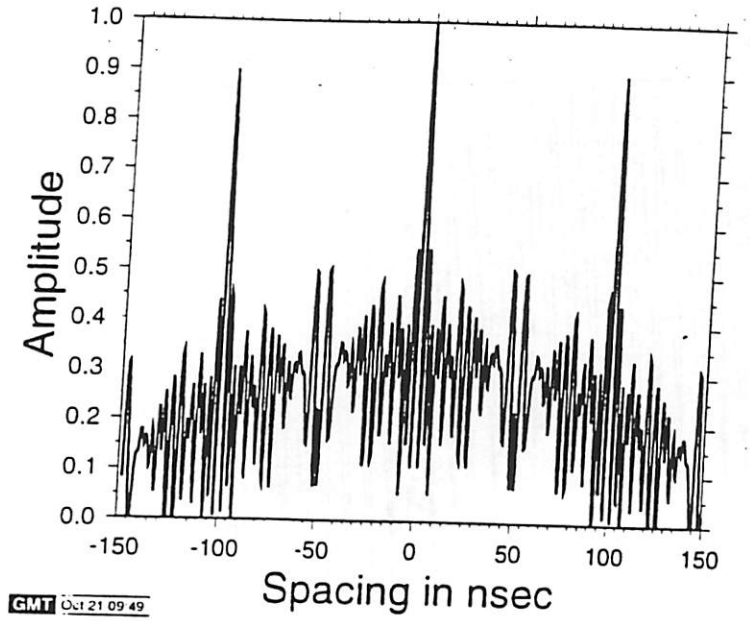


Fig. 4: Central part of delay resolution function with 8 channels at X band

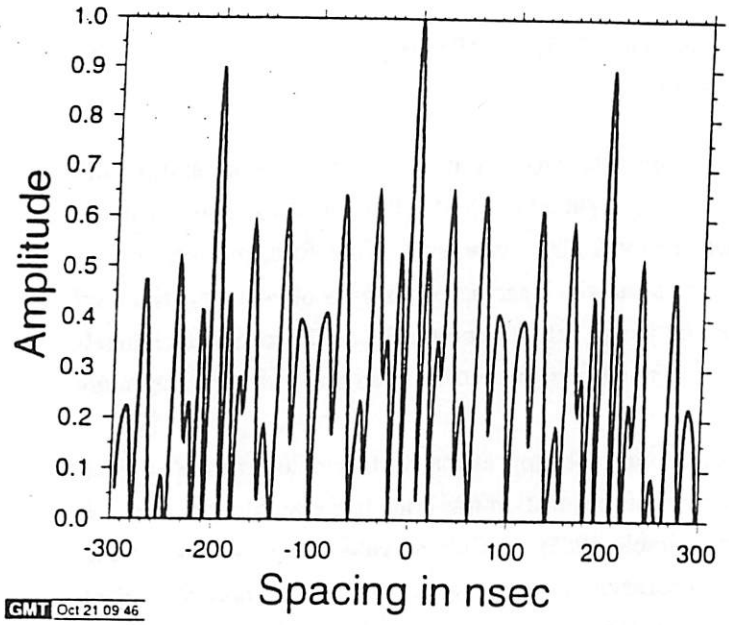


Fig. 5: Central part of delay resolution function with 6 channels at S band

# 4 Effects of Missing tracks

As we have seen in the previous section tracks are introduced in between the two extreme channels for an increase in SNR and for the suppression of sidelobes in the delay resolution function. Since each channel scheduled to be observed has its specific "purpose" the loss of a channel due to radio frequency interference, formatter failure, or recording deficits not only reduces the SNR by $1/\sqrt{(n-1)/n}$ but also distorts the delay resolution function. Figure 6 shows the central part DRF (just one ambiguity spacing of it) of the undisturbed (no RFI) Matera S band channels in the Europe-3/97 session (channels 2 and 6 are missing due to RFI). It is obvious that the sidelobes within the ambiguity spacing may easily be detected as the main lobe in case of low SNR or bandpass irregularities.

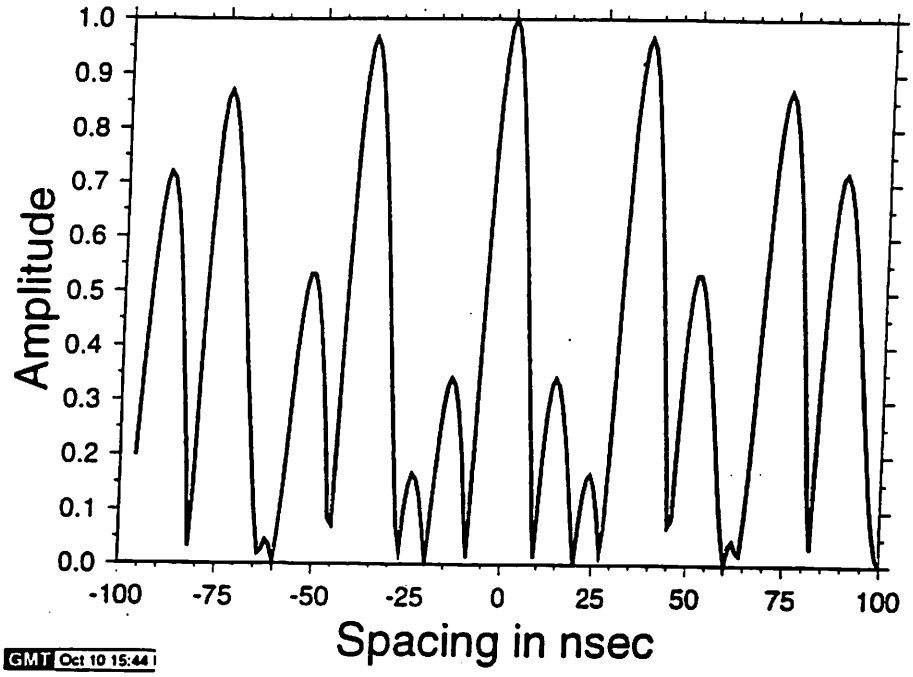


Fig. 6: Central part of Delay Resolution Function of Matera using only S band tracks 1, 3, 4, and 5

In the data analysis of the resulting group delays, for example with OCCAM or Calc/Solve, the deficit becomes even more obvious. Fig. 7 shows the delay residuals on the Matera - Yebes baseline where abnormally large deviations from the expected level of a few tens of picoseconds are easily discernable. The reason for this is that for a number of scans the fringe fitting process (FRNGE or fourfit) has indeed chosen the wrong peak generating pseudo- ambiguity levels of odd separations.

Generally, these observations have to be discarded since their separation from the main lobe may only be computed with low accuracy. However, the author has devised a routine which forces the fringe fitting process to home in on the correct peak. The procedure uses initial Solve delay residuals and converts them into FRNGE/fourfit multiband residual delays (correlator model residuals) and subsequently into search windows of about 10 nsec. With these search windows the fringe fitting process is repeated with a high success rate. However, all scans with missing tracks suffer from a reduced SNR which lead to reduced

data quality. Although this software is now available it should not become a routine requirement to use it.

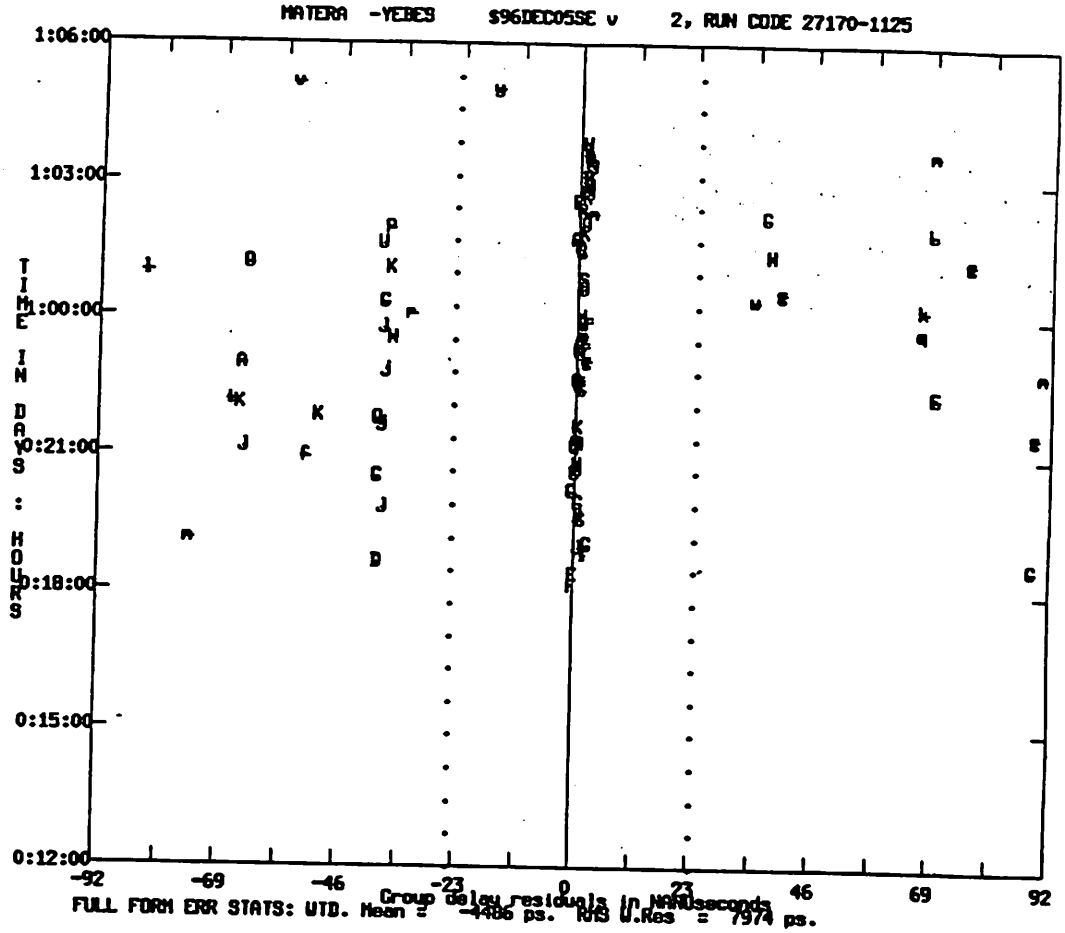


Fig. 7: Delay fit residuals on the baseline Matera - Yebes with pseudo-ambiguities caused by missing tracks

# 5 Conclusion

The ensemble of frequency channels in the geodetic VLBI Mark III setup serves the purpose of providing sufficient SNR and delay resolution with low sidelobes. Missing tracks reduce the SNR and require an iterative method to narrow the fringe fitting search window, a procedure which is rather laborious and non-routine. The staff at the observing stations and at the correlators should, therefore, take utmost care that all channels are recorded and processed properly.

# References

Beyer, W.; Laufzeitschätzung in digitalen Korrelationsinterferometern unter besonderer Betrachtung des MK-II-Systems des Max-Planck-Instituts für Radioastronomie; Mitteilungen aus den Geodätischen Instituten der Rheinischen-Friedrich-Wilhelms-Universität Bonn, No. 68; Bonn, 1985

Clark, T.A. et al.; Precision Geodesy Using the Mark III Very Long Baseline Interferometer System; IEEE Trans. on Geoscience and Remote Sensing, Vol. GE-23, No. 4, p. 438; July 1985

Robertson, D.S.; Geophysical Applications of Very Long Baseline Interferometry; Reviews of Modern Physics, 63, 4, p.899-918, 1991

Rogers, A.E.E; Very Long Baseline Interferometry with Large Effective Bandwidth; Radio Science, Vol. 5, p. 1239 - 1247; 1970.

Taylor, H., S.W. Golomb; Rulers, Part I: CSI Technical Report 85-05-01, Communication Science Institute, Univ. Southern California, Los Angeles, CA.; 1985

Whitney, A.R.; Precision Geodesy and Astrometry via Very Long Baseline Interferometry; PhD thesis, Massachusetts Institute of Technology, Cambridge, 1974

# Comparison of Space Geodetic Data Analysis Results at the CGS.

G.Bianco[1], R.Devoti[2], M.Fermi[2], C.Ferraro[3], R.Lanotte[3], V.Luceri[3], A.Nardi[2], R.Pacione[3], P.Rutigliano[3], C.Sciarretta[2] and F.Vespe[1]

1) Agenzia Spaziale Italiana, Centro di Geodesia Spaziale "G. Colombo", Matera, Italy
2) Nuova Telespazio SpA, Via Tiburtina 167, Rome, Italy
3) Nuova Telespazio SpA, Centro di Geodesia Spaziale "G. Colombo", Matera, Italy

**Abstract.** The space geodetic data analysis activities, in the fields of Global Positioning System (GPS), Satellite Laser Ranging (SLR) and Very Long Baseline Interferometry (VLBI), usually carried out at the Space Geodesy Center (CGS) of the Italian Space Agency (ASI) at Matera, make the comparison and combination of the results a natural objective. This work deals with the comparison of the analysis results, a step that we consider preliminary and necessary to the combination of the three techniques. VLBI results are used as reference for the comparison with a global SLR solution and a regional (European) GPS analysis. The kind of compared geodetic parameters depend on the particular solutions (global, regional) that we have computed: by comparing VLBI and SLR we try to assess the consistency of the solutions looking at the realization of the Terrestrial Reference Frame given by positions and velocities of the sites, while the comparison between VLBI and GPS has been performed looking at the time series of the baselines formed by sites hosting both the techniques.

## 1. Introduction

At the Space Geodesy Center (CGS) of the Italian Space Agency (ASI) are continuously acquired and analyzed data coming from the space geodetic techniques Global Positioning System (GPS), Satellite Laser Ranging (SLR) and Very Long Baseline Interferometry (VLBI).
The production of results from more than one technique make the following questions quite obvious: are the data analysis results comparable? Can we use more than one technique to improve our knowledge of physical phenomena?
This work regards the first item that we consider preliminary and necessary to the second one, although the comparison of the results of these independent techniques can be sometimes envisaged as a combination of the results themselves.
The starting point of this work are two VLBI solutions, a "global" (worldwide) and a "regional" (European) solution. The global VLBI solution is compared to a global SLR solution while the regional VLBI solution is compared to a regional GPS solution.
This kind of pairing comes from our choice of dealing with comparable levels of complexity in our starting solutions. For example both the SLR and VLBI global solutions solve for Earth orientation parameters (EOP) while the two VLBI and GPS regional solutions do not.
The kind of compared geodetic parameters depend on the particular solution. In the case of the global solutions the comparison is based on the consistency check of the two terrestrial reference frames (TRF), while for the two regional ones, it is based on the differences among the estimated baselines.

## 2. The SLR and VLBI global solutions

Table A summarizes the data statistics, the adopted models and strategies of the SLR and VLBI global solutions. The VLBI celestial reference frame is strictly linked to the quasar

positions while the SLR one is tied to the orbits of the two satellites: this difference could cause the presence of a scale factor between the two TRF. Moreover the *a-priori* TRF for the two solutions are different, namely the ITRF93 for SLR and ITRF94 [Boucher et al. 1996] for VLBI. The good quality levels of the solutions is guaranteed, in term of precision, by the tiny values of the WRMS of the post fit residuals: about 3 cm for the SLR and 41.2 ps for the VLBI.

| | VLBI | SLR |
|---|---|---|
| Software | • CALC/SOLVE | • GEODYNII/SOLVE |
| Data | • 1166 observing sessions from 1990 up to 1995.2 | • Jan. 86-Dec 95 (Lageos-I).<br>Nov. 92-Dec 95 (Lageos-II) |
| Celestial Reference Frame | • Value of nutation at January 2, 1990<br>• right ascension of the source 0420-014 at the value of the ICRF94<br>• IAU 1976 precession model | • Estimated LageosI and LageosII orbits<br>• DE200 Planetary Ephemerides<br>• IAU 1976 precession model<br>• IAU 1980 nutation model |
| Terrestrial Reference Frame | • Position of Westford fixed at the value of the ITRF94 and moved according to the NUVEL1A model<br>• Direction of the baseline Wettzell - Westford evolved according the NUVEL1A model, vertical rate at KAUAI fixed to zero<br>• EOP fixed at January 2, 1990 to the values of the IERS series 90C04 | • Position of Herstmonceux (lat, lon) and Washington (lat) fixed to the values predicted by ITRF93 model<br>• 3D velocity of Herstmonceux and Washington fixed to ITRF93 model. |
| Estimated Parameters | • Daily nutation adjustment<br>• Site positions at 1993.0 and velocities<br>• Source positions<br>• Daily EOP | • Satellite monthly state vectors<br>• Site positions at 1993.0 and velocities<br>• Daily EOP |
| Number of estimated parameters | • 1472 global and more than 259000 arc parameters | • more than 11000 parameters |
| Overall WRMS fit | • 41.2 ps with a reduced $\chi 2$ of 1.2 | • 0.0323 m |

**Table A:** Characteristics of the SLR and VLBI solutions.

More details for the SLR solution are in Bianco et al. 1996.
The comparison between the two solutions has been performed considering the realization of the TRF given by positions and velocities of the sites.

## 2.1 Comparison of the VLBI and SLR terrestrial reference frames

The comparison of the TRF is done by determining the rotation, translation and scale parameters that transform one system into the other. The 7 parameters are estimated in a least square sense using couples of co-located sites according to equation 1:

$$\mathbf{X}_{SLR} = (1 + d + \mathbf{R})\mathbf{X}_{VLBI} + \mathbf{T}. \qquad (1)$$

Co-located sites, even if not featuring simultaneous acquisitions, have been selected from the estimated site coordinates at 1993.0 of the two solutions and each couple has been translated to a common reference point by adding, to the estimated SLR position, the eccentricity vector (EV) to the VLBI site, known from local survey data. Before performing this operation, the

estimated SLR coordinates, in the ITRF93 frame, have been transformed into the corresponding ITRF94 value by means of the rototranslation and scale parameters provided by IERS.
The list of the co-located sites and the applied eccentricity vectors is in table b.

| Site code | | | Eccentricity vector (VLBI-SLR) | | |
|---|---|---|---|---|---|
| SLR | VLBI | | ΔX (m) | ΔY (m) | ΔZ (m) |
| 7834 | 7224 | Wettzell | 10.003 ± 0.003 | -46.149 ± 0.003 | 11.072 ± 0.003 |
| 7091 | 7205 | Haystack | -48.865 ± 0.001 | 12.264 ± 0.002 | 65.806 ± 0.002 |
| 7091 | 7209 | Westford | -247.002 ± 0.003 | -851.720 ± 0.004 | -800.428 ± 0.004 |
| 7105 | 7102 | Greenbelt | -33.112 ± 0.003 | -2.452 ± 0.003 | 4.398 ± 0.003 |
| 7295 | 7219 | Richmond | -60.877 ± 0.003 | 0.931 ± 0.002 | 44.212 ± 0.002 |
| 7080 | 7613 | Fort Davis | 6011.948 ± 0.004 | -3780.104 ± 0.010 | -4518.316 ± 0.007 |
| 7288 | 1513 | Goldstone | 5365.003 ± 0.025 | -8869.364 ± 0.025 | -7469.725 ± 0.025 |
| 7288 | 1515 | Goldstone | 2955.353 ± 0.011 | 4958.154 ± 0.011 | 8243.407 ± 0.011 |
| 7288 | 7222 | Goldstone | 323.113 ± 0.007 | -148.213 ± 0.013 | 43.993 ± 0.010 |
| 7853 | 7616 | Owens Valley | 1271.201 ± 0.011 | -772.872 ± 0.014 | -72.898 ± 0.014 |
| 7837 | 7227 | Shangai | -598.875 ± 0.010 | -469.603 ± 0.010 | 154.995 ± 0.010 |
| 7843 | 1545 | Canberra | -14458.353 ± 0.027 | 4638.716 ± 0.027 | 21870.004 ± 0.027 |
| 7210 | 1311 | Hawaii | -77839.511 ± 0.015 | 349863.795 ± 0.007 | 145626.295 ± 0.007 |
| 7939 | 7243 | Matera | -26.120 ± 0.007 | -67.073 ± 0.007 | 63.166 ± 0.007 |
| 7501 | 7232 | Hartebeesthoek | 41.652 ± 0.013 | -66.620 ± 0.014 | -8.187 ± 0.013 |
| 7543 | 7547 | Noto | 34.242 ± 0.003 | 67.907 ± 0.003 | -38.223 ± 0.003 |
| 7918 | 7108 | Greenbelt | 89.544 ± 0.004 | 111.625 ± 0.004 | 101.054 ± 0.004 |

**Table B:** List of the sites used for the 7 parameter transformation.

Those values have been taken from the paper of *Ray J.R. et al.* [1991] and from the IERS report on ITRF94. Different occupations for the same site have been considered separately. The variances associated to the eccentricity vectors, used in the analysis, are those from the local survey or propagated with a square law from the available values where necessary (namely, where the eccentricity value has been obtained by combining more than one value).
As it is known, the geographic coverage of the co-located sites is not completely satisfactory: there is a strong predominance of European and North American sites. For this reason also 'weakly' co-located sites (very extended eccentricity vector length), such as Orroral (7843) or moreover Hawaii (7210), have been analyzed.
Once the SLR estimates have been referred to the corresponding VLBI point, the residuals ($\underline{X}_{SLR} + \underline{EV} - \underline{X}_{VLBI}$) have been analyzed together with the associated variances (squared sum of the sigmas) in the 7-parameter transformation. The 7 parameters estimated from the 17 couples of co-located sites are listed in the first row of table c.
The computed values point out a global agreement in the realization of the static part of the terrestrial reference frame. In particular, it is worth to note that the scale factor from the two techniques appears substantially negligible, as previously shown by other similar analyses [Ray et al, 1991, Himwich et al, 1993]. The small value of this parameter, the only one involved in the comparison among baselines from different techniques and related to the dynamical modelling (e.g. GM), implies that the measurements of the same baseline of 1000km made by the two techniques differ for less than half a millimeter and implicitly confirms the goodness of the dynamic modelling used in the SLR data reduction. The highest difference in the parameters, already noted in the papers above, is found in the z-component.

| Rx (mas) | Ry (mas) | Rz (mas) | Scale factor (ppb) | Tx (mm) | Ty (mm) | Tz (mm) |
|---|---|---|---|---|---|---|
| 0.9±0.1 | -0.1±0.1 | 1.2±0.1 | -0.4±0.4 | -16±3 | 11±3 | 27±3 |
| estimates without Hawaii: | | | | | | |
| 1.2±0.1 | 1.0±0.2 | 1.4±0.1 | -1.2±0.4 | -37±4 | 12±3 | 45±4 |

**Table C:** Transformation parameters from VLBI to SLR solution.

The associated errors are formal 1-sigma. More realistic values could be obtained by rescaling the sigmas by the square root of the reduced $\chi^2$ (a factor of 2.7). Furthermore a sensitivity analysis has been performed by evaluating the variations obtained on the parameters while keeping out a site each time in the 7 parameter estimation. These variations are always within 3 unscaled sigmas with the only exception of the Hawaii site; its elimination from the estimation process, leads to the parameters listed in the second row of table c that, in the case of Ry, Tx and Tz, differ more than 3 formal sigmas from the previous values.

## 2.2 Comparison of the velocity fields under assumption of rigid plate

A synthetic comparison between the two solutions and their assessment to the NUVEL1A tectonic motion model may be attempted through the estimation of Eulerian poles for plates having a good (in terms of quantity and quality) coverage of sites. In our case this analysis can be done for Pacific, North America and Eurasia and allows to gather comparable information even in the case of not co-located sites.
The passage from cartesian velocities estimated for single sites to a plate Eulerian pole is modelled by the well-known equation: $\dot{\mathbf{X}} = \Omega \wedge \mathbf{X}$ that, handled in a least square sense, allows to relate the components of the $\dot{\mathbf{X}}$ velocity of each site to the components $(\Omega_1 \quad \Omega_2 \quad \Omega_3)^T$ of the rotation velocity of the underlying (if existing) plate.
The estimation of the Eulerian pole has been performed after a transformation from ITRF93 to ITRF93N for the SLR sites (to express SLR velocities in the NUVEL1A frame), by means of the rotation parameters derivatives as provided by IERS.
The results are summarized in table **D**.

| Pacific plate | SLR (7109. 7110. 7123. 7210. 7882. 7883) | VLBI (7241. 1311. 7298. 7617. 7251. 7223. 7310) | NUVEL1A |
|---|---|---|---|
| lat (deg) | -61 ± 1 | -63 ± 2 | -63 |
| lon (deg) | 95 ± 2 | 112 ± 17 | 107 |
| omega ($10^{-8}$ rad/yr) | 1.19 ± 0.02 | 1.11 ± 0.05 | 1.12 |

| North American plate | SLR (7046. 7080. 7091. 7109. 7112. 7122. 7295. 7918) | VLBI (7282. 7613. 7108. 7225. 7218. 7205. 7611. 7612. 7214. 7610. 7234. 7252. 7219. 7209. 7296. 7614. 7618. 1515) | NUVEL1A |
|---|---|---|---|
| lat (deg) | -2 ± 6 | 1 ± 3 | 2 |
| lon (deg) | -86 ± 3 | -86 ± 2 | -86 |
| omega ($10^{-8}$ rad/yr) | 0.36 ± 0.06 | 0.38 ± 0.02 | 0.36 |

| Eurasian plate | SLR (1181, 7236, 7545, 7550, 7805, 7810, 7835, 7839, 7834, 7837) | VLBI (7230, 7227, 7224, 7213, 7203, 1565) | NUVEL1A |
|---|---|---|---|
| lat (deg) | 57±1 | 56±5 | 51 |
| lon (deg) | -101±7 | -97±9 | -112 |
| omega ($10^{-8}$ rad/yr) | 0.47±0.02 | 0.44±0.03 | 0.41 |

**Table D**: Eulerian poles.

The errors associated to the estimates are formal 1-sigma errors scaled by the square root of the normalized $\chi^2$ of the fit, to take into account the good or bad fitting of the experimental values (cartesian velocities) to the assumption of rigid plate. The positions of the Eulerian poles reported in table **d** are shown in figure a.
The two geodetic solutions seem to bring globally the same tectonic information as the model. However, as we can see in figure a, the error ellipses associated to the VLBI estimates of the Eurasian and Pacific poles are larger than the SLR ones; this effect could be ascribed to the selection of the sites (those listed in the table) that has not been very strict, rejecting "pathological" cases only. A more accurate selection of the sites and a careful analysis of the residuals site by site should isolate specific further problems or justified discrepancies.
The refinement of this analysis goes beyond the scope of this work, whose aim is, above all, to establish a methodological procedure.

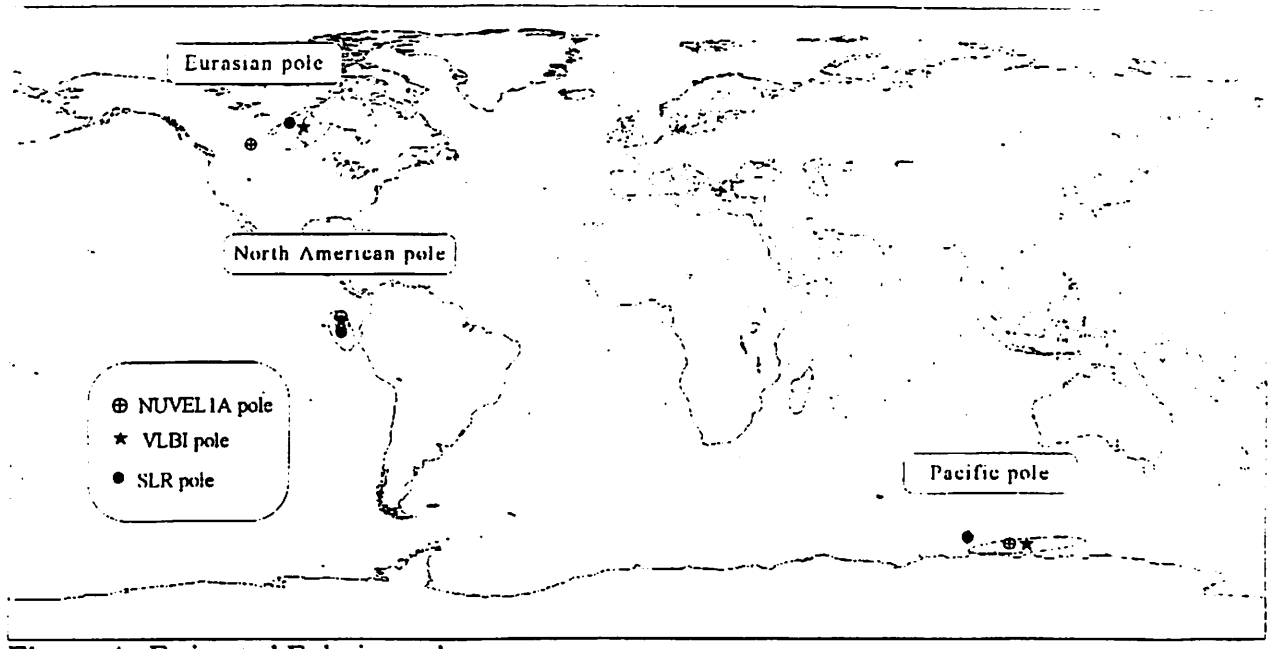


**Figure A:** Estimated Eulerian poles.

## 3. The GPS and VLBI regional solutions

The ASI/CGS participates to EUREF [Bruyninx et al. 1996] as local analysis center in the framework of the IGS pilot project for densification of the ITRF trough GPS regional analysis providing weekly solutions of the Italian GPS Fiducial Network (IGFN) [Bianco et al. 1993] from July 1996.

Table e summarizes the data statistics, the adopted models and strategies of the GPS and VLBI solutions.

The GPS solution is based on one year of daily station coordinate estimations. A fiducial approach is used: Matera coordinates and velocity are kept fixed to ITRF94 values, together with IGS final orbits and Earth rotation parameters. Double difference ambiguities, tropospheric scale factor and station coordinates are estimated. The VLBI solution [Lanotte et al. 1996] uses observing sessions from the EUROPE campaign. Wettzell coordinates have been fixed to the values of ITRF94 and its velocity modeled using the NUVEL1A. EOP and nutation time series are taken from the IERS series 90C04 [IERS 1993]. The two solutions have co-located sites (Madrid, Wettzell, Medicina, Matera and Noto) that allow to directly compare the geodetic estimated parameters. There is no temporal overlap between the GPS and the VLBI data span.

Since we are considering two regional solutions, a direct comparison of the TRF cannot have the same "global sense" as in the previous comparison between the SLR and VLBI worldwide solutions, however, interesting information could be derived by looking at the baselines time variations and velocity fields.

| | VLBI | GPS |
|---|---|---|
| Software | • CALC/SOLVE | • MicroCosm |
| Data | • 26 observing sessions from 1990 since 1995 (EUROPE campaign) | • Jul. 96-Aug 97 (data from IGFN, Wettzell and Madrid) |
| Celestial Reference Frame | • source coordinates from ICRF94<br>• EOP and nutation from the IERS series 90C04<br>• IAU 1976 precession model | • Satellite ephemerides and EOP from IGS final values<br>• DE200 planetary ephemerides<br>• IAU 1976 precession model<br>• IAU 1980 nutation model |
| Terrestrial Reference Frame | • Position of Wettzell at the value of the ITRF94 and moved according to the NUVEL1A model | • Position and velocity of Matera at the value of the ITRF94 |
| Geodetic Estimated Parameters | • Site positions and velocities | • Site positions |

**Table E:** Characteristics of the GPS and VLBI solutions.

### 3.1 Comparison of the VLBI and GPS baselines

The baseline length is independent from the transformation parameters, but not from the scale factor, then the baselines time series may show eventual site problems (for example environmental conditions for the GPS receivers), and weakness of analysis procedures. It is possible to make a comparison between the baseline time series, obtained from different techniques, only after reducing the coordinate values to common reference points. If the two techniques and their analysis procedures behave correctly, the two time series of the same baseline should be almost undistinguishable, as we have no reason to expect scale factor and its time derivative to affect baselines of the order of one thousand km, like the ones in our analysis, and not very rapidly varying for their plate position (Eurasia, Africa).
The estimated GPS site coordinates have been reported to the VLBI geodetic marker using the eccentricity vectors from ITRF94. A least square linear fit has been performed on the baselines to estimate a common rate for both VLBI and GPS and a different baseline value at an epoch for each technique.
Table f shows the estimated rates obtained using VLBI and GPS data separately, those using both data together and the differences between the two estimated values at an epoch.

| Baseline | VLBI rate (mm/yr) | GPS rate (mm/yr) | Combined rate (mm/yr) | GPS - VLBI offset (mm) |
|---|---|---|---|---|
| Madrid-Matera | 1.7 ± 1.0 | -15.3 ± 5.4 | -1.4 ± 2.2 | 13.9 ± 9.0 |
| Madrid-Medicina | 2.7 ± 0.7 | -11.7 ± 5.6 | 1.5 ± 1.6 | 2.4 ± 6.4 |
| Madrid-Noto | -0.6 ± 0.7 | -33.5 ± 5.6 | -4.6 ±2.1 | 13.6 ± 8.7 |
| Madrid-Wettzell | 0.2 ± 0.5 | -19.0 ± 5.5 | -1.0 ± 1.4 | 9.8 ± 5.5 |
| Matera-Medicina | -3.4 ± 0.5 | -11.4 ± 0.9 | -9.7 ± 0.8 | 34.2 ± 3.9 |
| Matera - Noto | 0.9 ± 0.9 | 2.2 ± 0.5 | 1.9 ± 0.4 | 0.4 ± 2.3 |
| Matera-Wettzell | -4.8 ± 0.8 | -3.8 ± 0.7 | -4.1 ± 0.6 | 12.9 ± 2.7 |
| Medicina-Noto | -4.6 ± 0.8 | -9.0 ± 1.1 | -7.2 ± 0.8 | 23.8 ± 4.0 |
| Medicina-Wettzell | -2.3 ± 0.6 | 1.0 ± 0.8 | -0.8 ± 0.5 | -0.6 ± 2.3 |
| Noto-Wettzell | -5.0 ± 1.0 | -2.8 ± 0.9 | -3.6 ± 0.7 | 12.1 ± 3.3 |

**Table F:** Comparison of the baseline rates.

Generally, the GPS results suffer the short data span covered in our analysis. In particular the GPS data used for Madrid cover the period from July up to December 1996 because after that

date the estimates of its position show dramatic worsening, probably due to the degradation of the acquired data. An example of baseline time series involving this station is in figure b.

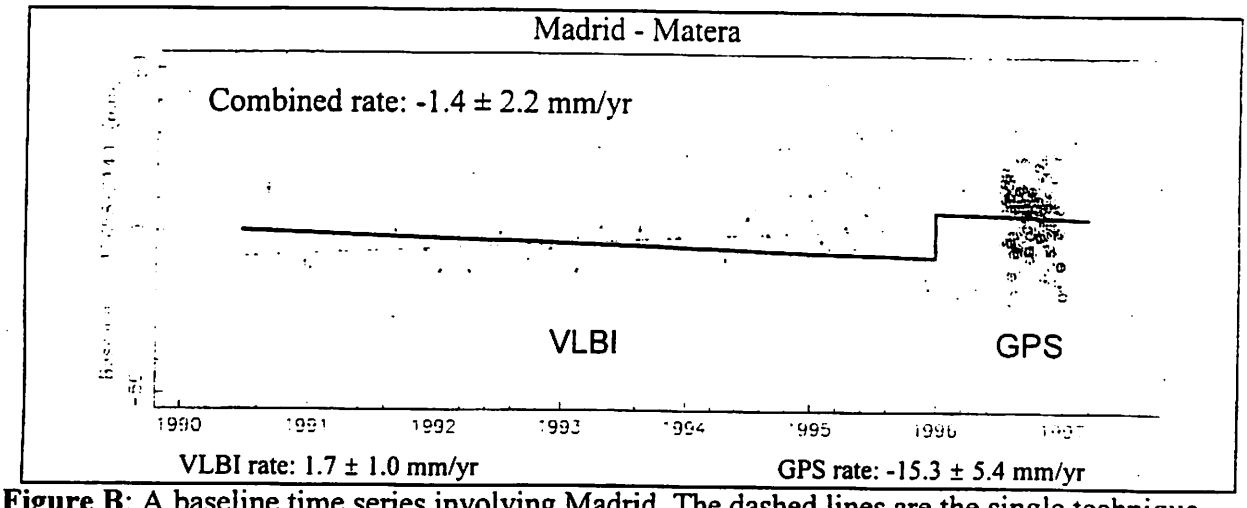


**Figure B**: A baseline time series involving Madrid. The dashed lines are the single technique data fit. The solid line is the combined fit. The jump on the solid line represents the offset in table **f**.

The assumption of linearity cannot be applied to the baselines time series with Medicina (figure c).

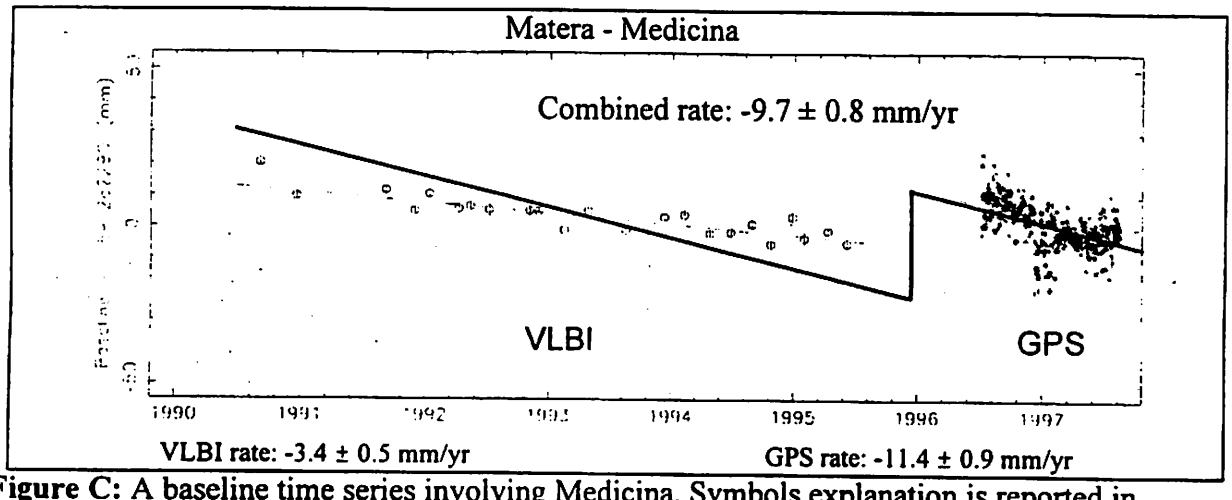


**Figure C:** A baseline time series involving Medicina. Symbols explanation is reported in figure **b**.

The time series of the baselines among Matera, Noto and Wettzell seem to be a good test case to compare the results but the short lapse of time covered by the GPS data dos not allow to draw any remarkable conclusion. These baselines are in figure d.

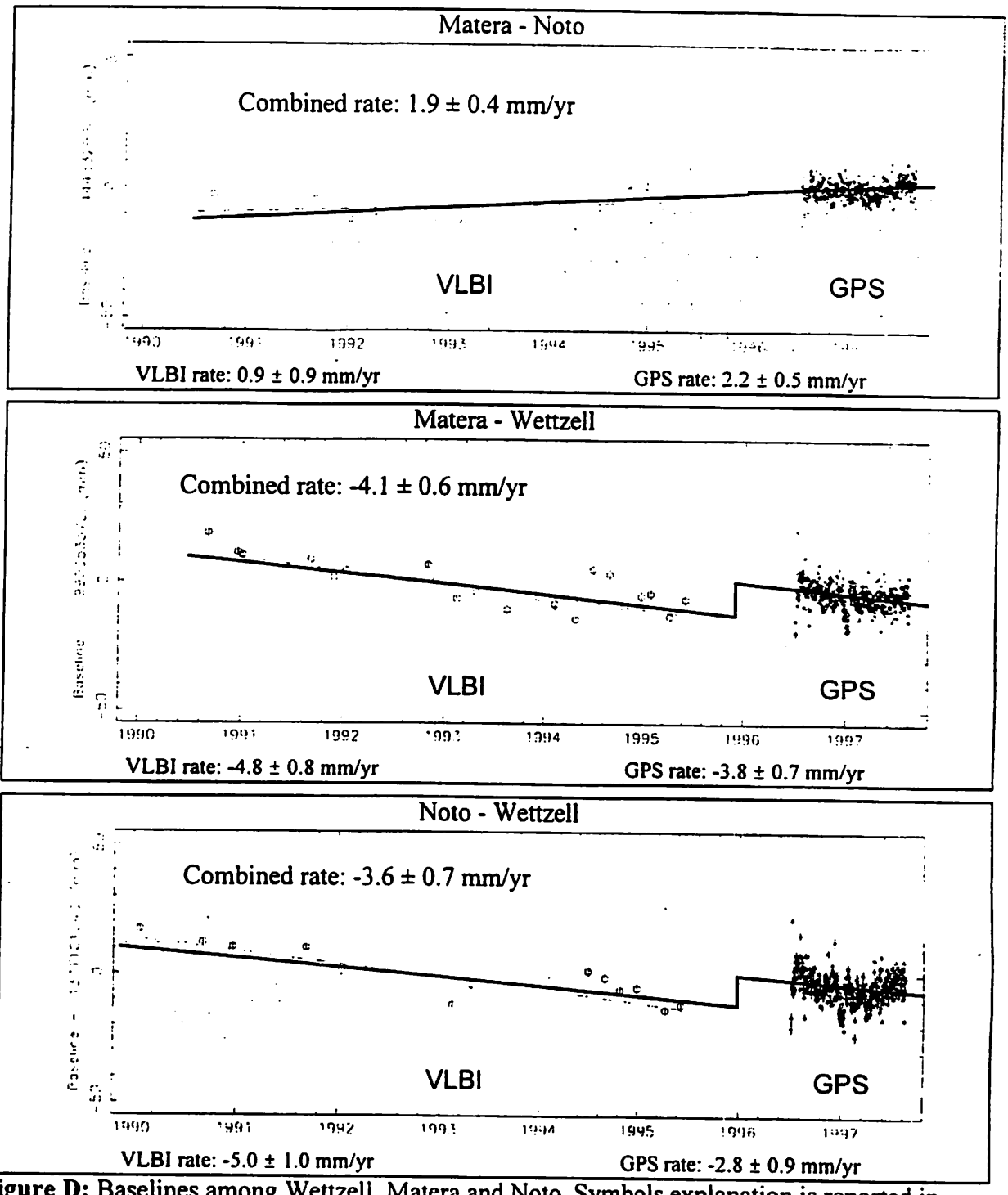


**Figure D:** Baselines among Wettzell, Matera and Noto. Symbols explanation is reported in figure **b**.

### 3.2 Comparison of the VLBI and GPS site velocities

The velocities used in the comparison have been obtained in different ways: for the VLBI directly from the solution while for GPS from a linear fit of the site positions.
They have been compared by estimating the 4 parameters present in equation 2, that is the time derivative of equation 1, to transform the GPS into VLBI velocity field.

$$\dot{\mathbf{X}}_{VLBI} = \dot{\mathbf{X}}_{GPS} + (\dot{d} + \dot{\mathbf{R}})\mathbf{X}_{GPS} \qquad (2)$$

This estimate has been done using only the Noto, Matera and Wettzell sites has suggested from the previous baseline time series analysis.

The estimated values for the 4 parameters are: $\dot{R}_x$=0.4±0.1 mas/yr, $\dot{R}_y$=0.06±0.03 mas/yr, $\dot{R}_z$=0.28±0.09 mas/yr and $\dot{d}$=0.22±0.08 $10^{-9}$ $yr^{-1}$.

After applying these parameters to the GPS velocities we obtain a new set of velocities that are more comparable with those from VLBI. In table g are the two velocity fields in the local topocentric refence frame, Up, East and North components, and in figure e are the horizontal velocities.

| Site | VLBI | | | GPS | | |
|---|---|---|---|---|---|---|
| | Up rate (mm/yr) | East rate (mm/yr) | North rate (mm/yr) | Up rate (mm/yr) | East rate (mm/yr) | North rate (mm/yr) |
| CAGLIARI | - | - | - | -3.4 ± 1.2 | 20.1 ± 0.6 | 13.8 ± 1.1 |
| EFFELSBERG | 2.5 ± 1.6 | 19.5 ± 0.3 | 13.4 ± 0.3 | - | - | - |
| MADRID | 7.4 ± 0.9 | 19.4 ± 0.2 | 16.2 ± 0.2 | 27.7 ± 10.4 | 41.9 ± 5.5 | 30.8 ± 9.8 |
| MATERA | -1.4 ± 1.0 | 23.8 ± 0.2 | 18.3 ± 0.3 | -1.2 ± 0.0 | 24.0 ± 0.0 | 18.7 ± 0.0 |
| MEDICINA | -2.7 ± 0.8 | 23.2 ± 0.2 | 15.7 ± 0.2 | -2.3 ± 1.1 | 30.3 ± 0.6 | 12.7 ± 1.1 |
| NOTO | 0.4 ± 1.0 | 21.9 ± 0.2 | 18.7 ± 0.3 | -1.6 ± 1.1 | 21.6 ± 0.6 | 17.1 ± 0.9 |
| ONSALA | 5.0 ± 0.8 | 18.4 ± 0.2 | 13.2 ± 0.2 | - | - | - |
| VENEZIA | - | - | - | -25.0 ± 1.8 | 16.6 ± 0.9 | 14.9 ± 1.8 |
| WETTZELL | 0.0 | 20.4 | 13.4 | -1.4 ± 1.2 | 20.4 ± 0.7 | 15.4 ± 1.2 |

**Table G:** Site velocities in the local topocentric reference frame.

These velocities reflect the site behavior seen in the previous baseline comparison. There is an agreement between the estimated velocities at Noto, Matera and Wettzell while Medicina and Madrid show significant discrepancy.

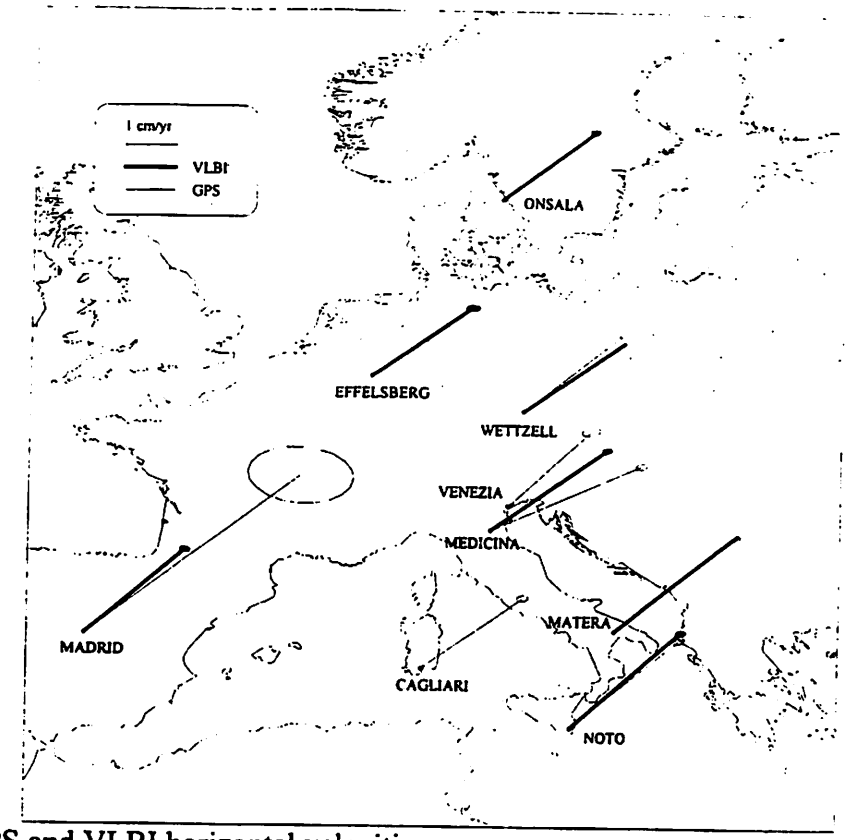


**Figure E:** GPS and VLBI horizontal velocities.

It is remarkable that this approach allow to densify the geodetic network of each technique improving the detail level of geodetic information in the area under investigation.

## 4. Future evolution of the work

The analysis activities at the ASI Space Geodesy Center in Matera are paced by several products, namely global solutions for VLBI and SLR, VLBI regional solution for the EUROPE campaign, regional GPS solution contributing weekly to IGS and a EOP SLR solution contributing to the IERS Bulletin B. All these activities, being continuously updated to meet the current standards, have a lot of common points and links that are worth to be explored at their deepest level. The two global SLR and VLBI follow-on solutions will be better aligned, e.g. by using the same a-priori terrestrial reference frame to constrain them and widening the overlapping period. In addition, the consistency analysis will be refined, by estimating together, along with the 7 "static" parameters, also their first time derivatives and look for the connections to the drifts from the EOP time series differences.
The benchmark of the GPS regional solution should benefit of its continuously increasing amount of estimates, making it more robust. This will bring to more meaningful comparisons with the SLR and VLBI solutions in the co-located sites. In addition, similar features of the reduction S/W we use for SLR and GPS analysis (GEODYN and MicroCOSM) have suggested us to explore the possibility of blending the two solutions at the level of normal matrix equations. This approach is still under study; it has been carried out at a 'functional' level, in the sense that the output in the form of normal matrices from the two S/W have been made compatible for the SOLVE S/W but to have results of some interest (e.g. for site position or Earth orientation parameters) we have to set up some proper test cases.

## References

Bianco G., Cenci A., Garramone L., Vespe F.; *"The Italian GPS Fiducial Network"*, Proceedings of the 1993 IGS Workshop, pages 42-48. Berne, 1993.

Bianco, G., Devoti R., Fermi M., Luceri V., Rutigliano P., and Sciarretta C., A contribution in the estimation of tectonic motion in crucial areas: the CGS96 solution, *Tectonophysics Special Issue for Wegener 96* (in press)

Boucher, C., Z. Altamini, and P. Sillard, Results and analysis of the ITRF94, *IERS Technical Note 20*, Observatoire de Paris, March 1996.

Bruyninx, C., W. Gurtner, and A. Muls, The EUREF Permanent GPS Network, Proceedings of EUREF symposium, Ankara, May 1996.

Himwich, W.E., M.M Watkins, C. Ma, D.S. MacMillan, T.A. Clark, R.J. Eanes, J.W. Ryan, B.E. Schutz, and B.D. Tapley, The consistency of the scale of the terrestrial reference frames estimated from SLR and VLBI Data, in Contributions of Space Geodesy to Geodynamics: Earth Dynamics, *Geodynamic series, volume 24*, 113-120, American Geophysical Union, 1993.

IERS Annual Report 1992, Central Bureau of IERS, Paris Observatory, July 1993.

Lanotte, R., G. Bianco, M. Fermi, P. Rutigliano, and G.R. Verdone, The CGS VLBI EUR96 Geodetic solution, Proceedings of the eleventh working meeting on European VLBI for geodesy and astrometry, edited by G. Elgered, Göteborg, 1996.

Ray, J.R., C. Ma, J.W. Ryan, T.A. Clark, R.J. Eanes, M.M. Watkins, B.E. Schutz, and B.D. Tapley, Comparison of VLBI and SLR geocentric coordinates, *Geophys. Res. Lett., 18(2)*, 231-234, 1991.

# Analysis of tectonic motion for the Ny-Ålesund VLBI station.

O. Titov*, B. R. Pettersen**

* Institute of Applied Astronomy, Russian Academy of Sciences, St.Petersburg, Russia.

** Norwegian Mapping Authority, N-3500 Hønefoss, Norway.

**Abstract**

The VLBI facility at Ny-Ålesund, Svalbard is one of the latest additions to the European VLBI network. Data from 74 observing sessions are presently available for analysis, covering a time span of almost 3 years. We present the results obtained with the OCCAM 3.4 program package and compare them to the predictions of the NUVEL1-A plate tectonic model.

## Introduction

The Ny-Ålesund VLBI station began operation in 1994. Analysis of the first experiments showed that the quality of observational performance is excellent (Titov, Zarraoa, Pettersen, 1996). Now the station participates actively in several international networks and provides reliable information for geodesy and geodynamics.

We have analyzed 74 VLBI experiments with participation of Ny-Ålesund station using the OCCAM 3.4 software (Zarraoa et al., 1989, see also Titov, this volume) to investigate tectonic motions of the Svalbard archipelago. The full time span of the data covers almost 3 years (04.10.1994–17.06.1997). We have selected two strategies for our analysis:

1. Celestial reference frame is fixed by the radiosource coordinates (ICRF 94). Terrestrial reference frame is fixed by *apriori* Earth orientation parameters published by IERS (EOP C04) and the coordinates of Wettzell as reference station. All experiments were processed by Kalman filtering in single-session mode.
2. Celestial reference frame is fixed by the radiosource coordinates (ICRF 94). Wettzell was selected as a reference station and we constrained the vertical motion of Kokee Park as well as the direction Wettzell–Fortaleza to fix the terrestrial reference frame. Station

coordinates are from ITRF 94; apriori velocities are from the NUVEL1-A model. Daily EOP values are estimated together with other parameters. Four VLBI stations (Wettzell, Kokee Park, Fortaleza, and Ny-Ålesund) have participated simultaneously in 30 experiments only. All of them were processed by Kalman filtering in single-session mode.

After estimation of individual positions we estimated a linear velocity for the Ny-Ålesund VLBI station using weighted least squares method. It appears that the solution 1 provides unrealistic velocity components (e.g. –18 mm/year in longitude). Obviously, it arises from the choice of reference frame as fixed by EOP. Some unexpected effects in polar motion could cause large velocity components because Ny-Ålesund is close to the North pole. Since baseline lengths do not depend on the choice of reference frame, the time series of baseline lengths from solution 1 is unaffected by this problem. We thus discuss the results for baselines: Ny-Ålesund–Wettzell, Ny-Ålesund–Gilmore Creek, Wettzell–Gilmore Creek.

In solution 2 the terrestrial reference frame is fixed only by coordinates of other stations. This allows realistic estimates of the velocity components of Ny-Ålesund to be obtained.

**Discussion**

Figures 1-3 show the time evolution of baseline lengths from solution 1. The results are in general agreement with the NUVEL1-A model (DeMets et al., 1994); the European baseline Wettzell–Ny-Ålesund is stable and both transcontinental baselines increase with velocities near 10 mm/year. Also, significant seasonal variations of baseline lengths are noted. The seasonal effects have been described earlier (McMillan and Ma, 1994; Zarraoa, 1995; Titov and Yakovleva, 1996) but their origin is not yet clear. They are able to distort an estimate of linear velocity for short and sparse time series. Therefore we also solved for two seasonal terms in addition to a linear regression fit. The first two column in Table 1 contain NUVEL1-A model velocities and our estimates from a linear fit with corresponding formal errors ($\pm 1\sigma$). The last three columns give our velocity estimates using a linear model plus seasonal terms; including amplitudes for annual and semiannual terms.

The baseline Wettzell–Gilmore Creek contains a significant annual signal. The other two baselines under study are two times shorter, so the annual signal is not so large. The

semiannual term is significant only for the baseline Ny-Ålesund–Wettzell. We note that the velocity estimates for transcontinental baselines are closer to NUVEL1-A model values when seasonal terms are included. Under the same approach the European baseline shows a larger deviation from NUVEL1-A as compared to the linear fit, but the formal error of the estimate is slightly improved. Nevertheless, none of the estimates for Ny-Ålesund–Wettzell exceed the $3\sigma$ level, so the conclusion is that no significant motion of the Ny-Alesund VLBI station relative to the European continent is detected.

| Baseline | NUVEL1-A | Linear model | Model with seasonal terms | Annual term | Semiannual term |
|---|---|---|---|---|---|
| NyAl-Wett | 0 | 0.9 +/- 0.8 | 1.5 +/- 0.6 | 2.2 +/- 0.8 | 3.3 +/- 0.8 |
| NyAl-Gilc | 10.8 | 9.8 +/- 1.2 | 10.0 +/- 1.3 | 4.5 +/- 1.4 | 2.2 +/- 1.3 |
| Wett-Gilc | 10.1 | 13.3 +/- 1.5 | 11.4 +/- 1.5 | 7.4 +/- 1.7 | 2.2 +/- 1.5 |

Table 1.

Estimates of baseline rates (in mm/year) and

amplitudes of annual and semiannual terms (mm)

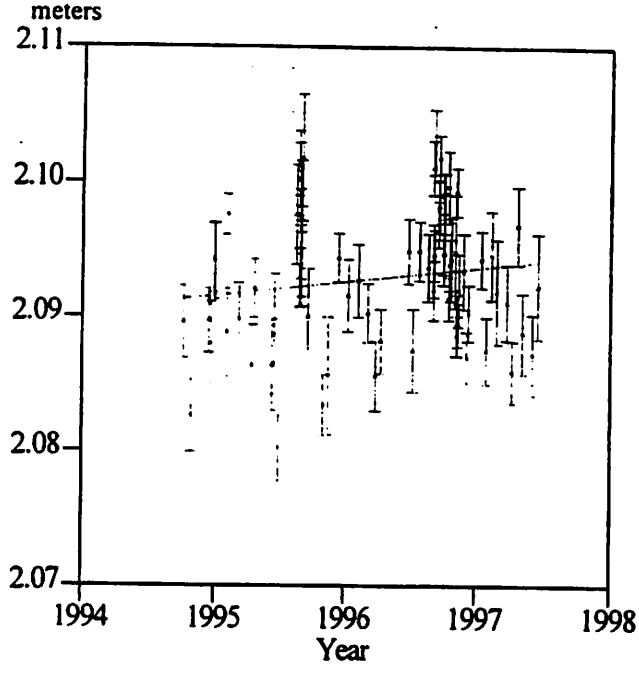


Fig.1

Evolution of NY-ÅLESUND – WETTZELL baselength

Rate: 0.9 +/– 0.8 mm/year

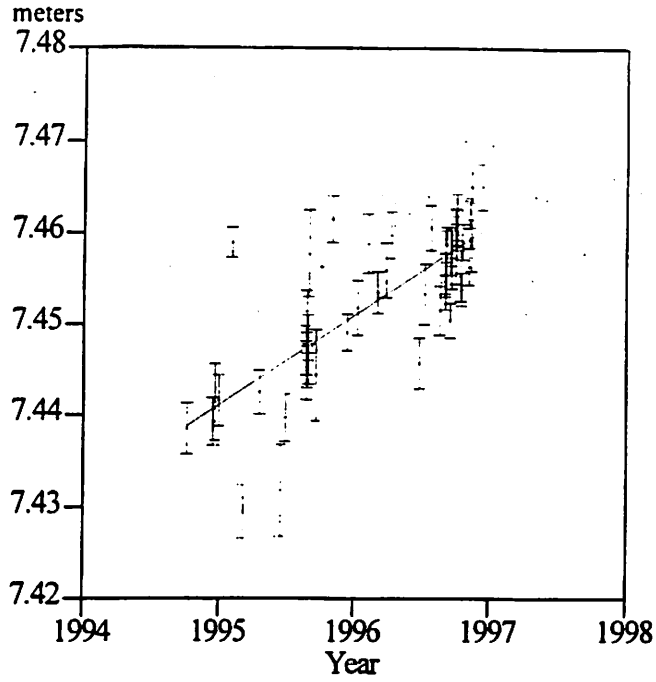


Fig.2
Evolution of NY-ÅLESUND – GILCREEK baselength
Rate: 9.8 +/– 1.2 mm/year

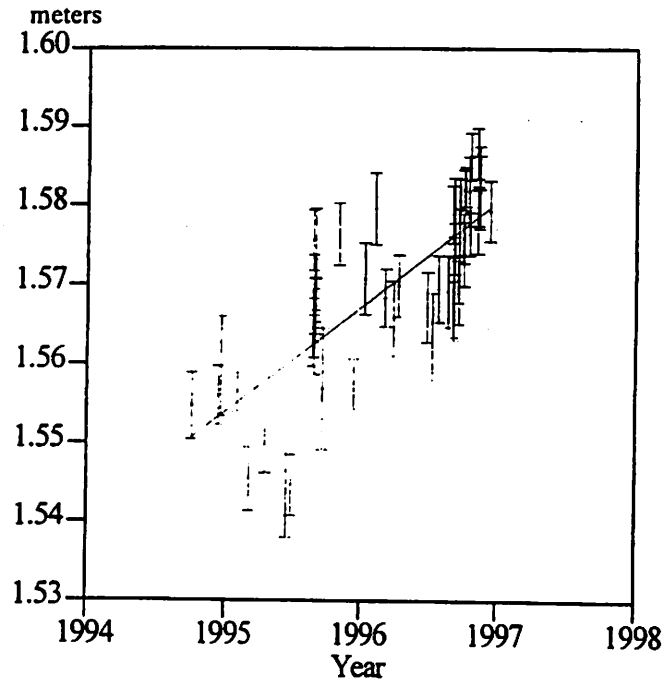


Fig.3
Evolution of WETTZELL – GILCREEK baselength
Rate: 13.3 +/– 1.5 mm/year

The evolution of the Ny-Ålesund station components from solution 2 are shown on Figs. 4–6. The estimated velocity components are in Table 2. The radial and latitude components are in a good agreement with NUVEL1–A values. The longitude component deviates a factor 2 from the NUVEL-1A value. This may be caused by the first 4 points in Fig. 6, which *may* be considered to deviate from the trend. Omitting them implies a velocity estimate of 9.4 +/- 3.4 mm/year. It is noteworthy, however, that the scatter for the longitude component in Fig. 6 is larger than for latitude in Fig. 5 . This is in contrast to the results for other VLBI sites where both horizontal components usually have comparable formal errors. The longitude component is thus sensitive to the choice of terrestrial reference frame (Ny-Ålesund is close to the North Pole), and the short time span of observations is in this case not enough for a reliable determination.

| Component | NUVEL1–A | Linear model |
|---|---|---|
| Radial | 0 | 0.4 +/- 3.6 |
| Latitude | 15.2 | 13.9 +/- 1.3 |
| Longitude | 12.7 | 6.0 +/- 2.4 |

Table 2.

Velocity estimates (in mm/year)

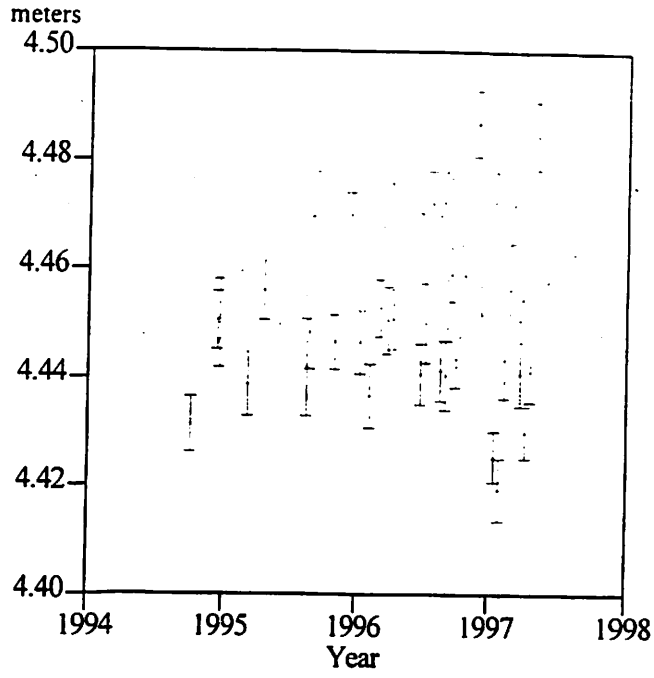


Fig.4
Evolution of Ny-Ålesund radial component
Rate: 0.4 +/– 3.6 mm/year

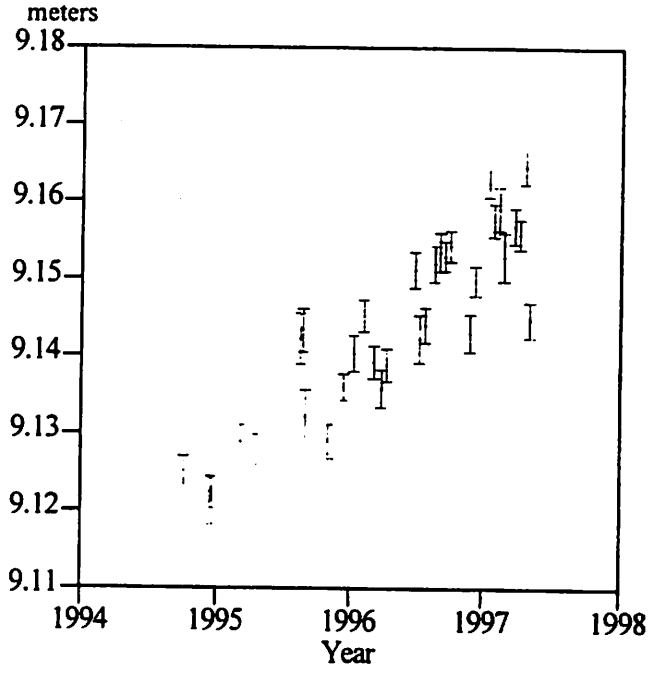


Fig.5
Evolution of Ny-Ålesund latitude component
Rate: 13.9 +/– 1.3 mm/year

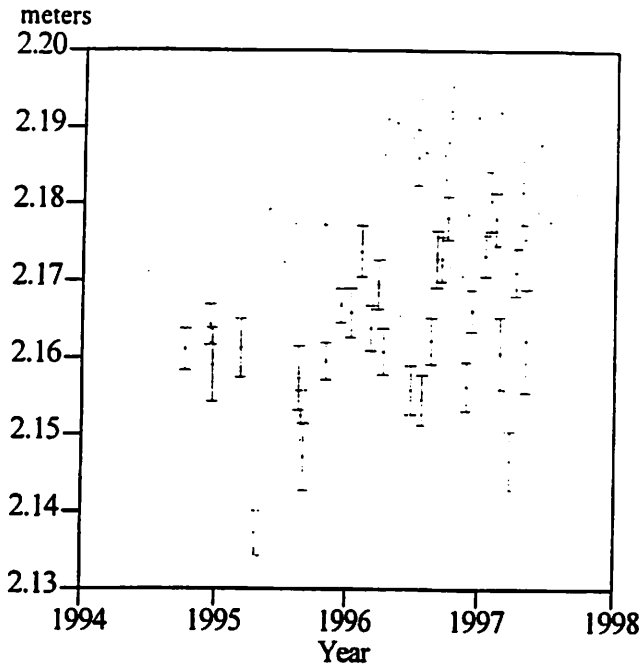


Fig.6
Evolution of Ny-Ålesund longitude component
Rate: 6.0 +/– 2.4 mm/year

**Conclusion**

Detailed analysis of the tectonic motion of the Ny-Ålesund VLBI station shows that there are no significant discrepancies with respect to the NUVEL1–A model. Seasonal effects do not distort essentially our estimates of linear trend for baselines Ny-Ålesund – Wettzell and Ny-Ålesund – Gilmore Creek. The accuracy of the longitudinal velocity component is worse than for latitude and comparable to that of the radial component. Probably, the peculiarity is caused by the closeness of the Ny-Alesund VLBI station to North Pole.

**References**

DeMets C., R.G. Gordon, D.F. Argus, S. Stein, (1994) *Effect on Resent Revision of the geomagnetic reversal time scale on estimates of current plate motions*. Geophys. Res. Let., 21, 2191–2194.

MacMillan D.S., C. Ma, (1994) *Very Long Baseline Interferometry Atmospheric Modeling Improvement*. J. Geophys. Res., **99**, 637–651.

Titov O., E. Yakovleva, (1996) *Spectral Analysis of the Baselength Time Series*, Proc. of the 11-th Working Meeting on European VLBI for Geodesy and Astrometry, ed. by G. Elgered, Onsala Space Observatory, 134–142.

Titov O., N. Zarraoa, B.R. Pettersen, (1997) *Ny-Alesund VLBI station: First Year Data Analysis*. Proceedings of IAA, vol.1, 80–88 (in Russian).

Zarraoa N., (1995) *VLBI in the far North. A closer look.* in Proc. of 10-th Meeting on European VLBI for Geodesy and Astrometry, 103–108.

Zarraoa N., A. Rius, E. Sardon, H. Schuh, J. Vierbuchen, (1989) OCCAM: A compact a transportable tool for the analysis of VLBI experiment. In A. Rius (ed.) Proc. of 7-th Working Meeting on European VLBI for Geodesy and Astrometry, 92–102.

# On the Relation Between Geodetic VLBI and Rain

Gunnar Elgered

Onsala Space Observatory, Department of Radio and Space Science, Chalmers University of Technology, SE–439 92 Onsala, Sweden

**Abstract.** This paper discuss two aspects of the influence of rain on geodetic VLBI. The first is the influence of rain on measurements of the excess propagation path using microwave radiometry. Previously, the microwave radiometer data themselves have been used to indicate when the quality is unacceptable. We here report on a field test to combine independent radar measurements of rain with the microwave radiometer data. The second aspect concerns the excess propagation path caused by the rain during VLBI observations. An excess propagation path is caused by free falling drops in the air as well as liquid water on the radome covering the antenna. We find no significant correlation between the estimated length residual of the Onsala–Westford baseline and the amount of rain observed at a nearby site during the VLBI experiment.

## 1 Introduction

Very-Long-Baseline Interferometry (VLBI) is often referred to as an all-weather technique. The reason is that the radiation in the microwave region (2–9 GHz in our case) can penetrate clouds and rain without too much attenuation. This means that the received signal is sufficiently strong in order to obtain a group delay estimation during all times, except perhaps during the very short periods with extremely high rain intensity. On the other hand the presence of liquid water in the atmosphere will introduce an additional excess propagation path [*Uzunoglu et al.*, 1977; *Liebe et al.*, 1989] which may decrease the accuracy of the estimated geodetic parameters.

Another effect caused by rain can be introduced through the use of Water Vapour Radiometer (WVR) data. The WVR observes the emission from the sky at two different frequencies. These observations are, thereafter, used to infer both the water vapour content—or the excess propagation path due to water vapour (the "wet" delay)—and the liquid water content. The WVR method relies on the assumption that all drops of liquid water have a size which is much less than the wavelengths observed. For the Onsala WVR the shortest wavelength is 10 mm, meaning that drops during rain can make such an assumption invalid. Furthermore, water can accumulate on the covers of the horn antennas of the WVR and is this case the drops will definitely degrade the accuracy of the inferred wet delay. The WVR data have so far been used in two different ways: (1) As independent wet delay estimates introduced as *a priori* information in the VLBI solution procedure [*Elgered et al.*, 1991]; (2) As statistical information of the wet delay variations, often resulting in a random walk variance specified in the VLBI solution when the VLBI data themselves are used to estimate the wet delay simultaneously with the geodetic parameters [*Jarlemark*, 1997].

In the first part of this paper we will use independent radar data to make an assessment of the influence of rain on the WVR results. In the second part we will study the 13 year long time series of length estimates for the Onsala–Westford baseline, and compare these estimates to the measured amount of rain at a site 11 km south of the Onsala observatory.

## 2 The Influence of Rain on Water Vapour Radiometry

This is a case study where we have analyzed WVR and radar data from August 24, 1997. We chose data from this day because it was a very cloudy day including many rain events. Figure 1 shows the results of the wet delay and the liquid water content inferred from the WVR using the standard

analysis. It is seen that no values for the liquid-water content are higher than 0.7 mm. The gaps in the time series are periods when the liquid-water content is higher than 0.7 mm and these data have been discarded. Note that the WVR was stopped at approximately 21 UT.

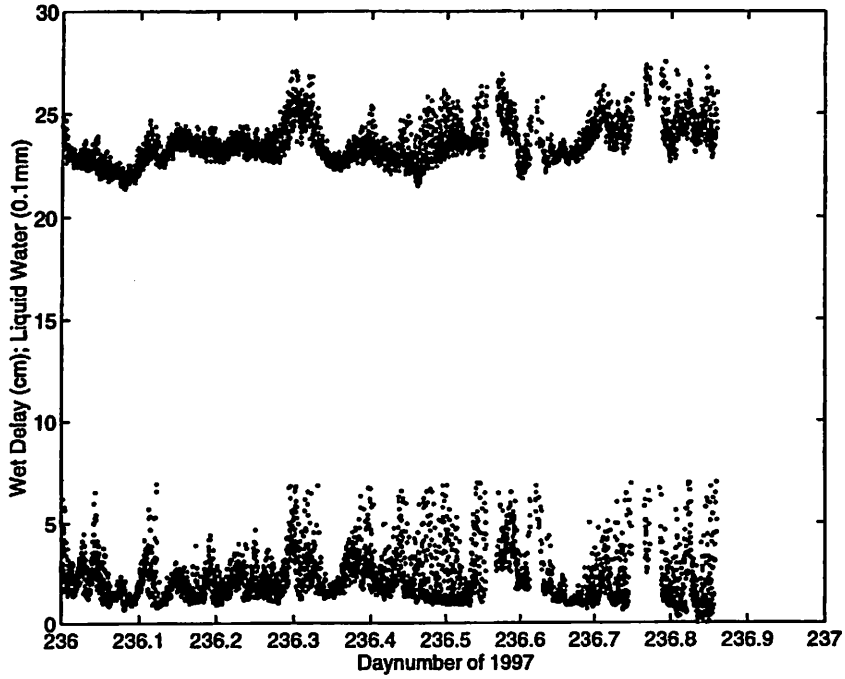


Figure 1: The wet delay and the liquid water content inferred from WVR data during August 24, 1997. Note the different scales for the two parameters. The upper curve is the wet delay, varying between 21 and 28 cm. The lower curve is the liquid-water content where all values higher than 0.7 mm have been discarded. All wet delay data corresponding to a liquid water content >0.7 mm are then also discarded.

A "Micro Rain Radar" was operating simultaneously with the WVR at a distance of approximately 20 m. The radar was rented for a field experiment using three different WVRs within the WAVEFRONT project [*WAVEFRONT*, 1997]. It is a Frequency Modulated-Continuous Wave (FM-CW) radar and is always measuring in the zenith direction [*Klugmann et al.*, 1997]. A picture of the radar is shown in Figure 2. The radar measures the velocity spectra of the falling drops. From these data the rain rate and the liquid water density can be inferred. During our field experiment the radar was operating to a height of 1200 m with a range resolution of 200 m. The data presented here is the rain rate at the height of 200 m (the height cell available that was closest to the ground level) and the integrated liquid-water content from the ground to the height of 1200 m. These two quantities are presented for August 24 in Figures 3 and 4.

When we compare the liquid-water content inferred from the WVR (Figure 1) with that from the radar (Figure 4) the results look very different. We must first note that the radar only senses liquid water up to 1200 m, whereas the WVR method is sensitive to all liquid water in the antenna beam through the atmosphere. A part of the difference could also be that the radar is less able to detect drops that are not falling, i.e., during periods of no precipitation. An instrument measuring the height of the cloud base and/or a radar with a longer range would have helped to understand the reason for the differences.

Turning back to the original problem of editing WVR data based on the argument that no large drops shall be allowed to influence the final results we can now combine the rain information obtained from the radar (Figure 3) with the original WVR data. We use the rain rate data to identify periods when rain is falling. Thereafter, we add $\pm 1$ minute to these periods and discard all the cor-

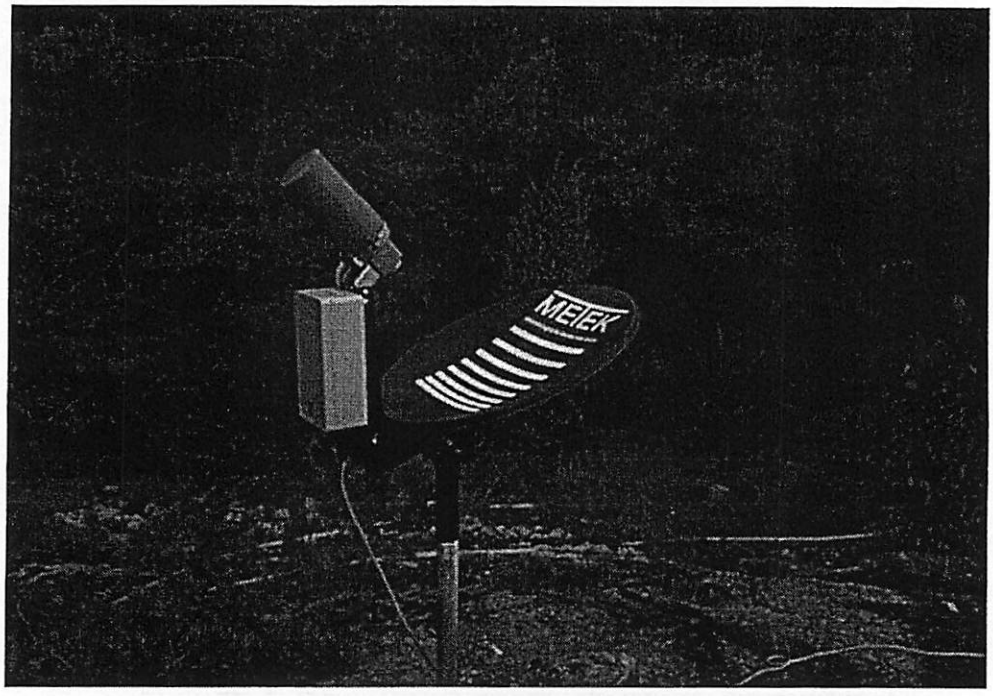


Figure 2: The FM-CW Doppler Radar. The offset parabola has a diameter of 60 cm.

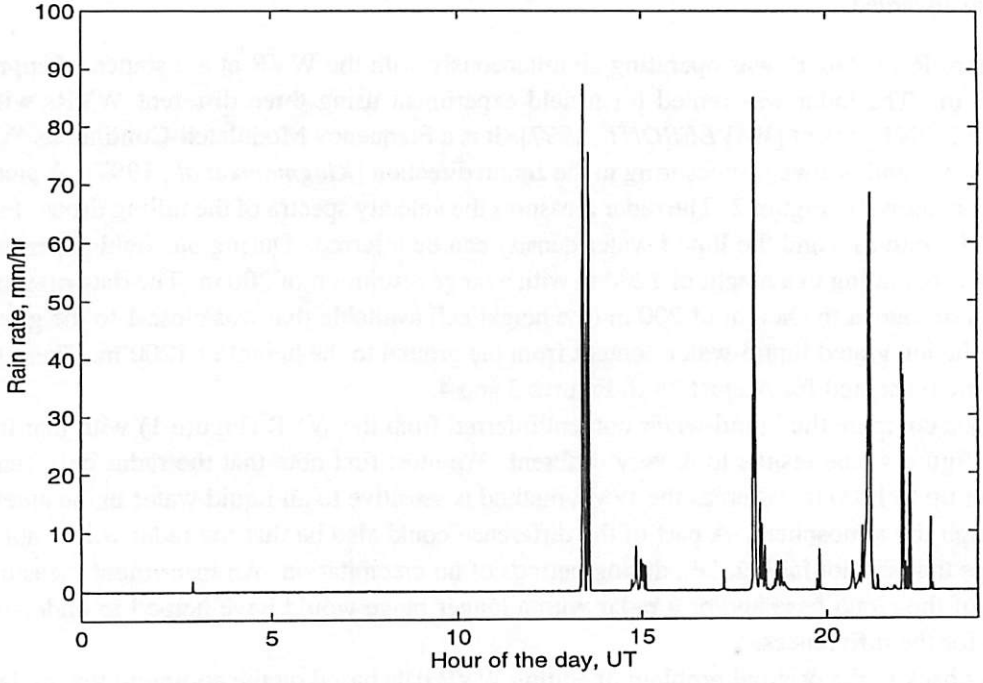


Figure 3: Radar measurements of the rain rate.

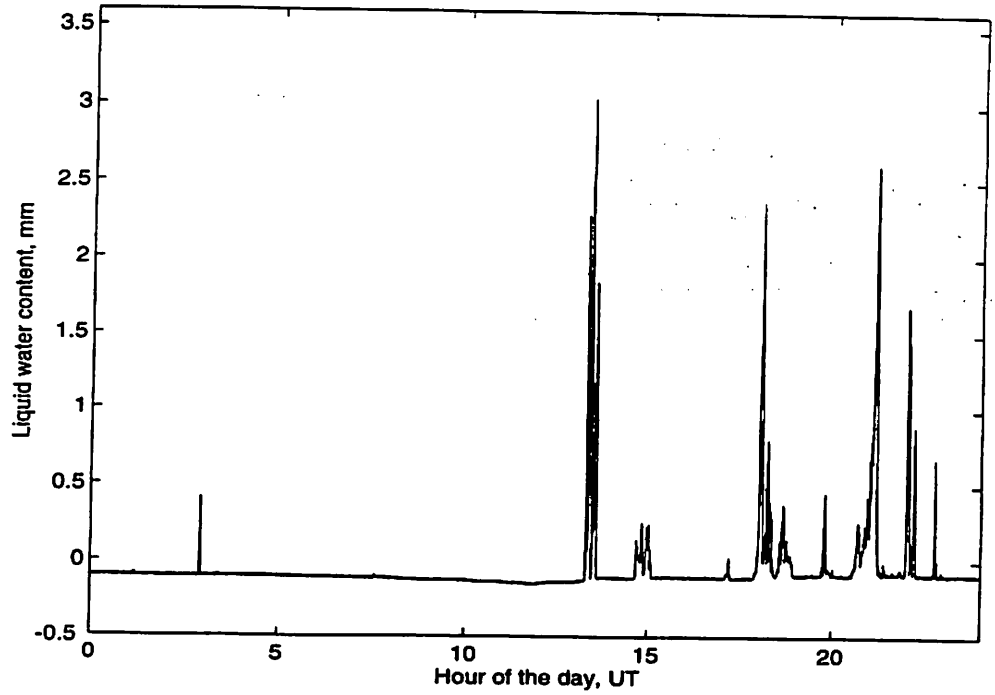


Figure 4: Radar measurements of the liquid water content in the height interval 0–1200 m.

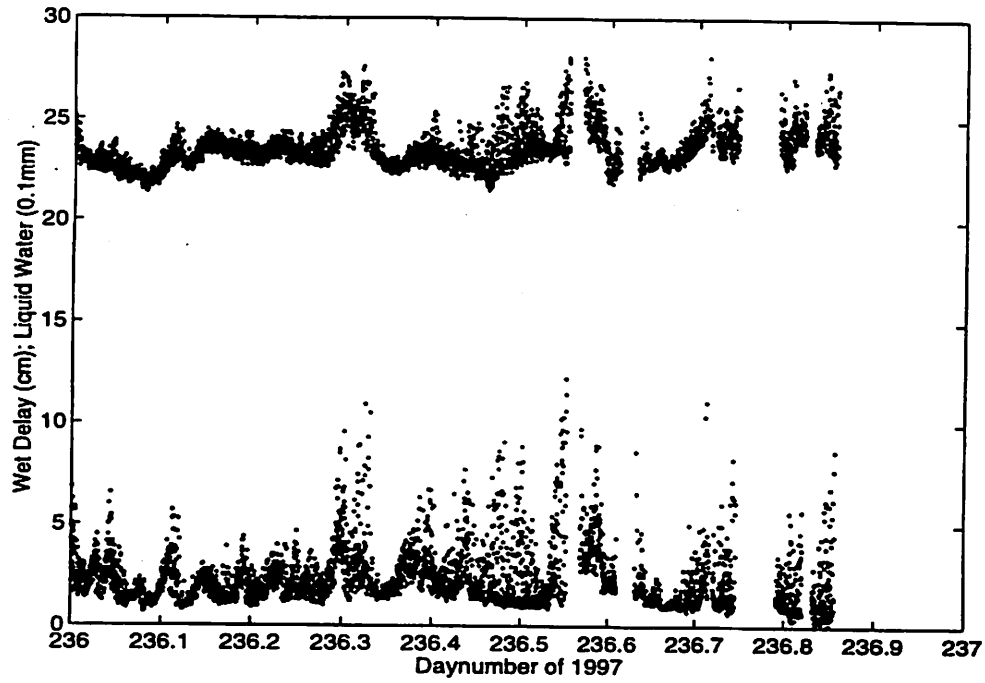


Figure 5: The wet delay and the liquid water content inferred from WVR data during August 24, 1997. Same as Figure 1 except that these data have been edited using the rain information shown in Figure 3.

responding WVR data. The result of this editing procedure is shown in Figure 5. When comparing these results to those from the standard analysis in Figure 1 some differences can be seen. The differences in the wet delay time series are, however, not dramatic. In order to make a more definite conclusion on the usefulness of the information provided by the radar more data are needed.

This editing technique will be improved to automatically handle long term drifting biases in the radar data and during times when radar data are available we anticipate to use these in the standard WVR data processing.

# 3 The influence of rain on estimated baseline lengths

We chose to study the estimated lengths of the Onsala–Westford baseline using data from 1982 to 1995. The estimated lengths are from the global solution 1014 available from NASA Goddard Space Flight Center (http://lupus.gsfc.nasa.gov). These data are shown in Figure 6. In the following we will investigate if the residuals about the fitted straight line to these data (see Figure 7) are correlated with observed amounts of rain. Rain data from this entire period have been archived at the weather station Nidingen, an island approximately 11 km south of the VLBI antenna (see Figure 8). We shall note two disadvantages associated with these data. The first is the distance between the VLBI site and the rain observations. The spatial variation of rain events are often more local. This is obvious also from the radar data presented in Section 2. The second disadvantage is that the rain data consist of a time series of the amount of rain collected during twelve hour long periods, from 6 UT to 18 UT and from 18 UT to 6 UT. Fortunately, VLBI experiments have often started around 18 UT but some uncertainty is introduced by the lack of synchronization.

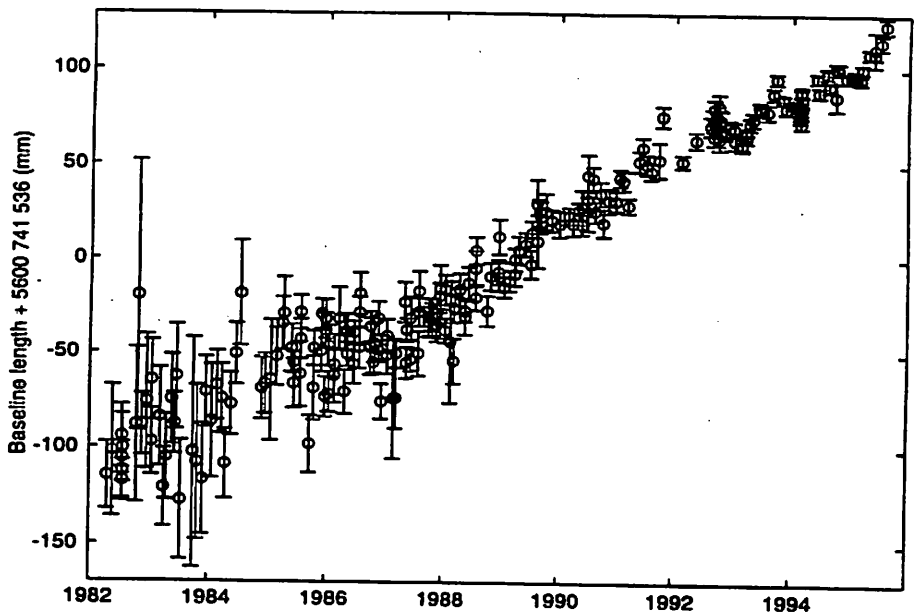


Figure 6: The estimated baseline length between Onsala and Westford.

Figure 9 show the baseline length residual, and the absolute value of the baseline length residual, plotted versus the estimated amount of rain using all the available data. The weighted correlation coefficient is insignificant, 0.02 and 0.03 for the two cases.

We have noted that in the time series of the geodetic VLBI data there was an important change at Onsala in March 1987, when the 20 m dish was first used to observe both the frequency bands. Before this date the S-band data were acquired with the 25.6 m antenna. This larger, but older and slower, antenna has no radome and must, therefore, be locked up during strong winds. Strong winds are correlated with rain fall and certainly more data were lost before 1987 when there was stormy

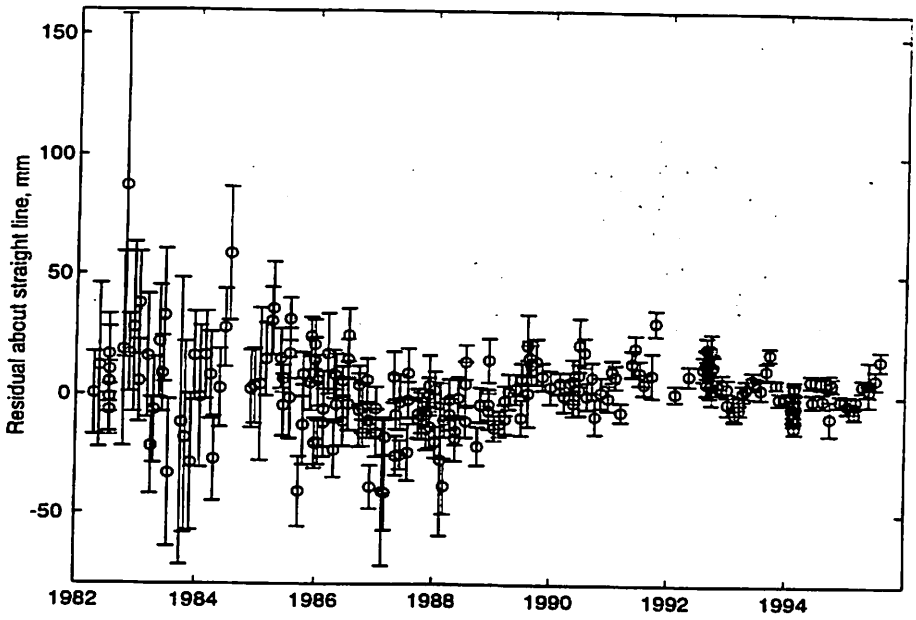


Figure 7: The residuals about a straight line fitted to the data in Figure 6. The mean value of 5600,741.536 m has been subtracted.

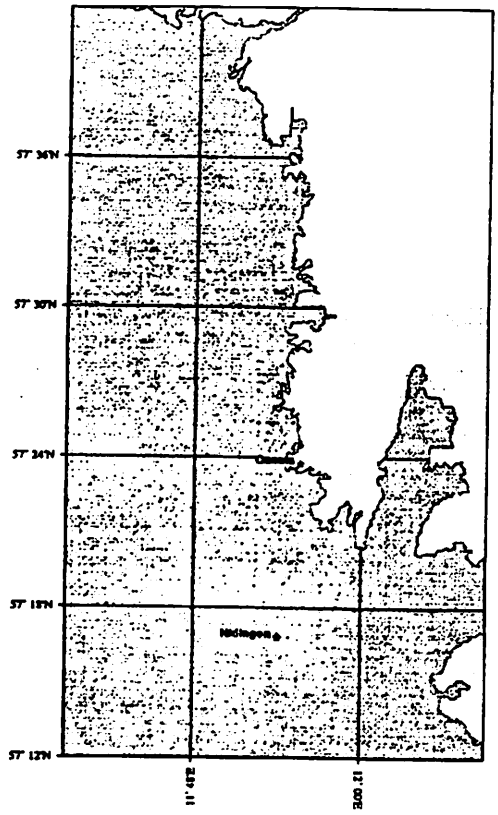

Figure 8: Map showing the location of the Onsala VLBI site and the weather station Nidingen, 11 km south of Onsala, where the rain data were acquired. The map was prepared using the GMT package [*Wessel and Smith*, 1995].

weather. Because the slewing speed of the 25 m antenna was low only 100–200 observations were typically acquired during a 24-hour experiment. This means that an additional loss of data could have a large impact on the resulting accuracy. It is therefore, interesting to split the data set into to smaller ones, one including data acquired before March 1987, and the other including data acquired during March 1987 and later. The resulting correlation plots are shown in Figure 10. Also here the weighted correlation coefficients are insignificant, 0.03 for the "old" data and 0.01 for the more recent data. We note, however, that the large formal errors typically occur during rain fall in the "old" data set. In fact we find a correlation of 0.23 and -0.08 between the formal error of the estimated baseline length and the amount of rain for the "old" and "new" data sets, respectively. This is an indication that there were less data acquired during rain when the 25.6 m antenna was used for the S-band observations.

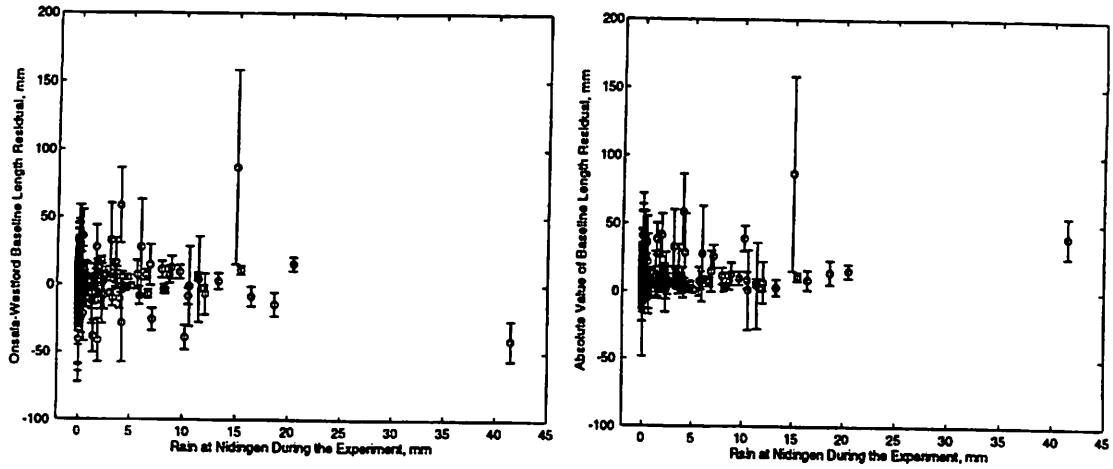


Figure 9: Correlation plots between the observed rain amount at Nidingen and the baseline length residual (left). The graph to the right shows the absolute value of the residual.

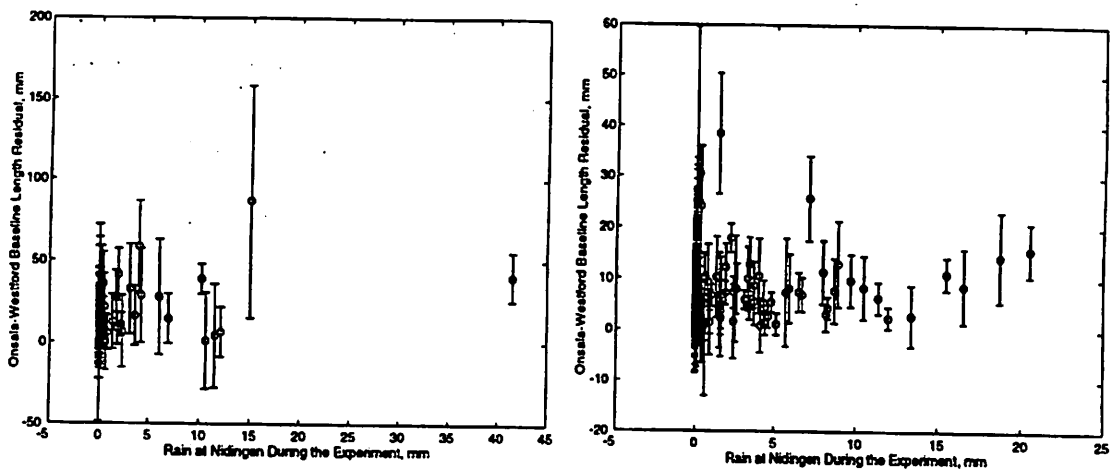


Figure 10: Correlation plots between the observed rain amount at Nidingen and the baseline length residual. Data from experiments up to February 1987 are shown to the left and data from March 1987 to date are shown to the right.

# 4 Conclusions

Radar measurements of the liquid water content and the rain intensity in the first 1200 m of the atmosphere have been compared to WVR data. The results obtained so far indicate that liquid water in the atmosphere is typically located at heights above 1200 m when no precipitation occurs. It also seems reasonable that the radar data are useful in terms of editing WVR data. Up to now the WVR data themselves have been used for this purpose. WVR data indicating a liquid water content above a certain threshold, often 0.7 mm, have simply been ignored. Using the alternative method and discard WVR data acquired during periods when the radar detects precipitation does not have a large impact on the time series of the wet delay inferred from the WVR for the one day long data set used. More data are, however, needed in order to make a solid statistical evaluation.

In the second part of the paper it was shown that there is no significant correlation between the residuals of estimated baseline lengths and the accumulated amount of rain measured 11 km from the Onsala VLBI site. The impact of the influence of rain on the geodetic VLBI data can be studied in much more detail in the future, given that we now have a colocated micro rain radar operating at the Onsala site. Rain events can be of very short duration and the lack of correlation observed could, at least partly, be explained by that such data automatically are removed from the VLBI solution by being characterized as "outliers". Other reasons for the lack of correlation is of course the 11 km distance between the VLBI site and the site of the rain observations; and that other error sources dominate in the error budget.

**Acknowledgement.** This research has made use of NASA Goddard Space Flight Center's VLBI terrestrial reference frame solution number 1014.

# References

Elgered, G., J.L. Davis, T.A. Herring, and I.I. Shapiro, Geodesy by radio interferometry: Water vapor radiometry for estimation of the wet delay, *J. of Geophys. Res.*, **96**, 6541–6555, 1991.

Jarlemark, P.O.J., Analysis of temporal and spatial variations in atmospheric water vapor using microwave radiometry, PhD thesis, *Technical Report 308*, School of Electrical and Computer Engineering, Chalmers University of Technology, Göteborg, 1997.

Klugmann, D., K. Heinsohn, and H.-J. Kirtzel, A low cost 24 GHz FM-CW doppler radar rain profiler, *Contr. to Atmospheric Physics*, **69**, 247–253, 1996.

Liebe, H.J., T. Manabe, and G.A. Hufford, Millimeter wave attenuation and delay rates due to fog/cloud conditions, *IEEE Trans. Antennas Propag.*, **AP–37**, 1617–1623, 1989.

Uzunoglu, N.K., B.G. Evans, and A.R. Holt, Scattering of electromagnetic radiation by precipitation particles and propagation characteristics of terrestrial and space communication systems, *Proc. IEE*, **124** (5), 417–424, 1977.

*WAVEFRONT Interim Progress Report*, IESSG, University of Nottingham, England, September, 1997.

Wessel, P., and W.H.F. Smith, New versions of the generic mapping tools released, *Eos Trans. American Geophys. Union*, **76**, 329, 1995.

# Activities and recent results in Geodynamics

P. Tomasi [1,2], F. Mantovani [1], M. Negusini [3], A. Orfei [1] and P. Sarti [1]

1 Istituto di Radioastronomia del CNR - Bologna - Italy
2 Istituto di Tecnologia Informatica Spaziale del CNR - Matera - Italy
3 Dipartimento di Geofisica, Università di Bologna - Bologna - Italy

**Abstract:**
In this paper we are presenting the activities of the Medicina station in VLBI and GPS. We are also presenting the most recent results from the Bologna VLBI analysis centre on the European stations velocity. In this analysis we have used all VLBI experiments containing at least three European stations belonging to the European VLBI core network. With this selection we have analysed almost 90 24-hours VLBI experiments. We have produced global solutions using least mean squares, determining positions and velocities for all the fixed European stations. Noto station in southern Italy shows a movement of about 5 mm/yr to North, North East in respect to stable Europe, while Matera shows similar velocity with slightly larger bending toward East. Medicina shows a small North East displacement.
Vertical movements are also found: few mm/yr positive for Onsala, and few mm/yr negative for Medicina and Noto in respect to Wettzell. Due to the present uncertainties on the vertical component determination, no final conclusions can be drawn on this component, even if for Onsala a positive motion is expected according to post-glacial rebound, while subsidence is believed to be the reason of negative vertical displacement in Medicina.

## VLBI activity

During 1997 the 32m antenna of the Medicina Station takes part to 19 VLBI experiments related to Geodesy. These observations are co-ordinated by different agencies and are included in geodetic VLBI programmes like EUROPE, CORE, VLBA.
The main aims of the projects can be summarised as follows (see the experiment cover letters for more details). The purpose of the EUROPE experiments is to determine the station co-ordinates and their evolution in the European geodetic network with high precision. Six experiments are planned during the 1997. The participating stations are all located in Europe.
The Medicina antenna is involved in six bimonthly co-ordinated astrometric/geodetic experiments in 1997 together with the full VLBA and other stations able to record in VLBA format. Three agencies have geodetic VLBI programmes that can make use of the same data set: USNO, which will perform repeated imaging and correction for source structure. These sources will establish a set of core reference sources with known structure and precisely known positions. NASA, which will analyse these data to determine a high accuracy terrestrial reference frame. The VLBA stations showed high peculiar transverse velocities. They also exhibit anomalous vertical motions. NRAO, which will use these sessions to provide a service to the users who require high quality positions for small number of sources. The Medicina telescope takes part to one out of three Celestial Reference Frame experiments designed to improve the determination of the celestial reference frame in the Southern Hemisphere and to provide a different geometry than that usually available to the DSN.
In 1997, six CORE (Continuos Observations of the Rotation of the Earth) experiments in which the Medicina telescope is involved are planned. The purpose of these experiments is to provide additional data for comparison of EOP measurements. The stations that participate in the CORE network are asked to maintain high performance standards. The accuracy goals require that stations

instrumental constants are known. The CORE requirements for the instrumentation at the stations is as follows:
a) a flexible and automatic frequency change
b) a Mark IV terminal
c) a TAC for the station timing system
d) a daily acquisition of GPS signals
The Medicina station fits the CORE requirements. The tape drive is now able to record both, thin and thick tapes. A total of 40 thin tapes has been ordered for the geodetic pool of tapes. Moreover, the X-band receiver has now a bandwidth of 800 MHz. The IF3, which operates in the range 600-900 MHz, has been added to increase the existing IF bandwidth (100-500 MHz). The Mark IV DAS is under the Field System 9.3.15 control.
Aside to these 'pure' geodetic VLBI programmes, the Medicina Station joined a network of geodetic stations for astrometric measurements, co-ordinated by the NASA Goddard Space Flight Center and US Naval Observatory VLBI Group, of the Mars Pathfinder Lander. Three sessions of observations were organized for July 18th and 21st and for September 12th. The main goals of these observations are:
a) determination of the Martian Precession Constant;
b) determine the relativistic precession of the perihelion of Mars to a few parts per thousands;
c) determine the Martian Length of Day to about 1 millisecond.

**GPS activity**
It is worth to mention that the Geodetic group of the Istituto di Radioastronomia is involved in GPS campaigns in which the Medicina station represent a fundamental point. The two main projects are:
a) WHAT_A_CAT (West Hellenic Arc and Calabrian Arc Tectonic).
b) SELF II (Sea Level Fluctuations) devoted to the Mediterranean sea for the aim to disentangle the real vertical movement of the mean sea level, from crustal vertical movement of tectonic or antropogenic origin, and for better understanding the interaction between vertical mean sea level fluctuations and climate processes.
c) A Turbo Rogue is permanently operating at the Medicina stations and the data are collected by the Italian Space Agency (ASI) in Matera. These data will be soon used to improve the VLBI results.
In order to analyse the data from these campaigns, the 'Bernese' package has been implemented on the HP 715/50 workstation.

**European VLBI data analysis**
We are presenting here the results from all the geodetic VLBI experiments including at least three European stations. The very first run was in May 1987, while the last in December 1996. About the sixty per cent of the experiments are purely European, the others contain also US stations, and only a few of them also the station of Hartebeesthoek (South Africa Republic).
All the experiments are analysed with CALC/SOLVE software package (Caprette et al., 1990) running on the HP 715/50 of the Institute of Radioastronomy in Bologna, Italy.
Most of the database used in the analysis were correlated and produced by the Goddard VLBI group, while the other, especially those concerning European experiments from 1993, were correlated and produced by the geodetic group of the Rheinische Universitaet of Bonn.
All the data base have been reprocessed individually using cable correction when available. In a few cases we have noticed that the cable correction degraded the result of the solution, and therefore it was not used. The cable correction for Onsala station has always been applied, since a lack of this information results in a bias of the position of the antenna (Ragne Carlsson, 1996).

The atmosphere and short period clock variations have been estimated using a piece wise linear function in segments of one hour. The reference station for position and clock is Wettzell, whenever this station is available. In very few cases, when this station was not available in the solution, another European station was used.
The complete set of data base has been processed with the batch programme GLOBL of the CALC/SOLVE package, in order to produce relative and total velocities of the antennas composing the network. GLOBL uses a least mean square procedure in which the position of the antennas at different epochs can be considered both global or arc parameters. In the first case this means that data of each daily experiment (arc) are to be considered as a whole in producing the velocities results, while in latter case the positions are estimated independently for each experiment. The first kind of solution is referred to as velocity solution, the second one as baseline solution. We have produced both kinds of solutions that are discussed in next section.

**Results**

The results are presented in tables 1, 2 and 3. Table 1 shows the longitudinal component of the baseline vector for all the stations composing the VLBI core network. The errors associated to baseline rates are less then a fraction of mm/yr. For baseline involving the "new" station of Ny Alesund and Simeiz we face different formal errors, sometime greater of one or even two order of magnitude then those of the most studied baselines. Especially the errors involving the station of Simeiz in Crimea are higher then any other and this leads to the consideration that the quality of data acquired at this antenna has to be improved. A general evaluation of results allows us to say that, considering previous baseline results, the general trend is confirmed.

| | Madrid | Matera | Medicina | Noto | Ny Alesund | Onsala | Simeiz | Wettzell |
|---|---|---|---|---|---|---|---|---|
| | mm/yr | mm/yr | mm/yr | mm/yr | mm/yr | mm/yr | mm/yr | mm/yr |
| Effelsberg | 0.3 ± 0.7 | -2.2 ± 1.3 | -2.6 ± 0.6 | -1.9 ± 2.9 | 1.2 ± 3.5 | 2.6 ± 0.8 | - | -0.5 ± 0.6 |
| Madrid | | 1.6 ± 0.5 | 2.1 ± 0.3 | -1.9 ± 0.4 | -0.6 ± 3.2 | -0.2 ± 0.4 | -3.3 ± 13.5 | -0.1 ± 0.3 |
| Matera | | | -2.5 ± 0.4 | 0.8 ± 0.5 | 0.4 ± 2.4 | -3.9 ± 0.7 | -10.3 ± 6.5 | -3.6 ± 0.5 |
| Medicina | | | | -3.7 ± 0.4 | -5.6 ± 0.9 | -2.0 ± 0.4 | -16.2 ± 12.2 | -2.3 ± 0.3 |
| Noto | | | | | -3.5 ± 3.4 | -4.7 ± 0.5 | -3.8 ± 12.1 | -5.0 ± 0.3 |
| Ny Alesund | | | | | | 1.0 ± 3.0 | 1.8 ± 9.0 | -0.6 ± 3.7 |
| Onsala | | | | | | | -4.0 ± 5.7 | -0.6 ± 0.2 |
| Simeiz | | | | | | | | -3.2 ± 7.3 |

**Table 1: baseline results**

The solutions produced via global velocity solution are shown in table 2 and 3, respectively for total and relative velocities, where the reference system is stable Europe, i.e. Wettzell fixed to NNR-Nuvel-1A model (Argus et al., 1991), and units are mm/yr. The azimuth angle is calculated clockwise in degrees from North. Figures 1 and 2 show horizontal velocity vectors and correspond to data contained in table 2 and 3 respectively.
Considering the results obtained for the horizontal relative velocity vector of table 3, the three Italian stations and Effelsberg show motions in perfect agreement with the results obtained from previous analysis. The Noto station shows an horizontal motion toward northern direction with a rate of 4.6 mm/yr. If we consider African plate motion in the NNR Nuvel 1A model, Noto residual velocity is 3.5 mm/yr with a direction of 144 deg..
Matera station shows a velocity of 5.7 mm/yr and a direction of 28 degrees. The two station seem to move slowly away as confirmed from the result of baseline solution (see tab. 1), even if with slightly lower velocity than in previous calculations. Probably Matera's movement is representative of the Adriatic block.

Medicina shows a velocity almost half of the Matera one: 2.5 mm/yr with a direction of 58 degrees from North, rotated of 28 degrees clockwise respect to the one of Matera.

| | Effelsberg | Madrid | Matera | Medicina | Noto | Onsala | Ny Alesund | Simeiz |
|---|---|---|---|---|---|---|---|---|
| azimuth (degrees) | 55.1 ± 0.3 | 53.1 ± 0.2 | 54.5 ± 0.2 | 56.7 ± 0.2 | 52.3 ± 0.2 | 54.5 ± 0.2 | 34.9 ± 1.7 | 66.8 ± 1.5 |
| Total horizontal vector (mm/yr) | 24.4 ± 0.1 | 25.7 ± 0.1 | 31.7 ± 0.1 | 28.5 ± 0.1 | 30.0 ± 0.1 | 23.0 ± 0.1 | 15.4 ± 0.5 | 32.5 ± 0.7 |

**Table 2: total velocities results**

Effelsberg shows a slow motion (1.1 mm/yr) with 170 degrees direction. Monitoring the relative movements of Effelsberg and Wettzell could help in understanding the phenomena that are believed to interest that part of continental Europe: a shallowing of continental crust that might prelude to the formation of a rift valley.

| | Effelsberg | Madrid | Matera | Medicina | Noto | Onsala | Ny Alesund | Simeiz |
|---|---|---|---|---|---|---|---|---|
| azimuth (degrees) | 171.3 ± 7.6 | 132.2 ± 3.8 | 28.8 ± 1.3 | 56.9 ± 1.9 | 7.1 ± 1.1 | 251.7 ± 6.1 | 251.7 ± 6.1 | 55.3 ± 8.7 |
| Horizontal velocity (mm/yr) | 1.1 ± 0.2 | 1.4 ± 0.1 | 5.7 ± 0.1 | 2.5 ± 0.1 | 4.6 ± 0.1 | 1.2 ± 0.1 | 5.0 ± 0.4 | 5.5 ± 0.7 |
| Vertical velocity (mm/yr) | 2.1 ± 0.8 | 2.3 ± 0.4 | 1.2 ± 0.6 | -3.0 ± 0.4 | -2.8 ± 0.4 | 3.4 ± 0.3 | 7.6 ± 1.8 | -6.2 ± 3.9 |

**Table 3: relative velocities results**

Ny Alesund velocity seems to be well characterised and shows a movement of 5 mm/yr in an East south-east direction. Even if the Norwegian antenna started to operate simultaneously with the Crimea one, there are more data available and this leads to more reliable results. Onsala presents a small velocity probably connected to the horizontal crustal deformation caused by post glacial rebound. Madrid starts to show a small movement toward East south-east with a direction calculated in almost 130 degrees.

| | Medicina | Onsala | Madrid | Noto | Matera | Effelsberg | Simeiz | Ny Alesund |
|---|---|---|---|---|---|---|---|---|
| azimuth (degrees) | 23.0 ± 2.1 | 175.1 | 229.4 ± 13.3 | 354.2 ± 1.1 | 341.2 ± 1.7 | 191.2 ± 9.0 | 256 ± 20 | 218 ± 7 |
| Horizontal velocity (mm/yr) | 2.0 ± 0.1 | 0.4 ± 0.1 | 0.3 ± 0.1 | 4.5 ± 0.1 | 3.7 ± 0.1 | 0.9 ± 0.2 | 2.4 ± 0.7 | 3.6 ± 0.5 |
| Vertical velocity (mm/yr) | -3.3 ± 0.3 | 0.0 | 1.3 ± 0.3 | -3.2 ± 0.4 | 2.3 ± 0.5 | 1.5 ± 0.7 | -3.2 ± 3.8 | 8.4 ± 1.8 |

**Table 4 : relative velocities with direction Onsala to Wettzell fixed**

Looking in details into the general behaviour of the horizontal velocity vectors on figure 2, it is possible to detect a rotation of the reference system. That is visible in particular for Ny-Alesund and Crimea, but it is also clear for Onsala, Effelsberg and Madrid. For the Italian stations the situation is

not so clear. In order to check this suggestion we have tried a new global velocity solution, adding a new constrain: in addition to Wettzell fixed to NNR Nuvel 1A model, we have also considered the direction Onsala to Wettzell fixed to the same model. In this reference system Onsala can only move along the direction to Wettzell, and any vertical or transverse component will be cancelled. The results for this solution are presented in Table 4 as velocities relative to the model, and the same data are visible in figure 3. In this reference system Onsala velocity disappears, as expected, but also the Effelsberg and Madrid velocities disappear as well. Moreover for NyAlesund and Crimea (Simeiz) stations the discrepancy with NNR Nuvel 1A model has been reduced. For the Italian stations the most visible effect is a rotation of the direction of the velocity vectors.
Results obtained for vertical motions can be discussed with a relative grade of confidence only for a few stations. First of all we can underline that the results show a general decrease of the errors associated with the previous calculations (Nothnagel et al., 1994, Tomasi e Negusini, 1996). We still suspect, anyway, that some biases originated by an incomplete parametrization of the troposphere could be present. Onsala and, even more, Ny Alesund show an uplift that can probably be connected to the post glacial rebound interesting the Fennoscandian area, even if the amount of this uplift is probably too large. However it should be pointed out that these are results relative to Wettzell.
Medicina shows a negative vertical motion of 3.0 mm/yr. It should be noticed that the Po valley and the area between Bologna and Ravenna present a subsidence at a rate of 5 to 10 mm/yr in the last 20 years. This fact was due to gas and water extraction that is certainly decreasing nowadays.
Noto presents a similar behaviour for vertical motion, but no such causes as those given above can be taken into consideration. This motion could be of tectonic origin.

**Conclusion**

The data set available for processing and producing VLBI geodetic data permits nowadays to reach an accuracy of the fraction of millimetre per year for horizontal relative velocities and of the order of millimetre per year for vertical displacements rates. The intensity and direction found with this work seem to be in good agreement with previous analysis except for a few cases. The difference in velocity between Matera and Noto is substantially confirmed even if a decrease in intensity of relative motion between them should be underline. Southern Sicily might be part of a separate microplate thus complicating the tectonic scenario in that area (Mantovani et al., 1995).
The motion of Medicina at half the rate of Matera provides new evidence for the behaviour of the Adriatic microplate, which could show a rotation and also suffer plastic deformation due to compressional stress generated by the subducting African plate (Heki, 1993).
Effelsberg is showing a small horizontal displacement when compared to Wettzell: this leads to the consideration that it might not be on stable Europe. Ny-Alesund results are now to be considered as good as those of the other older stations belonging to the network. Results from Crimea station, considering the short time span of the observations, are certainly of lower quality, presenting a data scatter about an order of magnitude larger then the other European stations. This is possibly due to the fact that the hydrogen maser is switched of between different observations, causing a lack of stability both in frequencies and clock.
Considering different constraints in the solution, we cannot rule out the presence of a small rotation of the reference system. If this is real, the discrepancy between model and results, will be reduced. However, this fact has to be investigated in the near future.
For the first time we have valid information on the vertical component of the velocity. Onsala uplift is probably caused by post glacial rebound, while Medicina subsidence is probably of antropogenic origin and Noto subsidence is most likely of tectonic origin.
Even if more work is needed, in particular for the vertical component, a complete scenario for the present day crustal motions in the Mediterranean region is now about to emerge.

## References

Argus, D.F., Gordon, R.G.: No-Net-Rotation Model of Current Plate Velocities Incorporating Plate Motion Model NUVEL-1, Geophysical Research Letters, Vol.18, p.2039-2042, Nov. 1991.

Campbell, J.: The European Geodetic VLBI Network - Status Report. Proceedings of the 8th Working Meeting on European VLBI for Geodesy and Astrometry: Dwingeloo, The Netherlands, June 13-14, 1991; Report MDTNO-R-9243, Survey Departement of Rijkswaterstaat, p. IV-22, Delft 1991.

Campbell, J., Hase, H., Nothnagel, A., Schuh, H., Zarraoa, N., Rius, A., Sardon, E., Tornatore, V., Tomasi, P.,: First Results of European Crustal Motion Measurements with VLBI; AGU Geodynamics Series, Vol.23, Contribution of Geodesy to Geodynamics: Crustal Dynamics, ISBN 0-87590-523-4, AGI Washington, 1993.

Caprette, D., Ma, C., Ryan, J.W.,: Crustal Dynamics Project data analysis - 1990, NASA Tech. Mem. 100765, Goddard Space Flight Center, Greenbelt, Md., 1990.

Heki, K.: Temporal Change of Terrestrial Reference Frame: Theory and Observation; Proceedings of the International Workshop for Reference Frame Establishment and Technical Development in Space Geodesy, iRiS'93, Communications research Laboratory, Tokyo, p.19-26, January 18-21, 1993.

Mantovani, E., Albarello, D., Tamburelli, C., Viti, M.,: Annali di Geofisica. Vol. XXXVIII, N. 1, 1995.

Nothnagel, A., Tomasi, P., Campbell, J.: Station Displacements in Italy Determined with VLBI, 1st Turkish International Symposium on Deformation, Sept. 1994, Istanbul.

Ragne Carlsson, T.,: Site Dependent Error Sources in Geodetic Very Long Baseline Interferometry, Technical report N. 224L, Chalmers University of Technology, Goteborg, 1996.

Tomasi, P.: More on European station Velocity; Proceedings of the IX Working Meeting for Geodesy and Astrometry, Campbell, J. and Nothnagel, A. editors, p.194, 1994.

Tomasi, P., Negusini, M.: South-western Europe deformation measured with VLBI

Tomasi, P., Negusini, M., Campbell, J., Nothnagel, A., Ryan, J.W.: Recent Results from European Geodetic VLBI; Proceedings of the 6th General Assembly of Wegener - St. Petersburg, Pearlman, M. editor, p. 344-366, 1995.

Zarraoa, N., Rius, A., Sardon, E.: Relative Motions in Europe Studied with a geodetic VLBI network, Geoph. Journ. Int., 117, p.763-768, 1994.

## Figures caption

**Figure 1:** Total horizontal velocity vectors (black arrows). Velocities predicted by Nuvel-1A model are also shown. For Italian stations both prediction for African and European velocities given by the same model are shown.

**Figure 2:** Relative horizontal velocities with respect to stable Europe (Wettzell fixed to Nuvel-1A model). Italian stations show residuals calculated both considering an European (black arrows) and an African (red arrows) behaviour.

**Figure 3: :** Relative horizontal velocities with respect to stable Europe (Wettzell fixed to Nuvel-1A model and Onsala - Wettzell direction also fixed to the same model) . Italian stations show residuals calculated considering an European behaviour.

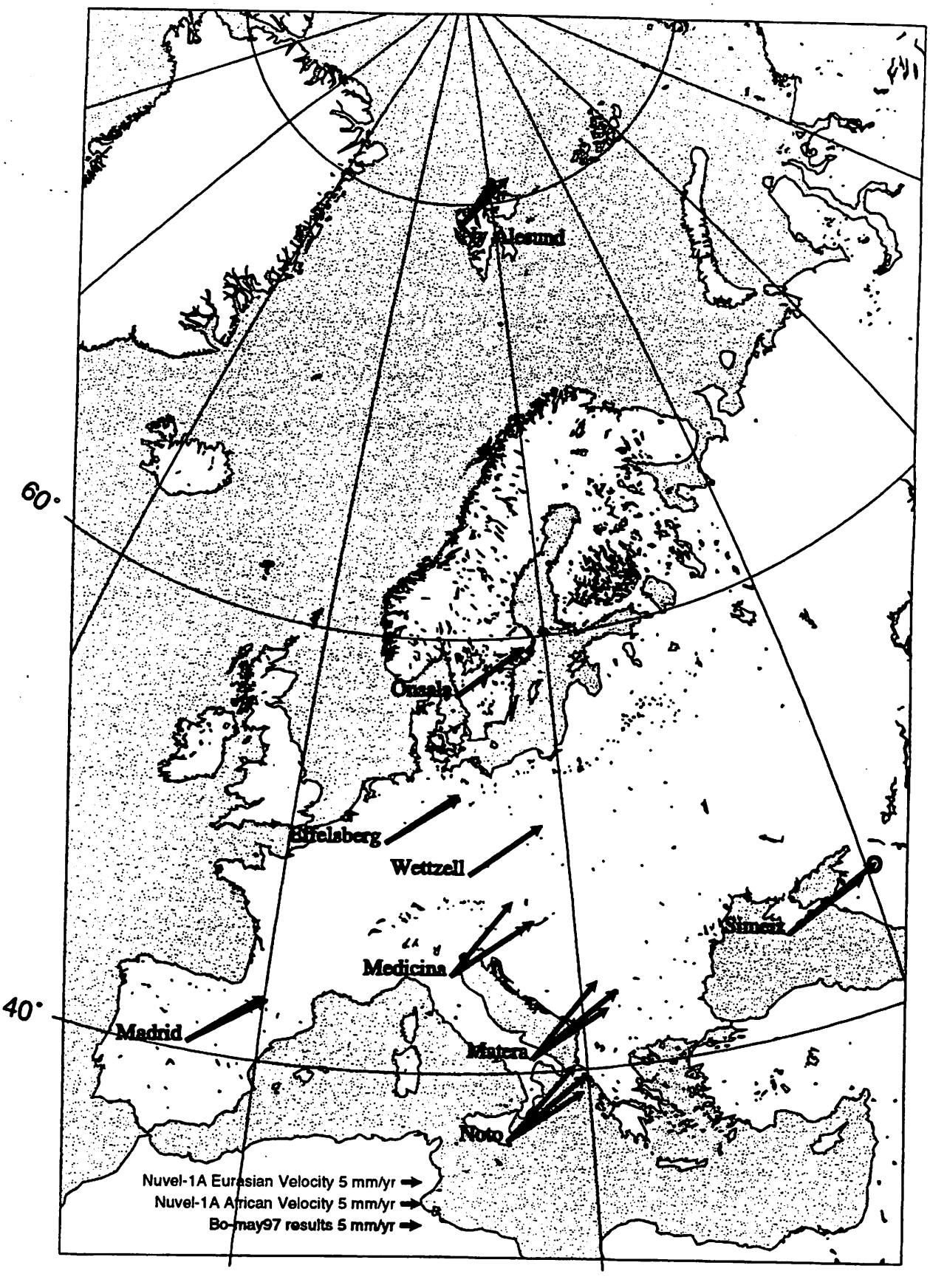
Ny Alesund
Onsala
Eifelsberg
Wettzell
Medicina
Matera
Noto
Madrid
Simeiz
60°
40°
Nuvel-1A Eurasian Velocity 5 mm/yr
Nuvel-1A African Velocity 5 mm/yr
Bo-may97 results 5 mm/yr

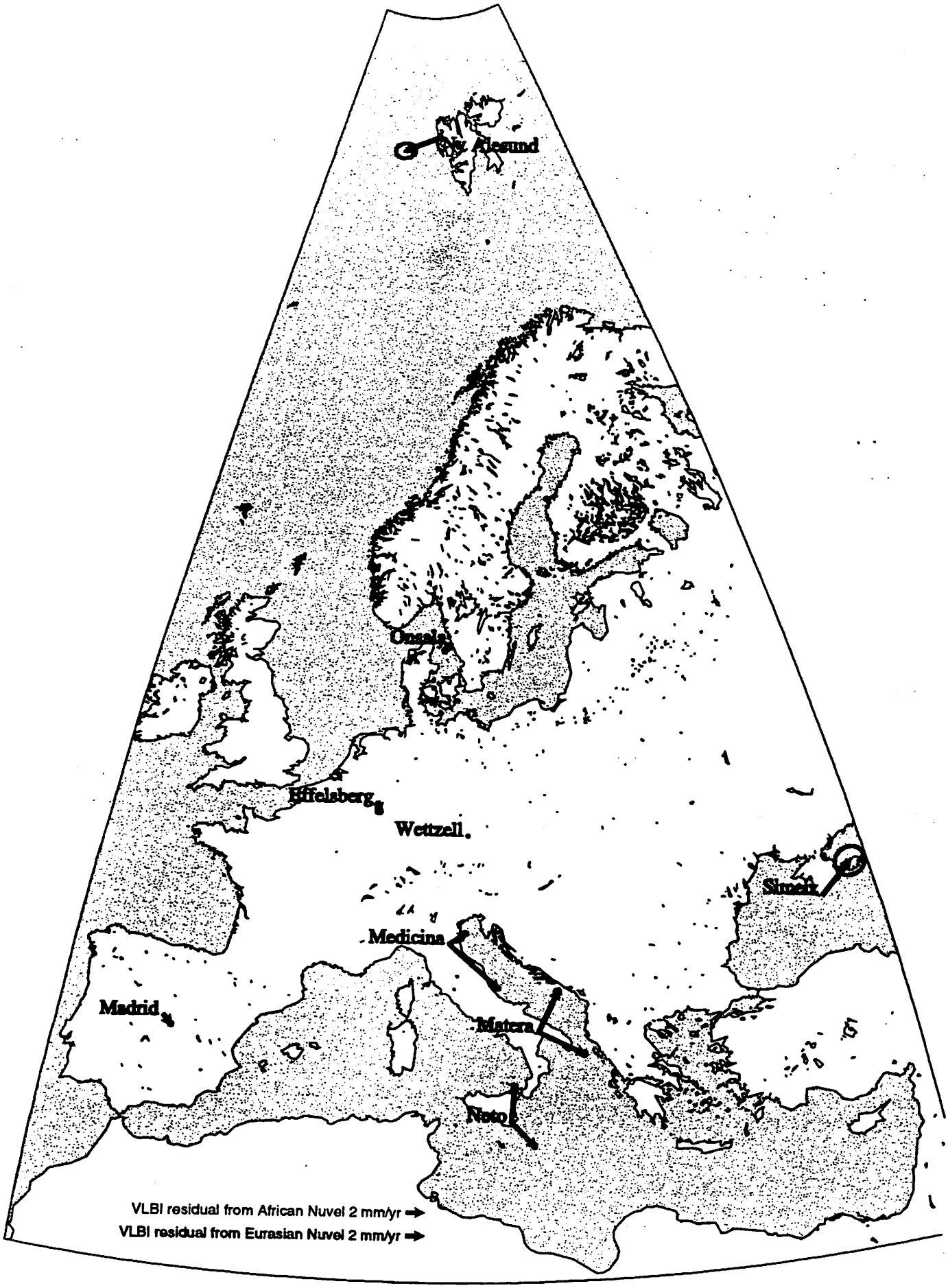
Ny Alesund
Onsala
Effelsberg
Wettzell
Simeiz
Medicina
Madrid
Matera
Noto
VLBI residual from African Nuvel 2 mm/yr
VLBI residual from Eurasian Nuvel 2 mm/yr

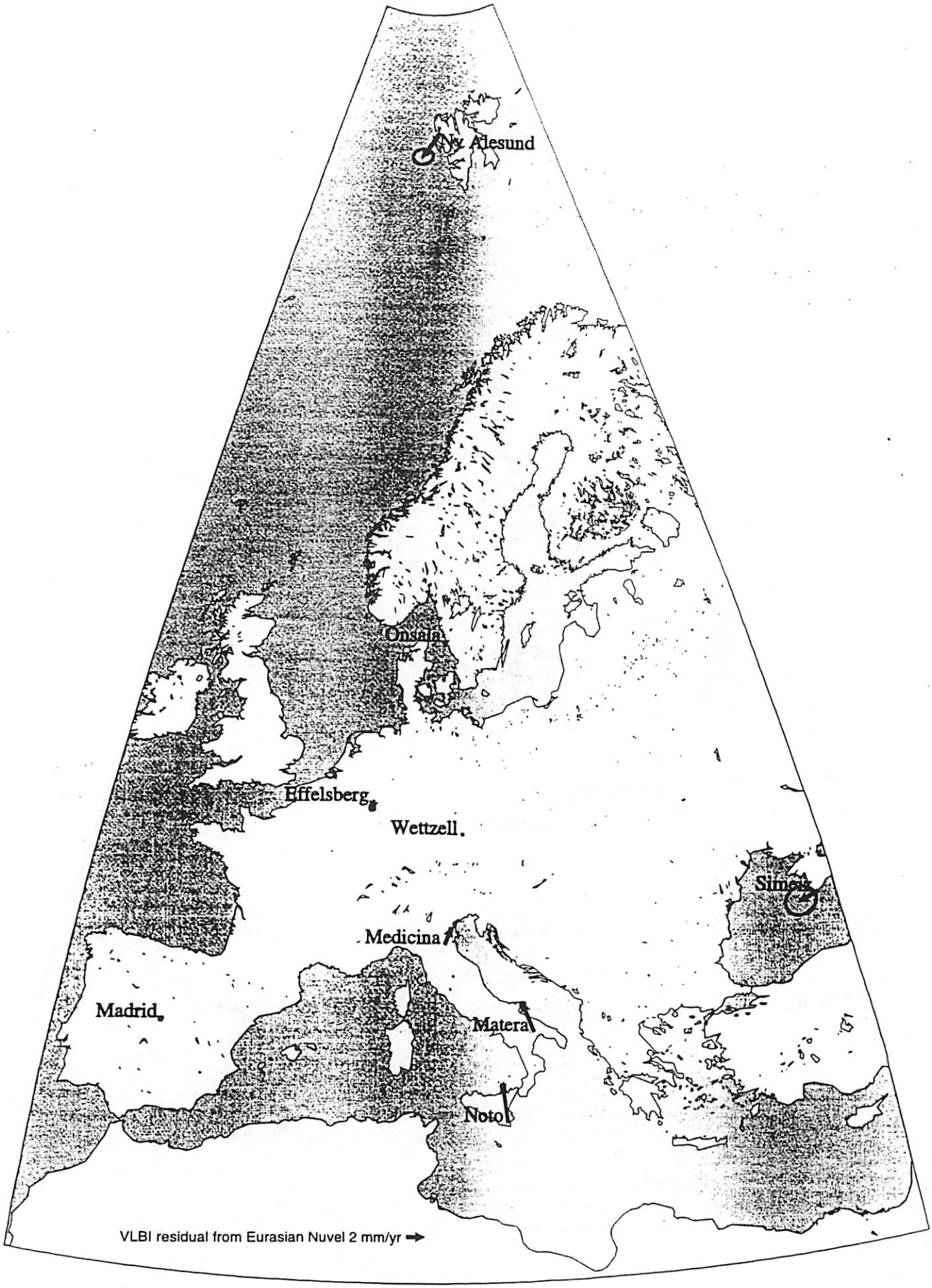
Ny Alesund
Onsala
Effelsberg
Wettzell
Medicina
Madrid
Matera
Noto
Simeiz
VLBI residual from Eurasian Nuvel 2 mm/yr

# Vertical site motion

## Geodynamic studies at Onsala Space Observatory

Hans-Georg Scherneck Jan M. Johansson Rüdiger Haas
T. Ragne Emardson

Chalmers University of Technology
Onsala Space Observatory
*S-439 92 Onsala, Sweden; hgs@oso.chalmers.se; Telefax +46 (31) 772-5590*

## Abstract

Geodynamic studies at Onsala Space Observatory currently pays special attention to the determination of vertical motion. The interest arises primarily as space techniques provide the necessary tools to separate the motions of the crust from variations of sea level. The sine qua non of such investigatons is a firm control of the global reference systems. We demonstrate some of the current weaknesses but also try show that GPS and VLBI can complement each other in achiving sufficiently high regional resolution together with global consistency.

We demonstrate the sensitivity of GPS by analyzing air pressure loading and tidal loading effects. First solutions look promising.

The vertical component in both VLBI and GPS is susceptable to atmospherical effects. We show results from atmospheric pressure loading as well as comparison from GPS based troposphere wave delay measurement with radiosonde data taken at Ny Ålesund.

## 1 Introduction

Vertical site motion in Europe shows, besides tectonic features in the Alpine region, predominant patterns believed to be caused by the isostatic rebound in response to the unloading of the pleistocene ice shield that vanished 10,000 years ago. The major interest in determining crustal vertical motion with space techniques arises since these methods work independently from the current sea level. Thus, by tying tide gauges into the network, residual sea level movement possibly relating to current melting of ice shields and global warming can be detected.

This is the ambition that drives the BIFROST project (BIFROST, 1996). Since summer 1993, more than twenty GPS stations have been operated continuously and data has been analyzed on a daily bases to provide 3-D determinations of site positions in a global reference frame. The regional station network comprises the SWEPOS

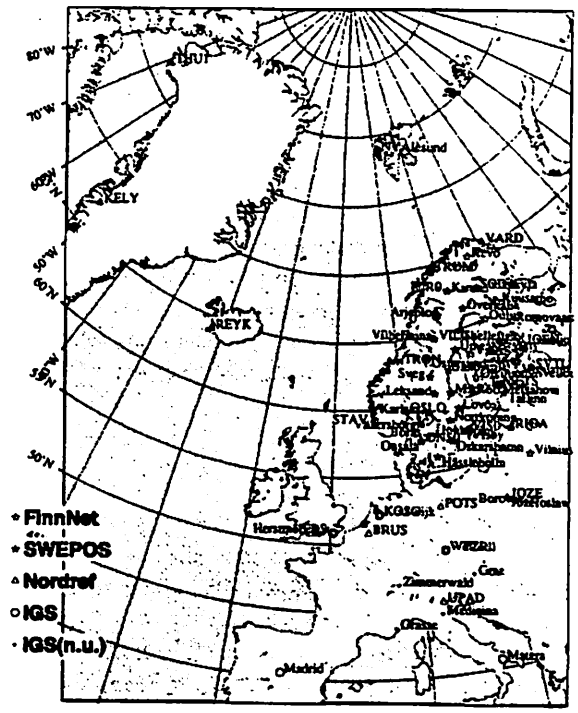


Figure 1: *GPS networks analyzed for Bifrost (SWEPOS, FinnNet, IGS) and EUREF (Nordref)*

GPS stations in Sweden, a joint effort of the National Land Survey of Sweden and our department, and since August 1996 also stations in the FinnNet network in Finland (12 stations). Data analysis is carried out with GIPSY (Webb and Zumberge, 1993)

Since 1996 Onsala Space Observatory functions as a regional processing centre for the European Reference Frame (EUREF). The contributed network NORDREF is spatially wider with stations as far as Greenland, but less dense. In accordance with the EUREF standards it is analyzed with Bernese Software (Rotacher et al., 1993). The networks are shown in Fig. 1.

The discussion in this presentation will focus on one of the primary goals of this project, the vertical sea level rates. As an exposé of the existing problems a preliminary result is shown in

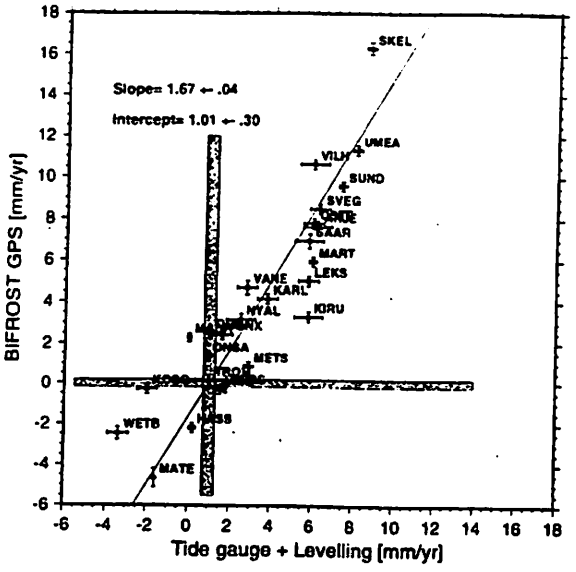


Figure 2: *Vertical rates from BIFROST GPS versus land emergence rates from tide gauge and precise levelling. Preliminary result shows unconvincingly large slope. A deviation from a unity slope is expected due to the rebound of the geoid; however, models suggest that geoid rebound in excess of 0.1 of the land emergence is unrealistic. The problems are discussed in the text.*

Fig. 2. The present flaws and shortcomings to be mentioned are mainly twofold. First, the intercept of the regression line between observed sea level (Ekman, 1996) and observed GPS vertical rates, which is indicative of a global change in sea level, is easily biased by a common mode of GPS site motion along a geocentric radius vector through the geographical centre of the region. In this way, the determination relies on the realisation of the geocentre at the stage of orbit modelling. Second, the slope of the regression line is indicative of the rebound of the geoid. (If tide gauges would detect a subsidence of the sea level with a systematic geographic pattern, but the GPS stations would not observe any vertical uplift, the change would solely reflect a gradual decrease of the gravity potential.) Model computations suggest a geoid uplift in the area scaling with land emergence at a ratio of at maximum 0.06 according to Ekman and Mäkinen (1996) or, alternatively, 0.08 according to the model used in Mitrovica et al. (1994). The regression slope corresponding to the 1:10 ratio is 1.09. The slope found in Fig. 2 is substantially larger. If not at a vastly unrealistic geoid rebound, this figure hints at a tilting of the reference frame. As long as this weekness cannot be cured, the resulting intercept of the regression line should not be interpreted in a physical context.

The data processing and analysis leading to this result are described in more detail in Scherneck et al. (1997). Data analysis proceeds in the nonfiducial approach (Heflin et al. 1992). The satellite orbits information used in the analysis is the combination product provided by the IGS.

In the nonfiducial method data is collected at reference stations (in the present case European sites operating for the IGS network), and analyzed together with the regional observations with loose constraints on the reference station positions. The results are mapped into an evolving frame given by the reference positions and motions as manifest in the ITRF files. This provides a daily series of site positions in the adopted frame.

To obtain station velocities, linear slopes versus time are estimated from the daily solutions in an additional stage following the mapping. Here, the rate of a purely corotating rigid frame at the respective station are subtracted by means of a three-parameter fit to the reference site velocities. By this the tectonic plate velocity is suppressed. Nonzero velocity in this frame is predominantly due to crustal deformation. Larson et al. (1997) suggested to estimate the rates on the basis of the unconstrained solutions and rather constrain the resulting velocities with respect to the ITRF station velocities. The advantage is less sensitivity to data degradation or outages at reference stations. We need to test their procedure in the presence of a suite of "discontinuous" ITRF's implicit in the orbits to check whether this offers an advantage as to unbiased vertical rate estimates.

## 2 Reference system consistency over the years

The major caveat of the project is the inconsistency and other limitations implied by the reference systems. Reference system information is used (1) for the mapping of the sites and (2) for orbit computation. Determination of vertical rates relies heavily on the stability of the geocentre (more precisely: its realisation at the stage of orbit computation). Aiming at consistent results would require to map estimated site coordinates into the same reference system to which the associated orbits relate. However, the accuracy of reference information generally improves over the years, which favours recent issues like those from IERS/IGN, Boucher et al. (1996, 1994). An alernative product can be obtained from JPL (Zumberge et al., 1997; Heflin, 1997).

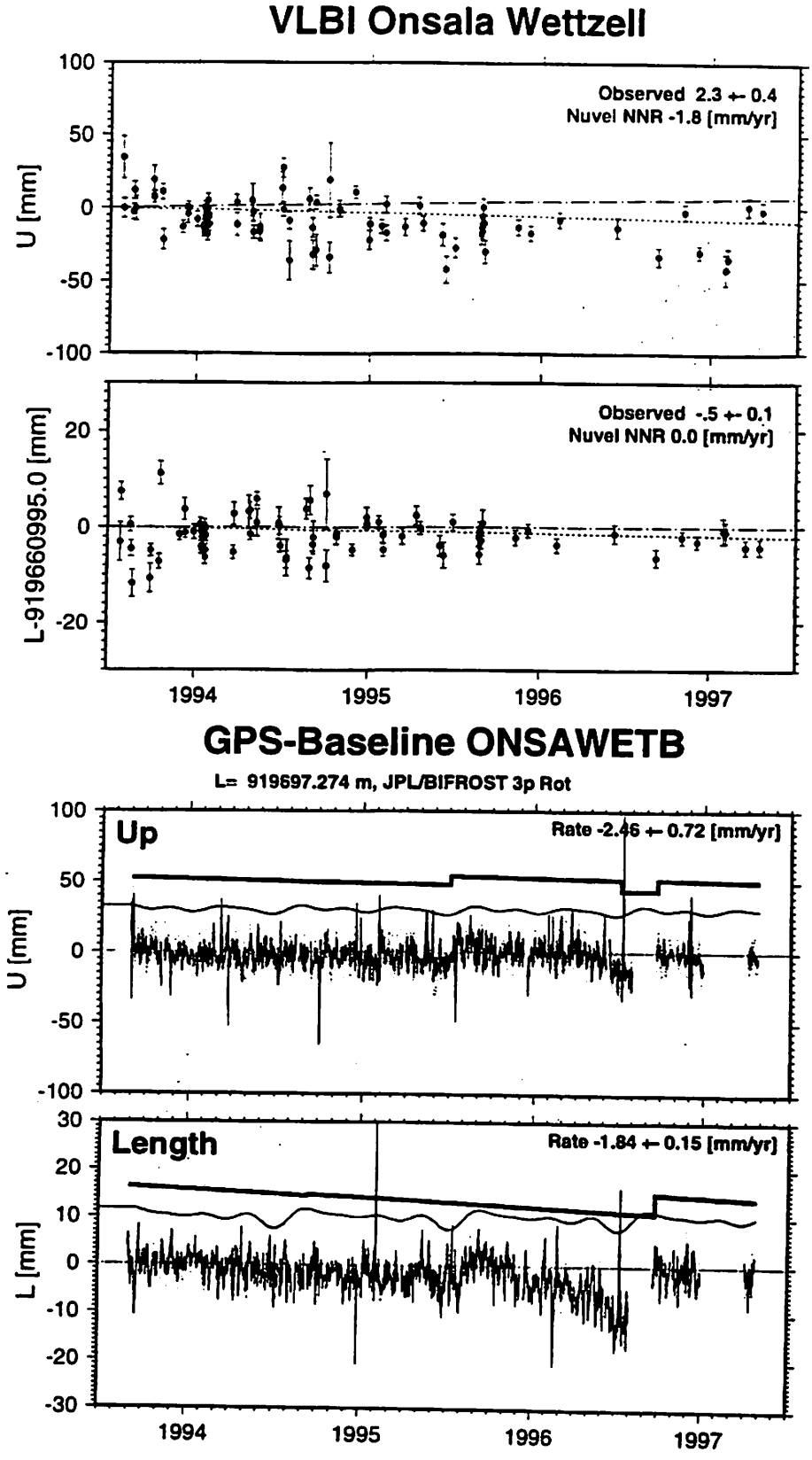


Figure 3: *Comparison of up-components determined with VLBI (top) and GPS (below) during the same range of years. To the GPS data we fit a persistent trend, a series of box-cars with offsets occurring at times of antenna/radome rearrangements, and an annual/seasonal harmonics series to account for solar heating or snow cover cycles. Notice the anomalous drift in the GPS vertical, which occurred due to receiver problems at Wettzell, starting in spring 1996, particularly in the length component. The VLBI determinations are so sparse in time that they do not exclude a similar behaviour.*

Fortunately, these two options are not mutually exclusive. One can compensate for the inconsistency indirectly introduced through the GPS orbits by subtracting the relative rotations and translations between the earlier ITRF's and the latest, pricipal frame.

Inspecting the vertical components implied by the ITRF motion parameters we find several problems:

- large differences within the same ITRF although there is no indication of tectonic motion;
- large differences at individual stations between different issues;
- the ensemble average of all European stations shows significantly different rates from issue to issue.

Inconsistencies on a per-station basis could could reflect monumentation problems as well as estimation errors or insufficient data. On top of these inconsistencies, the stability of GPS measurements at reference stations has not always been acceptable. Stations have temporarily been taken out of service, and even so important sites as Wettzell have had stability problems going on for months. Thus, a drift in network solutions can have three different origins, bad ITRF velocities, bad GPS data, and inconsistently handled reference systems. The former two are totally out of our control whereas we can mitigate the latter to some extent.

## 2.1 VLBI support for vertical reference stability

What can VLBI contribute to achieve consistent reference systems ? The importance of the geocentre realisation would exclude VLBI from the techniques that could solve the problem directly because of its translational invariance. On the other hand, the mean vertical station motion in Europe can be compared with VLBI solutions that are mapped into the ITRF since there is sufficient global coverage to avoid that the European bias swamps both VLBI and IGS-GPS. In Table 1 we show for comparison two TRF's, the JPL-GPS frame, the official (mapped) GSFC-VLBI results 1083c (Ma et al., 1997), and a "quick-and-dirty" result obtained from

$$\dot{r}_i = \frac{1}{N} \sum_{j \neq i} \dot{b}_{ij}$$

where

$$b_{ij} = r_i - r_j$$

assuming that

$$\sum_j \dot{r}_j = 0$$

Comparing with VLBI the table indicates that Heflin's vertical rates in Europe are slightly high, peaking at Onsala with an unconvincing 4 mm/yr, whereas all issues of IERS/IGN/ITRF show rates on the negative side, where Wettzell is stated to have considerable subsidence. Both issues ITRF93 and ITRF94 specify subsidence for Onsala.

The vertical rate determined from BIFROST GPS at Ny Ålesund, a station which has no rate in the ITRF93 and 94 because of its short history, compares well with refined tide gauge analysis by Breuer and Wolf (1995) who specify a land emergence rate (uplift relative sea level corrected for eustasy) of 2.5 ±0.7 mm/yr. The choice of reference frame in the BIFROST analysis turns out as uncritical; only a tendency towards higher rates with ITRF93 and ITRF94 is seen. Svalbard has been glaciated in the Pleistocene and is expected to rebound in a similar way as Fennoscandia, though in a smaller lateral scale. The GSFC solution 1083c specifies a negative rate, while the simple baseline summation displays insignificant motion.

The small reference frame effect on the Ny Ålesund vertical rates and the realism in the result are difficult to reconcile with the high rates found in the Gulf of Bothnia region.

Comparison of the baseline time series for Onsala-Wettzell, VLBI vs. GPS, shown in Fig. 3 exhibits a receiver problem at Wettzell during summer 1996. We notice the less frequent joint VLBI experiments after 1995. However, the joint VLBI experiments between the two stations have become so sparse after summer 1995 that a hypothesis of real site motion could not easily be dismissed on the basis of these results alone. The receiver problems have had a destabilizing effect on the day-to-day GPS network solutions in the form of transient signatures during that time period.

# 3 Vertical motion due to crustal loading

Using global fields of air pressure data at six hours interval we have computed a series of predicted loading displacements for most VLBI experiments since August 1993 and a large number of GPS stations in Scandinavia and for important ones in the rest of Europe. While all 3-D

Table 1: *Vertical rates in mm/yr in different international reference frames at European VLBI/GPS colocated stations, and determinations of vertical rates from BIFROST GPS. The column labeled VLBI(Ma--) is from the NASA-GSFC solution 1083c (Ma et al., 1997). Also shown is a simple, frame-independent estimate using global means over all baselines to the site in question (hgs). The mean values of the columns are compared as indicated by the arrow symbols.*

*The lower part of the table shows the BIFROST GPS result for Ny Ålesund mapped into each of the three different reference frames. The other station results are shown for the JPL frame only.*

| | Dome | Site | JPL(Heflin) | ITRF93 | ITRF94 | VLBI(hgs) | VLBI1083c(Ma--) |
|---|---|---|---|---|---|---|---|
| 1 | 13504M003 | KOSG | 1.8 | -2.4 | -0.8 | | |
| 2 | 13407S012 | MADR | 3.6 | 1.0 | 2.4 | 5.7 +-1.8 | 2.3 +-0.6 |
| 3 | 12734M008 | MATE | -0.5 | -4.9 | -1.7 | -2.3 +-0.7 | -1.1 +-0.5 |
| 4 | 10503S011 | METS | 6.7 | -0.2 | 0.2 | | |
| 5 | 10402M004 | ONSA | 4.5 | 1.9 | -1.1 | 1.0 +-0.5 | 2.0 +-0.2 |
| 6 | 10302M003 | TROM | 2.0 | -0.5 | -0.4 | | |
| 7 | 14201M009 | WETT | | -4.1 | -4.0 | -1.7 +-0.3 | -1.6 +-0.1 |
| 8 | 14201M010 | WTZR | -2.6 | -4.1 | -3.4 | | |
| | | | <== -2.9 ==> +-0.8 | | | | |
| | | | <========== | -1.6 ==> +-0.7 | | | |
| | | NYAL | | | | 0.7 +-1.0 | -1.0 +-0.6 |
| | Bifrost | NYAL | 2.8 +-0.6 | 3.1 +-0.8 | 3.1 +-0.8 | | |
| | | KOSG | 0.9 +-0.5 | | | | |
| | | MADR | 1.5 +-0.4 | | | | |
| | | MATE | -1.4 +-0.5 | | | | |
| | | METS | 4.6 +-0.5 | | | | |
| | | ONSA | 4.3 +-0.5 | | | | |
| | | TROM | 1.0 +-0.6 | | | | |

components can readily be predicted, the primary effect is found in the vertical with maximum displacements exceeding 10 mm. In that component the loading effect is largely proportional to local pressure with an admittance coefficient typically between -0.3 and -0.6 mm/hPa. In the course of 24 hours, deep water yields to the pressure in the so-called inverse barometer response, while shallow waters and basins require longer time scales to dissipate the excess mass. The land/sea coverage of the regional area, the spatial scale of pressure disturbances, and the dynamics of the water bodies in this order are responsible for a deviation of the admittance coefficient from a frequency-independent value. It may be as large as -0.8 mm/hPa like in the case of continent-scale anticyclones like those regularly parking over Russia and Siberia during winter.

Using global load convolution methods on realistic land/ocean grids with Green's loading functions (Farrell, 1972), admittance coefficients for each station can be computed from long time-series of predicted loading effects versus local pressure. If the predictions give successful noise reduction during a test epoch, the coefficient can be used henceforth on local pressure measurements since they might be more easily available. See Haas et al. (1997) for more details and references.

The global pressure fields and the load convolution method at the "uncooked" stage offer several advantages. First, 3-D displacements are computed; second, unusual pressure distributions can be handled; third, the method can be extended to incorporate hydrodynamic models of water bodies and thus to compute the combined and explicitly time-dependent ocean/land response.

In previous determinations from GPS data, van Dam et al. (1994) found very low correlation between predicted displacements and JPL solutions of GPS observations in northern Europe despite the fact that the pressure variations there are relatively large and rapid. Somewhat greater impact is found in VLBI data (van Dam and Herring, 1994; Haas et al., 1997).

In spite of using 1300 daily solutions of BIFROST GPS data, a clear correlation between day-to-day vertical position variations and predicted displacement has not been found at a significant level.

Recently we have used results from single-point positioning analysis at four stations, Mauna Kea (Hawaii), Reykjavik, Onsala, and Sundsvall (central Sweden). Sundsvall had the

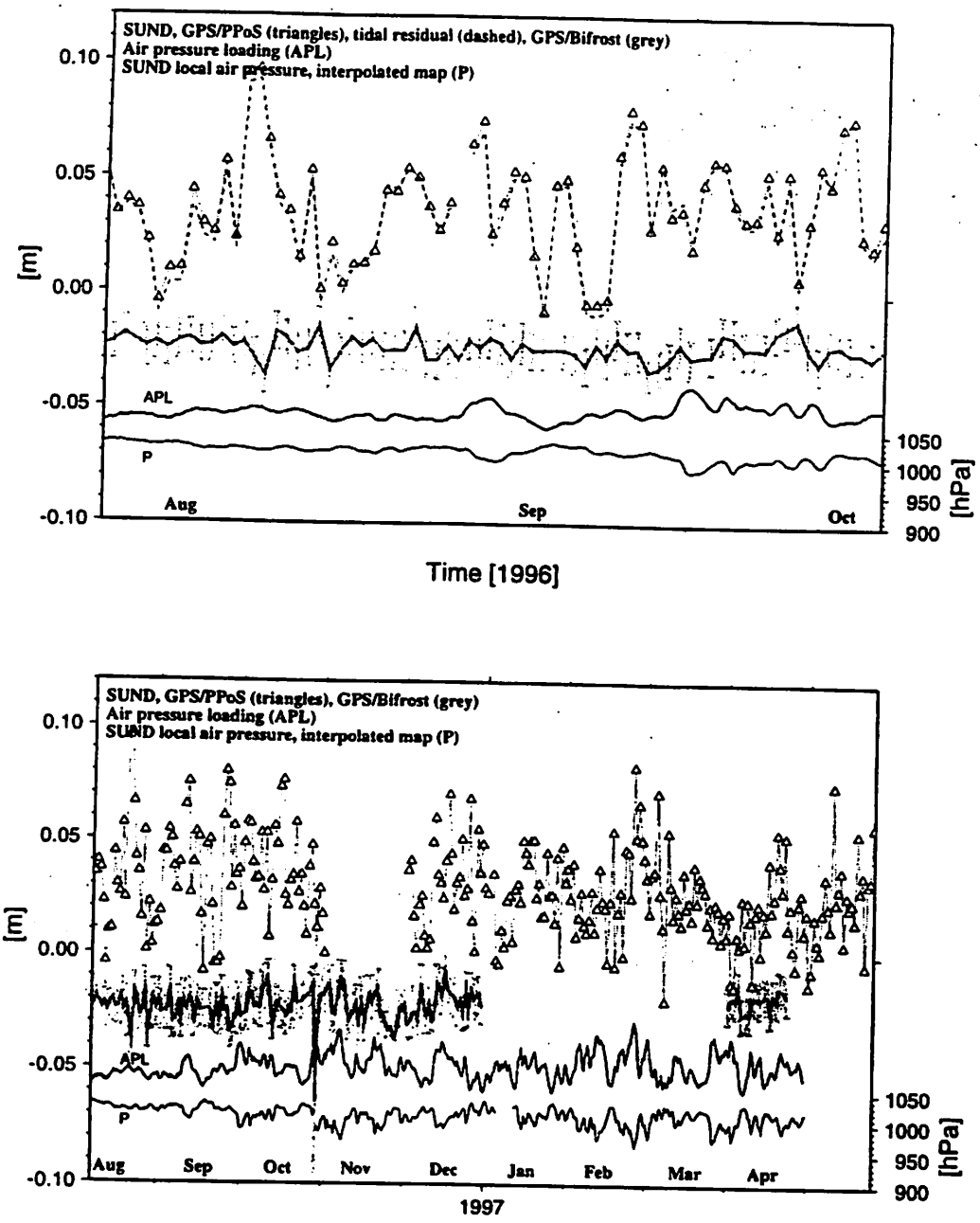


Figure 4: *Air pressure loading at Sundsvall, daily Bifrost GPS vertical estimates, and GPS one-hour vertical point-positioning estimates smoothed and resampled at 24 h interval. The lower frame zoomes in the first three months. Curves have been offset along the ordinate for clarity.*

Table 2: *Comparison of $M_2$ (principal semidiurnal lunar) tide terms detected in GPS point-position data and comparison with IERS standards ocean loading model. Also shown are VLBI determinations for Onsala.*

| Site | Observed Amplitude [m] | 95% | Observed Phase [deg] | Model Amplitude [m] | Model Phase [deg] |
|---|---|---|---|---|---|
| Sundsvall | 0.0097 | +-0.0005 | 100 | 0.0086 | 84 |
| Mauna Kea | 0.0145 | +-0.0011 | 137 | 0.0132 | 125 |
| Reykjavik | 0.0212 | +-0.0009 | -11 | 0.0205 | -22 |
| Onsala | 0.0011 | +-0.0009 | 6 | 0.0038 | 64 |
| Onsala (S) | 0.0041 | +-0.0008 | 23 | 0.0038 | 64 |
| Onsala (H) | 0.0035 | +-0.0005 | 106 | 0.0039 | 64 |
| Onsala (HS) | 0.0028 | +-0.0004 | 68 | 0.0038 | 64 |

(H) - Haas (1996); (S) - Sovers (1994),
(HS) - Haas & Schuh (1997)

Table 3: *Root-mean-square of GPS-determined residual tides from point-positioning data before and after subtracting ocean loading model.*

Ocean loading

Root Sum Square over 9 tides [mm]

| | Observed | Observed - model | |
|---|---|---|---|
| REYKJAVIK | 25.0 | 8.5 | |
| MAUNA KEA | 23.1 | 18.2 | *) |
| ONSALA | 10.8 | 9.8 | |
| SUNDSVALL | 8.5 | 7.5 | |

*) MAUNA KEA: The main error contribution is from K1 and K2 i.e. sidereal periods; 4.6 and 11.6 mm amplitude, respectively.

longest record and therefore was suitable for air pressure loading study. The data series used are shown in Fig. 4. The point-positioning solutions, although smoothed and resampled at 24 h interval to keep curve details comparable, show an order of magnitude higher RMS than the daily network determinations.

Observations, orbits, and troposphere model are the same as used in the Bifrost analysis. The major difference is the introduction of a precise clock solution into the satellite orbits. The sampling rate of the point-positioning solutions was set to one hour.

## 3.1 Tides

Tidal terms are included in the signal analysis in all cases. The point-positioning data is reduced with a solid earth tide model included, so residual tides would primarily be expected due to e.g. ocean loading. Results for the primary tide $M_2$ and comparison with the ocean loading model (Scherneck, 1991; McCarthy, 1996) is shown in Table 2. In all cases ocean loading is shown at significant levels (cf. Table 3), even at Sundsvall where the actual amplitudes are only at the millimeter level. Large descrepancies between GPS and model are found at Onsala; the VLBI determinations of neither Haas (1996) nor Sovers (1994) clarify the picture since large differences in both amplitude and phase appear to exist. Only recent VLBI analysis (Haas and Schuh, 1997) seems to corroborate the model and by the same token contradict the GPS result.

The analysis results for Sundsvall are shown in Table 4. We find comparably large amplitudes for tidal species that, observed on the rotating earth, are integer fractions of the sidereal day ($K_1$, $K_2$, $K_3$). The same is true of the other stations, Mauna Kea being the extreme example (5, 11, 1.4 mm). A candidate for generating these kinds of frequencies is related to orbit perturbations that are fixed in space and affect the spacecrafts at integer fractions (1, 1/2, 1/3) of the orbit revolution. The time duration is too short to single out orbit-unrelated perturbations as the nodal rate of the GPS system is only at a few degrees per year.

## 3.2 Air pressure loading

Due to data limitations we show results for air pressure loading only for the case of Sundsvall, for which we have more than 1000 samples of point-position determinations. The GPS data is analyzed for admittance of air pressure loading in a least-squares regression together with the tidal terms. The pressure loading is computed with the global convolution method. We also interpolate the global grids to the site for determination of a model-based pressure loading coefficient.

The VLBI value to which the result can be compared is obtained at Onsala, -0.16 mm/hPa (Haas et al., 1997). This value is still low compared to an expected, model-based coefficient of between -0.25 and -0.5 mm/hPa (Manabe et al., 1991). Using the local pressure interpolated from the global fields and the loading effect we obtain a "theoretical" (or model-based) air pressure loading admittance of -0.45 mm/hPa. Sundsvall is located further inland than Onsala, but that does not appear to have any substantial effect on the coefficient. Multiplied with the admittance of predicted loading effects into the GPS observations (0.32 ±0.06, c.f. Table 4), we arrive at an observed pressure admittance of 0.15 ±0.03 mm/hPa. This matches closely the VLBI result of 0.16 mm/hPa ±0.07 in Haas et al. (1997).

Table 4: *Results from analysis of ocean loading tides and air.pressure loading in GPS data from Sundsvall. Pointer (a) highlights admittance of predicted air pressure loading effects. Pointers (b) mark tidal species with periods related to the sidereal day.*

RESULTS: ADMITTANCE

SITE/FILE: S U N D S V A L L

Normalized Chi^2 of fit : 1.72D+00

| | #b | Dominating tide argum. numbers | Frequ. [cyc/d] | Amplit. [m] | Phase [deg] | Co..admittance parameter..Quad +- 95.0% conf | Gain | Cophase |
|---|---|---|---|---|---|---|---|---|
| Mf | 1 | 2 0 2 0 0 0 0 0 | .0732022 | 2.800D-02 | 141.5 | -.061943 +- .021969 .090617 +- .021680 | .109765 | 235.6 |
| Q1 | 3 | 2 1-2 0 1 0 0-1 | .8932441 | 1.596D-02 | 60.6 | -.021459 +- .045345 -.048541 +- .045290 | .053073 | 113.8 |
| O1 | 5 | 2 1-1 0 0 0 0-1 | .9295357 | 8.323D-02 | 97.0 | -.010895 +- .009354 -.028071 +- .009357 | .030112 | 111.2 |
| M1 | 7 | 2 1 0 0 1 0 0 1 | .9664463 | 6.519D-03 | 202.1 | .133265 +- .095712 .021351 +- .095700 | .134964 | 350.9 |
| P1 | 9 | 2 1 1-2 0 0 0-1 | .9972621 | 3.729D-02 | 156.8 | -.044380 +- .016252 -.009632 +- .016261 | .045414 | 167.8 |
| S1K1 | 11 | 2 1 1 0 0 0 0 1 | 1.0027379 | 1.013D-01 | 239.0 | .027931 +- .006886 -.032711 +- .006881 | .043014 | 49.5 |
| J1 | 13 | 2 1 2 0-1 0 0 1 | 1.0390296 | 6.635D-03 | 274.9 | -.004934 +- .108156 -.017907 +- .108143 | .018574 | 105.4 |
| 001 | 15 | 2 1 3 0 0 0 0 1 | 1.0759401 | 3.615D-03 | 200.1 | .081737 +- .265331 -.135467 +- .265201 | .158216 | 58.9 |
| 2N2 | 17 | 2 2-2 2 0 0 0 0 | 1.8645472 | 1.626D-02 | 275.7 | -.157428 +- .254423 .264830 +- .254349 | .308088 | 239.3 |
| N2 | 19 | 2 2-1 0 1 0 0 0 | 1.8959820 | 1.018D-02 | 299.1 | .007417 +- .056042 -.059009 +- .056067 | .059474 | 82.8 |
| M2 | 21 | 2 2 0 0 0 0 0 0 | 1.9322736 | 5.318D-02 | 335.5 | .000864 +- .011303 -.020677 +- .011305 | .020696 | 87.6 |
| L2 | 23 | 2 2 1 0-1 0 0 2 | 1.9685653 | 1.503D-03 | 191.9 | -.119886 +- .381740 .303790 +- .381686 | .326590 | 248.5 |
| S2 | 25 | 2 2 2-2 0 0 0 0 | 2.0000000 | 2.474D-02 | 35.3 | .036465 +- .024870 -.016759 +- .024869 | .040132 | 24.7 |
| K2 | 27 | 2 2 2 0 0 0 0 0 | 2.0054758 | 6.728D-03 | 297.1 | -.609678 +- .121446 -.550183 +- .121442 | .821224 | 137.9 |
| M3 | 29 | 3 3 0 0 0 0 0 2 | 2.8984104 | 3.250D-04 | 323.3 | -.176341 +-1.739183 .776827 +-1.739216 | .796590 | 257.2 |
| K3 | 31 | < EXP (iwt) > | 3.0082140 | 1.000D+00 | .0 | -.003123 +- .000624 -.000550 +- .000624 | .003171 | 170.0 |
| Apl | 33 | <^/hgs/Oload/smhi/apl/SUND_apl.ts> | | | | >>> .316147 +- .063530 <<< (a) | | |
| / | 34 | Linear 1/[year] | | | | -.017523 +- .001566 | | |

RESULTS: MAJOR TIDE AMPLITUDES, GREENWICH COPHASES

| | #pot.dvlp | frequ. | amplitude | | cophase | +- .950% conf | |
|---|---|---|---|---|---|---|---|
| Mf | 076 | .073202 | 3.0736D-03 | | 235.6 | +-6.2D-04 | |
| Q1 | 225 | .893244 | 8.4695D-04 | | 131.5 | +-7.2D-04 | |
| O1 | 257 | .929536 | 2.5062D-03 | | 128.9 | +-7.8D-04 | |
| M1 | 293 | .966446 | 8.7982D-04 | | 8.6 | +-6.2D-04 | |
| P1 | 310 | .997262 | 1.6935D-03 | | 185.4 | +-6.1D-04 | |
| S1K1 | 324 | 1.002738 | 4.3584D-03 | << | 67.2 | +-7.0D-04 | <<< (b) |
| J1 | 351 | 1.039030 | 1.2324D-04 | | 123.1 | +-7.2D-04 | |
| 001 | 378 | 1.075940 | 5.7189D-04 | | 76.6 | +-9.6D-04 | |
| 2N2 | 452 | 1.864547 | 5.0085D-04 | | 274.6 | +-4.1D-04 | |
| N2 | 474 | 1.895982 | 6.0553D-04 | | 118.2 | +-5.7D-04 | |
| M2 | 501 | 1.932274 | 1.1006D-03 | | 122.9 | +-6.0D-04 | |
| L2 | 526 | 1.968565 | 4.9095D-04 | | 283.8 | +-5.7D-04 | |
| S2 | 546 | 2.000000 | 9.9297D-04 | | 60.0 | +-6.2D-04 | |
| K2 | 556 | 2.005476 | 5.5253D-03 | << | 173.3 | +-8.2D-04 | <<< (b) |
| M3 | 629 | 2.898410 | 2.5888D-04 | | 310.2 | +-5.7D-04 | |
| K3 | 20016 | 3.008214 | 3.1712D-03 | << | 170.0 | +-6.2D-04 | <<< (b) |

Thus, in both VLBI and GPS data the pressure deformation signature is low and has similar attentuation. Still it would be premature to conclude that a process responsible for this would be common and therefore external to VLBI and GPS. There are a number of factors that affect the pickup of air pressure related signatures in data analysis. First there is the possibility that the troposphere model absorbs some of the vertical motion because of compatible stochastic signal properties (GIPSY GPS) or since it is easily approximated by piecewise linear functions (CALC/SOLVE VLBI). In the case of GPS there is the additional possibility that the crustal deformation is picked up by the orbit model since pressure loading effects are not reduced from the tracking data. Thus, the satellite range to a station that moves coherently with such an orbit would be unaffected.

# 4 Wet troposphere

We have estimated the water vapor at Ny-Ålesund using approximately two years of GPS data and compared these results with the integrated radiosonde profiles available. Figure 5 shows such a comparison for the months February, and July 1995. Note that pressure data have only been available at the times for the radiosonde launches. This means that these data have been interpolated to the times of the GPS estimates in order to calculate the wet delay. These wet delay estimates are therefore less reliable between the radiosonde measurements. The -1 cm GPS offset seen during winter lasts until June 1996 (not shown) for no obvious reason.

# 5 Conclusions

At various stages of the studies summarized in this paper it became clear how valuable VLBI is in constrianing and goading to reference frames. This in spite of the fact that the technique is insensitive to the centre of gravity of the earth. Mapping of the VLBI solutions onto the geocentre regularly leads to less anomalous vertical rates than the combined solutions as stated in the ITRF files.

The large number of daily GPS solutions, more than 1300 since the start of the BIFROST project, presents a favourable statistical basis on which station movement can be resolved at the sub-millimeter per year level. As regards sensitivity the two systems become comparable to each other as demonstrated by the analysis of air pressure and ocean loading effects. The notion that they are complementary in the aspect of earth rotation has lead to the now commencing CORE program. But also as regards aspects of baselines and vertical components of motion, both techniques support each other. The present contribution has certainly only scimmed at the surface of this synergetic potential.

The Onsala-Wettzell and Onsala-North America baselines are key baselines for the refinement of reference systems in support of the BIFROST investigations with the major aim to detect and seperate the vertical movements of the solid earth from that of the sea surface. The frequency of joint experiments involving Onsala have been slightly less after summer 1996. Direct use in satellite-VLBI combined solutions, however, argues for more dense observation programs.

# Acknowledgments

We are owing thanks to Frank Webb, JPL, for making the GPS point-position results available. Our studies are supported by various grants from the Natural Science Research Council of Sweden. Plotting programs have been contributed by Wessel and Smith (1996).

# References

BIFROST Project, Bennett, R.A., Carlsson, T.R., Carlsson, T.M., Chen, R., Davis, J.L., Ekman, M., Elgered, G., Elósegui, P., Hedling, G., Jaldehag, R.T.K., Jarlemark, P.O.J., Johansson, J.M., Jonsson, B., Kakkuri, J., Koivula, H., Milne, G.A., Mitrovica, J.X., Nilsson, B.I., Ollikainen, M., Paunonen, M., Poutanen, M., Pysklywec, R.N., Rönnäng, B.O., Scherneck, H.-G., Shapiro, I.I. and Vermeer, M., 1996. GPS measurements to constrain geodynamic processes in Fennoscandia, *EOS Trans. American Geophys. Union*, 77, 337+339.

Boucher, C., Altamimi, Z., Feissel, M., and Sillard, P., 1996. *Results and Analysis of the ITRF94*, IERS Technical Note 20, Observatoire de Paris, 157pp.

Boucher, C., Altamimi, Z., and Duhem, L., 1994. *Results and analysis of the ITRF93*, IERS Technical Note 18, Observatoire de Paris, 313 pp.

Breuer, D. and Wolf, D., 1995. Deglacial land emergence and lateral upper-mantle heterogeneity in the Svalbard archipelago—I. First results for simple load models, *Geophys. J. Int.* 121, 775–788.

Ekman, M., 1996. A consistent map of the postglacial uplift of Fennoscandia, *Terra Nova*, 8, 158–165.

Ekman, M. and Mäkinen, J., 1996. Recent postglacial rebound, gravity change and mantle flow

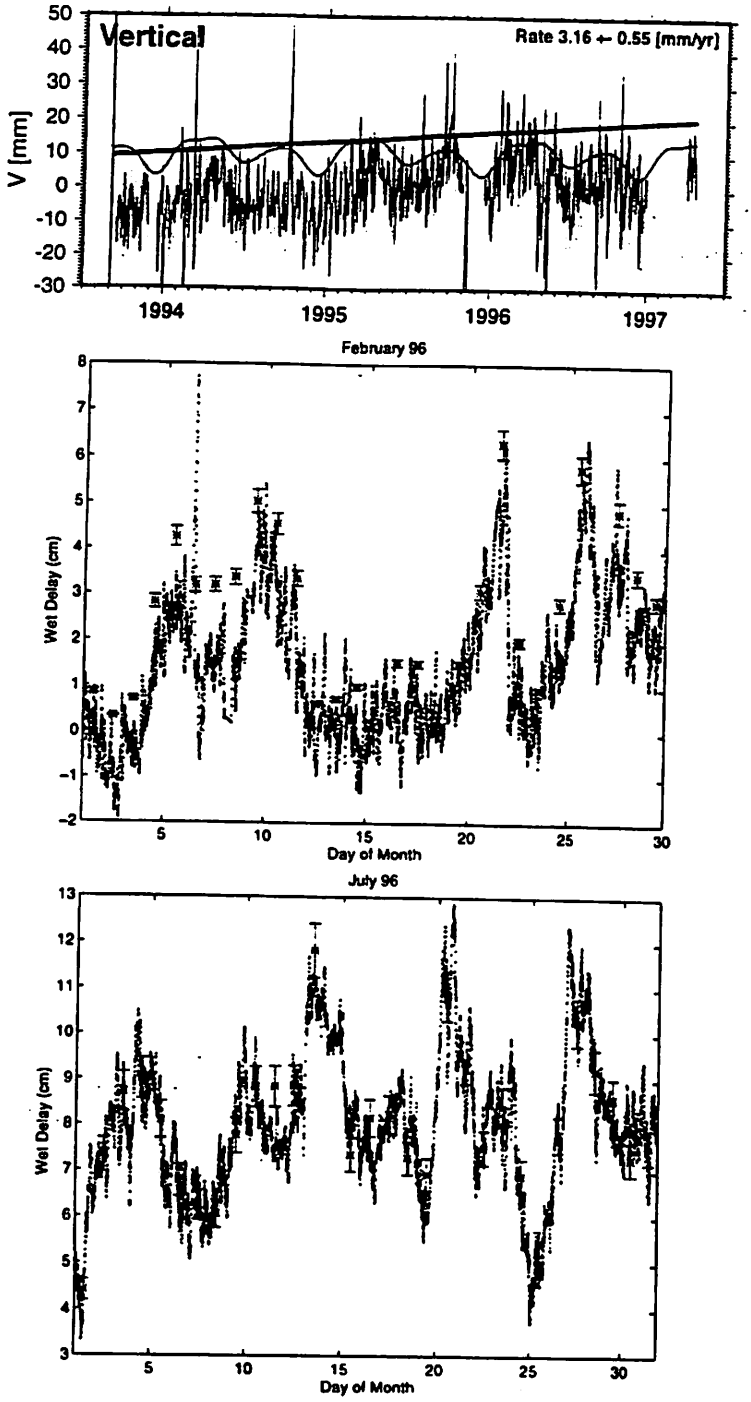


Figure 5: *Top frame shows GPS determination of vertical component at Ny Ålesund, Spitsbergen. Below a comparison between wet delay estimate from GPS with radiosonde (asterisks) for a winter (top) and a summer month (bottom) at Ny Ålesund. The offset seen in February disappears before July. Whether the disappearance is related to the 1 cm dip signature in the vertical can only be a matter of speculation.*

in Fennoscandia. *Geophys. J. Int.*, **126**, 229–234.

Farrell, W.E., 1972. Deformation of the earth by surface loads, *Rev. Geophys. Space Phys.*, **10**, 761-797.

Haas, R., 1996. *Untersuchungen zu Erddeformationsmodellen für die Auswertung von geodätischen VLBI-Messungen*. PhD-thesis, Deutsche Geodätische Kommission, Reihe C, Heft Nr. 466, 103 pp.

Haas, R., Scherneck, H.-G., and Schuh, H., 1997. Atmospheric loading corrections in geodetic VLBI and determination of atmospheric loading coefficients, *this issue*.

Haas, R. and Schuh, H., 1997. Ocean loading observed by geodetic VLBI, *Proc. 13th Int. Symp. Earth Tides*, in preparation.

Heflin, M.B., 1997. `http://-sideshow.jpl.nasa.gov/mbh/all/table.txt`

Heflin, M.B., Bertiger, W., Blewitt, G., Freedman, A., Hurst, K., Lichten, S., Lindqwister, U., Vigue, Y., Webb, F.H., Yunck, T., and Zumberge, J.F., 1992. Global geodesy using GPS without fiducial sites, *Geophys. Res. Lett.*, **19**, 131–134.

Larson, K.M., Freymueller, J.T., and Philipsen, S., 1997. Global plate velocities from the Global Positioning System. *J. Geophys. Res.*, **102**, 9961–9982.

Ma, C., Ryan, J.W., Vandenberg, N.R., 1997. `ftp://gemini.gsfc.nasa.gov/pub/REPORT97/-topocentric_velocities.1083c`

Manabe, S., Stao, T., Sakai, S., Yokoyama, K., 1991. Atmospheric loading effect on VLBI observations, in *Proc. AGU Chapman Conference on Geodetic VLBI: Monitoring Global Change*, NOAA Techn. Rep., NOS 137 NGS 49, pp. 111–122, U.S. Dept. of Commerce, NOAA/NOS, Rockville, MD.

McCarthy, D. D. (ed): *IERS Conventions* IERS Technical Notes 21, Observatoire de Paris, 94 pp. 1996, and `http://hpiers.obspm.fr/webiers-/general/syframes/convent/CONV.html`

Mitrovica, J.X., Davis, J.L. and Shapiro, I.I., 1994. A spectral formalism for computing three-dimensional deformations due to surface loads, 2. Present-day glacial isostatic adjustment. *J. Geophys. Res.* **99**, 7075–7101.

Rothacher, M., Beutler, G., Gurtner, W., Brockmann, E., and Mervart, L., 1993. *Bernese GPS Software (Version 3.4), 1993 Documentation*, Astronomical Institute, University of Berne.

Scherneck, H.-G., 1991. A parametrized solid earth tide model and ocean tide loading effects for global geodetic baseline measurements, *Geophys. J. Int.*, **106**, 677–694.

Scherneck, H.-G., Johansson, J.M., Mitrovica, J.X., and Davis, J.L., 1997: The BIFROST project: GPS determined 3-D displacement rates in Fennoscandia from 800 days of continuous observations in the SWEPOS network. *Tectonophysics*, submitted.

Sovers, O. J., 1994. Vertical ocean loading amplitudes from VLBI measurements, *Geophys. Res. Letters*, **21**, 357–360..

van Dam, T.M., and Herring, T.A., 1994. Detection of atmospheric pressure loading using very long baseline interferometry measurements. *J. Geophys. Res.*, **99**, 4505–4517.

van Dam, T.M., Blewitt, G., and Heflin, M.B., 1994. Atmospheric pressure loading effects on Global Positioning System coordinate determinations, *J. Geophys. Res.*, **99**, 23,939–23,950.

Webb F.H. and Zumberge J.F., 1993. *An Introduction to GIPSY/OASIS-II Precision Software for the Analysis of Data from the Global Positioning System*. JPL Publ. No. D-11088, Jet Propulsion Laboratory, Pasadena, Cal.

Zumberge, J.F., Heflin, M.B., Jefferson, D.C., Watkins, M.M., and Webb, F.H., 1997. Precise point positioning for the efficient and robust analysis of GPS data from large networks. *J. Geophys. Res.*, **102**, 5005–5017.

# Atmospheric loading corrections in geodetic VLBI and determination of atmospheric loading coefficients

Rüdiger Haas
Onsala Space Observatory (OSO)
S-43992 Onsala, Sweden, (haas@oso.chalmers.se)

Hans-Georg Scherneck
Onsala Space Observatory (OSO)
S-43992 Onsala, Sweden, (hgs@oso.chalmers.se)

Harald Schuh
Deutsches Geodätisches Forschungsinstitut (DGFI), Abt. I
Marstallplatz 8, 80539 München, Germany, (schuh@dgfi.badw-muenchen.de)

**Abstract** Redistribution of atmospheric masses (air pressure lows and highs) loads the Earth's surface. Large-scale deformation fields are generated with typical wavelengths of some hundred to some thousand kilometers. The periods of the loading variations are between a few days and some weeks but also include diurnal and seasonal signature. The air pressure variations can cause vertical displacements in the centimeter range and horizontal ones in the millimeter range.

We investigated the influence of atmospheric loading corrections on the results and the accuracy of geodetic VLBI experiments. Atmospheric loading corrections were calculated with three different methods (using local barometric pressure, using a two-coefficient model, using global convolution) and were applied in the analysis of EUROPE and R&D VLBI observations. The results (e.g. baseline lengths) change by a few mm when the corrections are applied but the post fit residuals and the baseline length repeatability do not improve significantly. Possible reasons for this are local effects at some VLBI stations and the absorption of the effect by clock and atmosphere parameters.

In a second study we determined atmospheric loading coefficients for 18 VLBI stations using a VLBI data set of 800.000 observations which covers 18 years. The correlation coefficients between these parameters determined empirically and those given by the theoretical model by MANABE et al. [1991] are higher than 0.7. Thus, the empirical results from VLBI prove the effect and in general confirm the theoretical model but for some VLBI stations significant differences from theory are revealed.

## 1 Introduction

Air pressure lows and highs (cyclones and anticyclones) can be regarded as time dependent redistribution of masses loading the Earth's surface. According to their geometry they generate large-scale deformation fields with several hundred to several thousand kilometers wavelength. Due to the velocity of the passing (anti-)cyclones, the periods of the loading function are between a few days and some weeks. There is also a diurnal pressure variation corresponding to the solar $S_1$ tide, resonances with other diurnal tides and an annual period of the global air pressure distribution. Such air pressure anomalies can cause vertical displacements in the centimeter range and horizontal displacements in the millimeter range.

The reaction of the oceans to barometric pressure variations (see e.g. WUNSCH and STAMMER [1997]) is of special importance. The dynamic reaction of the oceans depends on water depth, coastal geometry and velocity of atmospheric pressure systems. According to the model of a static oceanic response, often named 'inverted barometer hypothesis' [IHB], the atmospheric pressure variation on the oceans is compensated by redistribution of ocean water masses, so that no pressure variation is transfered to the ocean bottom. The other extreme is a non-static oceanic reaction, often named 'non-

inverted barometer hypothesis' [NIBH] in the literature, which means that the loading is transferred to the ocean bottom.

Space geodetic measurements (e.g. VLBI, GPS, SLR, LLR, GLONASS, DORIS) are affected by the loading effect due to the changing geometry between observing sites. Thus, in the analysis of space geodetic observations the loading effect should be corrected.

Theoretical studies on atmospheric loading effects have been published by RABBEL and ZSCHAU [1985], RABBEL and SCHUH [1986], VANDAM and WAHR [1987], MANABE et al. [1991], VANDAM and HERRING [1994] and SUN et al. [1995]. Different methods to calculate the effect have been developed in order to provide corrections for the analysis of space geodetic observations. Empirical studies on the effect have been published by MACMILLAN and GIPSON [1994] and VANDAM et al. [1994].

## 2 Calculation of atmospheric loading corrections

Three different methods to calculate the atmospheric loading effect of geodetic sites as a site specific displacement were used for our investigations. The common basis of these methods is a convolution of a loading pressure distribution with mass loading Green's functions. Different pressure distributions are used in the different methods and different parameterizations are given to calculate the site diplacements.

RABBEL and ZSCHAU [1985] used synthetic circular pressure distributions of different sizes and Green's functions for an elastic Earth. From regression calculations between the pressure and the calculated radial displacement $\Delta_R$ they developed a two coefficient formula which contains local and regional barometric pressure. In equation (1) the first coefficient (−0.55) is the coefficient for large scale pressure variations and the second one (−0.35) for small scale variations.

$$\Delta_R(t) \quad = \quad -0.55\,(\bar{p}_{2000km}(t) - \bar{p}) - 0.35\,(p(t) - \bar{p}) \tag{1}$$

The large scale pressure variation is computed as a difference between the mean barometric pressure $\bar{p}_{2000km}$ in a surrounding area of 2000 km around the station, and the reference barometric pressure $\bar{p}$ at the station. The small scale pressure variation is computed as a difference between the local barometric pressure $p(t)$ and the reference barometric pressure $\bar{p}$ at the station. Since local *and* regional barometric pressure are needed, this model needs a lot of efforts if someone wants to apply it properly. A mechanism for characterizing the pressure anomaly surrounding the site has been recommended by SOVERS and JACOBS [1996]. A modification to make the method more applicable is to enter the difference between the mean barometric pressure during the 24 hour VLBI experiment and the reference pressure as large scale pressure variation and the difference between the actual pressure and the mean value during the VLBI session (normally 24 hours) as small scale pressure variation [HAAS, 1996].

MANABE et. al [1991] worked with observed barometric pressure data of the Japanese Meteorological Agency [JMA] and Green's functions by FARREL [1972]. They calculated radial displacements of space geodetic stations by a global convolution of the barometric pressure data and determined regression coefficients between these calculated radial displacements and the local barometric pressure at the stations. Regression methods for horizontal displacements would require observed horizontal pressure gradients at the stations which is difficult to obtain. Finally, they provide atmospheric loading coefficents $\alpha_P$ for a number of space geodetic stations.

$$\Delta_R(t) \quad = \quad \alpha_p\,(p(t) - \bar{p}) \tag{2}$$

The radial displacement is computed with the site dependent atmospheric loading coefficient $\alpha_P$, local barometric pressure $p(t)$ and a local reference pressure $\bar{p}$ as shown in equation (2).

The third method gives all three components of the site displacement. It uses the pure global convolution of observed pressure distribution and Green's functions without any regression calculations.

This is feasable when the global barometric pressure data is given and the computed site displacements can be introduced into the data analysis.

$$\Delta_N(t) = -\int \cos(\alpha_{AZ})\, G_l(\psi)\, dM(\theta,\lambda,t) \quad (3)$$

$$\Delta_E(t) = -\int \sin(\alpha_{AZ})\, G_l(\psi)\, dM(\theta,\lambda,t) \quad (4)$$

$$\Delta_R(t) = \int G_h(\psi)\, dM(\theta,\lambda,t) \quad (5)$$

The three components of the station displacement can be calculated as shown in equations (3) to (5). In these equations $\Delta_N$, $\Delta_E$, $\Delta_R$ are the station displacements in north, east and radial direction, respectively. A loading mass at co-latitude $\theta$ and longitude $\lambda$ is denoted by $dM(\theta,\lambda,t)$, its azimuth with respect to the point of interest is denoted by $\alpha_{AZ}$. The angular distance between the loading mass and the point of interest is described by $\psi$. Mass loading Green's functions are denoted by $G_l(\psi)$ for the horizontal components and $G_h(\psi)$ for the radial component. Figure 1 shows schematically the situation for a global convolution using barometric pressure data given on a grid which are provided by several meteorological agencies like the European Center for Medium-Range Weather Forecasts [ECMWF], the Japanese Meteorological Agency [JMA] and the US National Meteorological Center [NMC].

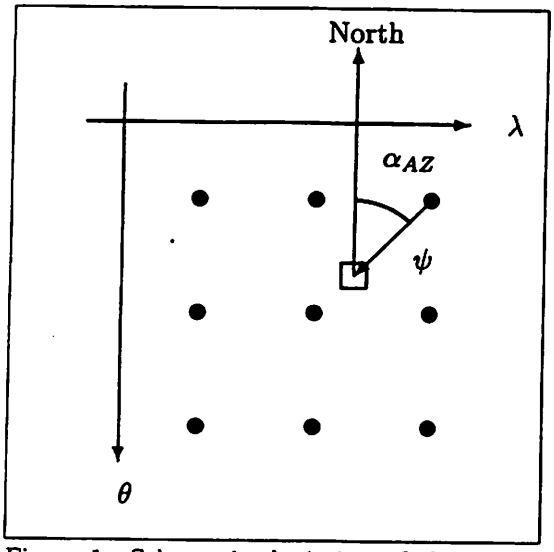


Figure 1: Schematic depiction of the global convolution method using barometric data given on a grid. The regular black dots denote grid points with pressure data, the square represents the space geodetic station for which the loading is computed

For our calculations with the pure global convolution method we used the data of the ECMWF given on a $1° \times 1°$ grid with temporal resolution of 6 hours. We calculated mean global pressure fields by averaging all 6 hour pressure fields. The loading effects due to this permanent field are always subtracted. As the loading fields accumulate with time, the difference between station coordinate estimates before and after an inclusion of the atmospheric loading corrections by global convolution will average to zero.

The graphs in figure 2 show the calculated radial displacements due to atmospheric loading for 7 stations during the CONT94 sessions of about two weeks in January 1994. Shown are the loading effects calculated with all three methods described before. For Wettzell (Germany) the agreement between the three methods is excellent, the discrepancies are in the range of only 1 mm. For Westford (Massachusetts, USA), Onsala (Sweden) and Gilcreek (Alaska, USA) the agreement is only good for some days out of the CONT94 sessions but there are also discrepancies of up to 5 mm between the different methods. For Ft. Davis (Texas, USA) and Los Alamos (New Mexico, USA) a clear offset of the effect calculated by the global convolution method with respect to the other two methods can be seen. For the island station Kokee (Hawai, USA) the effect calculated with the modified RABBEL and ZSCHAU method disagree with the other two which lie close together within 1 mm. Offsets between the curves are due to differences between the mean local pressure and the mean global pressure field, primarily due to the station height.

The graphs in figure 3 show the horizontal displacements for the stations in the CONT94 network, calculated with the global convolution method. The effects do not exceed $\pm$ 2.5 $mm$ and are minimal for the island station Kokee (Hawai, USA). Graphs a-g show displacements in east direction, graphs h-n in north direction.

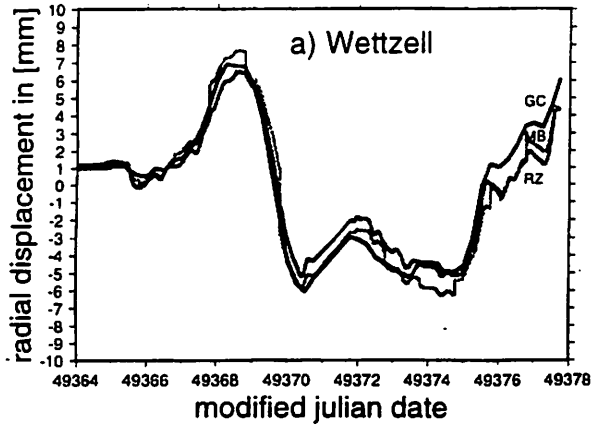


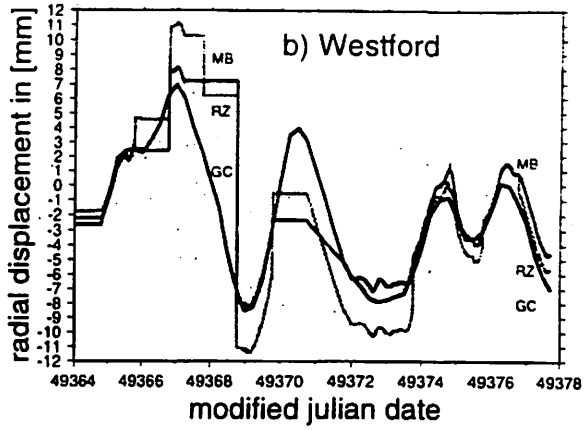


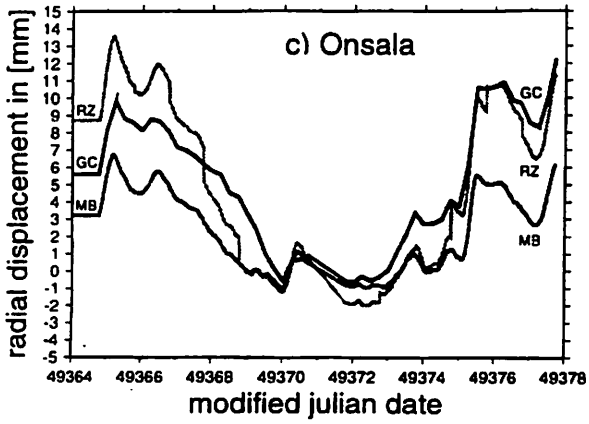


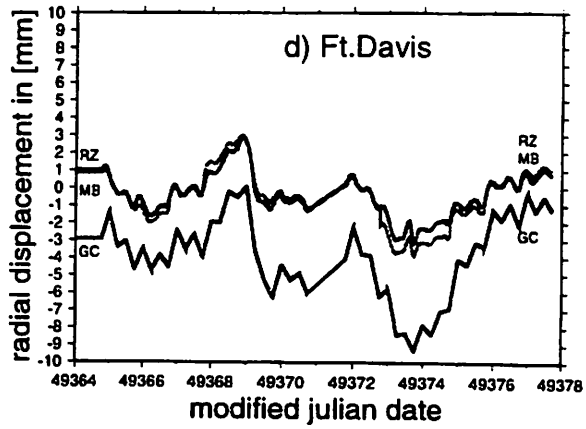


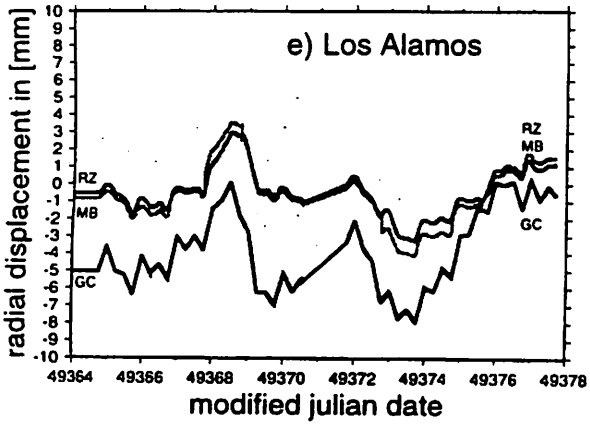


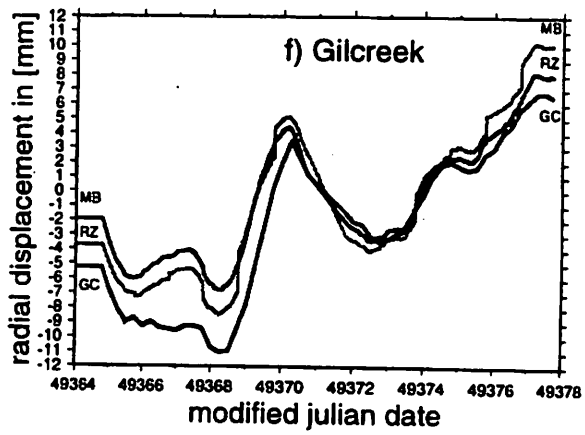


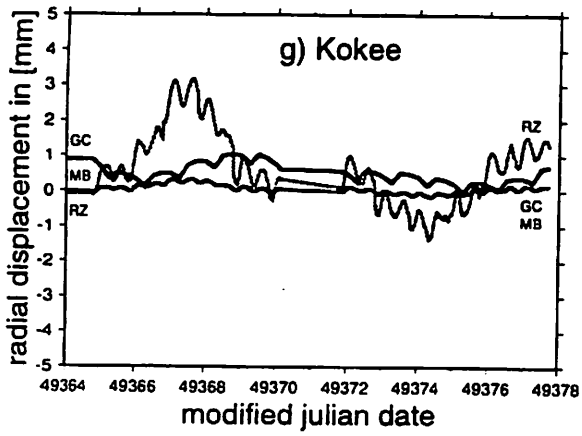


Figure 2: Graphs a-g show the calculated atmospheric loading effects in radial direction for the stations in the CONT94 network during 12 days in January 1994. The effects calculated with the atmospheric loading coefficients by MANABE et al. [1991] are denoted by MB. Those calculated with the modified version of the two-coeffients method by RABBEL and ZSCHAU [1985] are denoted by RZ and those calculated using the pure global convolution approach are denoted by GC.

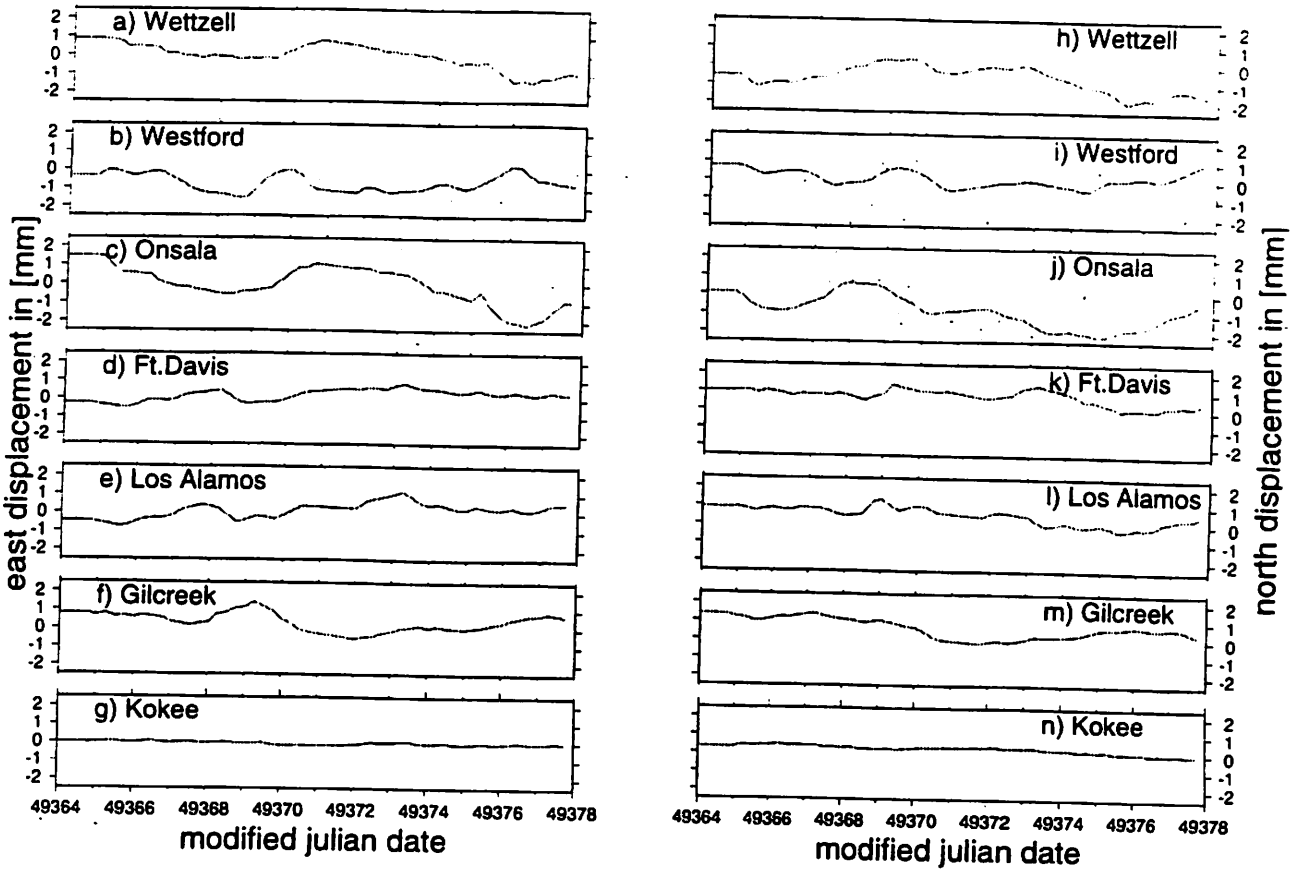


Figure 3: The graphs show the horizontal displacements in east (a-g) and north (h-n) direction, respectively, for the stations in the CONT94 network during 12 days in January 1994. The effects are calculated with the pure global convolution method described in chapter 2.

# 3 Application of atmospheric loading corrections to geodetic VLBI measurements

Using the three methods described in chapter 2 we applied the calculated loading effects to special subsets of the global geodetic VLBI data. We analyzed the EUROPE VLBI sessions and the R&D VLBI sessions from 1993 to the mid of 1995. The time span was restricted due to the restricted amount of global atmospheric pressure data that was available for us. The CALC/SOLVE VLBI data analysis software [MA et al., 1990] was modified to include the computed loading corrections. For the first two methods we entered the atmospheric pressure readings recorded during the VLBI sessions. For the global convolution method we used the global barometric pressure data of the European Center for Medium-Range Weather Forecasts [ECMWF] as described in chapter 2 and mass loading Green's functions for an elastic Earth [FARREL, 1972, SCHERNECK, 1991]. Shallow waters up to a depth of 200 m were treated as dry land, in deeper waters the IBH was assumed.

We then carried out the for so-called 'baseline solutions' which means, that the coordinates of each station were determined for each individual observing session except for one reference station. This allows to determine baseline evolution rates and the weighted root mean square [WRMS] values of the regression which can be used as a measure for the quality of the fit. Qualitatively the application of atmospheric loading corrections to the two testbases EUROPE and R&D sessions give similar results. Thus, we present in the following the results obtained from the R&D sessions, only.

Table 1 shows the effect of the application of atmospheric loading corrections on the estimated VLBI baselines from the analysis of the R&D VLBI sessions. The baseline lengths change by only a few mm or less. The largest length changes are +1.7 mm and −2.1 mm and occur on intercontinental baselines from Ft.Davis (Texas, USA) and Mauna Kea (Hawai, USA) to Wettzell (Germany) when the corrections obtained by pure global convolution calculation are applied.

Table 1: Effect of application of atmospheric loading corrections on baseline results from the analysis of the R&D VLBI sessions. Given are the differences Δl between the estimated results of MB, i.e. application of corrections with the MANABE et al. [1991] model, RZ, i.e. application of corrections using the modified RABBEL and ZSCHAU [1985] two-coefficient approach, GC, i.e. application of corrections computed from the pure global convolution method, and N, i.e. the reference results without application of atmospheric loading corrections.

| baseline | Δl [mm] | | | baseline | Δl [mm] | | |
|---|---|---|---|---|---|---|---|
| | MB-N | RZ-N | GC-N | | MB-N | RZ-N | GC-N |
| Ft.Davis-Gilcreek | −0.3 | +0.2 | +0.9 | Kokee-Onsala | −0.4 | −1.3 | −1.6 |
| Ft.Davis-Kokee | ±0.0 | ±0.0 | +0.7 | Kokee-Westford | +0.7 | +0.4 | +0.9 |
| Ft.Davis-Los Alamos | ±0.0 | ±0.0 | +0.3 | Kokee-Wettzell | −0.2 | −0.1 | −0.2 |
| Ft.Davis-Mauna Kea | −0.2 | ±0.0 | +0.1 | Los Alamos-Mauna Kea | +0.9 | ±0.0 | +0.4 |
| Ft.Davis-Onsala | −0.2 | −1.1 | +0.1 | Los Alamos-Onsala | ±0.0 | −1.0 | ±0.0 |
| Ft.Davis-Westford | ±0.0 | +0.1 | +1.0 | Los Alamos-Westford | +0.3 | +0.2 | +0.8 |
| Ft.Davis-Wettzell | +0.1 | +0.2 | +1.7 | Los Alamos-Wettzell | +0.2 | +0.2 | +1.5 |
| Gilcreek-Kokee | −0.3 | −0.1 | −0.2 | Mauna Kea-Onsala | +1.8 | ±0.0 | +0.9 |
| Gilcreek-Los Alamos | −0.2 | +0.2 | −0.3 | Mauna Kea-Westford | +1.3 | ±0.0 | +0.6 |
| Gilcreek-Mauna Kea | +0.4 | ±0.0 | +0.4 | Mauna Kea-Wettzell | −1.0 | ±0.0 | −2.1 |
| Gilcreek-Ny Ålesund | +0.3 | ±0.0 | −0.6 | Ny Ålesund-Onsala | ±0.0 | ±0.0 | −1.4 |
| Gilcreek-Onsala | −0.6 | −0.6 | −1.1 | Ny Ålesund-Westford | −0.2 | ±0.0 | −0.4 |
| Gilcreek-Westford | ±0.0 | +0.4 | +0.6 | Ny Ålesund-Wettzell | −0.1 | ±0.0 | −1.6 |
| Gilcreek-Wettzell | −0.4 | +0.3 | ±0.0 | Onsala-Westford | +0.3 | −0.7 | −0.3 |
| Kokee-Los Alamos | +0.1 | ±0.0 | +0.7 | Onsala-Wettzell | ±0.0 | −0.1 | +0.2 |
| Kokee-Ny Ålesund | +0.6 | ±0.0 | ±0.0 | Westford-Wettzell | +0.4 | +0.2 | +0.6 |

Table 2 shows the effect of the application of atmospheric loading on the repeatability of the baseline measurements from the analysis of the R&D VLBI sessions. The weighted root mean square [WRMS] values of the baseline lengths after determining a baseline rate for each of the baselines are given. The post fit residuals and the WRMS of the solutions do not change significantly. Possible reasons for the only slight changes are the absorption of the applied corrections by clock and atmosphere parameters. Simulations by RABBEL and SCHUH [1986] showed the influence of atmospheric loading on the estimated clock parameters. With all three methods the effect of atmospheric loading is at the verge of detectability and the repeatabilities do not point out a unique conclusion for a preferred method.

Table 2: Effect of application of atmospheric loading corrections on baseline results from the analysis of the R&D VLBI sessions. The WRMS for the baseline solutions after regression of baseline rates are given. N means the WRMS of a reference solution without application of atmospheric loading corrections. MB with application of corrections using the MANABE et al. [1991] model, RZ with application of corrections with the modified RABBEL and ZSCHAU [1985] two-coefficient approach and GC with application of corrections computed from the pure global convolution method.

| baseline | WRMS [mm] | | | | baseline | WRMS [mm] | | | |
|---|---|---|---|---|---|---|---|---|---|
| | N | MB | RZ | GC | | N | MB | RZ | GC |
| Ft.Davis-Gilcreek | 4.4 | 3.9 | 4.3 | 3.8 | Kokee-Onsala | 15.1 | 14.7 | 14.8 | 14.6 |
| Ft.Davis-Kokee | 7.3 | 7.4 | 7.2 | 7.5 | Kokee-Westford | 11.7 | 11.0 | 10.7 | 11.2 |
| Ft.Davis-Los Alamos | 1.8 | 1.8 | 1.8 | 1.7 | Kokee-Wettzell | 12.9 | 12.2 | 12.4 | 11.9 |
| Ft.Davis-Mauna Kea | 1.5 | 1.9 | 1.5 | 2.1 | Los Alamos-Mauna Kea | 1.3 | 1.6 | 1.3 | 1.9 |
| Ft.Davis-Onsala | 7.4 | 7.8 | 8.0 | 7.8 | Los Alamos-Onsala | 8.3 | 7.9 | 7.8 | 7.8 |
| Ft.Davis-Westford | 4.6 | 4.6 | 4.6 | 4.0 | Los Alamos-Westford | 3.6 | 3.4 | 3.4 | 3.3 |
| Ft.Davis-Wettzell | 8.0 | 7.3 | 7.8 | 6.6 | Los Alamos-Wettzell | 8.7 | 7.7 | 8.6 | 7.3 |
| Gilcreek-Kokee | 6.2 | 6.3 | 6.2 | 6.3 | Mauna Kea-Onsala | 9.9 | 9.1 | 9.9 | 8.6 |
| Gilcreek-Los Alamos | 3.9 | 3.7 | 3.9 | 4.0 | Mauna Kea-Westford | 2.5 | 1.6 | 2.5 | 1.0 |
| Gilcreek-Mauna Kea | 4.5 | 5.0 | 4.5 | 5.4 | Mauna Kea-Wettzell | 17.0 | 16.4 | 17.0 | 16.2 |
| Gilcreek-Ny Ålesund | 2.7 | 2.7 | 2.7 | 2.8 | Ny Ålesund-Onsala | 2.8 | 2.8 | 2.8 | 2.6 |
| Gilcreek-Onsala | 8.0 | 7.6 | 7.9 | 7.5 | Ny Ålesund-Westford | 3.6 | 3.9 | 3.6 | 4.1 |
| Gilcreek-Westford | 5.7 | 4.8 | 5.0 | 4.8 | Ny Ålesund-Wettzell | 2.3 | 2.3 | 2.3 | 2.3 |
| Gilcreek-Wettzell | 8.0 | 6.9 | 7.9 | 6.4 | Onsala-Westford | 8.1 | 8.2 | 8.2 | 8.3 |
| Kokee-Los Alamos | 7.2 | 7.2 | 7.1 | 7.6 | Onsala-Wettzell | 2.9 | 3.0 | 3.0 | 3.3 |
| Kokee-Ny Ålesund | 4.8 | 4.7 | 4.8 | 4.8 | Westford-Wettzell | 9.4 | 8.7 | 9.1 | 8.6 |

# 4 Estimation of atmospheric loading parameters from VLBI data

In order to estimate atmospheric loading parameters from geodetic VLBI data we implemented the model by MANABE et al. [1991] (see equation 2) which uses only local barometric pressure and site-specific loading coefficients. We then solved for the loading coefficients $\alpha_P$ for 18 VLBI stations from a VLBI data set of about 800.000 observations covering nearly 18 years. Those 18 stations contributed most of the observations to the global database and have reliable records of local barometric pressure. The defomation effects due to solid Earth tides were modelled including frequency and latitude dependence [HAAS, 1996] and a recent ocean loading model was applied [SCHERNECK, 1996] in order to prevent the propagation of errors of the deformation models into the estimates for atmospheric loading parameters. The chi-square of the solution decreased slightly by 0.2% when solving for the atmospheric loading parameters compared to a standard solution without the additional parameters. The results for the atmospheric loading parameters $\alpha_P$ are given in table 3 and figure 4.

The first three columns in table 3 show model parameters by MANABE et. al [1991] based on atmospheric pressure data of the Japanese Meteorological Agency [JMA] and model parameters by VANDAM and HERRING [1994] based on atmospheric data of the US National Meteorological Center [NMC]. Columns 4 to 5 show empirical results by MACMILLAN and GIPSON [1994] from VLBI data analysis and the empirical results by VANDAM, BLEWITT and HEFLIN [1994] obtained from GPS data analysis. The last column gives our recent results obtained from the analysis of an extensive VLBI data set.

Table 3: Model parameters and VLBI estimates of atmospheric loading coefficients $\alpha_p$. stations near the coast are marked by C (distance $\leq$ 200 km), stations far from the coast by I. Columns 1 and 2 give model parameters by MANABE et al. [1991] with atmospheric pressure data of the Japanese Meteorological Agency [JMA], column 3 gives model parameters by VANDAM and HERRING [1994] with atmospheric data of the US National Meteorological Center [NMC]. Column 4 presents the VLBI results by MACMILLAN and GIPSON [1994], column 5 the GPS results by VANDAM, BLEWITT and HEFLIN [1994]. The last column presents our results for the atmospheric loading parameters.

| | model values in [mm/hPa] | | | empirical results in [mm/hPa] | | |
|---|---|---|---|---|---|---|
| Station (I) inland or (C) coastal | MANABE et al. IBH JMA data (1991) $[\frac{mm}{hPa}]$ 1 | MANABE et al. NIBH JMA data (1991) $[\frac{mm}{hPa}]$ 2 | VANDAM and HERRING IBH NMC data (1994) $[\frac{mm}{hPa}]$ 3 | MACMILLAN and GIPSON VLBI data (1994) $[\frac{mm}{hPa}]$ 4 | VANDAM, BLEWITT and HEFLIN GPS data (1994) $[\frac{mm}{hPa}]$ 5 | HAAS, SCHERNECK and SCHUH (this paper) VLBI data (1997) $[\frac{mm}{hPa}]$ 6 |
| Algopark (I) | −0.435 | −0.453 | – | $-0.44 \pm 0.36$ | $-0.35 \pm 0.17$ | $-0.42 \pm 0.19$ |
| Greenbank (I) | −0.479 | −0.528 | −0.41 | $-0.17 \pm 0.12$ | – | $-0.73 \pm 0.17$ |
| Ft.Davis (I) | −0.532 | −0.547 | −0.55 | $-0.44 \pm 0.17$ | – | $-0.56 \pm 0.11$ |
| Gilcreek (I) | −0.432 | −0.536 | −0.45 | $-0.35 \pm 0.04$ | $-0.59 \pm 0.14$ | $-0.39 \pm 0.03$ |
| Hartebeesthoek (I) | −0.540 | −0.644 | – | $-0.16 \pm 0.20$ | – | $-0.24 \pm 0.12$ |
| Los Alamos (I) | – | – | – | – | – | $-0.17 \pm 0.17$ |
| Mojave (I) | −0.457 | −0.542 | −0.42 | $-0.30 \pm 0.09$ | $-0.80 \pm 0.47$ | $-0.27 \pm 0.11$ |
| Pietown (I) | – | – | – | – | – | $-0.30 \pm 0.15$ |
| Ovro (I) | −0.444 | −0.517 | – | – | – | $-0.36 \pm 0.43$ |
| Wettzell (I) | −0.442 | −0.523 | −0.46 | $-0.53 \pm 0.05$ | $-0.30 \pm 0.17$ | $-0.59 \pm 0.03$ |
| Madrid (I) | – | – | – | – | $-0.15 \pm 0.27$ | $-0.64 \pm 0.21$ |
| Haystack (C) | −0.369 | −0.458 | – | $-0.58 \pm 0.12$ | – | $-0.41 \pm 0.27$ |
| Kauai (C) | −0.053 | −0.638 | −0.26 | $-0.49 \pm 0.35$ | $0.35 \pm 0.77$ | $-0.43 \pm 0.14$ |
| Matera (C) | – | – | – | – | $-0.12 \pm 0.22$ | $-0.43 \pm 0.14$ |
| Medicina (C) | −0.431 | −0.563 | – | – | – | $-0.50 \pm 0.15$ |
| Onsala (C) | −0.254 | −0.517 | −0.32 | $-0.16 \pm 0.07$ | $0.00 \pm 0.11$ | $-0.16 \pm 0.04$ |
| Richmond (C) | −0.175 | −0.604 | −0.35 | $-0.16 \pm 0.07$ | – | $-0.20 \pm 0.19$ |
| Westford (C) | −0.366 | −0.454 | −0.43 | $-0.43 \pm 0.04$ | – | $-0.41 \pm 0.03$ |

Most of our results are significant and reasonable compared to the theoretical values. In general the theoretical models are confirmed, but there are also significant differences from theory for some stations. It can be seen from figure 4 that most of our VLBI results agree with theory within their formal error bars and as will be shown below, the correlation coefficient is higher than 0.7. Scaling the formal errors by a factor of 1.5 in order to get reasonable standard deviations, only the stations Hartebeesthoek (South Africa), Mojave (California, USA) and Onsala (Sweden) deviate from the IBH and the NIBH values by more than their scaled standard deviations. The stations Mojave and Hartebeesthoek in subtropical arid regions show significant discrepancies from the theoretical values which can be due to seasonal climatological coupling in these areas. Besides this, both stations have metal structure antennas which are probably stronger influenced by thermal deformation than other antennas. Moreover, both stations only took part in few observation sessions of the whole database and therefore their atmospheric loading parameters could only be weakly determined and got large formal errors. The atmospheric loading parameter of Onsala was determined to $-0.16 \pm 0.04$. Thus, it received a very small formal error, but completely disagrees with theory. The Onsala telescope is

located very close to the coast and is largely surrounded by the shallow water of the Kattegatt. From the theoretical point of view this should lead to an atmospheric loading effect like an inland station since shallow water reacts non-static. But there are probably strong wind driven ocean loading effects when the often strong westly winds press water into the bay surrounding the station Onsala. The wind driven ocean loading effects are not modeled by usual ocean loading models and could disturb the detection of the whole atmospheric loading effect at this station.

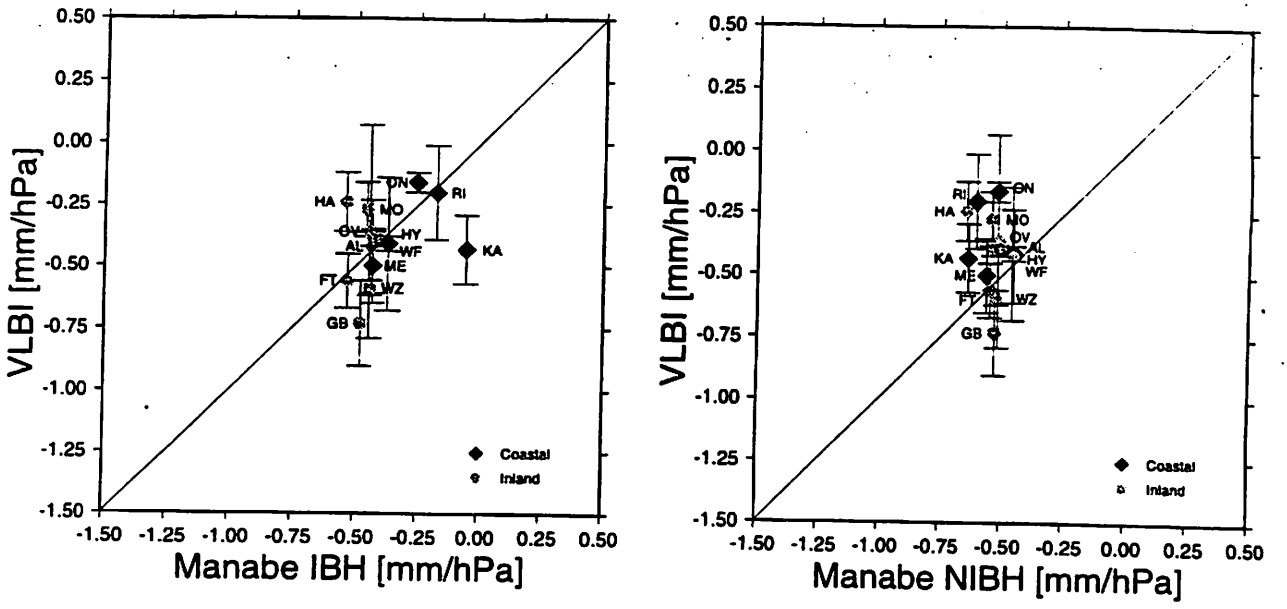


Figure 4: Correlation plots of model parameters (IBH left, NIBH right) and VLBI estimates of atmospheric loading coefficients for the station: Algopark (AL), Greenbank (GR), Ft.Davis (FT), Gilcreek (GI), Hartebeesthoek (HA), Mojave (MO), Wettzell (WZ), Haystack (HY), Medicina (ME), Onsala (ON) and Westford (WF), (circles = inland stations, diamonds = coastal stations (distance $\leq$ 200 $km$))

We also tested the validitiy of the inverted barometer hypothesis with our results obtained from VLBI data analysis, i.e. the VLBI results were compared with both, the parameters given by MANABE et al. [1991] for the IBH and those given for the NIBH.

The cross correlation coefficients r(x,y) between the theoretical atmospheric loading parameters $x_i$ of MANABE et al. [1991] and the empirical results $y_i$ obtained by VLBI were computed with equation (6) below. In this equation, $w_i$ are the weights of the results $y_i$. The weights are calculated from the formal sigmas $\sigma_i$ of the empirical results $y_i$ and an additional constant (const=0.10 $[mm/hPa]$), i.e. $w_i = 1/(\sigma_i + const)^2$.

$$r(x,y) = \frac{\sum_{i=1}^{n}(x_i \cdot (w_i \cdot y_i))}{\sqrt{(\sum_{i=1}^{n} x_i^2 \cdot \sum_{i=1}^{n}(w_i \cdot y_i)^2)}} \qquad (6)$$

Table 4 gives the correlation coefficients between the results of all stations, of only coastal stations and of only inland stations, respectively and the IBH and NIBH values by MANABE et al. [1991].

There is a small tendency that the IBH fits slightly better with the VLBI data than the NIBH, in particular for stations near the coast. Using all stations for which atmospheric loading coefficients have been determined, the correlation coefficients are 0.75 for the IBH and 0.73 for the NIBH. If we take only those stations which are closer than 200 km to the coast, the correlation is 0.78 for IBH and 0.73 for NIBH, respectively. For the other stations which are far from the coast, the relation changes and the correlation coefficents are 0.74 for the IBH and 0.75 for the NIBH.

Table 4: Cross correlation coefficients between model parameters and VLBI estimates of atmospheric loading coefficients.

| | IBH | NIBH |
|---|---|---|
| a) all stations regarded | 0.75 | 0.73 |
| b) only the stations near the coast regarded | 0.78 | 0.73 |
| c) only the stations far from the coast regarded | 0.74 | 0.75 |

# 5 Conclusions and outlook

Atmospheric loading corrections can be computed with different methods. The method supplying all three components of the site displacement applies a pure global convolution calculation based on observed barometric pressure data. Corrections due to atmospheric loading in the analysis of geodetic VLBI data influence the geodetic result only by a few mm or less and the postfit residuals and the baseline repeatability only change slightly. With all three methods used the atmospheric loading effect is on the limit of detectability and the repeatabilities do not point to a preferred method. Since the global barometric pressure data is provided only with a time resolution of 6 hours, further improvement using a combination of global pressure data and locally recorded pressure with better time resolution can be envisaged. Anyway, atmospheric loading corrections should be used routinely in the analysis of space geodetic data, even if the effect on the geodetic results still is small. Possible reasons are the absorption by clock and/or atmosphere parameters which has to be investigated further.

The determination of atmospheric loading parameters from geodetic VLBI data is successful. We determined atmospheric loading parameters for 18 stations from an extensive geodetic VLBI data set of about 800.000 observations, which is nearly 45 % of all geodetic VLBI data available. The correlation coefficients between the empirical results and the theoretical values by MANABE et al. [1991] is r=0.75. For stations close to the coast (distance $\leq$ 200 km) the correlation is higher to the IBH values (r=0.78) than to the NIBH values (r=0.73). Nevertheless there are some results that disagree with theory especially for the stations Hartebeesthoek (South Africa) and Mojave (California, USA) which are located in arid subtropical areas and the station Onsala (Sweden). The reason for the discrepancies can be seasonal climatological coupling and thermal effects for Hartebeesthoek and Mojave and wind driven ocean loading for Onsala.

For future work we plan to continue the investigations with a larger VLBI data set. An increased VLBI instrumental precision and VLBI phase solutions will improve the results of these investigations. Furthermore the question of IBH or NIBH should be studied in more detail and local deformations at the VLBI stations have to be considered.

**Acknowledgements.** We thank Dr. Axel Nothnagel (Geodätisches Institut der Universität Bonn [GIUB]) for making available the GIUB computer hard- and software to do numerous calculations. Rüdiger Haas is supported by the EU-TMR programme 1996-2000.

# References

[1] Farrell X.: *Deformation of the earth by surface loads*, Rev. Geophys. Space Phys., 10, 761-797, 1972

[2] Haas R.: *Untersuchungen zu Erddeformationsmodellen für die Auswertung von geodätischen VLBI-Messungen*, Ph.D. thesis, University of Bonn, DGK, Reihe C, Nr. 466, 1996

[3] Ma C., J. M. Sauber, L. J. Bell, T. A. Clark, D. Gordon, W. E. Himwich: *Measurement of horizontal motions in Alaska using very long baseline interferometry*, J. Geophys. Res., Vol. 95, No. B13, 21991-22011, 1990

[4] MacMillan D. S., J. M. Gipson: *Atmospheric pressure loading parameters from very long baseline interferometry observation*, J. Geophys. Res., Vol. 99, No. B9, 18081-18087, 1994

[5] Manabe S., T. Stao, S. Sakai, K. Yokoyama: *Atmospheric loading effect on VLBI observations*, Proceedings of the AGU Chapman Conference on Geodetic VLBI: Monitoring Global Change, 111-122, NOAA Technical Report NOS 137 NGS 49, U.S. Departement of Commerce, NOAA/NOS, Rockville, MD, 1991

[6] Rabbel W., J. Zschau: *Static deformations and gravity changes at the earth's surface due to atmospheric loading*, J. Geophys., 56, 81-99, 1985

[7] Rabbel W., H. Schuh: *The influence of atmospheric loading on VLBI-experiments*, J. Geophys., 59, 164-170, 1986

[8] Scherneck H. G.: *A parameterized Solid Earth Tide Model and Ocean Tide Loading Effects for Global Geodetic Baseline Measurements*, Geophys. J. Int., 106, 677-694, 1991

[9] Scherneck H. G.: *A comprehensive and tentatively complete summary of oceanic effects in space geodetic baseline measurements*, Proceedings of the 11th Working Meeting on European VLBI for Geodesy and Astrometry, 121-133, Onsala, 1996

[10] Sovers O. J., C. S. Jacobs: *Observation model and parameter partials for the JPL VLBI parameter estimation software "MODEST"-1996*, JPL publication 83-39, Rev. 6, 1996

[11] Sun H. P., B. Ducarme, V. Dehant: *Effect of the atmospheric pressure on surface displacements*, Journal of Geodesy, Vol. 70, 131-139, 1995

[12] VanDam T. M., J. M. Wahr: *Deformations of the Earth's surface due to atmospheric loading, effects on gravity and baseline measurements*, J. Geophys. Res., Vol. 92, 1281-1286, 1987

[13] VanDam T. M., T. A. Herring: *Detection of atmospheric pressure loading using very long baseline interferometry measurements*, J. Geophys. Res., Vol. 99, No. B3, 4505-4517, 1994

[14] VanDam T. M., G. Blewitt, M. B. Heflin: *Atmospheric pressure loading effects on Global Positioning System coordinate determinations*, J. Geophys. Res., Vol. 99, B12, 23939-23950, 1994

[15] Wessels P., W. H. F. Smith: *Free software helps map and display data*, EOS Trans. Amer. Geophys. U., Vol.55, 293-305, 1991

[16] Wunsch C., D. Stammer: *Atmospheric loading and the oceanic "inverted barometer" effect*, Rev. of Geophysics, Vol. 35, 1, 79-107, 1997

# INVESTIGATIONS OF FREQUENCY-DEPENDENT SOURCE STRUCTURE: 1038+52 A,B REVISITED

Richard W. Porcas [1] and María J. Rioja[2]
[1]*Max-Planck-Institut für Radioastronomie, Bonn, Germany*
[2]*Joint Institute for VLBI in Europe, Dwingeloo, The Netherlands*

## 1 Introduction

At mas and sub-mas angular scales, most extra-galactic radio sources exhibit some form of extended structure. Although perhaps undesirable for geodesists, this is not entirely unexpected. The radio power is believed to come from incoherent synchrotron emission. Kellermann and Pauliny-Toth (1969) have shown that the brightness temperature of such radiation cannot normally exceed $10^{12}$ K. This implies that sources with flux densities ca. 1 Jy at short cm wavelengths cannot be much smaller than ca. 1 mas. Of interest to astronomers are the morphology and spectral properties of such structure, since these provide constraints for understanding the physical properties of the emitting regions. Linear "jet-like" features are found to be common, strongly supporting the idea of collimated plasma outflow from a condensed, nuclear region.

Studying the spectral properties of mas emitting regions using VLBI presents a problem, since the normal use of "self-calibrated" visibility phases to make VLBI maps does not permit registration of maps at different frequencies at the mas level, except in special cases (e.g. Porcas and Patnaik, 1995). However, VLBI observations of close pairs of sources may result in a relative visibility phase measurement. For very close pairs, propagation and geometric model errors may be sufficiently diluted that relative astrometry between the sources, or mapping of one source using the other as a phase reference, can be made (e.g. Porcas and Rioja, 1996, Rioja and Porcas, 1996). If one of the sources is "point-like" and "achromatic" (no frequency-dependent sub-structure), a correct registration of maps of the other source at different frequencies can be achieved using relative astrometry. However, in realistic cases the structure of the reference source and its frequency-dependence must also be taken into account.

## 2 Observations of 1038+528A,B

We report here some results from multi-frequency VLBA+Effelsberg observations of the close quasar pair 1038+52 A and B (Owen, Porcas and Neff, 1978; Owen, Wills and Wills, 1980). Details of these 1995 observations are given in Porcas and Rioja (1996). Here we report on the frequency- dependent structure of both the A and B quasars, and on a new approach to making the "double registration" using the relative astrometric measurements at different frequencies.

Maps of both A and B quasars from our observations at 2.3, 8.4 and 15 GHz are presented in Figure 1. The map scales are very roughly the same at the three frequencies. The map resolu-

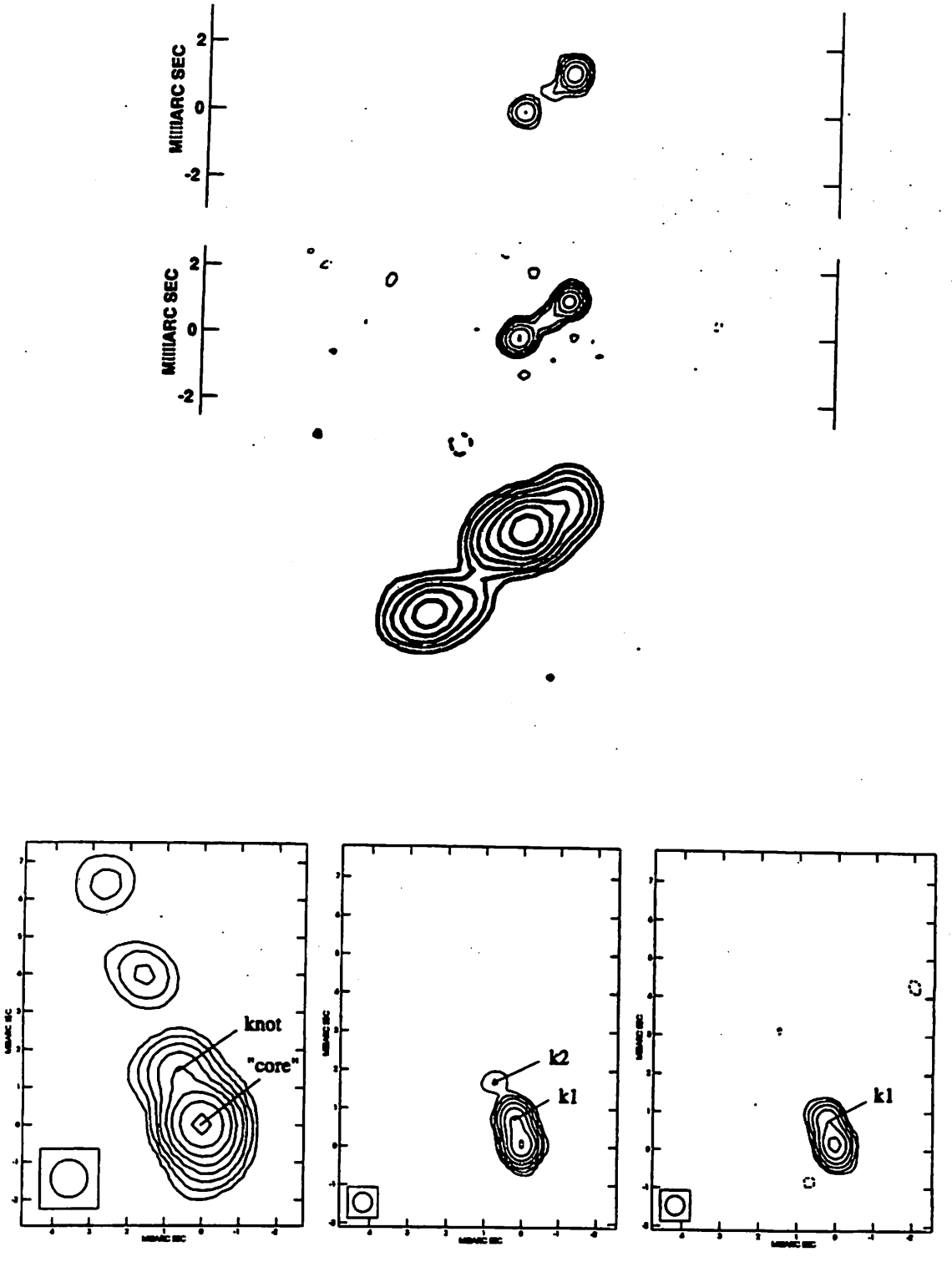


FIGURE 1

Top: Maps of 1038+52B at 15, 8.4 and 2.3 GHz (top down)

Bottom: Maps of 1038+52A at 2.3, 8.4 and 15 GHz (left to right)

tions at 15 GHz (without Effelsberg) and 8.4 GHz (including Effelsberg) are both 0.5 mas. At 2.3 GHz the "true" beam is nearly 4-times larger. Here we present "super-resolved" maps, using a CLEAN-algorithm restoring beam of 1.0 mas, in order to help in the detection and identification of components seen at 8.4 and 15 GHz which are just at the limit of the 2.3 GHz resolution.

## 3 Structure of 1038+528 B

Following Marcaide and Shapiro (1984) we identify the SE component of quasar B, seen at 8.4 and 15 GHz, with the central peak seen in the 2.3 GHz map. Because the A and B quasar structures are almost perpendicular in the sky plane, no other identification of "components" within B leads to a physically plausible astrometric registration of the maps of A. We refer to this as the "reference component" in B; our astrometric measurements are referred to the measured positions of the peak of this component in the maps of B at all three frequencies. In the registration of maps at different frequencies adopted by Marcaide and Shapiro (1984) these positions are the same at all frequencies. Note that this reference component is not identified with the "core" of quasar B, which is in fact the strong, NW component seen at 15 and 8.4 GHz, and which appears as a NW extension of the structure in the super-resolved 2.3 GHz map. We have shown elsewhere that there is a slow, outward motion of the reference component with respect to the core in B of ca. 13 micro-as per year (Rioja, 1993; Rioja et al, 1997; Rioja and Porcas, 1997). The extreme SE component seen at 2.3 GHz evidently has a very steep spectrum, as it is not detected above the limiting brightness level in either the 8.4 or 15 GHz maps.

## 4 Structure of 1038+528 A

The maps of quasar A show a bright peak of emission at the SW end of the structure at all three frequencies, and a "knotty" asymmetric extension to the NE in pa 15 - 25 degrees. At 2.3 GHz this jet extends out to at least 40 mas (see Figure 2). As pointed out by Marcaide and Shapiro (1984), the only physically plausible registration of the maps at 2.3 and 8.4 GHz results in a position of this bright peak which is frequency dependent. Radio astronomers usually refer to the bright peak at the base of such jets as the "core"; in this sense, the position of the "core" of 1038+52A is frequency-dependent. Marcaide and Shapiro reported a core shift of ca. 0.7 mas between 2.3 and 8.4 GHz. Core shifts are indeed expected from models of relativistic plasma jets (eg Blandford and Konigl, 1979), where opacity effects produce a rapid change of radio spectrum near the jet base. Marcaide et al (1985) parametrize the core shift with a power-law, $k\lambda^{\beta}$, with $0.7 < \beta < 2$. Our astrometric measurements of quasar A are referred to the measured position of the "core" peak at each frequency.

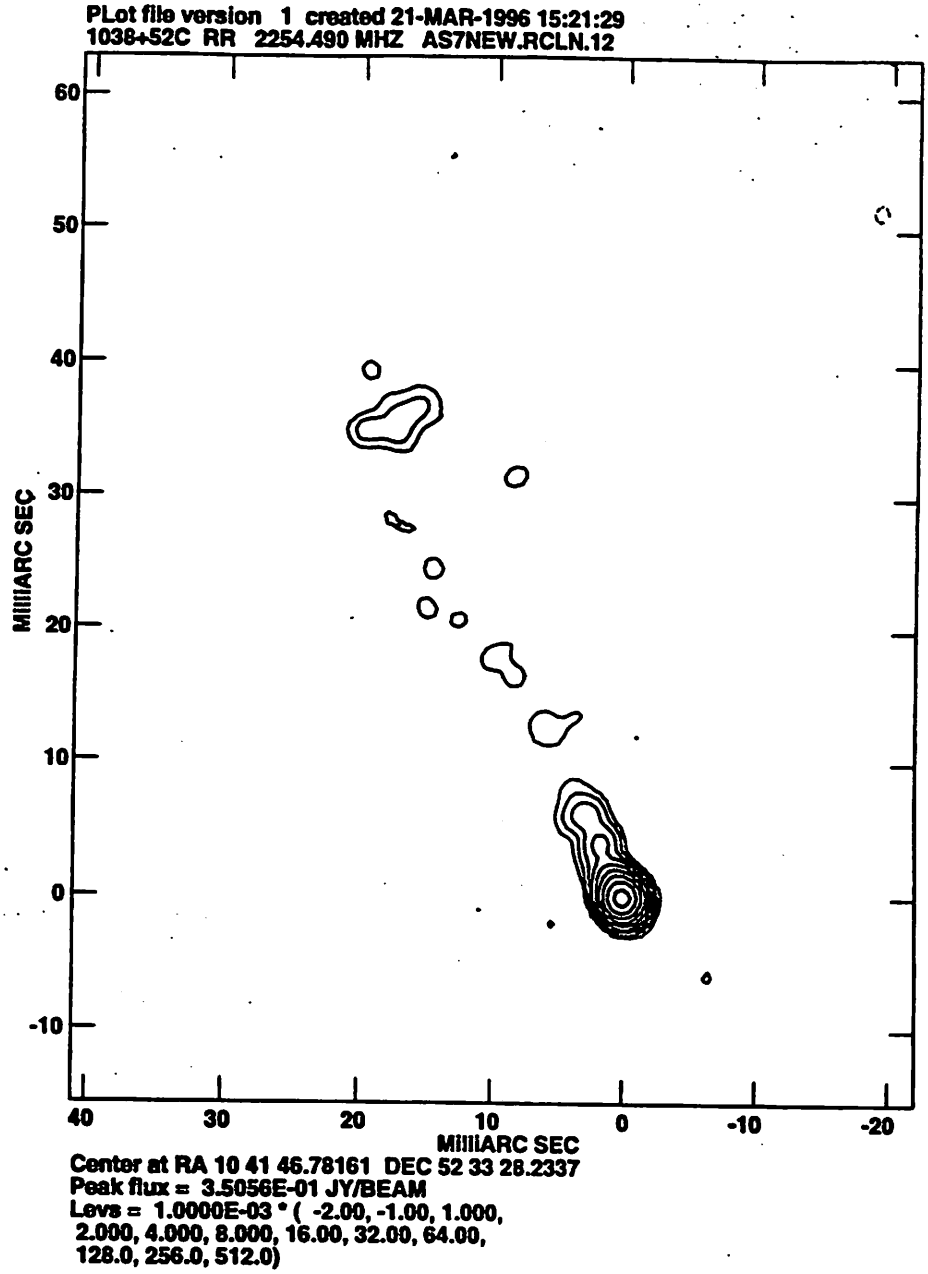


FIGURE 2

Map of 1038+52A at 2.3 GHz (1.8 mas beam)

# 5 New Astrometric Results

The astrometric measurements of the separations between the reference points in A and B, measured at each frequency, are shown in Figure 3. This includes measurements from three earlier epochs at 2.3 and 8.4 GHz, reported in Marcaide and Shapiro (1984), Marcaide et al (1994) and Rioja et al (1997). Our new three-frequency VLBA results are labelled "epoch 4". The origin of the plot represents the 8.4 GHz separation at epoch 1 (1981.3). The large offset of ca. 0.6 mas to the NE between the 2.3 and 8.4 GHz separations at epoch 4 clearly reflects the "core" shift in A. There is, however, no significant difference in the A-B reference-point separations between 8.4 and 15 GHz.

# 6 New Approach to the Registration

Our new three-frequency observations of 1038+52A,B produce a number of puzzles, which have caused us to re-examine the size of the A "core" shift, and the registration of the maps at different frequencies.

1) The A-B reference-point separations at 8.4 and 15 GHz are essentially identical; the measured difference is $< 20$ micro-as. Because the A and B source axes are roughly orthogonal, this implies both that there are no masureable opacity effects in A leading to a core-shift, and no position offset of the B reference component, between 8.4 and 15 GHz. This is surprising in view of the relatively large apparent shift in the A core position between 2.3 and 8.4 GHz; it leads to the conclusion that either the exponent $\beta$ in the core-shift formula is higher than previously supposed ( $> 2$ ) or that the "true" 2.3/8.4 GHz core shift has been over-estimated.

2) The size of the 2.3/8.4 GHz core shift in A (0.52 mas) is very close to the distance between the core and the first jet knot component ("K1") seen at 8.4 GHz and 15 GHz (0.65 mas). This is illustrated in Figure 4, where we have superposed a plot of the A-B measured separations (corrected for the motion of the B reference component) on to the 8.4 GHz map of A. The large crosses indicate the position of the 2.3 GHz "core", under the assumption (adopted by Marcaide and Shapiro) that the positions measured for the reference component in B coincide. If we consider K1 as a distinct, physical component, with a steeper spectral index than that of the 8.4 GHz core, it is clear that in 2.3 GHz maps, with a poorer resolution, these features will become blended into a single "core" component, with a position closer to K1 than would occur with a smaller beamwidth. In this way, the shift of the A "core" position with frequency is confused, and probably over-estimated, by the use of different resolutions at different frequencies.

It is tempting to ask whether, in fact, an alternative registration of maps can be made by actually identifying the 2.3 GHz A "core" with the 8.4 GHz knot K1. This results in a NW displacement of the 2.3 GHz position w.r.t the 8.4 GHz position of the reference component in B, but not quite in the direction of the B core.

3) There is a second knot, K2, visible in the 8.4 GHz map of quasar A, with a larger PA w.r.t. K1

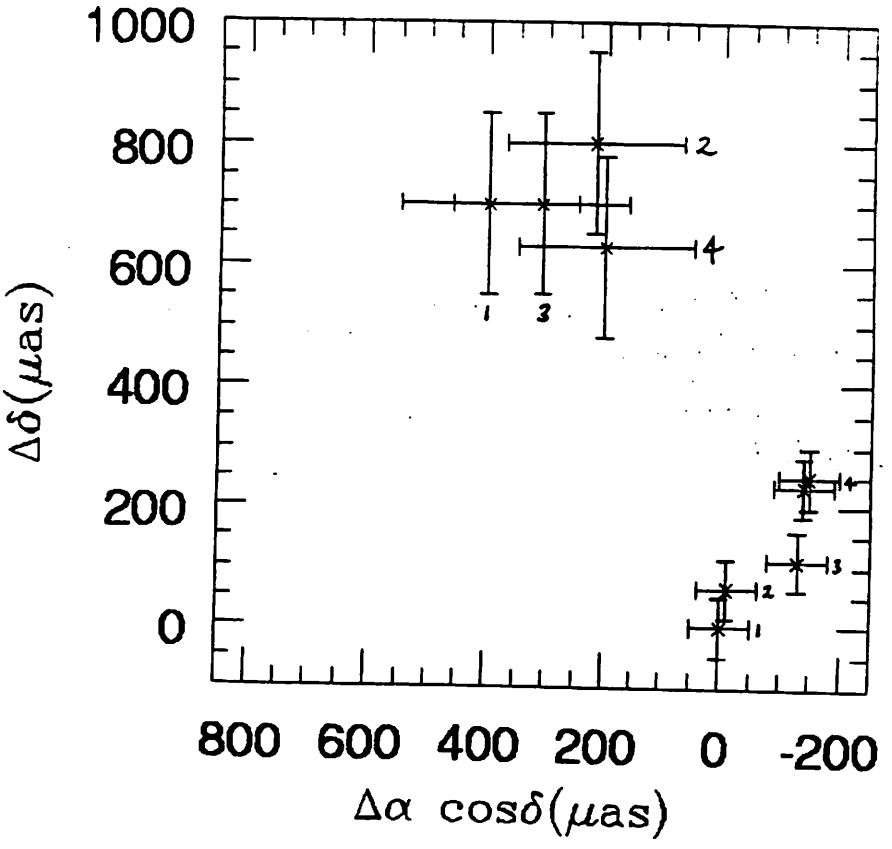


FIGURE 3 Astrometric A - B separations at different frequencies and epochs. Origin is 8.4 GHz separation at epoch 1. Large crosses are 2.3 GHz. Higher small cross at epoch 4 is 8.4GHz

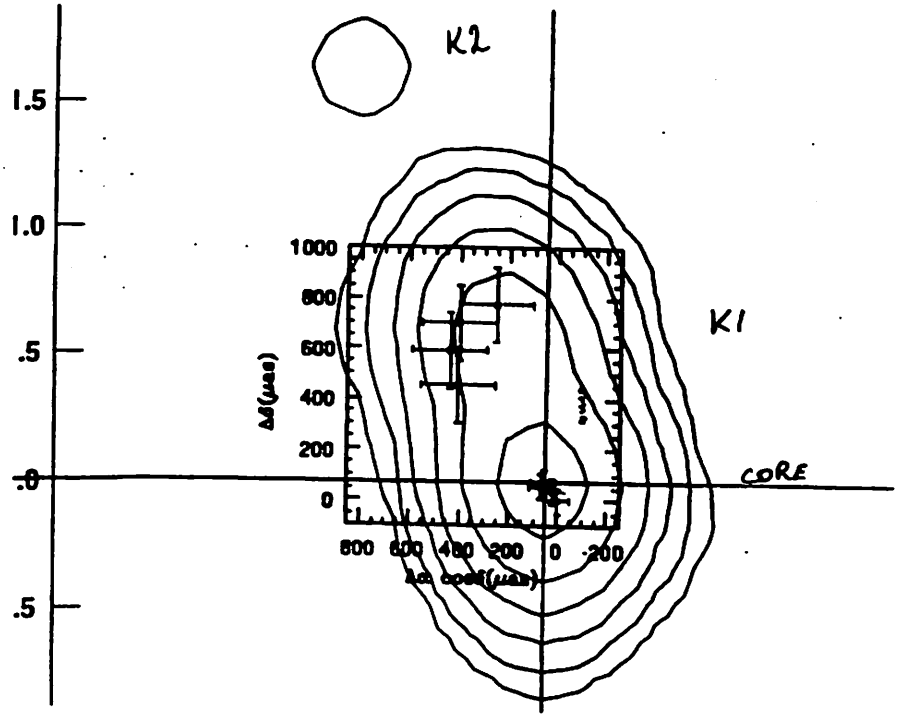


FIGURE 4 Corrected A - B separations superposed on 8.4 GHz A map

than K1 w.r.t. the core. This bend towards a larger PA is also seen in our super-resolved 2.3 GHz map, as an extension of the "core" (labelled "knot"). Because of the similarity of the positions and PAs of K2 and this 2.3 GHz "knot", it is again tempting to try a registration based on the identity of these (presumably optically thin) components. Again, this results in an offset, mainly to the W, between the 2.3 and 8.4 GHz positions of the B reference component.

4) At epoch 4 (and at epochs 1 and 3) there is a significant displacement of the 2.3 GHz "core" component from the 8.4 GHz source axis defined by the core-K1 separation (see Figure 4), using the registration adopted by Marcaide and Shapiro for epoch 1. This again suggests that perhaps some part of the difference between the A-B separations at different frequencies arises from a frequency-dependent position of the B reference component. We have investigated this possibility in the following ways. We used model fitting to measure the distance between the reference component and the core in B at different frequencies. There was no significant difference between the separations at 8.4 and 15 GHz. Although the measurement at 2.3 GHz has larger errors because the two features are only barely resolved, we did indeed find that the separation is smaller than at 8.4 and 15 GHz by ca. 0.28 mas. This might indicate the existence of opacity effects in the core of B. Alternatively, there may be beam-blending effects with the larger 2.3 GHz beam, of the sort which we believe play an important role in quasar A. In Figure 5 we present one-dimensional cuts along the main source axis for A and B at the three frequencies. As is clear from both these plots and the maps, there appears to be a significant level of emission between the core and reference components in B at 8.4 and 15 GHz. This might indeed contribute to a shift of the reference component position towards the core in B at 2.3 GHz.

In view of the above evidence for frequency-dependent positions in both A and B quasars, we adopted a new approach to the registration problem, similar to that used by Rioja (1993) to disentangle possible temporal changes in both sources. We allowed frequency-dependent position offsets in both sources, but required these to be along special, fixed directions in the two sources, defined by the "local" jet axis directions (137 degrees in B; 15 degrees in A). This gives a unique decomposition of the difference in the A-B separations at two frequencies, and leads to a new registration in which the 2.3 GHz position of the B reference component is offset 0.26 mas from the 8.4 GHz position towards the B core; the 2.3 GHz A "core" is offset by 0.55 mas from the 8.4 GHz core towards K1. Interestingly, a natural consequence of this registration, unimposed by the constraints, is that the 2.3 and 8.4 GHz positions of the B core are essentially the same, and the 2.3 GHz "knot" in A follows well the curved jet path defined by the 8.4 GHz core and knots K1 and K2. In Figure 6 we show the 8.4 GHz maps of both A and B, with the positions of 2.3 GHz components superimposed, for the "traditional" and new registrations. We have also applied this 2-vector decomposition to the measured A-B 2.3/8.4 GHz separation differences at epochs 1, 2 and 3; this yields 2.3/8.4 GHz position offsets of the B reference component of 0.22, 0.04 and 0.29 mas respectively, towards the core.

## 7 Conclusions

Our three-frequency VLBA + Effelsberg study of the structures of the close quasar pair 1038+52 A, B leads us to the following conclusions:

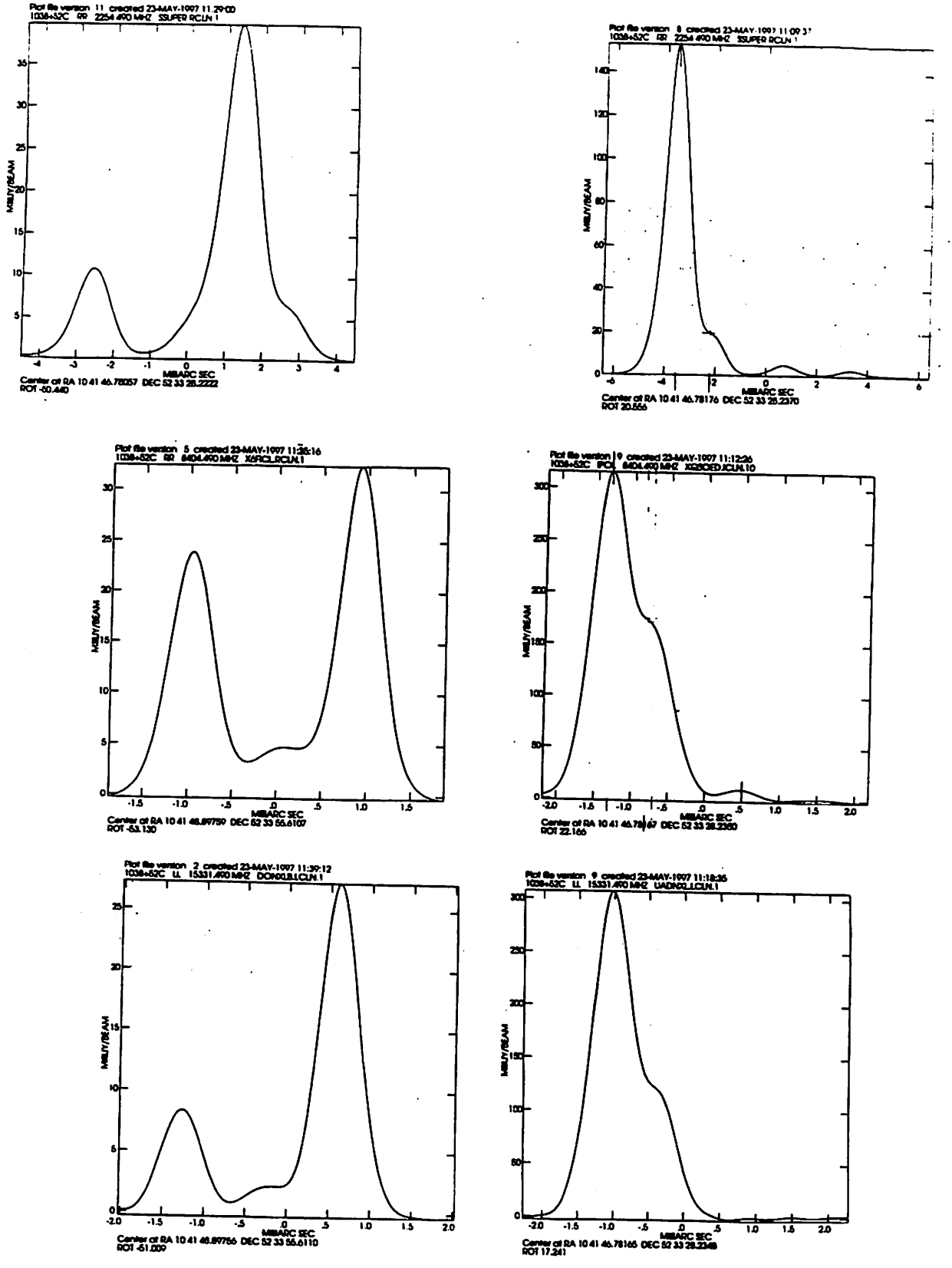


FIGURE 5

Cuts along the source axis of: (left) 1038+52B (right) 1038+52A

Top to bottom: 2.3 GHz, 8.4 GHz, 15 GHz

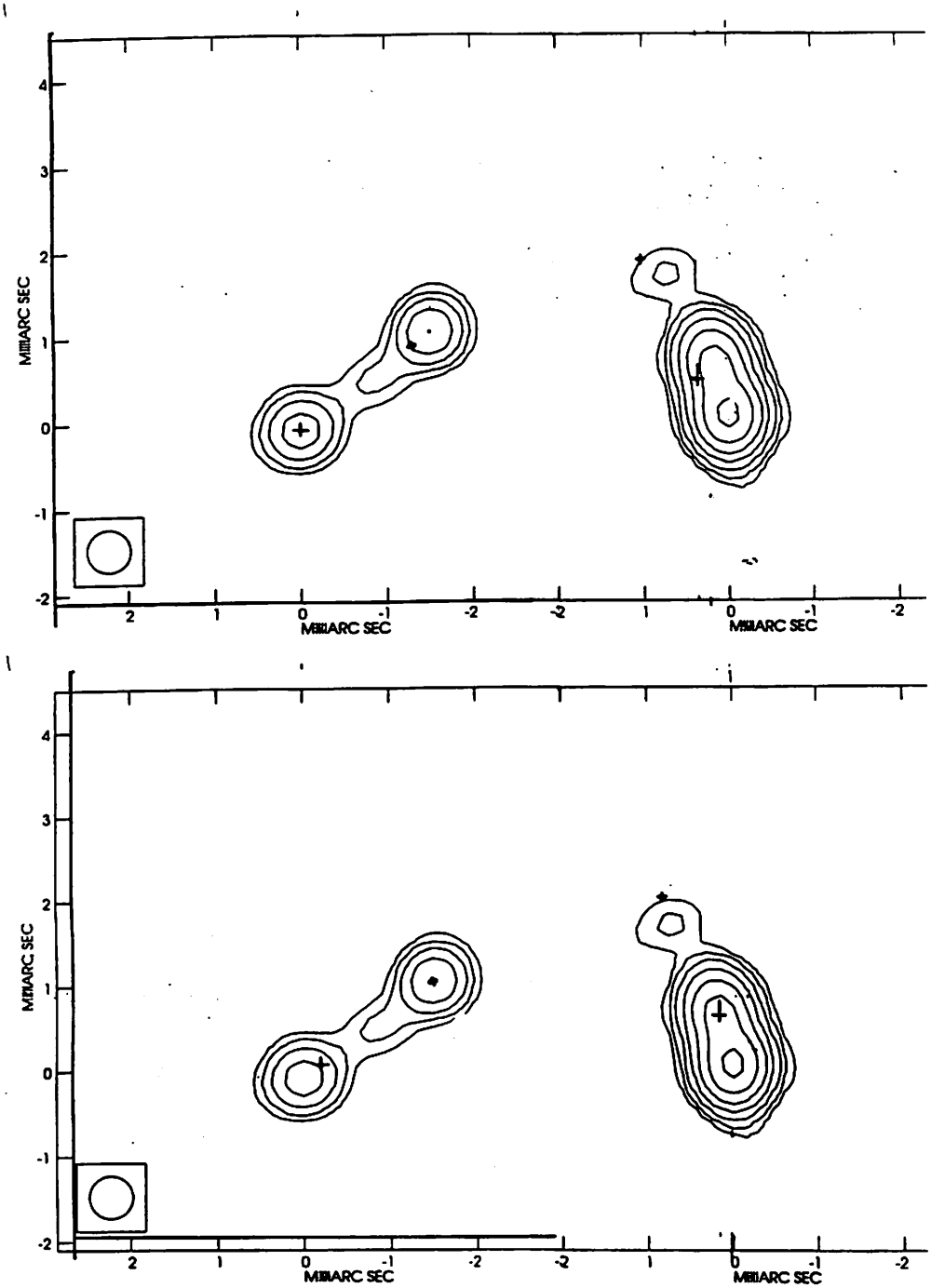


FIGURE 6

Maps at 8.4 GHz of (left) 1038+52B and (right) 1038+52A, with positions of the 2.3 GHz components marked with crosses

Top: Registration assumimg B reference component is achromatic

Bottom: Registration assuming offsets are in local jet direction

1) We confirm the difference between the A and B reference point separations at 2.3 and 8.4 GHz, as reported by Marcaide and Shapiro (1984). However, there is no detectable difference between the separations measured at 8.4 and 15 GHz.

2) To interpret the frequency-dependent structure of either quasar, the relative positions of the reference points at different frequencies within each quasar have to be established (map registration), using the separation measurements between the sources, and arguments of physical plausibility. The fact that the source axes are almost perpendicular is a powerful aid for this source pair, and provides a compelling argument that the reference features at 8.4 and 15 GHz are coincident in both 1038+52A and 1038+52B. Between 2.3 and 8.4 GHz, any physically plausible registration results in an offset between reference points in 1038+52A ; we also assume there may be offsets in 1038+52B.

3) The different resolutions of the VLBI beams at 2.3 GHz and 8.4/15 GHz must be taken into account when making a correct registration of maps at different frequencies, and when interpreting any offsets between positions of map "components" at different frequencies. Distinct components with different spectral characteristics may be resolved at the higher resolution, but blended at the lower. It is thus a dangerous assumption that a "component" (even an optically thin one) seen in a VLBI map has a uniform spectral distribution and a frequency-independent position.

4) To circumvent the dangers of assuming that any components have frequency- independent positions, we adopted a new strategy for registering the maps at 2.3 and 8.4 GHz, which permits frequency-dependent position offsets in both 1038+52 A and B, but which are constrained along the local jet directions. Although the main justification for this procedure is simplicity, it does lead to a very plausible registration of the 2.3 and 8.4 GHz maps of both quasars. Surprisingly, it independently produces the result that there is no detectable core-shift in quasar B between 2.3 and 8.4 GHz.

5) With the 8.4/15 GHz and 2.3/8.4 GHz registrations desribed above, we can now summarise the frequency-dependence within the two quasar structures. For 1038+52B, the reference component has the same position at both 8.4 and 15 GHz. Because the measured core to reference component separations also agree, the cores must also have the same position; thus the cores are coincident at 2.3, 8.4 and 15 GHz, within our measurement errors. The positions of the reference component coincide at 8.4 and 15 GHz, but at 2.3 GHz it is offset by ca. 0.25 mas in the direction of the core. We attribute this to the effects produced by the larger beam at 2.3 GHz, blending substructure which is separately resolved at the higher frequencies.

For 1038+52A, the reference ("core") components coincide at 8.4 and 15 GHz, but at 2.3 GHz it is offset by 0.55 mas towards the knot component K1. We suspect that emission from the jet component K1, seen at 8.4 and 15 GHz, is blended with the "true core" emission at 2.3 GHz to give the observed "core" component. Whilst there may be a "core-shift" reflecting opacity effects near the base of the jet, measurements made at different frequencies with different resolutions cannot give a good estimate of it, since the value obtained will depend on the different beamwidths used. Note, for example, that our "core" positions at 8.4 and 15 GHz would both shift towards K1 if we used the larger 2.3 GHz beam to restore the maps - and by different amounts, since the strength

of the K1 emission compared to that of the core is different at 8.4 and 15 GHz (see Figure 5) ! We treat our measured offset within A of 0.55 mas as an upper-limit to any such shift. The absence of any detectable shift between 8.4 and 15 GHz supports the conclusion that any true core-shift is less than that previously reported.

## 8 Acknowledgements

María J. Rioja acknowledges support for her research by the European Union under contract CHGECT920011.

## 9 References

Blandford, R.D. and Konigl, A., 1979, ApJ, 232, 34

Marcaide, J.M.M and Shapiro, I.I., 1984, ApJ, 276, 56

Marcaide, J.M.M et al, 1985, A+A, 142, 71

Marcaide, J.M.M et al, 1994, AJ, 108, 368

Kellermann, K.I. and Pauliny-Toth, I.I.K, 1969, ApJL, 155, L71

Owen, F.N., Porcas, R.W. and Neff, S.G., 1978, AJ,83, 1009

Owen, F.N., Wills, B.J. and Wills, D., 1980, ApJL,235,L57

Porcas, R.W. and Patnaik, A.R., 1995, Proc.10th Working Meeting, 188

Porcas, R.W. and Rioja, M.J., 1996, Proc. 11th Working Meeting, 209

Rioja, M.J., 1993, Proc. 9th Working Meeting, 152

Rioja, M.J. and Porcas, R.W., 1996, Proc. 11th Working Meeting, 219

Rioja, M.J. and Porcas, R.W., 1997, Proc. IAU Colloq. 164, Socorro (in press)

Rioja, M.J. et al, 1997, A+A, 325, 383

V. Tornatore, F. Migliaccio

DIIAR - Sez. Rilevamento - Politecnico di Milano

# A RIGOROUS STATISTICAL APPROACH FOR CENTROIDS DETERMINATION

## Abstract

A software to obtain a rigorous estimation of the positions of each individual component of images consisting of blended components has been developed. The elementary case with two components has been analized. The software takes advantage of a probabilistic approach to the problem of cluster analysis. This can be seen as a set of procedures which allow to subdivide sets of data into groups with homogeneus characteristics. The problem can be defined in the following way : to estimate a distribution which is a 'mixture' of two or more distributions. Once the number of distributions and their family has been identified, the problem can be solved as a parameter estimation. The least squares method was applied although not in a straightforward way. As a first test of the algorithms, two sets of simulated data were used.

## 1. Introduction

The images of brightness of radiosources present some internal structure which can be interpreted as the overlapping of individual components; the positions of the so called centroids of emission of these components are of great interest for both astrometry and geodesy. Our idea is to treat this problem as a type of cluster analysis with its statistical background.
The problem is that of refining procedures to subdivide data into homogeneus groups. Cluster analysis can be seen as a set of procedures which allow to subdivide sets of data into groups with internal homogeneous characteristics (a sort of internal coherence) dissimilar from one another. To reach this goal several methods based on different criteria have been developed over the last 30 years.
From our point of view, it is mostly fruitful to use a statistical model for the data. According to our approach the problem of cluster analysis can be defined in the following way: to estimate a distribution which is a "mixture" of two or more distributions according to the equation

$$L(x|\underline{p},\underline{\vartheta}) = \sum_{i=1}^{M} p_i f_i(x|\underline{\vartheta}^{(i)}) \qquad (1)$$

where:

$M$ = number of distributions which form the "mixture" distribution
$p_i$ = probability of having data in the $i$-th distribution
$\underline{\vartheta}^{(i)}$ = parameters of the $i$-th distribution

Once the distribution family has been identified, the problem can be solved as a parameter

estimation, where the parameters are $\underline{p}$ and $\underline{\vartheta}$.
We assume to know $M$, i.e. the number of groups present in the data, from an application of one of the many discrete procedures described in literature [4].
The standard method to estimate the parameters could be the maximum likelihood criterion, stating that the estimate of the parameters must be such as to maximize the likelihood function:

$$\prod_k L(x|\underline{p},\underline{\vartheta}) = Max \tag{2}$$

This gives rise to equations which are non linear and contain partial derivatives of $L$: to linearize them, the second order derivatives of $L$ must be introduced. This means that the equations are of increasing complexity, which is true also from the numerical point of view as the functions $L$, $\partial L$ and $\partial^2 L$ must be computed summing the contributions coming from all the data points.
A simpler method, such as the least squares principle, can be used if we work in the following way.
Let us suppose to have data laying on an area which is regularly divided into $m$ regions $R_i$, $(i = 1, \cdots, m)$, each one containing $N_i$ points:

$$\begin{array}{rcl} N_i & = & N[x \in R_i] \\ \sum_{i=1}^m N_i & = & N_{tot} \end{array} \tag{3}$$

The probability of having one point in $R_i$ is represented by:

$$P_i = P\{x \in R_i|\underline{p},\underline{\vartheta}\}, \tag{4}$$

which allows to write:

$$\nu_i(\underline{p},\underline{\vartheta}) = N_{tot}P\{x \in R_i|\underline{p},\underline{\vartheta}\} = N_{tot}\int_{R_i} L(x|\underline{p},\underline{\vartheta})dx, \tag{5}$$

$\nu_i$ being the "theoretical" number of points to be found in $R_i$.
As it is known [6], the following asymptotic result holds

$$\sum_{i=1}^m \frac{(N_i - \nu_i(\underline{p},\underline{\vartheta}))^2}{\nu_i(\underline{p},\underline{\vartheta})} \sim \chi^2_{m-1-k} \tag{6}$$

$k$ = number of parameters to be estimated .

This justifies the principle

$$\sum_{i=1}^m \frac{(N_i - \nu_i(\underline{p},\underline{\vartheta}))^2}{\nu_i(\underline{p},\underline{\vartheta})} = Min(x|\underline{p},\underline{\vartheta}) \tag{7}$$

which is strictly analogous to least squares both from the intuitive point of view ( (7) states that $N_i$ have to be close to $\nu_i$) as well as from the statistical point of view because the target function has the same distribution as that of the ordinary least squares principle.

Afterwards we approximate $\nu_i(p,\underline{\vartheta})$ with $\tilde{\nu}_i$ in the denominator, thus obtaining the modified principle

$$\sum_{i=1}^m (\delta N_i)^2 = \sum_{i=1}^m \frac{(N_i - \nu_i(x|p,\underline{\vartheta}))^2}{\tilde{\nu}_i} = Min(p,\underline{\vartheta}); \tag{8}$$

The reason of this approximation is that $\nu_i$ in the denominator appear as weights in the l.s. target function and we know that the l.s. solution depends weakly on the weights.

Two remarks are in order:

- the least squares principle cannot be applied staightforwardly to the vector with components $(N_i - \nu_i)$, when the regions $R_i$ cover the support of the probability distribution: as such a vector (asimptotically) has a singular covariance matrix [7]:
- it can be proved that the estimators $(\hat{\underline{p}}, \hat{\underline{\vartheta}})$ so obtained are consistent, i.e. when $N_{tot} \to \infty$, $(\hat{\underline{p}}, \hat{\underline{\vartheta}}) \to (\underline{p}, \underline{\vartheta})$ in probability.

## 2. A bi-dimensional, two-gaussians case

We now consider a bidimensional set of data with the distribution of data resulting from the mixture of two Gaussian densities.

$$L(\underline{x}|\underline{p}, \underline{\vartheta}) = pf_1(\underline{x}|\underline{\vartheta}_1) + (1-p)f_2(\underline{x}|\underline{\vartheta}_2) \tag{9}$$

where

$$f_{x,y}(x,y) = \frac{1}{2\pi \det C}\, e^{-\frac{1}{2}\left([(x-\mu_x)(y-\mu_y)]C^{-1}\left[\begin{smallmatrix} x-\mu_x \\ y-\mu_y \end{smallmatrix}\right]\right)} \tag{10}$$

$$\underline{x} = \begin{vmatrix} x \\ y \end{vmatrix} \qquad C = \begin{vmatrix} \sigma_x^2 & \sigma_{xy} \\ \sigma_{xy} & \sigma_y^2 \end{vmatrix} \tag{11}$$

The parameters to be estimated are $\underline{\vartheta}_1, \underline{\vartheta}_2, p$

$$\underline{\vartheta}_1 = \begin{vmatrix} \mu_{x1} \\ \mu_{y1} \\ \sigma_{x1}^2 \\ \sigma_{y1}^2 \\ \sigma_{xy1} \end{vmatrix} \qquad \underline{\vartheta}_2 = \begin{vmatrix} \mu_{x2} \\ \mu_{y2} \\ \sigma_{x2}^2 \\ \sigma_{y2}^2 \\ \sigma_{xy2} \end{vmatrix} \tag{12}$$

The available information is represented by $N_{ij}$ = number of points in a set of area elements of the real plane.
The observation equation can be written in the form :

$$\nu_{ij}(\underline{\vartheta}) = pN_{tot} \int_{Q_{ij}} f_1(\underline{x}|\underline{\vartheta}_1)dQ + (1-p)N_{tot} \int_{Q_{ij}} f_2(\underline{x}|\underline{\vartheta}_2)dQ \tag{13}$$

As the equation is non linear in the parameters, it has to be linearized. We set

$$\begin{array}{llll}
p = \tilde{p} + \delta p & & & \\
\mu_{x1} = \tilde{\mu}_{x1} + \delta\mu_x; & \mu_{x2} = \tilde{\mu}_{x2} + \delta\mu_x \\
\mu_{y1} = \tilde{\mu}_{y1} + \delta\mu_y; & \mu_{y2} = \tilde{\mu}_{y2} + \delta\mu_y \\
\sigma_{x1}^2 = \tilde{\sigma^2}_{x1} + \delta\sigma_{x1}^2; & \sigma_{x2}^2 = \tilde{\sigma^2}_{x2} + \delta\sigma_{x2}^2 \\
\sigma_{y1}^2 = \tilde{\sigma^2}_{y1} + \delta\sigma_{y1}^2; & \sigma_{y2}^2 = \tilde{\sigma^2}_{y2} + \delta\sigma_{y2}^2 \\
\sigma_{xy1} = \tilde{\sigma}_{xy1} + \delta\sigma_{xy1}; & \sigma_{xy2} = \tilde{\sigma}_{xy2} + \delta\sigma_{xy2}
\end{array}$$

The resulting linearized equation is :

$$\nu_{ij}(\underline{\vartheta}) = \nu_{ij}(\tilde{\underline{\vartheta}}) + \frac{\partial \nu_{ij}(\tilde{\underline{\vartheta}})}{\partial p}\delta p + \sum_{i=1}^{5} \frac{\partial \nu_{ij}(\tilde{\underline{\vartheta}})}{\partial \vartheta_{1i}}\delta \vartheta_{1i} + \sum_{i=1}^{5} \frac{\partial \nu_{ij}(\tilde{\underline{\vartheta}})}{\partial \vartheta_{2i}}\delta \vartheta_{2i} \qquad (14)$$

where the expression of partial derivatives versus $p$ is

$$\frac{\partial \nu_{ij}(\underline{\vartheta})}{\partial p} = \frac{N}{2\pi}\left\{\frac{1}{\sqrt{k_1}}\int_{Q_{ij}} e^{-h_1/2}dQ - \frac{1}{\sqrt{k_2}}\int_{Q_{ij}} e^{-h_2/2}dQ\right\}$$

and the expressions of partial derivatives versus the parameters defining the two gaussians are the following

$$\begin{aligned}
\frac{\partial \nu_{ij}}{\partial \mu_{x_1}} &= \frac{Np}{2\pi(k_1)^{\frac{3}{2}}}\int_{Q_{ij}} (l_1\sigma_{y_1}^2 - g_1\sigma_{xy_1})e^{-h_1/2}dQ \\
\frac{\partial \nu_{ij}}{\partial \mu_{y_1}} &= \frac{Np}{2\pi(k_1)^{\frac{3}{2}}}\int_{Q_{ij}} (g_1\sigma_{x_1}^2 - l_1\sigma_{xy_1})e^{-h_1/2}dQ \\
\frac{\partial \nu_{ij}}{\partial \sigma_{x_1}^2} &= \frac{-Np}{4\pi(k_1)^{\frac{3}{2}}}\int_{Q_{ij}} \left[\sigma_{y_1}^2 - \frac{(l_1\sigma_{y_1}^2 - g_1\sigma_{xy_1})^2}{k_1}\right] e^{-h_1/2}dQ \\
\frac{\partial \nu_{ij}}{\partial \sigma_{y_1}^2} &= \frac{-Np}{4\pi(k_1)^{\frac{1}{2}}}\int_{Q_{ij}} \left[\sigma_{x_1}^2 - \frac{(g_1\sigma_{x_1}^2 - l_1\sigma_{xy_1})^2}{k_1}\right] e^{-h_1/2}dQ \\
\frac{\partial \nu_{ij}}{\partial \sigma_{xy_1}} &= \frac{Np}{2\pi(k_1)^{\frac{3}{2}}}\int_{Q_{ij}} \left[\sigma xy_1 + \frac{1}{k_1}(g_1\sigma_{x_1}^2 - l_1\sigma_{xy_1})\cdot\right. \\
&\qquad \left.\cdot(l_1\sigma_{y_1}^2 - g_1\sigma_{xy_1})\right] e^{-h_1/2}dQ,
\end{aligned}$$

setting

$$\begin{aligned}
l_1 &= x - \mu_{x_1} \\
g_1 &= y - \mu_{y_1} \\
k_1 &= \det C_1 = \sigma_{x_1}^2\sigma_{y_1}^2 - \sigma_{xy_1}^2 \\
h_1 &= \frac{1}{k_1}(l_1^2\sigma_{y_1}^2 - 2l_1g_1\sigma_{xy_1} + g_1^2\sigma_{x_1}^2)
\end{aligned}$$

The derivatives with respect $\underline{\vartheta}_2$ can be written analogously.

## 3. Experiments with simulated data

A software implementing the above equations has been written and tested on two sets of simulated data. The simulations were realized by sampling two sets of $N_{tot} = 1000$ data from two normal bidimensional distributions characterized by the "true" values of the parameters displayed in the first column of Table 1.

In simulation $A$ the two clusters have a little overlapping area, while in $B$ the overlapping area is quite large (see Fig. 1).

We assumed to have no information about the data distribution but the fact that the data belonged to two normal densities. The ten parameters of the two distributions and $p$ are the parameters to be estimated by the "least squares" principle (8). As the problem we are treating is non linear, the solution can be found according to an iterative procedure, where the new approximate values at each step are equal to the solutions of the previous step.
Before starting this procedure, we established a simple criterion to obtain approximate values of the parameters to be estimated. We used the straight line in figure 1 as a border line to roughly separate the two groups : then means, variances and covariances of the two samples so obtained were the starting values. Based on these values, the least squares solution was applied. The number of iterations necessary to obtain stable results was 6.
The results obtained for the estimates of the parameters of the two distributions are satisfactory. Table 1 summarizes the 'true', approximate and estimated values for each parameter. In particular, the estimated values of the components of mean values of each gaussian are very close to the 'true' values used for both simulations.

| Data from simulation A | | | |
|---|---|---|---|
| Parameter | "True" value | Approximate value | Estimated value |
| $p$ | 0.3000 | 0.3160 | 0.3039 |
| $\mu_{x_1}$ | 0.0000 | 0.1000 | 0.0258 |
| $\mu_{y_1}$ | 0.0000 | 0.0900 | 0.0693 |
| $\sigma^2_{x_1}$ | 1.0000 | 0.7000 | 0.8344 |
| $\sigma^2_{y_1}$ | 1.0000 | 1.2000 | 1.0961 |
| $\sigma_{xy_1}$ | 0.0000 | -0.1000 | −0.0888 |
| $\mu_{x_2}$ | 3.0000 | 3.0600 | 3.0438 |
| $\mu_{y_2}$ | 3.0000 | 3.0600 | 3.0257 |
| $\sigma^2_{x_2}$ | 0.5000 | 0.4800 | 0.5013 |
| $\sigma^2_{y_2}$ | 1.0000 | 0.9000 | 1.0122 |
| $\sigma_{xy_2}$ | 0.1000 | 0.5000 | 0.3408 |

| Data from simulation B | | | |
|---|---|---|---|
| Parameter | "True" value | Approximate value | Estimated value |
| $p$ | 0.3000 | 0.3030 | 0.2641 |
| $\mu_{x_1}$ | 0.0000 | -0.0800 | −0.1721 |
| $\mu_{y_1}$ | 0.0000 | 0.0500 | 0.0148 |
| $\sigma^2_{x_1}$ | 1.0000 | 0.5000 | 0.6231 |
| $\sigma^2_{y_1}$ | 1.0000 | 1.3000 | 1.1353 |
| $\sigma_{xy_1}$ | 0.0000 | -0.2000 | −0.1497 |
| $\mu_{x_2}$ | 2.0000 | 2.0800 | 2.0017 |
| $\mu_{y_2}$ | 2.0000 | 2.0200 | 1.9349 |
| $\sigma^2_{x_2}$ | 0.5000 | 0.4300 | 0.5291 |
| $\sigma^2_{y_2}$ | 1.0000 | 0.9800 | 1.1390 |
| $\sigma_{xy_2}$ | 0.1000 | 0.4000 | 0.3821 |

Table 1

SIMULATION A

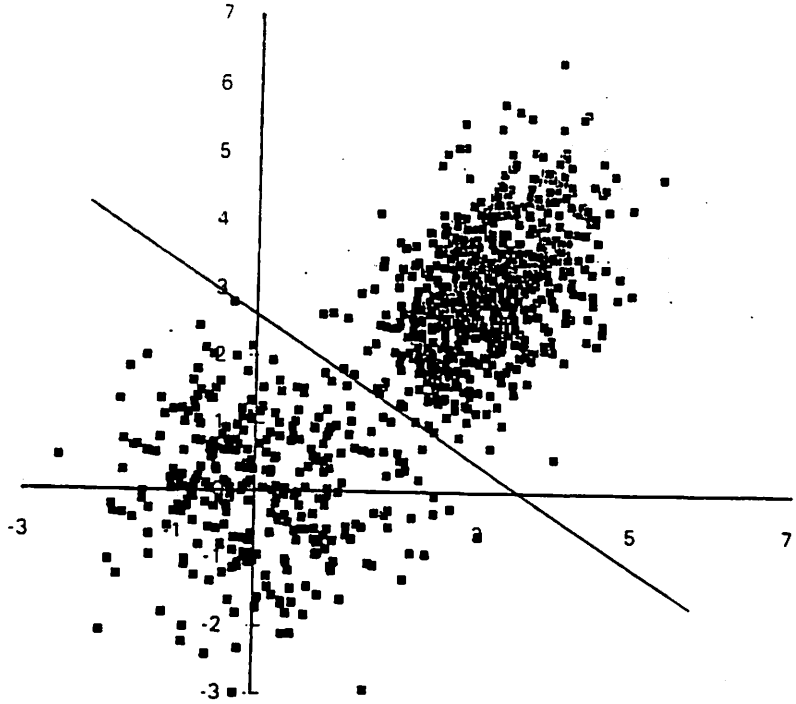


SIMULATION B

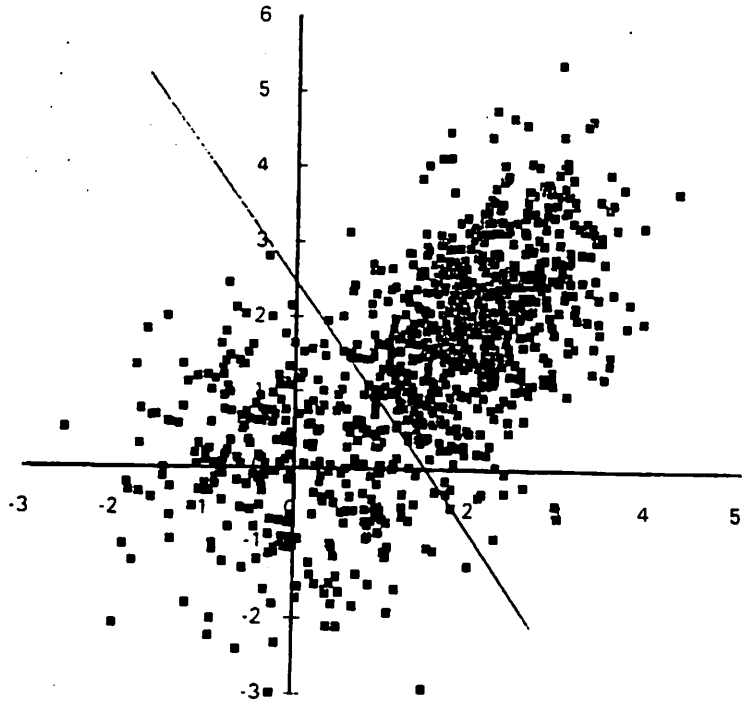


Figure 1: Graphical rappresentation of the simulations in the x,y plane.

As a check, we made some computations changing the starting approximate values finding that the solution gave the same estimates for the values of parameters.
The next step of this work will be to use the software developed to determine the centroids of emission of individual component of a radiosource consisting of two blended components.

In this case in the observation equation the value $N_{tot}$ will be substituted by the total flux density of the radiosource; each element of the grid of map values of the radiosource will be associated to the corrisponding area element $Q_{ij}$. The $Q_{ij}$ are the area elements in the right ascension declination plane.
We feel confident to find good estimates of the coordinates of these centroids since they correspond to the components of the mean values of each gaussian distribution, which are are the better estimated parameters of the problem in the case of simulations presented here.

# References


[1] B. Crippa, L. Mussio (1993). "Data compression and evaluation by cluster analysis", Proceedings of ISPRS Commission I Workshop on "Digital sensors and systems".

[2] A. de Haan (1991). "Fundamentals of cluster analysis", Proceedings of ISPRS Tutorial on "Mathematical aspects of data analysis".

[3] R.O. Duda, P.E. Hart (1973). "Pattern classification and scene analysis", J. Wiley and Sons.

[4] L. Kaufman, P.J. Rousseeuw (1990). "Finding groups in data", J. Wiley and Sons.

[5] J.S. Lim (1990). "Two-dimensional signal and image processing", Prentice Hall.

[6] A.M. Mood, F.A. Graybill, D.C. Boes (1983). "Introduction to the theory of statistics", McGraw-Hill.

[7] F. Migliaccio, F. Sanso', V. Tornatore, "Clusters and probabilistic models for a refined estimation theory", Bollettino di geodesia e scienze affini, in press

# LIST OF PARTICIPANTS AT THE 12TH WORKING MEETING ON EUROPEAN VLBI FOR GEODESY AND ASTROMETRY

Andersen, Per Helge
Norwegian Defence Research Establishment,
Box 25, N-2007 Kjeller, Norway.
Tel: +47 63 80 74 07
Fax: +47 63 80 72 12
per-helge.andersen@ffi.no

Campbell, James
Geodetic Institute,
University of Bonn,
Nussallee 17,
D-53115 Bonn, Germany
Tel:+49-228-733565 or -732621
Fax: +49-228-732988
CAMPBELL@sn-geod-1.geod.uni-bonn.de

Carlsson, Ragne
Onsala Space Observatory
S-439 92 Onsala
Sweden
Tel: +46 31 772 5575
Fax: +46 31 772 5590
rtc@oso.chalmers.se

Colucci, Pino
Nuova Telespazio C.P. Aperta
Centro di Geodesia Spaziale
I-75100 Matera, Italy
Tel: +39 835 377291
Fax: +39 835 334951
colucci@geodaf.mt.asi.it

Elgered, Gunnar
Onsala Space Observatory
Chalmers University of Technology
S - 439 92 Onsala, Sweden
tel (direct) +46 31 772 5565
fax +46 31 772 5590
kge@oso.chalmers.se

Haas, Ruediger
Onsala Space Observatory
Chalmers University of Technology
S-43992 Onsala, Sweden
tel.: +46 31 772 5530
fax.: +46 31 772 5590
haas@oso.chalmers.se

Hase, Hayo
Institut für Angewandte Geodäsie
Fundamentalstation Wettzell
D-93444 Kötzting, Germany
Tel.: +49 9941 603-0, resp.-104, -333
Fax: +49 9941 603 222
hase@wettzell.ifag.de

Hernes, Gunn Marit
Geodesidivisjonen
Statens kartverk
N-3500 Hønefoss, Norway
Tel: +47 32 11 81 00
Fax:+47 32 11 81 01
gunn.marit.hernes@gdiv.statkart.no

Holland, David
Statens kartverk
Geodetisk observatorium
N-9173 Ny-Ålesund, Norway
Tel: +47 79 02 70 10
Fax:+47 79 02 71 48
david.holland@gdiv.statkart.no

Jarlemark, Per
Onsala Space Observatory
S-439 92 Onsala, Sweden
Tel: +46 31 772 5560
Fax: +46 31 772 5590
poj@oso.chalmers.se

Johansson, Jan
Onsala Space Observatory
Chalmers University of Technology
S-439 92 Onsala, Sweden
Tel. +46 31 772 5558
fax. +46 31 772 5590
jmj@oso.chalmers.se

Kilger, Richard
Fundamental Station Wettzell
D-93444 Kötzting, Germany
Tel:+49 9941 603 263
Fax.+49 9941 603 222
kilger@wettzell.ifag.de

Kristiansen, Oddgeir
Geodesidivisjonen
Statens kartverk
N-3500 Hønefoss, Norway
Tel: +47 32 11 81 00
Fax:+47 32 11 81 01
oddgeir.kristiansen@gdiv.statkart.no

Lanotte, Roberto
Nuova Telespazio SpA
Centro di Geodesia Spaziale
Contrada Terlecchia
I-75100 Matera, Italy
Tel: +39 835 377238
Fax:+39 835 334951
lanotte@alpha.mt.asi.it

Lopez-Fernandez, Isaac
Centro Astronomico de Yebes
Apartado 148
E-19080 Guadalajara, Spain
Tel:+34 49 290311/37
Fax:+34 49 290063
isaac@cay.oan.es

Mantovani, Franco
Instituto di Radioastronomia
Via P.Gobette 101
I-40129 Bologna, Italy
Tel:+39 516 399377
Fax:+39516 399431
FMANTOVANI@astbo1.bo.cnr.it

Mathisen, Olav
Institutt for kartfag
Norges landbrukshøgskole
Postboks 5034
1432 ÅS, Norway

Nardi, Anthonio
Nuovo Telespazia SpA,
Via Tiburtina 167
Roma, Italia

Nothnagel, Axel
Geodetic Institute
University of Bonn
Nussallee 17
D-53115 Bonn ,Germany
Tel.: +49 228 733562
Fax.: +49 228 732988
nothnagel@uni-bonn.de

Pettersen, Bjørn Ragnvald
Statens kartverk
N-3500 Hønefoss, Norway
Tel: +47 32 11 81 00
Fax: +47 32 11 81 01
bjorn-ragnvald.pettersen@statkart.no

Plag, Hans Peter
Geodesidivisjonen
Statens kartverk
N-3500 Hønefoss, Norway
Tel: +47 32 11 81 00
Fax:+47 32 11 81 01
Email:hans.peter.plag@gdiv.statkart.no

Porcas, Richard
Max-Planck-Institut für Radioastronomie
Auf dem Huegel 69
D-53121 Bonn, Germany
Tel: +49 228 525288
Fax: +49 228 525229
porcas@mpifr-bonn.mpg.de

Reinhold, Andreas
Bundesamt für Kartografie und Geodäsie
Agency Leipzig
Karl Rothe Strasse 10-14
D-04105 Leipzig, Germany
Tel: +49 341 5634 421
Fax: +49 341 5634 415
ar@leipzig.ifag.de

Rekkedal, Svein
Geodesidivisjonen
Statens kartverk
N-3500 Hønefoss, Norway
Tel: +47 32 11 81 00
Fax:+47 32 11 81 01
svein.rekkedal@gdiv.statkart.no

Rius, Antonio
IEEC/UB-CSIC-UAB-UPC
Edif. NEXUS,104
Gran Capita, 2-4,
E-08034 Barcelona, Spain
Tel:+34 3 280 2088
Fax:+34 3 280 6395
rius@ieec.fcr.es

Scherneck, Hans-Georg
Onsala Space Observatory
S-439 92 Onsala, Sweden
Tel: +46 31 772 5556
Fax: +46 31 772 5590
hgs@oso.chalmers.se

Schuh, Harald
DGFI, Abteilung 1
Marstallplatz 8
D-80539 München, Germany
Tel: +49 89 23031 214
Fax: +49 89 23031 240
schuh@dgfi.badw-muenchen.de

Sorgente, Mauro
Max Planck Institut für RadioAstronomie
Auf dem Hugel 69
D-53121 Bonn, Germany
Tel: +49 228 525 219
sorgente@mpifr-bonn.mpg.de

Tangen, Leif Morten
Geodetisk observatoriun
Statens kartverk
N-9173 Ny-Ålesund, Norway
Tel:+47 79 02 70 10
Fax:+47 79 02 71 48
leif.morten.tangen@gdiv.statkart.no

Titov, Oleg A.
Institut of Applied Astronomy,
Zhdanovskaya st. 8
St.Petersburg 197042, Russia.
Tel:+7 812 230 74 13
Fax:+7 812 230 74 13
titov@isida.ipa.rssi.ru

Tornatore, Vincenza
c/o DIIAR Politecnico di Milano
Piazza Leonardo da Vinci 32
I-20133 Milano, Italy
Tel:+39 223 996504
Fax:+39 223 996530
vlbi@ipmtf4.topo.polimi.it

Tuccari, Gino
Instituto di Radioastronomia
Consiglio Nazionale delle Riecerche,
P.O.box 141
I-96017 Noto (Siracusa), Italy
Tel:+39 931 824108
Fax:+39 931 824122
tuccari@ira.noto.cnr.it

ISBN 82-90408-41-2